ENGINEERING FUNCTIONAL HEPATIC TISSUE USING BIOLOGIC SCAFFOLDS COMPOSED OF LIVER EXTRACELLULAR MATRIX

by

Denver Michael Faulk

Bachelor of Science in Chemical and Biomedical Engineering,

Carnegie Mellon University, 2008

Submitted to the Graduate Faculty of

Swanson School of Engineering in partial fulfillment

of the requirements for the degree of

Doctor of Philosophy

University of Pittsburgh

2015

UNIVERSITY OF PITTSBURGH

SWANSON SCHOOL OF ENGINEERING

This dissertation was presented

by

Denver Michael Faulk

It was defended on

August 10, 2015

and approved by

Stephen F. Badylak, DVM, PhD, MD, Professor, Department of Surgery

Anthony J. Demetris, MD, Professor, Department of Pathology

Paulo A. Fontes, MD, Associate Professor, Department of Surgery

John F. Patzer, PhD, Professor, Department of Bioengineering

William R. Wagner, PhD, Professor, Department of Surgery

Dissertation Director: Stephen F. Badylak, DVM, PhD, MD, Professor,

Department of Surgery

ENGINEERING FUNCTIONAL HEPATIC TISSUE USING BIOLOGIC SCAFFOLDS COMPOSED OF LIVER EXTRACELLULAR MATRIX

Denver Michael Faulk, PhD

University of Pittsburgh, 2015

Liver disease is a leading cause of mortality in the United States resulting in over 30,000 deaths annually. Allogenic liver transplantation represents the treatment of choice for end-stage liver failure, but the shortage of viable donor livers, the need for immunosuppressive drugs, and high cost are all limiting factors. The concept of whole organ engineering of the liver has emerged as a potential solution. This approach involves perfusion decellularization of a xenogeneic liver followed by repopulating the resultant three-dimensional biologic scaffold with an autologous cell source. Current limitations preventing this approach from becoming a clinical reality include the re-establishment of a non-thrombotic microvasculature and an effective method for delivering functional parenchymal cells to their native location within the three-dimensional scaffold.

The first objective of this work was to determine the effects of commonly used decellularization agents upon the resulting scaffold and its ability to support endothelial cell attachment and growth. Results showed that when a tissue is decellularized with harsh anionic detergents, such as sodium dodecyl sulfate, it is stripped of naturally occurring bioactive components and the native fiber architecture of the extracellular matrix is significantly damaged. Conversely, when less harsh non-ionic detergents are used for decellularization, such as Triton X-100, the resulting scaffold maintains the native microstructure of the extracellular matrix

resulting in improved endothelial cell attachment. Thus, the choice of detergents used for tissue decellularization can have a marked effect upon the integrity of the resultant bioscaffold.

The second objective of the present work was to systematically investigate key variables associated with reconstructing a functional hepatic vascular network. Four factors of endothelial cell seeding (1) rate of media perfusion, (2) seeding density, (3) duration of culture, and (4) the addition of an anti-thrombotic heparin coating were investigated by means of two outcomes: endothelial coverage of the scaffold vasculature and cell viability. Within three days of culture, seeded human endothelial cells attached to the three-dimensional liver scaffold, displayed a normal flattened appearance, and formed microvasculature throughout.

The final objective of this work was to develop a preferred method of delivering hepatocytes to achieve effective and viable cell engraftment, anatomically appropriate spatial location, and functionality. Two hepatocyte seeding techniques were developed and evaluated: (1) syringe injection through the Glisson's capsule and (2) infusion through portal and hepatic veins. Metabolic activity and cell viability of the engrafted hepatocytes was evaluated by quantification of albumin and urea production, engrafted cell morphology, and expression of hepatic specific genes. Results also showed high hepatocyte viability (>80%), excellent cell morphology, albumin and urea production, and hepatocyte specific gene expression with the syringe injection technique. The findings from this work represent notable steps toward clinical translation of whole organ engineering.

TABLE OF CONTENTS

LIST OF TABLES

LIST OF FIGURES

PREFACE

The pursuit of a doctorate involves a process of one's growth and development as a researcher. This maturation can go forward only with the help and support of others. I am thankful to many people whose continuous guidnace and feedback were essential to my success during my doctoral work. First and foremost I am indebted to Dr. Stephen Badylak for accepting me into his laboratory and facilitating the completion of my doctoral studies. I will forever value his support and the opportunity to participate in such an interdisciplinary environment focused on translational medicine.

Thank you to my committee members; Dr. William Wagner, Dr. Paulo Fontes, Dr. Anthony Jake Demetris, Dr. Jack Patzer and once again to Dr. Stephen Badylak for their dedication to my development and for the valuable insights that they provided to this body of work. Their ideas and criticisms helped me to improve my ability to conduct thorough research.

The Department of Bioengineering has given unrelenting support. I especially thank Dr. Harvey Borovetz and Dr. Sanjeev Shroff for their dedication to the institution and their continuing support of my endeavors. The administrative staffs were invaluable friends and colleagues who keep the gears turning: Jocelyn Runyon, Eve Simpson, Allyson LaCovey, Rachel Thomas, Allie Giel, Nicholas Mance, Glenn Peterson, Linda Askren, Courtney Euker, and Alison Hall.

I would not have had a chance ever to develop the skills necessary to pursue my doctorate without first having the opportunity to participate in undergraduate research. Dr. Athanasios Makalaris fostered my passion for biomedical engineering by accepting me into his biological systems engineering laboratory at Imperial College London in 2007. He gave me the freedom to make key decisions, allowed me to roam in and out of lab at odd hours, and never discouraged

my ideas, no matter how naïve they were. Thank you to Dr. Badylak for accepted me into his lab for a summer internship in 2008, and to Tiffany Sellaro for her mentorship while I first learning about liver tissue engineering. It was during this time that my passion for whole organ engineering of the liver was born. Thank you to Larry Robinson for his guidance and mentorship as well as everyone else at Proctor and Gamble during my time there. Thanks to Dr. Karen Christman for graciously accepting me into her lab at the University of California San Diego. Finally, thank you to Dr. Michael Helmrath and his staff at Cincinnati Children's Hospital for all of their guidance and support.

I am also thankful to my fellow colleagues for assisting me in developing the skill sets necessary for the performance of experiments that were key to this endeavor. I look forward to their continued friendship and to additional intellectual discussions. I and truly thankful to Lisa Carey for her friendship as we started in the Badylak Lab at the same time, took classes and trained to be clinical engineers together. A special thanks to Dr. Ricardo Londono for conducting all of my animal surgeries and to Brian Sicari for bestowing wisdom upon me and inspiring me to reach my full potential. Dr. Christopher Carruthers, Dr. Matthew Wolf, Dr. Christopher Medberry, Jenna Dziki, Catalina Pineda Molina, Lindsey Saldin, and Timothy Keane were an incredibly herd of graduate students. They were critical to my development as a researcher and I thank them all for their assistance and friendship over the years. Harleigh Warner, Justin Wildemann, Sophie Hollands, Prishanti Patel, Yolandi van der Merwe, and Abigail Loneker were excellent undergraduate researchers who contributed immensely to the completion of this work.

I am thankful for the patience and mentoring of the post-docs, staff scientists and laboratory managers: Dr. Li Zhang, Janet Reing, Scott Johnson, Dr. Christopher Dearth, Dr. Jeremy Kelly, Dr. George Hussey, Dr. Michelle Scarllet, Dr. Lisa White, Dr. Kristen Jones, Dr. Ale Costa, Dr. Luai Huleihel, Ilea Swinehart, Deanna Rhoads, Lori Walton, and Dr. Neil Turner. The assistance of Dr. Donna Stolz and Jonathan Franks from the Center for Biologic Imaging at the University of Pittsburgh was critical to successful acquisition and analysis of data from both two-photon microscopy and scanning electron microscopy. The support of my colleagues at the UPMC artificial heart program strengthened my clinical perspective of cardiovascular disease and treatment: Dr. Richard Schaub, Douglas Lohmann, Donald Severyn, Erin Driggers, and Michael McCall.

The National Institute of Health (F31 Predoctoral Fellowship), the National Science Foundation (Graduate Research Fellowship Program), the McGowan Institute of Regenerative Medicine, and the ARCS foundation provided the funding necessary for the completion of this work. For this assistance I shall always be thankful.

Without family and friends such work would be without purpose. To my mother and father: Thank you for believing in me and instilling in me a sense of purpose. You supported my development without boundaries, and were always there for me. I would also like to thank Monica Faulk, Mary Beth Spore, Joe Spore, Alex Spore, Sarah Reif, Molly DiMatteo, Anthony Dimatteo, Emily Lowder, and the rest of my friends and family for always providing a good laugh and perspective.

Finally, to my wife, Bridget, and to my son, Michael: I am forever grateful for your love and support no matter the hour, dedication, and sacrifice. You have both encouraged me to always remain positive, to laugh, and to enjoy life. Your support has been essential to my success. I dedicate this body of work to you.

1.0 BIOLOGIC SCAFFOLDS FOR TISSUE ENGINEERING AND REGENERATIVE MEDICINE APPLICATIONS

1.1 ABSTRACT

This chapter reviews the use of naturally occurring biomaterials for tissue repair and regeneration and the effects of tissue source and processing methods for these materials upon the host response. The pros and cons of naturally biologic scaffolds are discussed. Methods for preparation of biologic scaffolds are shown to have a critical effect upon functionality of the device. The mechanisms by which biologic scaffolds composed of extracellular matrix (ECM) can alter the default wound healing response from the well described pro-inflammatory and scarring events toward a more constructive remodeling response, i.e., the site appropriate formation of functional tissue, are discussed in detail. The information discussed in this chapter is the foundation and justification for using naturally derived biologic scaffolds for engineering functional hepatic tissue.

1.2 INTRODUCTION

1.2.1 Naturally Occurring Biomaterials

Naturally occurring biomaterials are commonly used as surgical mesh devices for a number of clinical applications and are increasingly recognized in regenerative medicine for their inductive properties in tissue and organ engineering. Ventral hernia repair is one of the most frequent clinical applications of ECM scaffolds. Most surgical mesh devices used for ventral hernia repair are composed of synthetic materials with robust mechanical strength, and are

typically incorporated quickly into the host tissue [1-5]. While these mesh materials provide more than enough strength to prevent hernia recurrence, such devices are associated with non-trivial complications including adhesion, infection, fistula formation, and contraction [6-8]. Additionally, the innate immune response to the synthetic materials is classically a chronic pro-inflammatory foreign body reaction that promotes fibrotic encapsulation. This fibrotic encapsulation is associated with long-term patient discomfort, which can lead to revision surgery and surgical mesh removal [9]. The intensity of the inflammatory response to an implanted mesh may be linked to the degree of tissue ingrowth and scar formation, and modulation of this response can have marked downstream effects [10]. Surgical mesh materials composed of naturally occurring allogeneic or xenogeneic extracellular matrix (ECM) have been used as an alternative to synthetic materials to abrogate the foreign body response, prevent infection, and minimize or avoid excessive fibrosis [11-14]. In these circumstances, facilitating a constructive host remodeling response is an advantage to the dense scar tissue deposition in the response to synthetic mesh materials [15]. This logic has also justified the use of ECM scaffolds in applications such as breast reconstruction, where constructive remodeling is preferred to dense scar tissue.

Naturally derived ECM is a material consisting of the secreted structural and functional components of resident cells. The specific composition and ultrastructure of ECM will vary depending on the source tissue. The composition of ECM scaffolds includes a complex mixture of molecules arranged in unique three-dimensional (3-D) patterns that are ideally suited to the tissue from which the ECM is harvested. The ECM provides signals which cue cell migration, proliferation, and differentiation[16-22]. Maintaining the native ultrastructure and composition of the ECM during the tissue/organ decellularization process is essential for optimal outcomes

with biologic scaffolds[23-27]. ECM scaffold materials are derived from a variety of tissues and organs including blood vessels [28-30], ligaments[31] heart valves[32-38], skin [39], nerves[40, 41], skeletal muscle, tendons[42, 43], small intestinal submucosa (SIS)[44-46], heart[47, 48], urinary bladder[49-51] and liver [52]. Although a number of studies have been conducted with many different ECM materials, the most comprehensive studies regarding structure-function relationships have been reported for urinary bladder matrix (UBM) and SIS. ECM scaffold materials are biodegradable unless processed with crosslinking agents, and their degradation products have been shown to be important bioactive contributors to the constructive remodeling process [53, 54]. Furthermore, incomplete removal of cellular material from the source tissue results in an undesirable host remodeling response [55]. A more detailed discussion of the mechanisms by which naturally occurring biologic materials support constructive remodeling can be found later in this chapter, in section 1.5.

Table 1. Examples of clinical products composed of decellularized tissues.

Product	Tissue Source	Application	Manufacturer
Alloderm®	Human dermis	Soft tissue	Lifecell Corp.
AlloMax™	Human dermis	Soft tissue	Bard Davol
Allopatch HD™	Human dermis	Tendon, breast	Musculoskeletal Transplant Foundation
GraftJacket®	Human dermis	Soft tissue	KCI
Strattice™	Porcine dermis	Soft tissue	Lifecell Corp.
Permacol™	Porcine dermis	Soft tissue	Tissue Science Laboratories
TissueMend®	Bovine dermis	Soft tissue	Stryker Corp.
Veritas®	Bovine dermis	Soft tissue	Synovis Surgical
Suspend™	Human fascia lata	Pelvic organ prolapse	Coloplast
Freestyle®	Porcine heart valve	Valve replacement	Medtronic Inc.
Prima Plus	Porcine heart valve	Valve replacement	Edwards Lifesciences Inc.
OrthAdapt®	Equine pericardium	Soft tissue	Synovis Orthopedic and Woundcare Inc.
Lyoplant®	Bovine pericardium	Dura mater	B. Braun Melsungen AG
Surgisis®	Porcine small intestine	Soft tissue	Cook Biotech Inc.
CuffPatch™	Porcine small intestine	Rotator cuff	Athrotek
Restore®	Porcine small intestine	Soft tissue	DePuy Orthopaedics
CorMatrix ECM®	Porcine small intestine	Pericardium, cardiac	CorMatrix® Cardiovascular Inc.
MatriStem®	Porcine urinary bladder	Soft tissue	Acell Inc.

1.2.2 Synthetic Biomaterials

New generations of synthetic biomaterials which attempt to mimic the native extracellular matrix are being developed at a rapid pace for use as three-dimensional scaffolds. Poly(glycolic acid) (PGA), poly(lactic acid) (PLA), and the copolymer PLGA have been extensively used as synthetic 3D scaffold biomaterials. Biomimetic synthetic polymers have been created to elicit

specific cellular functions and to direct cell-cell interactions. The use of synthetic materials for regenerative medicine applications can be effective, but there are inherent limitations to the use of synthetic materials. Of note, synthetic or chemically crosslinked biologic materials, invariably elicit a foreign body response.

Generally, the presence of an absorbable component as part or the entirety of a synthetic device or a natural device results in a less severe foreign body response than a nondegradable device. The effective ability of the host to effectively degrade and remodel an implanted biomaterial facilitates the integration of the implanted device with surrounding tissue and minimizes the formation of dense capsule formation.

1.2.3 Utilizing Nature's Engineered Scaffold Material

Individual ECM components or combinations of specific ECM components have been used as substrates for in vitro cell culture systems for several decades. Although cell culture substrates composed of proteins such as collagen type I, laminin, and fibronectin have facilitated cell attachment, proliferation, and differentiation, these systems are far from physiologically relevant. The lack of an intact ECM structure negatively affects cell–cell interaction, cell–ECM interaction, physical–chemical influences, and the effects mechanical stimuli upon the cultured cells. As a result, the cells in culture eventually lose their functional cell phenotype and initiate a de-differentiation process. Studies have shown that intact ECM provides a more favorable substrate than the use of individual components of ECM for the growth and differentiation of various cell types. Squamous epithelial, fibroblastic (Swiss 3T3), glandular epithelial (adenocarcinoma), and smooth muscle-like (urinary bladder) cells cultured on SIS-ECM

maintained superior expression of tissue-specific phenotype than those same cells cultured on plastic, Vitrogen, or Matrigel. In a study that used human islet cells, SIS enhanced the insulin producing function of the cells in-vitro better than islets cultured on standard islet substrates[56-58]. Lin et al. compared hepatocytes cultured on L-ECM to the well-characterized hepatocyte culture models, double-gel (sandwich) cultures, and adsorbed collagen monolayers. Hepatocytes survived up to 45 days on L-ECM, and several liver-specific functions, such as albumin synthesis, urea production, and P- 450 IA1 activity, were significantly greater than the growth and metabolism of cells cultured on collagen[59].

In summary, there is an increasing body of evidence that tissue specific signals are present within the ECM from each tissue and organ. This property may be important in selected regenerative medicine strategies.

1.3 ECM COMPOSITION AND TISSUE-SPECIFIC ULTRASTRUCTURE

The ECM provides a physical substratum for the attachment and spatial organization of cells[60]. Well-known biophysical properties such as ECM composition and 3-dimensional surface topography play an important role in cell phenotype and behavior[61-65]. The 3-dimensional surface topography of ECM derived from different tissues includes variation in pore diameter, distance between the pores[66], surface texture[64, 67], hydrophobicity, hydrophilicity, and the presence or absence of a basement membrane. In addition to surface topography, the spatial presentation of the surface proteins contacting the cells can alter cell attachment, migration, proliferation, and differentiation (**Figure 1**).

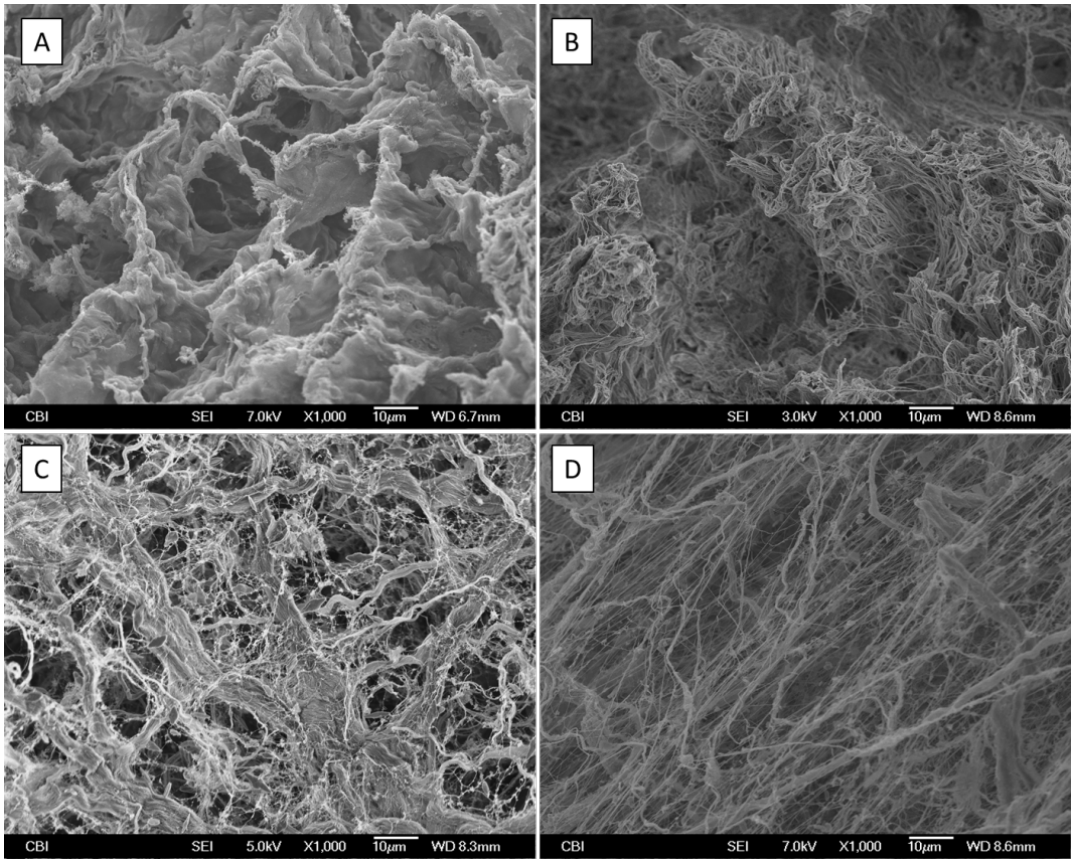

FIGURE 1. SEM images of naturally occurring ECM scaffold derived from (A) adrenal, (B) dermal, (C) liver, and (D) and pancreas tissues. These images demonstrate a distinct, tissue specific architecture.

Studies have suggested that tissue- and organ-specific ECM can promote site-appropriate differentiation of progenitor cells[68, 69] and maintain site-appropriate phenotype in *in vitro* culture systems[70]. Since the ECM of each tissue and organ is produced by the resident cells and logically represents the ideal scaffold or substrate for these cells, it is intuitive that a substrate composed of a tissue specific ECM would be favorable for that tissue's cells. It has been shown that biologic ECM scaffolds support tissue-specific cell phenotype. Hepatic sinusoidal endothelial cells maintained their differentiated phenotype longer when cultured on

ECM derived from the liver compared to sinusoidal endothelial cells cultured on ECM derived from small intestine or urinary bladder[70]. These results suggest that ECM biologic scaffolds provide a set of unique, tissue-specific signals that are dependent upon the tissue from which an ECM is derived. Lin et al. compared rat hepatocytes cultured on porcine liver ECM biologic scaffolds to well-characterized hepatocyte culture models (type-I collagen sandwich configuration or a single layer of type-I collagen)[59]. Hepatocytes survived up to 45 days on a sheet form of porcine liver ECM and several liver-specific functions such as albumin synthesis, urea production, and P-450 IA1 activity were markedly enhanced compared with the growth and metabolism of cells cultured on a single layer of type-I collagen.

Zeisberg *et al*. isolated liver-derived basement membrane matrix from human or bovine liver, and used the substrate for culture of human hepatocytes[71]. Human hepatocytes adhered more efficiently to liver-derived basement membrane matrix and expressed lower levels of vimentin and cytokeratin-18, which are markers of hepatocyte dedifferentiation, compared with hepatocytes cultured on Matrigel or type-I collagen. However, maintenance of liver-specific functions *in vitro* was not reported[71].

Biologic scaffolds composed of ECM provide a more physiologically relevant culture substrate compared to reconstituted ECM proteins and have unique biochemical profiles that are dependent upon the tissue from which an ECM scaffold is derived. Minimally processed ECM scaffolds and gels, such as PLECM, provide a combination of ECM proteins derived from the liver that are in physiologically relevant amounts (e.g. Type-I, IV, VI, III, XI, XIX, heparin sulfate proteoglycan, ECM-bound growth factors, laminin, biglycan, tenascin, fibronectin)[67, 72, 73].

1.4 ROLE OF ECM IN ORGAN DEVELOPMENT

ECM represents the secreted products of the resident cells of each tissue and organ and is in a state of dynamic reciprocity with its surrounding microenvironment [74]. The structure and functional molecules of the ECM provide cues that affect cell migration and cell proliferation [16, 54, 75], cell differentiation [72, 76-79], and modulate the host innate immune response [53, 80-82]. The creation of an ECM biologic scaffold involves decellularization of a source tissue or organ with the ultimate goal of preservation of the native ECM ultrastructure and composition. Reviews of tissue decellularization techniques and their effect upon ECM properties are available [83, 84]. When properly processed to remove cellular antigens that may cause an adverse host immune response while maintaining as much as possible of the native architecture and biologically active molecules, ECM scaffolds can promote the formation of site-appropriate tissue, constructive remodeling [85] after injury. It is likely that the three-dimensional ultrastructure, surface topology, surface ligand landscape, and composition of the ECM all contribute to these constructive effects. These characteristics of ECM make it the ideal biological scaffold to promote constructive and functional remodeling of tissues and organs.

While it is beyond the scope of this chapter to detail all of the components of the extracellular matrix it is important to note that many of the main components, specifically several forms of collagen, are evolutionarily highly conserved across all metazoans [86] [87]. The matrix consists of a complex mixture of proteins, glycans and molecules that, while diverse in form and function, play very important roles in embryonic development by influencing cell

behavior and differentiation. As tissue matures the ECM assumes roles to maintain cell and organ function, to serve as a communication network between cells, and to provide the role of structural support for the organs.

The embryonic role of ECM begins immediately fertilization and attachment to the uterine wall [88-90]. As matrix is synthesized and secreted during the blastula and gastrula stages [91], molecules such as laminin become determinant in the separation of germ layers. The importance of ECM in development has been recognized for well over 20 years [92, 93] and has been the subject of several recent reviews [94-98]. Early stages of development rely upon the ECM to guide cellular proliferation and migration. Basement membranes, a form of ECM, are responsible for endodermal cell migration of the developing blastocyst [99]. ECM-cell interactions have been shown to be responsible for epithelium to mesenchymal transformation [100] interactions [101] and mesenchymal cell spreading [102] throughout the embryo.

Individual ECM components have been extensively investigated as to specific roles in development. For example, an ECM molecule specific to the developing sea urchin, and only expressed during development, is thought to be critically important for gastrulation [103]. Fibronectin is required for mesoblast cell migration and the emigration of primitive streak cells [104]. Tenascin has been speculated to be involved in forming initial barriers between epithelium and mesenchyme [105].

Following initial germ layer formation and early cell fate determination, ECM becomes involved in both morphogenesis and organogenesis of the developing embryo. Morphogenesis refers to the general shaping of the embryo or parts thereof. ECM proteins are responsible for basic axis patterning of the developing embryo [106], paraxial mesoderm to epithelial transformation in the chick [107] and somite formation [108, 109]. The morphogenesis of

branching structures involves the degradation and deposition of ECM in a highly dynamic but repeated pattern of bifurcation [110] also seen in glomeruli formation in the developing kidney [111].

Hyaluronic acid (HA) has been shown to be crucial for basic patterning of the digits and proper skeletal elongation [112, 113]. Early muscle morphogenesis, myoblast and myotube alignment, is driven by fibronectin deposited by neighboring connective tissue [114]. Collagens and non-collagenous glycoproteins are required for neuronal cell migration and early brain morphogenesis [115].

As development continues, organogenesis, the formation of the internal organs, begins as tissue differentiates and specializes. Changes in temporal and spatial arrangement of ECM drive cellular architecture of the developing organs, as seen in the developing brain [116] and heart [117].

ECM components, specifically HA, are responsible for initiating chondrogenesis and the maturation of those chondrocytes. The changes in the ECM brought about by the chondrocytes leads to full maturation of cartilage and formation of synovial joints, a process that may continue with osteoblasts during osteogenesis [113, 118].

Hemonectin expression during development matches the changing pattern of hematological development, moving from the yolk sac to the liver and spleen and eventually to the bone marrow of the developing mouse. While hemonectin is not exclusively expressed in these developing blood locations the patterning of this extracellular matrix molecule appears crucial to granulocyte production [119].

In summary, while the ECM was originally thought to mainly function as structural support for the cells [120], it is now clear that dynamically reciprocal communication between

cells and ECM allows for continual modification of the microenvironment that is associated with the physical structure of the ECM [121]. However there is ample evidence to show that the physical properties of ECM, such as stiffness, drive some of the morphogenesis of the developing embryo. The complex twisting the embryo undergoes during development, specifically gastrulation, is highly dependent on the mechanical properties of the ECM present [122]. One of the major structural difficulties observed during development is that neighboring organs may develop and grow at different rates. The ECM must be structurally deposited and/or remodeled in ways that allow for this differential growth otherwise defects may occur [123].

This structural and signaling role is also seen in blastemal limb regeneration as developmental recapitulation occurs. It has been shown that the regenerating blastemal ECM takes on instructive roles that cause muscle cells to dedifferentiate, migrate and possibly proliferate. Temporal changes due to cell-ECM interactions then drive undifferentiated cells down required lineages [124]. The blastemal tissue has also been shown to be less stiff than the residual muscle in the remaining stump and this physical difference may play a role in cellular migration and behavior [125].

ECM constituents have also been extensively studied in the context of stem cell biology, though content is outside the scope of this chapter. However it has clearly been shown that ECMs can be used to maintain stem and progenitor cell potency but are also crucial for determining stem cell lineage fate [126, 127].

Understanding the embryonic genesis and patterning of the ECM and how it influences and is influenced by cells is important for regenerative medicine strategies that attempt to recapitulate these processes. This concept has been reviewed by Caplan (2003) in the context of skeletal defects but can be used to form more general guidelines for the entire field.

1.5 PRODUCTION OF NATURALLY OCCURRING BIOMATERIALS FROM DECELLULARIZED TISSUES

Decellularization of anatomically distinct tissues to produce an ECM bioscaffold has been reported for hollow organs such as small intestinal, urinary bladder[128, 129], and dermis[130] as well as solid organs such as liver[131] and heart[132]. The use of these bioscaffolds to support tissue reconstruction varies, from bridging repairs to structural replacement (i.e. heart valves[133, 134]). There have been several comprehensive reviews of commonly used decellularization methods, which will be briefly discussed below[84, 129, 135].

While the specific methods used to decellularize the tissue can vary greatly, the physical form of the resulting extracellular matrix (ECM) can vary greatly. Hollow organs such as the urinary bladder or small intestine are typically incised and split opened, thus forming a sheet-like structure. The sheet form can be air dried or lyophilized and further processed into a comminuted powdered form. The sheet form is typically very thin; therefore, multiple sheets can be laminated together by vacuum pressing to increase strength of the resulting multilayer construct. Lamination can also be used to create more complex 3-D shapes such as tubes by molding the sheets around a mandrel. Lamination however is limited by the nature of the starting sheets and by casting requirements of particular shapes.

The sheet form of ECM has many advantages, not the least of which is that it is usually rapidly produced, often requiring only a couple of processing steps and easily scaled for mass production. The sheet or laminate sheet form lends itself well to patch, bridging or soft tissue

reinforcement applications for which robust strength is usually required. The comminuted form in contrast, is well suited for filling of volumetric injuries and can be applied by minimally invasive methods such as injection.

The maintenance of 3-dimensional organ morphology has recently emerged as a method for organ engineering[136]. Organs such as the heart, liver, kidney, and lung are decellularized by using the native vasculature to deliver decellularizing agents. This method leaves the organ as semi-transparent in appearance while retaining the shape of the native organ with intact vasculature. The benefit of this method is the ability to subsequently connect the vasculature of the decellularized organ to the recipient circulatory system. Re-endothelialization of the 3-D ECM construct is necessary to prevent thrombosis.

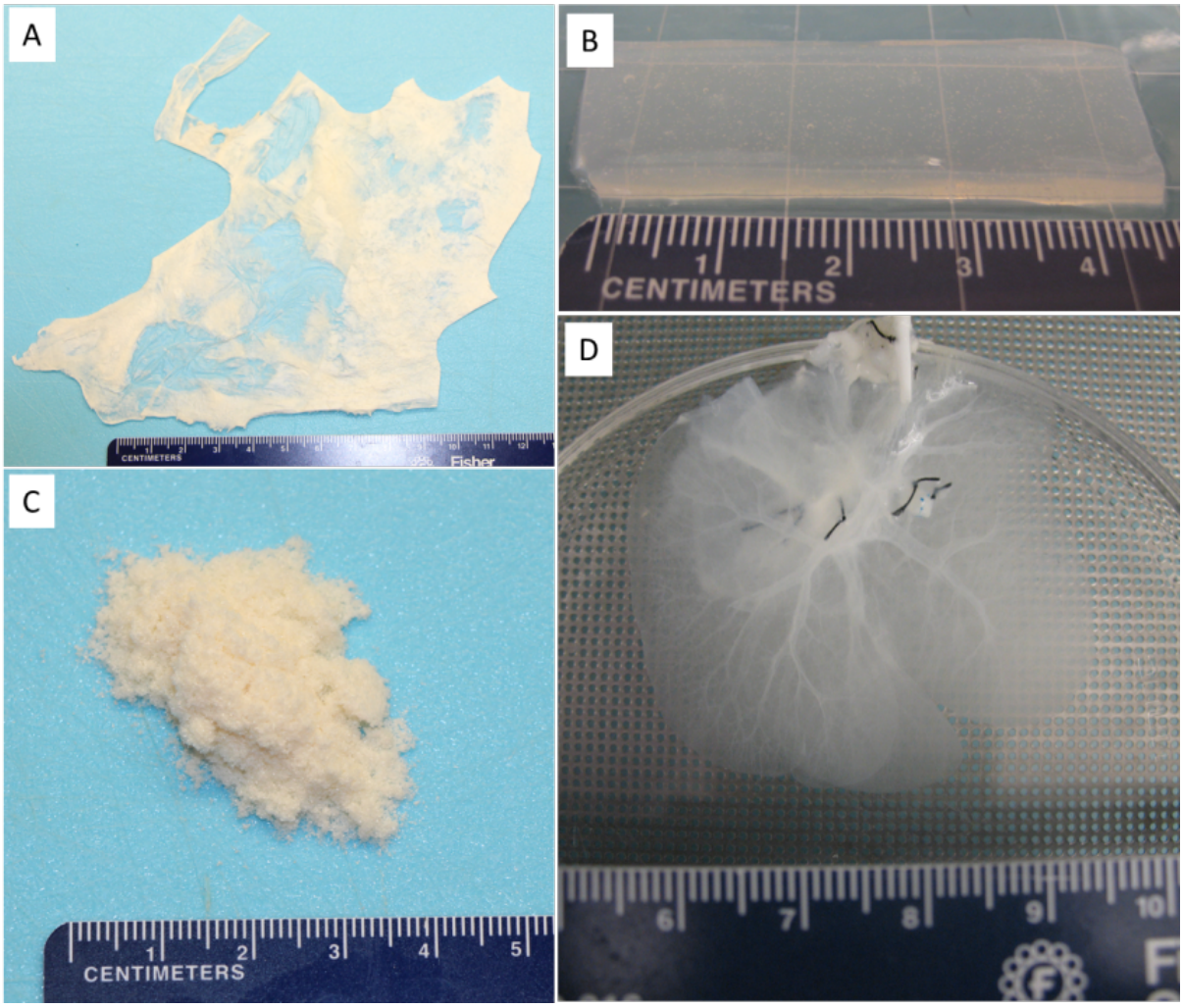

FIGURE 2. Naturally occurring scaffolds processed in various formats: (A) sheet, (B) hydrogel, (C) powder, and (D) 3D whole organ.

1.5.1 Techniques Used to Decellularize Tissue

The most effective agents for decellularization of each tissue and organ will depend upon many factors, including the tissue's cellularity (e.g. liver vs. tendon), density (e.g. dermis vs. adipose tissue), lipid content (e.g. brain vs. urinary bladder), and thickness (e.g. dermis vs. pericardium).

It should be understood that all cell removal agents and methods will disrupt ECM composition and ultrastructure. Minimization of these undesirable effects rather than complete avoidance is the objective of optimal decellularization.

The optimal recipe of of decellularization agents is dependent upon tissue characteristics such as thickness and density, the agents being used, and the intended clinical application of the decellularized tissue. Prior to applying decellularization agents, undesirable excess tissue may be removed to simplify the cell removal process. Cell removal may focus on retention of key ECM components such as the basement membrane. Mechanical or physical methods may be used to facilitate decellularization. For thin tissue structures such as urinary bladder, intestine, pericardium, and amnion, the most commonly used decellularization techniques include freezing and thawing, mechanical removal of undesirable layers such as muscle or submucosa, and relatively brief exposure to easily-removed detergents or acids followed by rinsing. Thicker tissue structures such as dermis may require more extensive biochemical exposure and longer rinse times. Fatty, amorphous organs and tissues such as adipose tissue, brain, and pancreas often require the addition of lipid solvents such as alcohols. The complexity and length of the decellularization protocol is usually proportional to the degree of geometric and biologic conservation desired for the post-processed tissue (e.g. macrostructure, ultrastructure, matrix and basement membrane proteins, growth factors, etc.), especially for composite tissues and whole organs.

Regardless of the decellularization method chosen, minimizing the disruption of matrix molecules is of paramount importance. The method used to decellularize the tissue can be broadly divided into physical, enzymatic or chemical techniques with many protocols mixing various methods and agents to optimize decellularization while maintaining native structure and

composition. Physical methods typically involve separation of the epithelial and muscular layer of an organ from the adjacent submucosal layers but can also include freezing or osmotic shock with hyper- and/or hypotonic solutions.

While there are many potential enzymatic methods of disrupting cells, trypsin is one of the most commonly used and effective enzymes. Trypsin cleaves peptide chains mainly at the carboxyl side of the amino acids lysine or arginine, except when either is followed by proline. This results in cellular detachment from the matrix and cell lysis. One of the disadvantages of using enzymes is the destruction of matrix proteins, especially with prolonged exposure which can also disrupt the native matrix architecture. Following enzymatic treatment the tissue must be thoroughly rinsed to remove or inactivate any remnant enzyme and to remove cellular material. Enzymes are often used in conjunction with other methods in a step-wise process to facilitate dislodgement of the cells while follow-up methods target the remaining, often damaged, cells.

Chemical methods of decellularization are varied in nature and mechanism of action. Detergents, changes of pH, and solvents or chelators can all be effectively used to decellularize tissue. Detergents comprise some of the most commonly used chemicals for decellularization, including sodium dodecyl sulfate (SDS), deoxycholate and Triton X-100. SDS and deoxycholate are ionic detergents that solubilize cellular membranes but also disrupt protein-protein interactions that may damage the ECM ulstrastructure and protein integrity. Triton X-100 is a non-ionic detergent that disrupts lipid interactions while leaving protein interactions intact. Zwitterionic detergents, such as CHAPS, mix properties of both ionic and non-ionic detergents but are less commonly used.

Placing tissues in acidic or alkaline solutions can effectively disrupt cells but can also irreversibly damage ECM proteins. Peracetic acid (PAA) is a relatively weak acid that has been

widely used as a decellularizing agent and a disinfectant, especially with ECMs such as small intestinal submucosa (SIS) and urinary bladder matrix (UBM), which have a thin cross-sectional area.

Following cell lysis, the membranes and cytoplasmic debris must be removed from the matrix, which is usually accomplished by aggressive rinsing in sterile water. This washing procedure also serves to remove any remnant detergents or enzymes from the decellularization process. The use of iso-, hyper- or hypotonic washing solutions can facilitate additional cell lysis as a physical method of decellularization as described above.

1.5.2 Criteria for Decellularization

Following decellularization the tissue usually assumes a pale or translucent quality. However, macroscopic appearance alone is insufficient to determine the extent of decellularization. While there is no universal consensus for criteria for adequate decellularization, standard metrics are beginning to emerge. It has been proposed that three relatively stringent criteria must be met to establish sufficient decellularization: 1) tissue must have less than 50ng of dsDNA per mg of dry weight, 2) DNA fragments less than 200 bp in length and 3) no visible nuclear material in histologic analysis with DAPI or H&E[84, 137, 138].

Failure to completely decellularize a tissue leads to negative outcomes upon in-vivo implantation, including a pro-inflammatory response with recruitment of M1 macrophages and subsequent fibrosis[139]. Such a reaction is likely caused in part by damage associated molecular pattern (DAMP) molecules and can lead to seroma formation, sterile abscess formation, and chronic inflammation[140].

1.5.3 Chemical Crosslinking and Sterilization

Following decellularization, further processing of the ECM can include dehydration, lyophilization, and/or comminution. Once comminuted, the powder can be enzymatically solubilized (e.g., pepsin) to produce a liquid form that can be subsequently induced to gel[130, 141-144]. This soluble form allows for minimally invasive applications such as needle or catheter based injections[143]. The viscosity of the soluble ECM can be adjusted so that it can be induced to conform to the contours of native tissue or irregularly shaped tissue defects. Although solubilization of an ECM scaffold obviously destroys the 3-dimensional architecture, entrapped growth factors and newly created bioactive cryptic peptides may be released.

Terminal sterilization of an ECM bioscaffold is required prior to in-vivo implantation. Gamma irradiation, e-beam, glutaraldehyde , ethylene oxide and peracetic acid have all been used as methods of sterilization and have been extensively evaluated for their effect on bioscaffold mechanical and biological integrity. In addition to sterilization, glutaraldehyde effectively crosslinks ECM proteins. Other chemical agents, such as carbodiimide and genipin, are also crosslinking agents prior to sterilization. Chemical crosslinking of ECM proteins (e.g. collagen) stabilizes and strengthens the ECM structure and severely inhibits in-vivo degradation. Chemically crosslinked and non-degradable ECM elicits a foreign body response very similar to non-degradable synthetic polymer scaffolds (e.g., polypropylene).

1.5.4 Source Material of ECM

Surgical mesh materials composed of ECM are harvested from a variety of allogeneic or xenogeneic tissue sources, including dermis, urinary bladder, small intestine, mesothelium,

pericardium, and heart valves, and from several different species. Although there have been no reported differences in the host remodeling response as a function of species source, there are clear differences with respect to age[145], anatomic location of the source tissue, and other factors[138]. The potential for disease transmission to humans is much less for a xenogeneic ECM compared to allogeneic (human) ECMs. Although a certain amount of biologic variability is unavoidable with naturally occurring biomaterials, such variability can be minimized by controlling for factors such as age, weight, breed, and diet of the source animals.

1.6 MECHANISMS BY WHICH BIOMATERIALS SUPPORT CONSTRUCTIVE REMODELING

ECM scaffolds can change the default wound healing response from the well described pro-inflammatory and scarring events toward a more constructive remodeling response[146]. Site appropriate formation of functional tissue has been shown for a variety of anatomic locations including dermis[147], esophagus[148], skeletal muscle[149-151], and heart[143, 152-156], temporomandibular joint meniscus, among others. There currently exists strong evidence for three mechanisms by which biomaterials support constructive remodeling: (1) contribution from bioactive cryptic peptides released during the process of in-vivo ECM degradation[157, 158], (2) recruitment of endogenous stem and progenitor cells to the site of ECM remodeling[157, 158] and (3) modulation of the host immune response toward an M2-Th2 phenotype[53, 140, 159, 160].

1.6.1 Cryptic Peptides and Bioactive Molecules

The host response to an ECM that is not chemically crosslinked is distinctly different from the response to synthetic scaffold materials and from the response to either purified components of ECM such as collagen I or chemically crosslinked forms of ECM. The purified components elicit a specific response to the particular molecule: for example, angiogenesis in response to VEGF or bone formation in response to BMP. The specific response may be desirable for particular medical/surgical needs but typically lacks the complex constructive wound healing response observed when the intact ECM is used as a reparative scaffold. It has been shown that MMPs can cause release of matricryptic peptides from ECM, such as endostatin[161], restin[162], and arrestin[163]. Macrophages can release matricryptic angiostatic factors from ECM[164]. Degradation and remodeling of the ECM by heparanases can release bioactive matricryptic peptides[165, 166].

ECM scaffolds in preclinical studies have been shown to result in constructive tissue remodeling, promote angiogenesis, and to resist deliberate bacterial infection[146, 167]. In vitro studies have shown that degradation of ECM generates low molecular weight peptides with biological properties such as chemotaxis, angiogenesis, and antimicrobial activity[168, 169]. In contrast, intact ECM does not possess such activity[170], suggesting that these biological activities are associated with and dependent upon the products of ECM degradation, rather than molecules present in intact ECM. Low molecular weight peptides isolated from acid-hydrolyzed small intestinal submucosa (SIS-ECM) have been shown to possess chemotactic activity for primary murine adult liver, heart, and kidney endothelial cells and to promote vascularization in vivo in Matrigel plug assays[171]. A recent study has shown that in vivo degradation of urinary

bladder-derived ECM can produce bioactive matricryptic peptides that cause chemotaxis of multi-potential progenitor cells[172]. Previous studies have also shown that subcutaneous implantation of porcine SIS-ECM induces migration of bone marrow-derived cells to the site of constructive remodeling[173], and that this phenomenon is associated with complete degradation of the ECM scaffold.

The concept of functional matricryptic peptides is not new. During ECM degradation, many large insoluble molecules present within the matrix are reduced to fragments which possess biological activities that are not possessed by the parent molecules. In addition to proteolysis-generated bioactive fragments, functional sites of the parent molecules that are hidden and inactive within the ECM can also become active due to conformational changes[174]. Some of the ECM molecules that have been shown to possess this property are collagen[162, 175, 176], fibronectin[177], laminin[178-180], and hyaluronan[181], all of which are present in ECM scaffold materials[146].

1.6.2 Recruitment of Progenitor Cells to the Site of Injury

The second mechanism of site-specific ECM scaffold remodeling involves the recruitment of multipotent or lineage-directed progenitor cells by scaffold degradation products. Both the age and species of the tissue from which the ECM is harvested have an effect upon this chemoattractant potential. Transitional ECM instructs cell behavior in both the blastema and in mammalian skeletal muscle regeneration. Especially tenascin-C, hyaluronic acid and fibronectin[182].

Studies have shown degradation products of human fetal skin-derived ECM possess stronger chemoattractant activity for skin-specific lineage-directed stem and progenitor cells than do degradation products of human adult skin-derived ECM. In addition, degradation products of porcine adult skin-derived ECM showed stronger chemoattractant activity than degradation products of human adult skin-derived ECM. These results suggest that ECM degradation products from younger tissue sources may have more potent chemoattractant activity for local tissue stem or progenitor cells than older tissue sources, and that the species of the tissue source also has an effect on chemoattractant activity.

The early gestation human fetus (less than 24 weeks gestation), unlike the later-gestation fetus or adult, is able to heal incisional skin wounds without scarring[183]. This scarless wound healing ability of fetal skin may be due to the fetal cells and/or the fetal ECM. Fetal platelets, inflammatory cells, and fibroblasts all demonstrate differences from their adult counterparts that may contribute to the scarless wound healing phenomenon. Fetal ECM contains a higher proportion of type III collagen and a greater concentration of hyaluronic acid than ECM of adult skin. Unwounded fetal skin at gestational ages associated with scarless wound healing has also been shown to express low levels of TGFβ1, high levels of TGFβ3, and increased expression of matrix metalloproteinases, a family of proteases associated with ECM degradation and remodeling[184]. Although studies have not addressed the relative contribution of cells vs. ECM to scarless fetal wound healing, it appears clear that the ECM, which represents the secreted product of local cells, contains signaling molecules that can affect stem and progenitor cell activity.

The results of a previous study show that degradation products of ECM possess chemoattractant activity for local tissue progenitor and stem cells, and that this chemoattractant

activity may decline as a function of the age of the tissue from which the ECM is harvested[185], and that ECM may vary between different species. These findings add a new perspective to the role of ECM in wound healing and the differences between fetal and adult wound healing. Though fetal ECM is not a likely candidate for tissue engineering/regenerative medicine applications because of the scarce availability of the raw material, these findings could be applied to the development of methods to induce migration of lineage-directed progenitor cells to tissue sites in need of repair, thereby facilitating a regenerative tissue response rather than default scar tissue formation.

1.6.3 Modulation of the Host Immune Response – Push Towards an M2 Constructive Remodeling Macrophage Phenotypes

The exact mechanisms by which certain biologic mesh materials are capable of modulating the host macrophage population towards a more constructive remodeling phenotype are not fully understood. However, it has been shown that the presence of large amounts of cellular remnant material as a result of ineffective tissue decellularization and chemical cross-linking have detrimental effects upon the host remodeling response[53, 147, 186]. This response is not surprising in the case of xenogeneic cellular components, such as the α-Gal epitope, which may be recognized by the host immune system and elicit an immune response following implantation. Other molecules, including those associated with cell death, are also known to have potent immunomodulatory effects. These cell-death-associated molecules, collectively termed damage-associated molecular pattern molecules (DAMPs), are recognized by pattern recognition receptors on cells of the innate immune system. Therefore, large amounts of these molecules

within biologic materials that derive from mammalian tissues as a result of inefficient removal during processing or due to cellular death upon implantation may have detrimental effects upon the ability of ECM scaffold materials to promote constructive tissue remodeling.

Macrophages are a heterogeneous subset of the mononuclear cell population involved in the host response to implanted materials. Macrophages are activated in response to tissue damage or infection, causing an increase in the production of cytokines, chemokines, and other inflammatory molecules to which they are exposed. Recently, macrophage phenotype has been characterized based on distinct functional properties, surface markers, and the cytokine profile of the microenvironment. Polarized macrophages are referred to as either M1 or M2 cells, mimicking the Th1/Th2 nomenclature.

Macrophages are a plastic cell population capable of sequentially changing their polarization in response to local stimuli during the process of wound healing. The macrophages participating in the host response to an implanted material are exposed to multiple stimuli including cytokines and effector molecules secreted by cells including other macrophages that are participating in the host response, microbial agents, epitopes associated with the implanted biomaterial, and the degradation products of the biomaterial, among others. Therefore, it is logical to assume that the host macrophage response after implantation of a biomaterial is modulated via “cross-talk” between macrophages and the other cells involved in the host response as well as factors within the local microenvironment.

Considerable variability has been seen in the host immune response to xenogeneic biologic scaffolds depending upon the source of the ECM, method of decellularization and the presence of any modifications such as chemical crosslinking. Crosslinking of ECM with carbodiimide has been correlated with delayed degradation, a chronic mononuclear cell accumulation around the device and a foreign body reaction.

Pro-inflammatory responses toward biomaterials are typically associated with encapsulation and a foreign body reaction. However, the bioactive and bioinductive molecules within the extracellular matrix (ECM) that induce polarization are unclear, although it is likely that cellular remnants such as damage associated molecular patterns (DAMPs) retained within the scaffold may play a role. Investigation of the immunomodulatory effects of common ECM scaffolds. Results showed that tissue source, decellularization method and chemical crosslinking modifications affect the presence of the well-characterized DAMP - HMGB1. In addition, these factors were correlated with differences in cell proliferation, death, secretion of the chemokines CCL2 and CCL4, and up regulation of the pro-inflammatory signaling receptor toll-like receptor 4 (TLR4). Inhibition of HMGB1 with glycyrrhizin increased the pro-inflammatory response, increasing cell death and up regulating chemokine and TLR4 mRNA expression. This suggests the importance of HMGB1 and other DAMPS as bioinductive molecules within the ECM scaffold. Identification and evaluation of other ECM bioactive molecules will be an area of future interest for new biomaterial development.

2.0 DECELLULARIZATION AND CELL SEEDING OF WHOLE LIVER BIOLOGIC SCAFFOLDS COMPOSED OF EXTRACELLULAR MATRIX

2.1 ABSTRACT

Liver failure causes over 30,000 deaths every year in the United States alone, with over 2 million deaths estimated worldwide. When this process occurs in a healthy individual, it is termed acute liver failure (ALF) or fulminant hepatic failure (FHF). On the other hand, when loss of liver function complicates an existing chronic liver disease, the term 'acute-on-chronic liver failure' is commonly utilized [187]. Loss of liver function leads to deficiencies in synthesis of proteins, including clotting factors, albumin, and antiproteases. Accumulation of ammonia and other toxic byproducts (i.e. bilirubin) normally metabolized by the liver is typically associated with multiple organ failure, jaundice, coagulopathy, encephalopathy, hepatic coma and brain death [188].

The definitive treatment for patients with end-stage liver disease is orthotropic transplantation. However, this option is limited by the disparity between the number of patients needing transplantation and the number of available livers. This issue is becoming more severe as the population ages and as the number of new cases of end-stage liver failure increases. Patients fortunate enough to receive a transplant are required to receive immunosuppressive therapy and must live with the associated morbidity. Whole organ engineering of the liver may offer a solution to this liver donor shortfall. It has been shown that perfusion decellularization of a whole allogeneic or xenogeneic liver generates a three-dimensional ECM scaffold with intact macro and micro architecture of the native liver. A decellularized liver provides an ideal transplantable scaffold with all the necessary ultrastructure and signaling cues for cell

attachment, differentiation, vascularization, and function. In this chapter, an overview of complementary strategies for creating functional liver grafts suitable for transplantation is provided. Early milestones have been met by combining stem and progenitor cells with increasingly complex scaffold materials and culture conditions.

2.2 INTRODUCTION

2.2.1 Concept of Whole Organ Engineering

Allogeneic liver transplantation is the "gold standard" for patients with end-stage liver disease but is limited by its high cost and the severe donor organ shortage [189]. Both xenotransplantation and hepatocyte transplantation represent alternative therapies, but these approaches have had limited clinical success. Xenotransplantation could provide a limitless supply of donor organs; however, previous attempts have resulted in hyperacute rejection and death. Hepatocyte transplantation offers much promise for correcting nonemergency conditions such as genetic defects of the liver. Delivery of isolated hepatocytes in suspension is typically performed by intravenous or peritoneal administration. This mode of cellular therapy aims to take advantage of hepatocyte ability to regenerate and reconstitute liver functions upon engraftment into the spleen or liver. However, low efficiency of engraftment, long-term immunosuppression from the use of allogeneic cells, and a lag time of 48 hours for the transplanted hepatocytes to become functional *in vivo* have limited the clinical success [190, 191]. Biohybrid artificial liver (BAL) devices provide temporary support for patients waiting for an allogeneic liver transplant, and since the liver can regenerate, the temporary support provided

by BAL may allow sufficient time for this process. However, the lack of a reliable cell source combined with the inability of BAL to maintain the functionality of hepatocytes for long periods of time has limited its clinical utility [192].

These therapeutic challenges have catalyzed the concept of whole organ engineering using three-dimensional biologic scaffolds composed of extracellular matrix (ECM). Whole organ engineering of the liver is based upon three fundamental concepts: 1) the native ECM of the liver represents an ideal and required substrate for liver regeneration, 2) three-dimensional acellular liver scaffolds retain the three-dimensional macrostructure, the native microvascular network, and the bile drainage system; allowing for complete recellularization of all native cell types, and 3) liver regeneration can be promoted when reseeded three-dimensional acellular liver grafts are placed in the appropriate three-dimensional microenvironment, specifically, in-situ in patients with liver failure. The general approach taken for engineering functional liver tissue with ECM scaffolds can be found in **Diagram 1**.

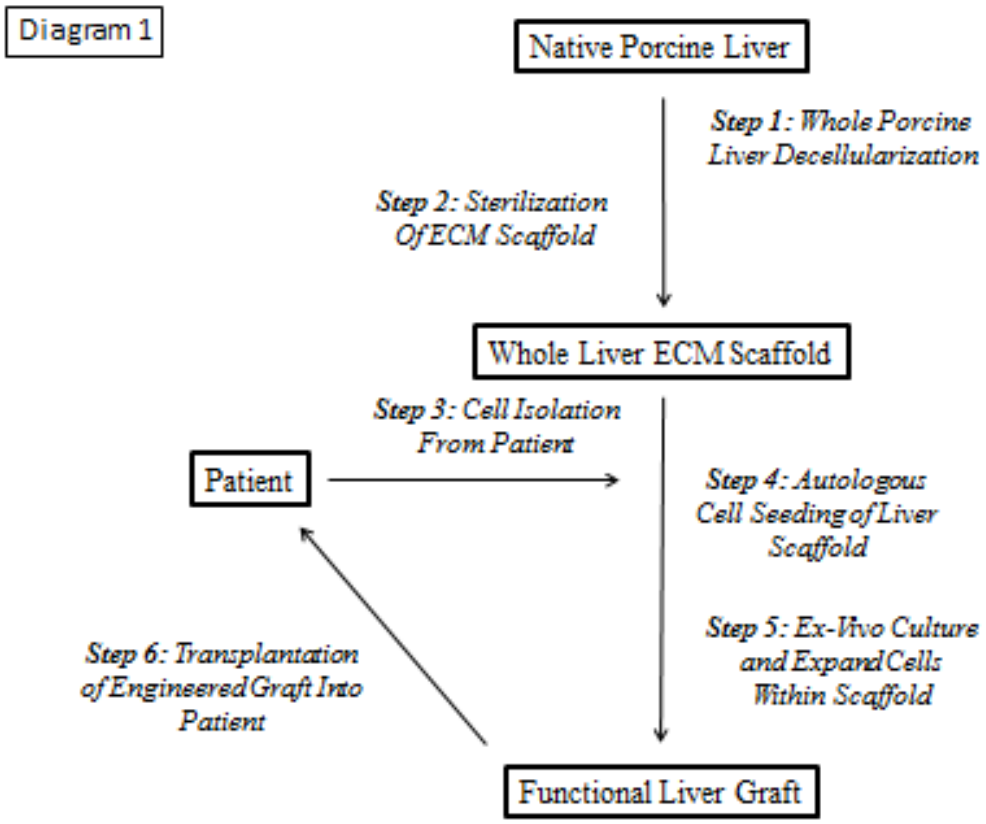

Liver ECM represents the secreted product of the resident cells of the liver, and it is therefore logical that L-ECM is the ideal microenvironment in which hepatocytes can maintain their phenotype and functionality. The liver ECM (i.e., stroma) has also been shown to be essential for liver generation following injury. Whole liver decellularization can be accomplished by vascular perfusion with a cocktail of enzymes, proteases, detergents, and hypotonic saline rinses that completely remove all cellular elements while largely maintaining the native composition and ultrastructure of the underlying three-dimensional matrix [193-195]. The creation of a functional liver has not been accomplished to date, but several intermediate milestones have been reached by tissue engineers of the heart [196], liver [24, 193-195, 197-200], lung [25, 201-203], pancreas [204], and kidney [205, 206]. By integrating increasingly

complex cell combinations, scaffold materials and culture environments, these efforts have successfully recapitulated different aspects of organ development and provided valid lessons that can be applied to future liver tissue engineering work.

2.2.2 Overview of the Liver

The liver is an organ of the digestive tract and is located in the abdominal cavity. It is the second largest organ of the body (skin being the largest), weighs ~1200-1600 grams in an adult human, and receives ~25% of the cardiac output [207]. Anatomically, it is separated into a large right and a small left lobe. The blood supply to the liver comes from two major blood vessels on its right lobe: the hepatic artery (one-third of the blood) and the portal vein (two-thirds). The portal vein brings nutrient- and hormone-rich venous blood from the spleen, pancreas, and small intestines to the liver for processing before entry into the systemic circulation. The hepatic veins drain directly into the inferior vena cava posterior to the liver. The liver possesses a remarkable capacity to regenerate itself after injury. Within a few weeks after partial hepatectomy (surgical removal of two-thirds of the liver), liver mass can return to pre-surgery levels[208].

In order to engineer a microenvironment for liver cells that maintains their key phenotypic functions, one can look at the precisely defined architecture of the liver in vivo where hepatocytes interact with extracellular matrix, nonparenchymal cells and soluble factors (i.e. hormones). In the repeating functional unit of the liver called the lobule, hepatocytes are arranged in unicellular plates along the sinusoid where they experience homotypic cell interactions. Lobules are polyhedrons (typically pentagonal or hexagonal) that are centered on a draining central vein. Portal triads at each corner of a lobule contain portal venules, arterioles

and bile ductules. Sinusoids are small capillaries coursing through the space of Disse, which lacks a basement membrane and is lined by a fenestrated endothelium. Hepatocytes constitute ~70% of the liver mass. Several types of junctions (i.e. gap junctions, cadherins, and tight junctions) and bile canaliculi at the interface of hepatocytes facilitate the coordinated excretion of bile to the bile duct and subsequently to the gall bladder. Several types of nonparenchymal cells including stellate cells, cholangiocytes (biliary ductal cells), fenestrated sinusoidal endothelial cells, and Kupffer cells (macrophages) interact with hepatocytes to modulate their functions. Furthermore, hepatocytes are sandwiched between layers of extracellular matrix in the space of Disse, the composition of which varies along the length of the sinusoid[209]. Finally, physiochemical gradients (i.e. oxygen, hormones) provide hepatocytes in various parts of the sinusoid with different functions. Therefore, a precisely defined micro-architecture, coupled with specific cell-cell and cell-matrix interactions allows the liver to carry out its many diverse functions.

2.2.3 Hepatic Specific Functions

The liver can be simply described as the chemical factory of the body with over 500 functions. Some of these functions include protein synthesis (albumin, clotting factors), cholesterol metabolism, bile production, glucose and fatty acid metabolism, and detoxification of endogenous (bilirubin, ammonia) and exogenous (drugs and environmental compounds) substances. Subset of liver-specific functions (i.e. detoxification) has to be retained in an engineered hepatic tissue for it to be effective in cell-based therapies for liver disease.

The liver is the major organ for the biotransformation of xenobiotics, which can enter the body either intentionally (drugs) or unintentionally (environmental toxins). Xenobiotics undergo three phases of metabolism in hepatocytes. Phase I is the first-pass metabolism of lipophilic compounds into water-soluble metabolites for the purpose of removal from the body. Phase I reactions are mainly mediated by the cytochrome P450 enzyme family (CYP450) which specializes in oxidation and reduction reactions. The key CYP450 isoforms in human liver include 1A2, 2A6, 2C9, 2C19, 2D6, 2E1 and 3A4. Of these enzymes, CYP3A4 is present in the highest quantity and participates in the biotransformation of over 50% of current xenobiotics. Phase II enzymes conjugate highly polar molecules such as glucose, sulfate or glutathione to xenobiotics and/or their metabolites. The highly polar products of phase II are transported out of hepatocytes via the bile canaliculi into the bile, or they are released back into the blood for excretion via the kidneys (sometimes referred to as Phase III). Metabolites can be de-conjugated by gut bacteria and reabsorbed, which leads to a repeat of phase I-III metabolism in the liver (sometimes called enterohepatic recirculation). Though the aforementioned sequence of events in the liver is typically referred to as ‘metabolic detoxification’, many xenobiotics can be metabolized into pharmacologically active or highly toxic compounds [210].

Within the liver lobule, hepatocytes are partitioned into three zones based on morphological and functional variations along the length of the sinusoid from the portal triad to the central vein [211]. Zonal differences have been observed in many hepatocytes functions, including oxidative energy metabolism, carbohydrate metabolism, lipid metabolism, nitrogen metabolism, bile conjugation, and xenobiotic metabolism [212, 213]. Such compartmentalization of gene expression is thought to underlie the liver’s ability to operate as a ‘glucostat’. Zonal differences in expression of CYP450 enzymes has also been implicated in the zonal

hepatotoxicity observed with some xenobiotics [214]. Possible modulators of zonation include blood-borne hormones, oxygen tension, pH levels, extracellular matrix composition, and innervation.

2.3 EXTRACELLULAR MATRIX AS A BIOLOGIC SCAFFOLD

Biologic scaffolds composed of allogeneic or xenogeneic ECM have been used in millions of human patients to reconstruct a variety of tissues including the skin [215], body wall [216, 217], urinary bladder [218], and rotator cuff [218], among others. The ECM is in a state of dynamic reciprocity with resident cells in response to changes in the microenvironment and has been shown to provide cues that affect cell migration and cell proliferation [219-221], cell differentiation [83, 84, 172, 222, 223], and host innate immune response modulation [80, 185, 223, 224].

The creation of an acellular ECM scaffold involves decellularization of a source tissue or organ with the ultimate goal of preserving the native ECM ultrastructure and composition. Reviews of tissue decellularization techniques and their effect upon ECM properties are available [54, 225], and new techniques are continually being developed for application to whole organs. The deleterious *in vivo* effects of ineffective decellularization with the retention of residual cellular material are recognized [55]. However, definitive quantitative standards for effective decellularization of whole organs have yet to be established. This topic will be further discussed in section 3.2.

Biologic scaffold materials are typically, but not always, marketed and regulated as surgical mesh devices. These materials are composed of ECM harvested from a variety of allogeneic or xenogeneic tissue sources including dermis (e.g., AlloDerm® Lifecell Corp.), urinary bladder (e.g., MatriStem®, Acell Inc), small intestine (e.g., Biodesign® Cook Biotech Inc.), mesothelium (e.g., Meso BioMatrix™, Kensey Nash Corp.), and pericardium (e.g., Lyoplant®, B. Braun Melsungen AG), among others. Clinical products composed of ECM have been manufactured from many of these tissues and from a variety of species including human, porcine, bovine, and equine. There is evidence that tissue specific bioscaffolds are preferred, or even required, for functional reconstruction of whole organs such as lung and liver. However, tissue specificity of the biologic scaffold does not appear to be a requirement for reconstruction of many tissues such as skeletal muscle [226], esophagus [227-230], and urinary bladder [231, 232]. The mechanisms by which ECM bioscaffolds facilitate functional and constructive tissue remodeling include positive effects upon cell mitogenesis and chemotaxis [54, 75, 185, 233], cell differentiation [72, 76, 77, 79, 234], and modulation of the host innate immune response [53, 80-82, 138, 235]. It is likely that the three-dimensional ultrastructure, surface topology, surface ligand landscape, and composition of the ECM all contribute to these constructive effects.

2.3.1 Innate Host Response to ECM Scaffolds

Macrophages are a heterogeneous subset of mononuclear phagocytes that play an important role in the host response to implanted biomaterials. The macrophages participating in the host response following implantation of a biomaterial are exposed to multiple stimuli including cytokines and effector molecules secreted by cells (including other macrophages)

active at the implantation site, microbial agents, epitopes associated with the implanted biomaterial, and the degradation products of the biomaterial, among others [236]. Similar to the Th1/Th2 paradigm, populations of macrophages can be classified phenotypically and functionally along a spectrum ranging from cytotoxic/pro-inflammatory types (designated as M1 "classically activated" macrophages) or wound healing/anti-inflammatory types (designated as M2 "alternatively activated" macrophages) [82]. It has been shown that in response to the implantation of ECM scaffolds, cytokine expression is consistent with a predominant M2 and Th2 response. Macrophages are required for scaffold degradation *in vivo* and determine the overall remodeling outcome [81, 138].

2.3.2 ECM Degradation

It has been shown that most ECM scaffolds are rapidly degraded *in vivo*. A previous study showed that ^{14}C labeled ECM scaffolds were 60% degraded at 30 days post implantation and 100% at 90 days post-surgery in a model of canine Achilles tendon repair. During this period, the scaffold was populated and degraded by host cells and resulted in the formation of site-specific functional host tissue[237]. The major mechanism of excretion of the degraded scaffold was via hematogenous circulation and elimination by the renal excretion. Recent findings suggest that the degradation products of ECM scaffolds are bioactive [54, 169, 185, 234, 238]. One of the biologic effects of ECM degradation products is the recruitment of tissue specific stem and progenitor host cells to the site of degradation [75, 185, 238]. Therefore, not only does a biologic scaffold, such as liver ECM, modulate the host innate immune response

toward a constructive phenotype [53, 81, 82], but a biologic scaffold also has the potential to recruit endogenous progenitor cells to the site which can participate in the reconstitution of functional liver tissue. It is expected that the three-dimensional L-ECM scaffolds will also rapidly degrade and be replaced by new matrix secreted by the seeded hepatocytes.

2.3.3 Liver Specific ECM

As previously stated, tissue specific bioscaffolds are required for constructive remodeling of select tissues, including the liver. This requirement may be due to the selective nature of hepatocytes, which are notorious for losing functional phenotype quickly in culture. The use of complex ECM substrates derived from mammalian tissues for effective hepatocyte culture began more than two decades ago. Early culture models utilized ECM substrates derived from either rat liver or the Engelbreth-House sarcoma mouse tumor (i.e., Matrigel). Rat hepatocytes cultured on type-1 collagen show less cell attachment and survival compared to rat hepatocytes cultured upon a biomatrix derived from solubilized rat liver. This result further demonstrates that liver specific ECM is important in maintaining cells introduced to a decellularized scaffold.

ECM substrates derived from porcine, bovine, and human livers have been used to improve hepatocyte survival, polarity and liver-specific functions in vitro. Lin et. al. compared rat hepatocytes cultured on ECM biologic scaffolds derived from porcine liver (PLECM) to well characterized hepatocyte culture models (type-1 collagen sandwich configuration or a single layer of type-1 collagen) [59]. Hepatocytes survived up to 45 days on a sheet form of PLECM

and several liver-specific functions such as albumin synthesis, urea production, and P-450 IA1 activity were markedly enhanced compared to the growth and metabolism of cells cultured on a single layer of type-1 collagen.

In a previous study, two different biologic substrates were compared for their ability to support primary human hepatocyte function *in vitro*: porcine-liver-derived extracellular matrix (PLECM) and Matrigel [52]. Albumin secretion, hepatic transport activity, and ammonia metabolism were used to determine hepatocyte function. Hepatocytes cultured between two layers of PLECM or Matrigel showed equally high levels of albumin expression and secretion, ammonia metabolism, and hepatic transporter expression and function. In another study, three different acellular ECM scaffolds were investigated in a physiologically relevant *in vitro* culture model for their ability to maintain hepatic sinusoidal endothelial cell (SEC) phenotype [70]. The cell culture model used SECs only or a coculture of SECs with hepatocytes on ECM substrates derived from the liver (L-ECM), bladder (UBM-ECM), or small intestinal submucosa (SIS-ECM). The effect of the ECM substrate upon SEC dedifferentiation was evaluated using scanning electron microscopy (SEM) and confocal microscopy. When SECs alone were cultured on uncoated glass slides, collagen I, UBM-ECM, or SIS-ECM, SECs showed signs of dedifferentiation after 1 day. In contrast, SECs alone cultured on L-ECM maintained their differentiated phenotype for at least 3 days, indicated by the presence of many fenestrations on SEC surface, expression of anti-rat hepatic sinusoidal endothelial cells mouse IgG MoAb (SE-1), and lack of expression of CD31. When SECs were cocultured with hepatocytes on any of the ECM scaffolds, the SECs maintained a near-normal fenestrated phenotype for at least 1 day. However, SEM revealed that the shape, size, frequency, and organization of the fenestrations varied greatly depending on ECM source. At all-time points, SECs cocultured with hepatocytes

on L-ECM maintained the greatest degree of differentiation. This study demonstrated that the acellular ECM scaffold derived from the liver maintained SEC differentiation in culture longer than any of the other tested substrate materials and that contact and crosstalk between different cell types of the same tissue may also be beneficial to preserving or promoting proper function. The conclusion of these studies supports the hypothesis that L-ECM provides a preferred substrate and microenvironment for maintaining hepatic cell viability and function

2.3.4 Methods of Liver Decellularization and Scaffold Processing

Isolating the extracellular matrix from an intact liver requires a process that removes cellular material, while preserving the ultrastructure, composition, and ligand landscape of the underlying matrix. Minimal damage to vascular structures is essential for eventual re-endothelialization, anastomosis, and in-vivo implantation of three-dimensional liver scaffolds. Removal of cells from their integrin-bound anchors and intercellular adhesion complexes while maintaining extracellular matrix surface topography and resident ligands is challenging. A combination of physical, ionic, chemical, and enzymatic methods are typically used to accomplish decellularization. Organs, such as the heart [23, 48, 239], liver [24, 195], kidney [205], Pancreas [204], and lung [201], have been decellularized by using each organ's vascular network to deliver decellularizing solutions. This method leaves the organ semitransparent in appearance while retaining the ultrastructure of the whole organ with intact vascular basement membranes and architecture. Re-endothelialization of the denuded vascular network is necessary to support blood flow and to prevent thrombosis. Reviews of tissue decellularization techniques and their effect upon ECM properties are available [83, 84].

The most effective protocol for the decellularization of a liver will depend upon characteristics of the source liver, including species (e.g., porcine vs. non-human primate), age (e.g., neonatal vs. adult), and lipid content (e.g., high vs. low fat diet). Regardless of the processing method used, preservation of the native hepatic matrix composition and ultrastructure is the primary objective. All methods used for decellularization are inherently disruptive with unavoidable adverse effects upon the native architecture and key proteins and/or growth factors. However, the extent of disruption can be minimized with careful consideration of the method used.

2.3.5 Current Methods of Whole Liver Decellularization

In 2008, perfusion decellularization was reported as a technique to generate acellular whole organ scaffolds from cadaveric organs [23]. In this approach, decellularizing agents are delivered via the native vasculature of the organ and are thereby equally distributed across the entire mass of the organ. By applying physiologic perfusion pressures, decellularization solutions can effectively permeate the organ via arteries, arterioles and capillaries and remove cellular debris via the venous system, thereby minimizing their retention within the scaffold. The minimum exposure of the source organ to the decellularization solutions lowers the risk of the chemical or physical alterations of ECM proteins and growth factor loss, thus facilitating the generation of a more biocompatible scaffold for organ engineering. Although previous studies utilizing perfusion decellularization have reported a combination of SDS, Triton X-100 and PBS perfusion, the ideal detergent recipe must be tailored to the specifics of the harvested liver (i.e.

species and age). There have been several published methods for generating an acellular liver scaffold. An overview of these methods can be found in **Table 2**. Perfusion decellularization of whole liver generates an acellular ECM scaffold with intact three-dimensional anatomical structures and patent vasculature conduits that can be re-endothelialized. Decellularized liver scaffolds have been shown to be free of significant DNA content and nuclear fragments, while retaining major ECM proteins (collagen I, III, laminin, fibronectin and glycosaminoglycans).

Table 2. Methods of Whole Liver Decellularization

Author	Species	Protocol time	Temp (°C)	Perfusion inlet	Detergents used	Flow rate or pressure	Protocol overview
Shupe et al[11]	Rat	6 h	Room	Inferior Vena Cava	1% Triton X-100 2% Triton X-100 3% Triton X-100 0.1% SDS	5 ml/min	• 100 ml PBS • 300 ml of 1% Triton X-100 • 300 ml of 2% Triton X-100 • 300 ml of 3% Triton X-100 (300 ml each) • 300 ml of 0.1% SDS • 300 ml PBS
Uygun et al[9]	Rat	4 days	4°	Portal Vein	0.01% SDS 0.1% SDS 1% SDS 1% Triton X-100	1 ml/min	➢ 1 × PBS overnight ➢ 0.01% SDS for 24 h ➢ 0.1% SDS for 24 h ➢ 1% SDS for 24 h ➢ Distilled water for 15 min ➢ 1% Triton X-100 for 30 min ➢ 1 × PBS for 1 h ➢ 0.1% peracetic acid for 3 h ➢ Sterile PBS containing antibiotics up to 7 days
Soto-Gutierrez et al[7]	Rat	2 days	−80°Room 37° Room	Inferior Vena Cava	3% Triton X-100	8 ml/min	• 1 × PBS • 0.02% Trypsin/0.05% EGTA @ 37C for 2 h • Water for 15 min • 2 × PBS for 15 min • 3% Triton X-100/0.05% EGTA for 18–24 h • Water for 15 min • 2 × PBS for 15 min • 0.1% peracetic acid/4% EtOH for 1 h • 2 × PBS for 15 min twice • Water for 15 min twice

Table 2 (continued).

Author	Species	Protocol time	Temp (°C)	Perfusion inlet	Detergents used	Flow rate or pressure	Protocol overview
Bao et al[10]	Rat	2 days	4°	Portal Vein	1% SDS 0.5% SDS 0.25 SDS 1% Triton X-100	25 mmHg	➢ Heparinization ➢ Deionized water (20 ml) containing heparin sodium (50 U/ml) ➢ Deionized water containing 10 mM adenosine overnight ➢ 1% SDS for 4 h ➢ 0.5% SDS for 4 h ➢ 0.25% SDS for 4 h ➢ Deionized water for 20 min ➢ 1% Triton X-100 for 1 h ➢ 1 × PBS with 100U/ml Penicillin-G, 100U/ml Streptomycin, and Amphotericin B for 12 h
Barakat et al[6]	Porcine	–	Room 4°	Portal Vein	0.25% SDS 0.5% SDS	80 mmHg	• 6–10 L of distilled water • 20 L of 0.25% SDS in distilled water via PV • Storage in 0.25 SDS at 4 °C for 28 h • 40 L of 0.5% SDS • 20 L of distilled water • 10% formalin • 40 L of PBS
Zhou et al[5]	Murine	6 h	37°	Portal vein	1% SDS 1% Triton X-100	5 ml/min	➢ Heparinized PBS for 15 min ➢ 1% SDS for 2 h ➢ 1% Triton X-100 for 30 min
Baptista et al[14]	Rat & Ferret	–	Room	Portal vein	1% Triton X-100	5 ml/min	• Distilled water (40× the volume of the liver) • 1% Triton X-100 with 0.1% ammonium hydroxide (50× the volume of the liver) • Distilled water wash
Mirmalek-Sani et al[12]	Porcine	–	4° Room 4°	Hepatic Artery	1% Triton X-100 2% Triton X-100 3% Triton X-100 0.1% SDS	50 ml/min	➢ PBS containing 10 U/ml sodium heparin ➢ 1% Triton X-100 ➢ 2% Triton X-100 ➢ 3% Triton X-100 ➢ 0.1% SDS ➢ 1 × PBS for several days
Nari et al[15]	Rabbit	2 days	−80° Room	Inferior Vena Cava	3% Triton X-100 0.1% SDS	6-10 ml/min	• 0.02% Trypsin/0.05% EDTA for 4 h • 3% Triton X-100 and 0.05% EGTA. Three times for 2 h each. 16 h. Three times for 2 h each. • 0.1% SDS for 4 h • 3% Triton X-100 and 0.05% EGTA for 14 h • 1 × PBS • Deionized water • 4% Ethanol for 1 h
Wang et al[16]	Murine	6 h	Room	Portal Vein	1% SDS 1% Triton X-100	5 ml/min	➢ 50 mL of sterile PBS (containing 12.5 U/mL heparin) ➢ PBS containing 100 units/ml penicillin and 100 ug/ml streptomycin. ➢ 1% SDS for 2 h ➢ 1% Triton X-100 for 30 min ➢ 1 × PBS for 3 h

2.3.6 Criteria for Decellularization

Following whole liver decellularization, the organ usually assumes a pale or translucent quality. However, macroscopic appearance alone is insufficient to determine the extent of decellularization. While there is no universal consensus on criteria for adequate decellularization, standard metrics are beginning to emerge. Three relatively stringent criteria have been proposed to establish sufficient decellularization: specifically, the remaining ECM scaffold must have 1) less than 50ng of dsDNA per mg of dry weight, 2) DNA fragments less than 200 bp in length, and 3) no visible nuclear material in histologic analysis with DAPI or H&E [84].

Failure to completely decellularize a tissue leads to negative outcomes upon *in vivo* implantation, including a pro-inflammatory response with associated M1 macrophages and subsequent fibrosis. Such a reaction is likely caused in part by damage associated molecular pattern (DAMP) molecules and can lead to seroma formation, sterile abscess formation, and chronic inflammation. A recently published study determined the association between decellularization efficacy and host response by qualitative and quantitative methods[240]. ECM devices containing significantly more cellular material showed a predominantly M1 pro-inflammatroy macrophage response while ECM device containing less DNA resulted in a macrophage response predominantly of an M2 phenotype. Other studies have shown that a scaffold that contains cellular material promotes a clear M1 phenotype macrophage response at 3 days; whereas, the equivalent acellular scaffold promotes a strong M2 phenotype [36]. Rieder et al. have shown that decellularization can reduce the chemotactic potential of heart valve tissue for macrophages but does not inhibit the activation of macrophages although they did not study

macrophage polarization [60]. Ariganello et al. have shown that in vitro exposure of a macrophage cell line to decellularized tissue elicited lower esterase and phosphatase activity consistent with a subdued inflammatory response comparable to the M2 phenotype [35].

2.3.7 The Effects of Detergents on ECM Scaffolds

The choice of detergent used for whole liver decellularization is an important factor because the recellularization process will be dependent on the integrity of the remaining substrate. Each detergent, depending on its chemical characteristics, has unique and distinct effects on ECM composition and structure. Less harsh detergents, such as Triton X-100 or other non-ionic detergents are preferred for maintaining the native ECM structure and composition compared to detergents such as SDS, which can denature essential ligands and proteins within the ECM.

Detergents commonly used in the decellularization of organs and tissues include triton X-100 [131, 241], 3-[(3-cholamidopropyl)dimethylammonio]-1-propanesulfonate (CHAPS) [18], deoxycholic acid [132], and sodium dodecyl sulfate (SDS) [23, 242-245]. Detergents can solubilize cell membranes and dissociate DNA from proteins, making them attractive for the decellularization process. Ionic detergents can be more effective for cellular removal than non-ionic and zwitterionic detergents [40]. However, subjecting tissue to harsh detergents, such as SDS, can disrupt the ECM structure [246], eliminate growth factors [67], and/or denature essential proteins [35].

In chapter 5, a study is described in which four detergents commonly used for decellularization of tissues and organs were systematically evaluated and compared for their effect on the basement membrane complex (BMC) [247]. The ability of the resulting scaffold to support human microvascular endothelial cells (HMECs) in vitro was determined. This study is relevant because the success of whole liver engineering will be critically dependent upon the re-endothelialization of the organ's vasculature. The detergents investigated were 3% Triton X-100, 4% sodium deoxycholate, 8 mM CHAPS, and 1% SDS. Key findings of this study were as follows:

Collagen Content

Scaffolds treated with 3% Triton X-100, 8 mM CHAPS and 4% sodium deoxycholate retained a soluble collagen content similar to that of the non-detergent water control. Treatment with 1% SDS resulted in a significant loss of detectable soluble collagen. This finding suggests that detergent treatment with SDS resulted in either a decrease in soluble collagen present or modification of the molecular structure of this collagen to the point of insolubility.

GAG Content

Scaffolds treated with 3% Triton X-100, 4% sodium deoxycholate and 8 mM CHAPS retained GAG similar to that of the water control, while scaffolds treated with 1% SDS retained a smaller amount of detectable GAG than the water control.

Elastin Content

Scaffolds treated with Triton X-100 and sodium deoxycholate retained elastin fibers: whereas, CHAPS had no visible elastin fibers, and SDS had only a small amount of thin fragmented fibers.

Fiber Network Analysis

Differences in scaffold surface fiber organization and evidence of collagen fiber denaturation were apparent from both SEM inspection and the results of automated image algorithms. SDS and CHAPS caused marked alterations of collagen fiber architecture while Triton X-100 and sodium deoxycholate were better tolerated and showed the surface of the BMC maintained an appearance that more closely resembled that of the no-detergent control. These structural changes and the associated changes in the ligand landscape provide insight into the results of the cell seeding experiments. When HMECs were cultured on basement membrane exposed to the chosen detergents, clear differences were seen in cell morphology, confluence, infiltration depth, and integrin β-1 expression.

ECM-Cell Interactions

HMECs cultured on the BMC prepared with 3% Triton X-100 had a similar level of confluence, infiltration depth, and phenotype compared to cells cultured on scaffolds treated with type I water (control). These HMECs were characterized by a flat morphology. HMECs cultured on the BMC prepared with 8 mM CHAPS were less confluent, had a greater infiltration depth, and an atypical phenotype compared to HMECs cultured on the control. HMECs cultured on scaffolds prepared with 4% sodium deoxycholate were less confluent, had a similar infiltration depth, and

an atypical phenotype compared to cells cultured on a no-detergent control. HMECs cultured on scaffolds prepared with 1% SDS had a similar percentage of confluence, similar infiltration depth, but a less normal phenotype compared to cell cultured on a no-detergent control.

HMECs cultured on the BMC prepared with 8 mM CHAPS and 1% SDS had a lower number of cells stain positive for integrin β-1 compared to HMECs cultured on the BMC not subjected to a detergent. HMECs cultured on the BMC prepared with 3% Triton X-100 and 4% sodium deoxycholate had a similar percentage of cells expressing integrin β-1 compared to cells cultured on the no-detergent control tissue. The percent of cells positive for Ki67 was below 3% for all groups, and no significant differences were seen when comparing to the control.

This study shows that each detergent, depending on its chemical characteristics, has distinct effects on ECM composition and structure. Less disruptive detergents, such as Triton X-100 or other non-ionic detergents are preferred for maintaining the native ECM structure and composition compared to more harsh detergents, such as SDS, which can denature essential ligands and proteins within the BMC. The disruption or denaturation of the native BMC architecture can negatively impact the interaction of cells with the scaffold. The results of this study can aid in the formulation of tissue and organ decellularization protocols such that the native biological activity of the resulting extracellular matrix scaffold is maximally preserved.

2.3.8 Enzymes

There have been several published methods for generating biologic scaffolds composed of ECM, each of which describes a unique and specific recipe of enzymes and detergents to be used on the source tissue. Trypsin is an enzyme commonly used in the decellularization process because it is

a well-characterized protease naturally found in the digestive tract of many vertebrates. As a protease, trypsin disrupts cell adhesion molecules (i.e. integrins) and cleaves peptide bonds with remarkable specificity.

Trypsin can disrupt both cell-cell and cell-ECM bonds as well as cleave cell surface proteins. In conjunction with EDTA, an ion chelating agent that disrupts cell-cell cadherin adhesions, trypsin is a powerful decellularization agent. Perfusing an organ with a solution of trypsin/EDTA is an effective initial step in the process of whole organ decellularization. However, the perfusion with trypsin is time dependent and must be performed at low concentrations to preserve the proteins within the ECM to the maximum extent possible. The combination of trypsin followed by a detergent is typically necessary to achieve complete decellularization.

2.4 STERILIZATION OF WHOLE LIVER SCAFFOLDS

Recellularization and implantation of a whole liver scaffold will obviously require sterility. Gamma irradiation, e-beam, glutaraldehyde, ethylene oxide and peracetic acid have all been used as methods of sterilization and have been extensively evaluated for their effect on bioscaffold mechanical and biological integrity. In addition to sterilization, glutaraldehyde effectively crosslinks ECM proteins. Other chemical agents, such as carbodiimide and genipin, are also crosslinking agents, which can be used prior to sterilization. Chemical crosslinking of ECM proteins (e.g. collagen) stabilizes and strengthens the ECM structure and severely inhibits *in vivo* degradation. However, sterilization techniques that also crosslink must be avoided because crosslinked ECM scaffolds have been shown to elicit a foreign body response very similar to

non-degradable synthetic polymer scaffolds (e.g., polypropylene) [138]. This response is predominantly M1 in nature, causing fibrosis leading to chronic inflammation [80].

2.5 WHOLE LIVER ECM SCAFFOLD RECELLULARIZATION

There have been several published methods for cell seeding a whole liver ECM scaffold. An overview of these methods can be found in **Table 3**. The methods employed in recellularization of whole-organ scaffolds are typically adaptations of techniques from a wide range of procedures including traditional cell culture, tissue-engineering methods, cell-transplantation therapies, and isolated-organ perfusion. The recellularization process can be considered in two major steps. The first is cell seeding, in which the goal is distribution of appropriate cell types to all areas of the three-dimensional liver scaffold. The second is perfusion culture, which is typically utilized to prepare the cells for *in vivo* function by exposing them to physiological conditions.

Table 3. Published Methods for Cell Seeding a Whole Liver ECM Scaffold.

Author	ECM scaffold source species	Cell types	Number of cells	Method of cell delivery	Culture duration	Implantation site	Duration of graft survival
Baptista et al[1,4]	Ferret	Human fetal liver cells Human umbilical vein endothelial cells	7.0×10^7 3.0×10^7	Portal vein perfusion	7 days	n/a	n/a
Bao et al[10]	Rat	Rat Hepatocytes	1.0×10^8	Portal vein perfusion	6 h	In series with native liver via end-to-end anastomosis with the portal vein	72 h
Barakat et al[6]	Porcine	Human fetal stem cells Human fetal liver cells	3.5×10^8 1.0×10^9	Portal and hepatic vein perfusion	3, 7, 13 days	Into the infrahepatic space by using the recipient portal vein and infrahepatic inferior vena cava as an inflow and outflow, respectively	2 h
Soto-Gutierrez et al[7]	Rat	Mouse hepatocytes	5.0×10^7	Injection or portal vein perfusion	7 days	n/a	n/a
Uygun et al[9]	Rat	Rat hepatocytes	5.0×10^7	Portal vein perfusion	14 days	Heterotopic, following unilateral nephrectomy	8 h

The first challenge in recellularization of decellularized liver scaffolds is its repopulation with an appropriate mixture and number of cells as well as directing each cell type to necessary niches within the scaffold to match the native distribution. In addition, non-parenchymal cells

such as fibroblasts and endothelial cells enhance the functional phenotype of the hepatocytes and contribute to the organization of the cellular architecture of the liver.

Endothelial cells are necessary to provide a non-thrombogenic barrier for the decellularized liver matrix and assure that blood flow *in vivo* is confined to the vascular spaces and that the parenchymal cells are protected from the shear stress created by the flow. A major advantage of whole-organ scaffolds is the presence of intact vascular networks, but full utilization of this vascular system to direct flow within the tissue *in vivo* requires adequate endothelialization. Functional long-term endothelialization of a liver bioscaffold has yet to be demonstrated, although initial attempts have been promising in showing endothelial cell attachment. Strategies to improve the endothelialization of three-dimensional organ constructs are under investigation.

2.5.1 Delivery of Cells Within a Decellularized Scaffold

Seeding techniques currently employed in recellularization of whole-organ grafts are essentially adaptations of the approaches employed in cell-transplantation therapies. Cells are either injected directly into the organ or injected into the circulation with the expectation that the cells will home to the injury site. These techniques include intramural injection of cells or infusion of cells into the vasculature followed by continuous perfusion.

In the report for whole-rat heart recellularization, recellularization occurred with 50–75×10^6 neonatal cardiac cells delivered in five injections of 200 μl each into the anterior left ventricle with a seeding efficiency of approximately 50% [23]. This approach resulted in approximately 34% of recellularization proximal to the injection sites with decreasing

percentages distally. Furthermore, 2×10^7 endothelial cells were placed by direct infusion into the aorta, which yielded 550.7 ± 99 cells per mm^2 on the endocardial surface and 264.8 ± 49.2 cells per mm^2 within the vascular tree after 7 days of perfusion culture.

A study conducted by Soto-Gutierrez et al. compared three different methods for hepatocyte seeding of a three-dimensional liver scaffold. The three evaluated methods were (1) direct parenchymal injection, (2) multistep infusion, or (3) continuous perfusion. The three-dimensional liver matrix reseeded with the multistep infusion of hepatocytes generated ~90% of cell engraftment and supported liver-specific functional capacities of the engrafted cells, including albumin production, urea metabolism, and cytochrome P450 induction [195].

2.5.2 Cell Type and Source

Hepatocytes are the parenchymal cells of the liver and account for approximately 80% of all liver cells [248]. Hepatocytes perform most of the functions of the liver and work in concert with a number of other cell types to perform the functions essential for survival of the individual. The non-parenchymal cells (NPCs) of the liver include sinusoidal endothelial cells, Kupffer cells, and stellate cells [248]. It is likely the addition of liver-derived NPCs will be necessary in the recellularization of a three-dimensional liver scaffold. Co-cultivation of primary human hepatocytes with other cells types can maintain liver-specific functions for several weeks *in vitro* [249]. Liver-derived NPCs as well as non-hepatic endothelial cells, epithelial cells, and fibroblasts have been co-cultured with hepatocytes to maintain hepatocyte morphology and a

variety of synthetic, metabolic, and detoxification functions of the liver. Bhatia et al. have provided an extensive summary of studies used to preserve hepatocyte-specific functions *in vitro* through co-culture with other cells [250].

The cell source used to seed three-dimensional ECM scaffolds is an open and unanswered question. Availability of human donor livers for hepatocyte isolation is inadequate: thus, alternatives to autologous primary hepatocytes should be considered. Induced pluripotent stem cell populations are attractive due to their typically rapid and extensive proliferation and their potential to be used without immunosuppressant drugs. However, many questions regarding induced pluripotent stem cells remain unanswered. The in vitro differentiation state of stem cells that leads to optimal survival in vivo is unknown. It is believed that early-stage progenitor cells may be more efficient than fully differentiated liver cells because they can give rise not only to hepatocytes but also to other cell types (non-parenchymal liver cells) including bile duct epithelial cells required for the formation of the sophisticated hepatic anatomy.

2.5.3 Construction of a Vascular Network

It has previously been shown that the basement membrane and elastin fibers of the vascular network of the decellularized liver matrix were intact following whole liver decellularization [195]. A corrosion cast of the liver matrix was created and showed the existence and preservation of the entire vascular system (portal vein, hepatic artery vasculature, central vein and biliary tract) similar to normal liver. This vascular network integrity is an important feature for subsequent endothelialization. These denuded vascular conduits must be re-endothelialized to prevent coagulation. Prevention of blood coagulation is typically difficult to achieve and failure

to do so hinders long-term in vivo testing of engineered livers. Blood contact is normally restricted to the endothelium, and the coagulation cascade is initiated if blood is exposed to tissue collagen through direct and indirect interactions of collagen with platelet glycoprotein surface receptors. Unless the graft has been fully endothelialized to conceal collagen, coagulation will occur when the graft is exposed to circulating blood. Coagulation can be prevented in vivo by covering the vascular bed in the decellularized liver matrix with endothelial cells. In practice, achieving near-perfect endothelial cell coverage of the vasculature in the scaffold is challenging. A potential solution is to deposit heparin throughout the vasculature of the scaffold.

2.6 CHALLENGES AND FUTURE DIRECTIONS

The key limiting step for successful implementation of an engineered liver is the establishment a functional non-thrombotic vascular network throughout. Several groups have attempted the implantation of a seeded ECM construct, only to have it thrombose shortly after implantation. Furthermore, delivering all cell types to their native spatial location and recapitulating the liver's complex cellular organizations is challenging. The liver is composed of several distinct cell types, including hepatocytes, sinusoid endothelial, Kupffer, stellate and biliary epithelial cells. These cells function in a highly sophisticated and integrated manner, which is difficult to engineer in-vitro. However, it is believed that liver regeneration can be promoted when seeded three-dimensional acellular liver grafts are placed in the appropriate three-dimensional microenvironment, specifically, in-situ in patients with liver failure. Studies aimed at successful implantation of an engineered liver graft in pre-clinical large animal models are in progress.

3.0 OBJECTIVE

A regenerative medicine strategy for the reconstitution of functional liver tissue is proposed. This whole organ replacement strategy that is based upon the concept that functional hepatic tissue can be engineered by the effective delivery of autologous hepatic parenchymal and non-parenchymal cells within a 3-dimensional liver scaffold composed of liver extracellular matrix (3D L-ECM). This approach would include immediate or near immediate in-situ transplantation of the cell seeded scaffold, providing the requisite perfusion by the host circulation that supplies appropriate microenvironmental cues, nutrients, and signaling factors necessary for liver regeneration. The long-term goal of this work is to establish the decellularization, recellularization and transplantation criteria necessary to produce the first fully functional bioengineered liver for organ transplantation

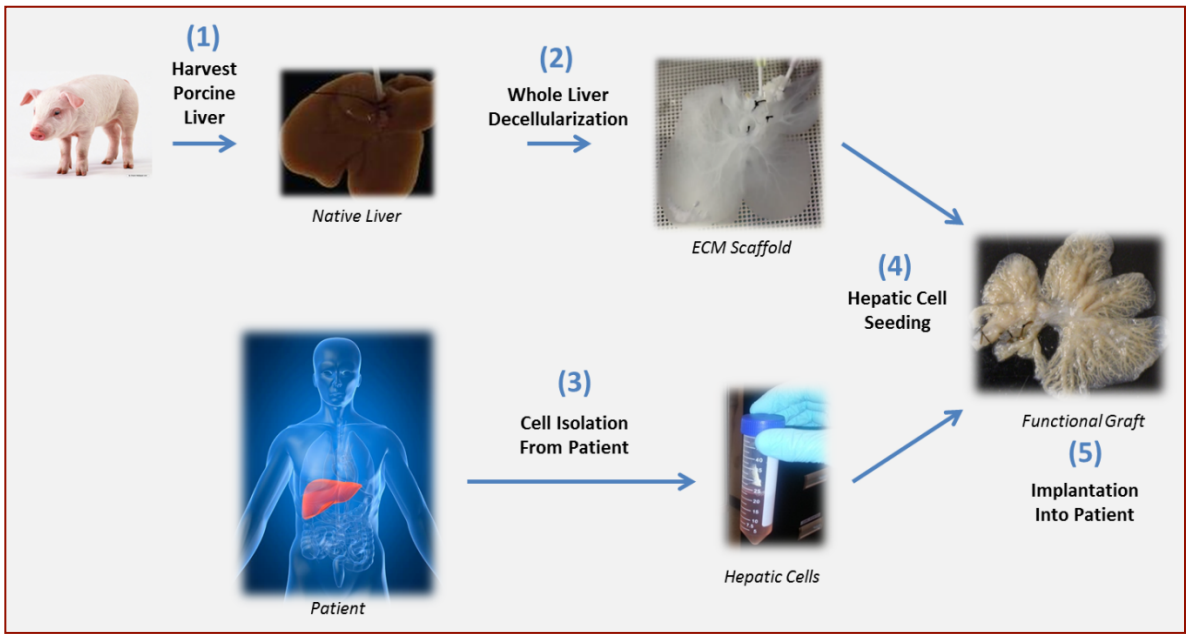

Figure 3. Conceptual overview of a regenerative medicine strategy for engineering functional liver tissue. Healthy porcine livers would be harvested and decellularized to produce a three-dimensional biologic scaffold composed of liver specific ECM. This scaffold would subsequently be seeded with the patient's cells to produce a functioning autologous liver graft suitable for implantation into the patient.

4.0 CENTRAL HYPOTHESIS AND SPECIFIC AIMS

The central hypothesis for this following work is that a whole organ biologic scaffold composed of hepatic ECM is ideal for engineering a fully functional liver graft because (1) it provides the necessary hepatic microenvironment for seeded cells and (2) it elicits a constructive immune response following in-vivo implantation.

4.1 Specific Aim 1: To determine the effects of decellularization agents on the interation between 3D L-ECM scaffolds and seeded parenchymal and non-parenchymal cells.

Hypothesis: Decellularization agents change the ultrastructure and composition of the ECM scaffold, and thus, the behavior of seeded cells.

Rationale: The decellularization of tissues for the purpose of utilizing the extracellular matrix (ECM) as a bioscaffold for reconstructive surgical procedures or whole organ engineering involves the use of various enzymes, detergents and mechanical/physical methods[16, 83, 84]. During the process of decellularization, parenchymal and non-parenchymal (e.g., vascular endothelium) cells within the source tissues are destroyed and/or removed[52, 83, 84, 251-253]. The remaining vascular network, devoid of endothelial cells, has been proposed as a potential guide and substrate for revascularization[23]. Therefore, determining the effects of decellularization methods upon the structure and composition of the scaffold, as well as the scaffold's ability to support hepatic cells in culture, is critical for subsequent recellularization.

4.2 Specific Aim 2: To reconstruct a vascular venous and arterial network within a decellularized rat liver scaffold.

Hypothesis: Preferred seeding of endothelial cells will be accomplished via the infusion of small numbers of cells into all vascular inlets of the decellularized scaffold (1) portal vein, (2) hepatic vein, and (3) hepatic artery. Increased seeding density and media perfusion rate will result in high vascular formation within the scaffold.

Rationale: It has been shown that L-ECM is a preferred substrate for sinusoidal endothelial cells[52] and, but effective delivery of endothelial cells into the sinusoidal vascular structures is challenging. Several attempts to repopulate 3D L-ECM scaffolds by perfusion techniques have shown partial success [24, 195]. However, no one has taken a systematic approach to investigating key seeding/culture variables associated with the reconstruction of a functional hepatic vascular network. Furthermore, re-endothelialization of both the venous and arterial networks has yet to be achieved. Multiple delivery methods, flow rates and cell concentrations will be tested. Each seeding technique will be evaluated for cell survival, liver specific functions, spatial distribution and cellular adhesion complexes.

4.3 Specific Aim 3: To develop preferred methods for seeding hepatocytes within a decellularized rat liver, achieving cellular attachment, survival, and prolonged graft functionality.

Subaim 1: Compare two seeding methods (1) direct parenchymal injection (2) infusion via the vascular network
Subaim 2: Systematic evaluation of key seeding variables (1) cell concentration, (2) injection volume, and (3) the addition of NPCs
Subaim 3: Combined the preferred hepatocyte seeding method with the endothelial cell seeding technique developed in Specific Aim 2

Hypothesis: Seeding of hepatocytes within a decellularized pig liver will be accomplished via small volume syringe into the scaffold's parenchymal space with a minimized injection volume.

Rationale: It has been shown that L-ECM is a preferred substrate for hepatic parenchymal cells[52] and for hepatic sinusoidal endothelial cells[70], but effective delivery of cells within a honey-combed shaped, 3-dimensional network of hepatic cords and vascular structures is challenging. Several attempts to repopulate 3D L-ECM scaffolds by perfusion techniques have shown partial success [24, 195] and we have recently shown 90% engraftment efficiency with a multistep perfusion method [195]. However, spatial distribution of seeded hepatocytes was not uniform. It is likely that the autologous cells for use in eventual clinical translation will be limited in number and it is critical that an optimal method for cell delivery be developed. 3D L-ECM scaffolds will be seeded with hepatic parenchymal and non-parenchymal cells. Multiple delivery methods, flow rates and cell concentrations will be tested. Each seeding technique will be evaluated for cell survival, liver specific functions, spatial distribution and cellular adhesion complexes.

5.0 THE EFFECT OF DETERGENTS ON THE BASEMENT MEMBRANE COMPLEX OF A BIOLOGIC SCAFFOLD MATERIAL

5.1 ABSTRACT

The basement membrane complex (BMC) is a critical component of the extracellular matrix (ECM) that supports and facilitates the growth of cells. This study investigates four detergents commonly used in the process of tissue decellularization and their effect upon the BMC. The BMC of porcine urinary bladder was subjected to 3% Triton-X 100, 8mM 3-[(3-cholamidopropyl)dimethylammonio]-1-propanesulfonate (CHAPS), 4% sodium deoxycholate or 1% sodium dodecyl sulfate (SDS) for 24 h. The BMC structure for each treatment group was assessed by immunolabeling, scanning electron microscopy (SEM) and second harmonic generation (SHG) imaging of the fiber network. The composition was assessed by quantification of dsDNA, glycosaminoglycans (GAG) and collagen content. The results showed that collagen fibers within samples treated with 1% SDS and 8 mM CHAPS were denatured, and the ECM contained fewer GAG compared with samples treated with 3% Triton X-100 or 4% sodium deoxycholate. Human microvas- cular endothelial cells (HMEC) were seeded onto each BMC and cultured for 7 days. Cell–ECM interactions were investigated by immunolabeling for integrin b-1, SEM imaging and semi-quantitative assessment of cellular infiltration, phenotype and confluence. HMEC cultured on a BMC treated with 3% Triton X-100 were more confluent and had a normal phenotype compared with HMEC cultured on a BMC treated with 4% sodium deoxycholate, 8 mM CHAPS and 1% SDS. Both 8 mM CHAPS and 1% SDS damaged the BMC to the extent that seeded HMEC were able to infiltrate the damaged sub-basement membrane tissue, showed decreased confluence and an atypical phenotype. The choice of detergents used

for tissue decell- ularization can have a marked effect upon the integrity of the BMC of the resultant bioscaffold.

5.2 INTRODUCTION

The decellularization of tissues for the purpose of utilizing the extracellular matrix (ECM) as a bioscaffold for reconstructive surgical procedures or whole organ engineering involves the use of various enzymes, detergents and mechanical/physical methods[16, 84, 135]. During the process of decellularization, parenchymal cells within the source tissues and organs such as the dermis, small intestine, urinary bladder, liver and lung are destroyed and/or removed[84, 130, 135, 253-255]. However, the less abundant but equally important non-parenchymal cells are also removed in the process. Such cells include the endothelial cells of the resident vascular network structures and any site appropriate epithelial cell populations. The remaining vascular network, devoid of endothelial cells, has been proposed as a potential guide and substrate for revascularization[23, 241, 256, 257]. Therefore, the effects of decellularization methods upon the structure and composition of the basement membrane complex (BMC) are critical for subsequent in-vitro or in-vivo recellularization.

There have been several published methods for decellularizing tissues and generating biologic scaffolds composed of ECM, each of which describes a unique and specific recipe of enzymes and detergents. Commonly used detergents include Triton X-100[131, 241], 3-[(3-cholamidopropyl)dimethylammonio]-1-propanesulfonate (CHAPS)[18], sodium deoxycholate[132], and sodium dodecyl sulfate (SDS)[23, 242-245]. Detergents are able to solubilize cell membranes and dissociate DNA from proteins, making such agents attractive for

the decellularization process. Studies have shown that ionic detergents can be more effective for cellular removal than non-ionic and zwitterionic detergents[40]. However, subjecting tissue to harsh detergents, such as SDS, can disrupt the ECM structure[246], eliminate growth factors[258], and/or denature essential proteins[35].

The present study compared the effects of four commonly used decellularization agents upon the BMC and its ability to support endothelial cells in vitro. The findings have relevance for decellularization strategies used in the production of ECM derived biologic scaffolds and whole organ engineering.

5.3 MATERIALS AND METHODS

5.3.1 Scaffold Preparation and Decellularization

Porcine urinary bladders were obtained from animals (~120 kg) at a local abattoir (Thoma's Meat Market, Saxonburg, PA). Bladders were frozen (>16 h at −80 °C) and thawed completely before use. The BMC and underlying lamina propria were isolated and harvested from the bladders as previously described [50, 253, 259]. The tissue was then placed in 0.02% Trypsin/0.05% EGTA solution for two hours at 37^{o}C with physical agitation to detach cells from the extracellular matrix. Tissue samples were then subjected to either, 3% Triton-X 100 (Sigma-Aldrich), 8 mM CHAPS (Sigma-Aldrich), 4% sodium deoxycholate (Sigma-Aldrich) , 1% SDS (Bio-Rad), or Type I water (non-detergent control) for 24 hours with physical agitation (300 rpm on an orbital shaker). Scaffolds were next rinsed with 1X PBS for 15 min followed by water for 15 min and each repeated. A 24 hour 1X PBS wash followed. Scaffolds were subsequently rinsed with 1X

PBS followed by water for 15 min each and repeated. Lastly, scaffolds were sterilized via gamma irradiation at a dose of 2 x 10^6 RADS.

5.3.2 dsDNA Quantification

Scaffolds were digested in 0.6% Proteinase K solution for at least 24 hours at 50°C until no visible tissue remained. Phenol/Chloroform/Isoamyl alcohol was added and samples were centrifuged at 10,000xg for 10 min at 4°C. The top aqueous phase containing the DNA was transferred into a new tube. Sodium acetate and ethanol was added to each sample and the solution was mixed and placed at -80°C overnight. While still frozen, the samples were centrifuged at 4°C for 10 min at 10,000xg. Supernatant was discarded and all residual alcohol was removed. Pellet was suspended in TE buffer. Double stranded DNA was quantified using Quant-iT PicoGreen Reagent (Invitrogen Corp., Carlsbad, CA, USA) according to the manufacturer's instructions. The dsDNA assay was performed in duplicate, and was performed two times.

5.3.3 Preparation of Urea-Heparin Extracts for Growth Factor Assays

Three hundred (300) mg of ECM powder was suspended in 4.5 ml of urea-heparin extraction buffer. The extraction buffer consisted of 2 M urea and 5 mg/ml heparin in 50 mM Tris with protease inhibitors [1mM Phenylmethylsulfonyl Fluoride (PMSF), 5 mM Benzamidine, and 10 mM N-Ethylmaleimide (NEM)] at pH 7.4. The extraction mixture was rocked at 4^{o}C for 24 hours and then centrifuged at 3,000 g for 30 minutes at 4^{o}C. Supernatants were collected and 4.5

ml of freshly prepared urea-heparin extraction buffer was added to each pellet. Pellets with extraction buffer were again rocked at 4°C for 24 hours, centrifuged at 3,000 g for 30 minutes at 4°C, and supernatants were collected. Supernatants from first and second extractions were dialyzed against Barnstead filtered water (three changes, 80 to 100 volumes per change) in Slide-A-Lyzer Dialysis Cassettes, 3500 MWCO (Pierce, Rockford, IL). The concentration of total protein in each dialyzed extract was determined by the bicinchoninic acid (BCA) Protein Assay (Pierce, Rockford, IL) following the manufacturer's protocol, and extracts were frozen in aliquots until time of assay.

5.3.4 Growth Factor Assays

Concentrations of basic fibroblast growth factor (bFGF),and vascular endothelial growth factor (VEGF) in urea-heparin extracts of dermis samples were determined with the Quantikine Human FGF basic Immunoassay (R&D Systems, Minneapolis, MN), and the Quantikine Human VEGF Immunoassay (R&D Systems). Manufacturer's instructions were followed for both growth factor assays. Each assay for bFGF and VEGF was performed in duplicate, and each growth factor assay was performed two times. Results are reported as mean ± standard error. It should be noted that growth factor assays measured the concentration of each growth factor and did not measure growth factor activity.

5.3.5 Soluble Collagen and Sulfated GAG Quantification

10 mg ECM/ml (dry weight) were enzymatically digested in a solution of 1 mg/ml porcine pepsin (SigmaeAldrich, St. Louis, MO) in 0.01 N HCl under a constant stir rate for 72 h at room temperature. The pH neutralized pepsin digests were diluted and assayed for soluble, triple helical collagen content using the Sircol Collagen Assay (Biocolor Ltd., Carrickfergus, United Kingdom) per the manufacturer's instructions. The pH neutralized pepsin digest were also analyzed for total protein recovered using the BCA protein assay (Pierce). A pepsin buffer solution was used as the negative control and subtracted from the signal. Similarly, 50 mg/ml of powdered ECM in 100 mM Tris (pH 7.5) was digested with 0.1 mg/ml proteinase K (Sigma) at 50 ºC for 24 h with gentle agitation. The proteinase K digests were then assayed for sulfated GAG concentration using the Blyscan Sulfated Glycosaminoglycan Assay (Biocolor Ltd.) per the manufacturer's instructions. All results were normalized to dry weight tissue. Assays were performed in duplicate on three independent samples for each treatment group.

5.3.6 Histologic Staining and Immunolabeling of the BMC

Formalin fixed scaffolds were embedded in paraffin and cut into 5μm sections. Sections were either stained with Hematoxylin and Eosin (H&E), Movat's Pentachrome, or used for immunolabeling. For immunolabeling, slides were manually deparaffinized, placed in Citrate Antigen Retrieval Buffer (10 mM, pH 6), and heated to 95°C for 20 min. Slides were then cooled to room temperature, rinsed in 1X PBS three times for 3 min, placed in humidity chamber to incubate for 1 hr with blocking solution (2% Goat Serum, 1% BSA 0.1% Triton X-100 0.1%

Tween) at room temperature, then incubated overnight at 4°C with anti-collagen I antibody (Sigma-Aldrich, C2456, 1:1000) in blocking solution. Slides were then rinsed with 1X PBS as above, treated with 3% hydrogen peroxide in methanol solution for 30 min, and re-rinsed. Biotinylated secondary antibody Horse Anti-Mouse IgG (Vector Labs, 1:100) was then applied for 30 min. Slides were rinsed as above, ABC solution applied for 30 min in humidity chamber at 37°C, re-rinsed, and 3,3'-diaminobenzidine (DAB, Vector Labs) was applied under microscope. To stain collagen IV (ab6586, Abcam, 1:500), laminin (L9393, Sigma-Aldrich, 1:100), and Collagen VII (C6805, Sigma-Aldrich, 1:10) the same protocol as used for collagen I was applied with an added 0.05% pepsin in 0.01 mM hydrochloric acid for 15 minutes in humidity chamber at 37°C following citrate acid buffer antigen retrieval. Staining for collagen VII also used a blocking solution that contained 4% goat serum and 2% BSA, and a 1 hour hydrogen peroxide incubation time. After DAB staining, all slides were counterstained with hematoxylin, dehydrated and manually coverslipped using standard mounting medium. Images were taken at the luminal interface of the tissue.

5.3.7 Analysis of the ECM Fiber Network of the BMC Luminal Surface

A complete set of fiber network descriptors was collected from SEM images of each BMC including: pore size distribution, node density (number of fibers intersections per μm^2), and fiber diameter. Porosity was described by the mean of the pore size (μm^2) histogram. Automated extraction of these fiber architectural features was achieved with an algorithm, which has been previously described in detail [260]. Briefly, the SEM image was digitally processed by a cascade of steps including equalization with a 3x3 median filter, local thresholding through the

Otsu method, thinning, smoothing, morphological operators, skeletonization, binary filtering for Delaunay network refinement, and ultimately the detection of fiber network architecture and its descriptors. For each treatment group ten images were analyzed.

5.3.8 Quantification of Collagen Fiber Denaturation via SHG

To both visualize and quantify the integrity of the collagen fiber network of the basement membrane, intact samples were imaged enface from the surface of the BMC with an Olympus FV1000 multiphoton system (MPM). The Olympus FV1000 MPM system was operated with Olympus Fluroview software, and was equipped with a Chameleon ultra diode-pumped laser, and a 25x XL Plan N objective with a N.A. of 1.05 and a field of view of 500 um. The excitation wavelength was chosen at 800 nm at a 5% laser transmissivity. The photomultiplier voltage was maintained at 400 V across all samples for subsequent signal intensity analysis. The emission wavelength was received by a filter set to 400±100nm for second harmonic generation signal of collagen. Image scans were performed at a depth of 25 μm, 50 μm, 75 μm, and 100 μm to encompass the BMC with a sampling speed set to 2 μs/pixel with a 2 line Kalman filter. Image sections were then imported into ImageJ for intensity analysis through a background subtraction, and then applying the integrated density function whereby area*intensity. This parameter provides a relative measurement of the SHG signal. It has previously been found that denaturation of collagen fibers results in the destruction of the SHG due to the loss of the noncentrosymmetric crystalline structure at the molecular level[261]. Additional image stacks were acquired for select samples with an incremental z-step of 0.5 μm to a depth of 100 μm for 3D reconstruction and visualization using Imaris software.

5.3.9 Endothelial Cell Seeding and Culture

Sterilized scaffolds were placed with the BMC luminal surface facing up in a 6 well plate. HMECs (a gift from Francisco Candal, Center for Disease Control and Prevention, Atlanta, GA) were cultivated in MCDB-131 medium containing 10% fetal bovine serum, 2 mM L-glutamine, 100 U/mL penicillin and 100 ug/mL streptomycin. MCDB-131 medium was from Invitrogen (Carlsbad, CA); all other reagents for cell growth were from Thermo Fisher Hyclone (Logan, Utah). Cells were grown at 37°C in 5% CO_2 and were harvested for seeding when they were approximately 100% confluent. HMECs were seeded on the BMC surface of each treatment group in triplicate. A total of 1 x 10^6 cells were cultured on each scaffold within a 2cm diameter stainless steel culture ring containing 5 ml of culture medium. Scaffolds were then placed in an incubator at 37°C in 5% CO_2 for 24 hrs of culture, at which time the culture rings were removed and the seeded scaffolds were transferred to a new 6 well plate with fresh media. Culture media was then replaced on day 2 and day 5. After 7 days of culture, seeded scaffolds were fixed in 10% neutral buffered formalin, gluteraldehyde, or liquid nitrogen for subsequent analysis.

5.3.10 Immunolabeling of Seeded HMECs

After 7 days of culture samples were fixed in formalin for at least 24 hours, embedded in paraffin and cut into 5 μm transverse sections. Sections were either stained with Hematoxylin and Eosin (H&E), or used for Ki67 and integrin β-1 immunolabeling. Slides for immunolabeling were deparaffinized and rehydrated with decreasing concentration of alcohol and water. Antigen retrieval was performed with Citrate Antigen Retrieval Buffer (10mM, pH6). Retrieval buffer

was heated until a boiling point was reached, slides were immersed, removed from heat, and cooled for 20 min. Slides were washed with 1X PBS 3x for 3 min each. 0.05% Pepsin digest was applied to samples for 15 min minutes in humidity chamber at 37°C. Blocking solution was applied (2% Goat serum 1% BSA 0.1% Triton 0.1% Tween) for 1hr at room temp. Slides were washed with 1X PBS as above. Rabbit anti-integrin β-1 (Abcam, AB52971, 1:1000) in blocking buffer was applied to each sample. Rabbit anti-Ki67 (Abcam, AB15580, 1:100) in blocking was applied to each sample on a separate slide. The samples were then incubated at 4°C overnight. Slides were washed with 1X PBS as above. Alexa-Flour 594 goat anti rabbit (Invitrogen, 1:200) was applied for 1 hr at room temperature for the anti-integrin β-1sample. Alexa-Flour 488 goat anti rabbit (Invitrogen, 1:200) was applied for 1 hr at room temperature for the anti-Ki67 samples. Slides were washed with 1X PBS as above. Coverslips were added with anti-FADE containing DAPI (Invitrogen, P36931). Analysis of apoptosis in tissue sections was performed with a DeadEnd™ Colorimetric TUNEL System (Promega Corp. PR-G7130) according to the manufacturer's specifications.

5.3.11 Semi-Quantitative Scoring of HMECs

Fixed seeded scaffolds were embedded in paraffin and cut into 5µm sections. Sections were stained with H&E and images were taken of the HMECs. The images were then evaluated by five blinded investigators using a standardized system as previously described [258]. Criteria included cellular infiltration, confluence, and cell phenotype. Associated descriptions of these metrics can be found in Table 4 and graphical examples in supplementary Fig. 3 All aspects were evaluated on a scale of 0 to 100.

Table 4. Definitions and descriptions of the metrics used for semi-quantitative scoring of the HMEC.

Confluence (%)	The confluence score is defined as the percentage of the BMC surface covered with cells. A score of 100 would indicate a fully coated surface with adjoining cells and no gaps.
Phenotype (%)	They phenotype score is defined as the percentage of healthy appearing cells. A healthy cell is flat and fully adhered to surrounding tissue and other cells. An unhealthy is round and not adhered to the surrounding tissue or other cells.
Infiltration (%)	The infiltration score is defined as the percentage of the total depth in which cells have migrated within the tissue. For example, if cells are found halfway into the tissue, this would correspond to an infiltration score of 50.

5.3.12 Scanning Electron Microscopy

SEM was used to examine the surface topology of urinary bladders treated with each detergent. Scanning electron micrographs were also taken of the HMEC seeded scaffolds after 7 days of culture on each sample. Samples were fixed in 2.5% glutaraldehyde in 1X PBS, cut into blocks of approximately $8mm^3$, and washed thoroughly in 1X PBS for three times at 15 minutes each. Samples were then fixed in 1% OsO_4 in 1X PBS for 15 minutes each, dehydrated in graded series of alcohol (30%-100%) baths for 15 minutes each. Samples were then critically point dried with hexamethyldisiloxane mounted on studs, sputter coated, and stored in a desiccator until imaged. SEM images were captured using a JEOL 6335F Field Emission SEM with backscatter detector.

5.3.13 Statistical Analysis

Results are shown as averages ± standard error. A one-way analysis of variance was performed to determine whether a particular detergent group was significantly different, followed by a post-hoc Dunnets test to determine whether any detergent treatment was different from the non-detergent control group ($p<0.05$).

5.4 RESULTS

5.4.1 dsDNA Content

No visible nuclei were observed by imaging of Hematoxylin and Eosin stained sections for any of the detergent groups **(Figure 4C-G)**. Double stranded DNA quantification of the scaffolds showed that each detergent caused markedly greater removal of the dsDNA compared to treatment with Type I water **(Figure 4B)**. Scaffolds treated with 1% SDS contained less dsDNA than those treated with 8 mM CHAPS ($P<0.05$) or 4% sodium deoxycholate ($P<0.05$). 1% SDS was the only detergent able to meet a previously established decellularization criterion of 50 ng dsDNA/mg tissue **(Figure 4F)** [135].

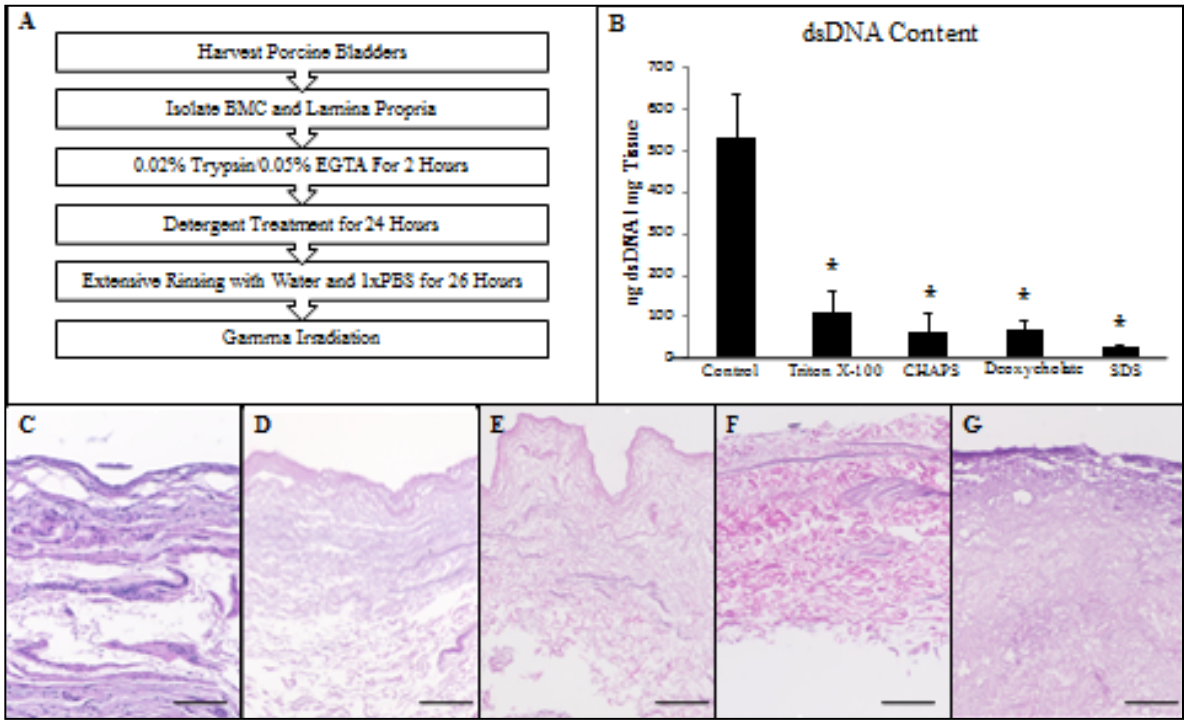

Figure 4. (A) Overview of the process used to prepare the BMC scaffolds. (B) Double-stranded DNA quantification of the scaffolds treated with each detergent showed significant removal compared with those treated with Type I water. H&E stained sections of BMC scaffolds prepared with (C) no detergent, (D) Triton X-100, (E) CHAPS, (F) sodium deoxycholate and (G) SDS. No signs of nuclear material are visible for any of the detergent groups. Scale bar represents 200 μm.

5.4.2 Collagen and Sulfated GAG Content

While scaffolds treated with 3% Triton X-100, 8 mM CHAPS, and 4% sodium deoxycholate retained a soluble collagen content similar to that of the water control, treatment with 1% SDS resulted in a significant loss of detectable soluble collagen **(Figure 5B)**. The assay used detected only soluble collagen, therefore non-soluble remnant collagen may still be present. This finding

suggests that detergent treatment with SDS resulted in either a decrease in soluble collagen present or modification of the molecular structure of this collagen to the point of insolubility. The greater amount of soluble collagen for Triton X-100 compared to the water control is an artifact of the normalization to dry weight. More specifically, the relative density of ECM to total weight is increased after decellularization for Triton X-100 after removal of cellular content compared to the water control. Scaffolds treated with 3% Triton X-100, 4% sodium deoxycholate, and 8mM CHAPS retained GAGs similar to that of the water control, while scaffolds treated with 1% SDS retained a lesser amount of detectable GAGs than the water control **(Figure 5C)**.

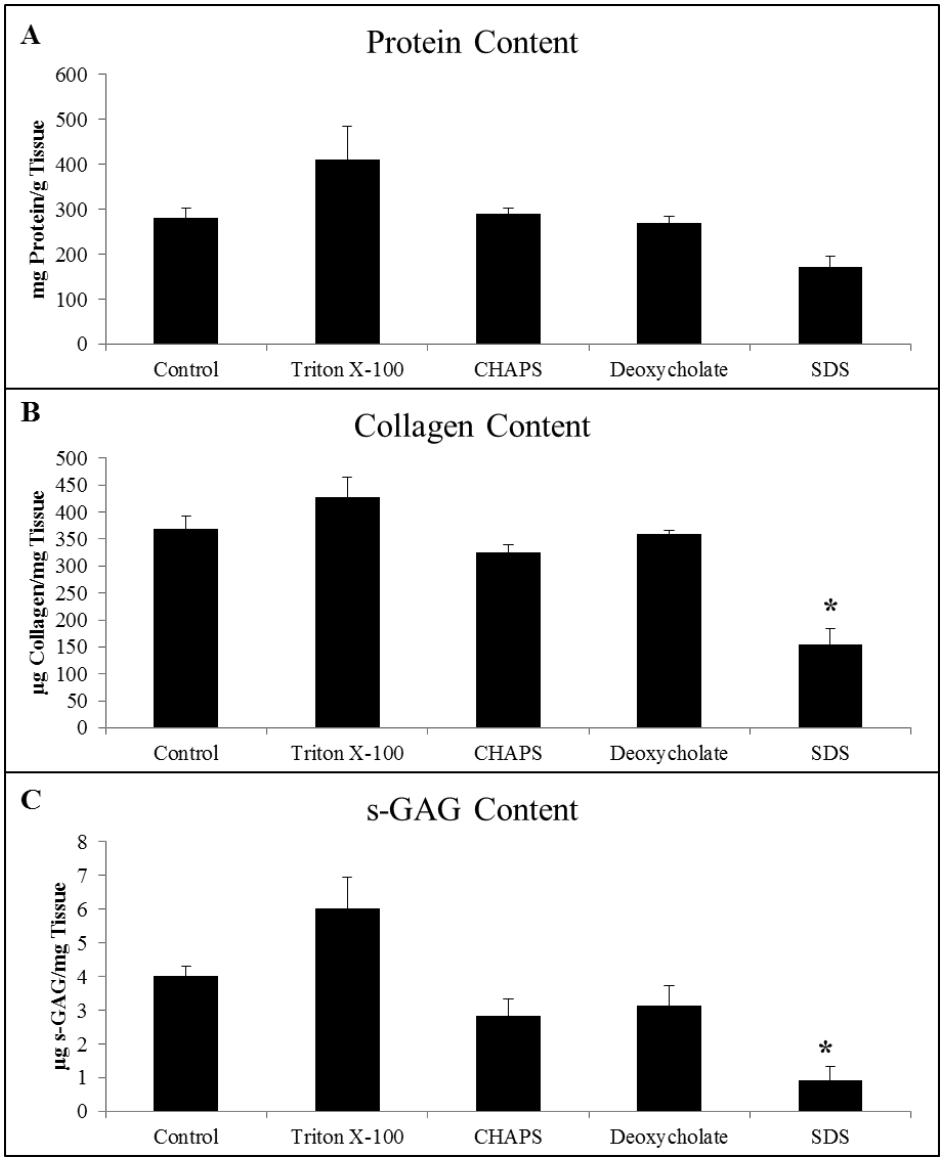

Figure 5. Biochemical assays to quantify soluble protein from (A) pepsin extract, (B) collagen and (C) sulfated GAG normalized to dry weight tissue. Graph shows mean ± standard error, and ⁄ indicates significance at $p < 0.05$ compared with the water control group.

5.4.3 Immunolabeling

The no detergent control showed positive staining at the basement membrane surface of collagen I, collagen IV, collagen VII, and laminin **(Figure 6A)** as previously reported[67]. All scaffold treatments were positive for collagen I staining **(Figure 6A)**. No treated scaffolds stained positive for collagen IV, VII, or laminin except for Triton X-100 and sodium deoxycholate treated scaffolds, both of which had positive expression of collagen IV **(Figure 6A)**. However, this positive staining was not localized to the surface as would be expected for an intact basement membrane.

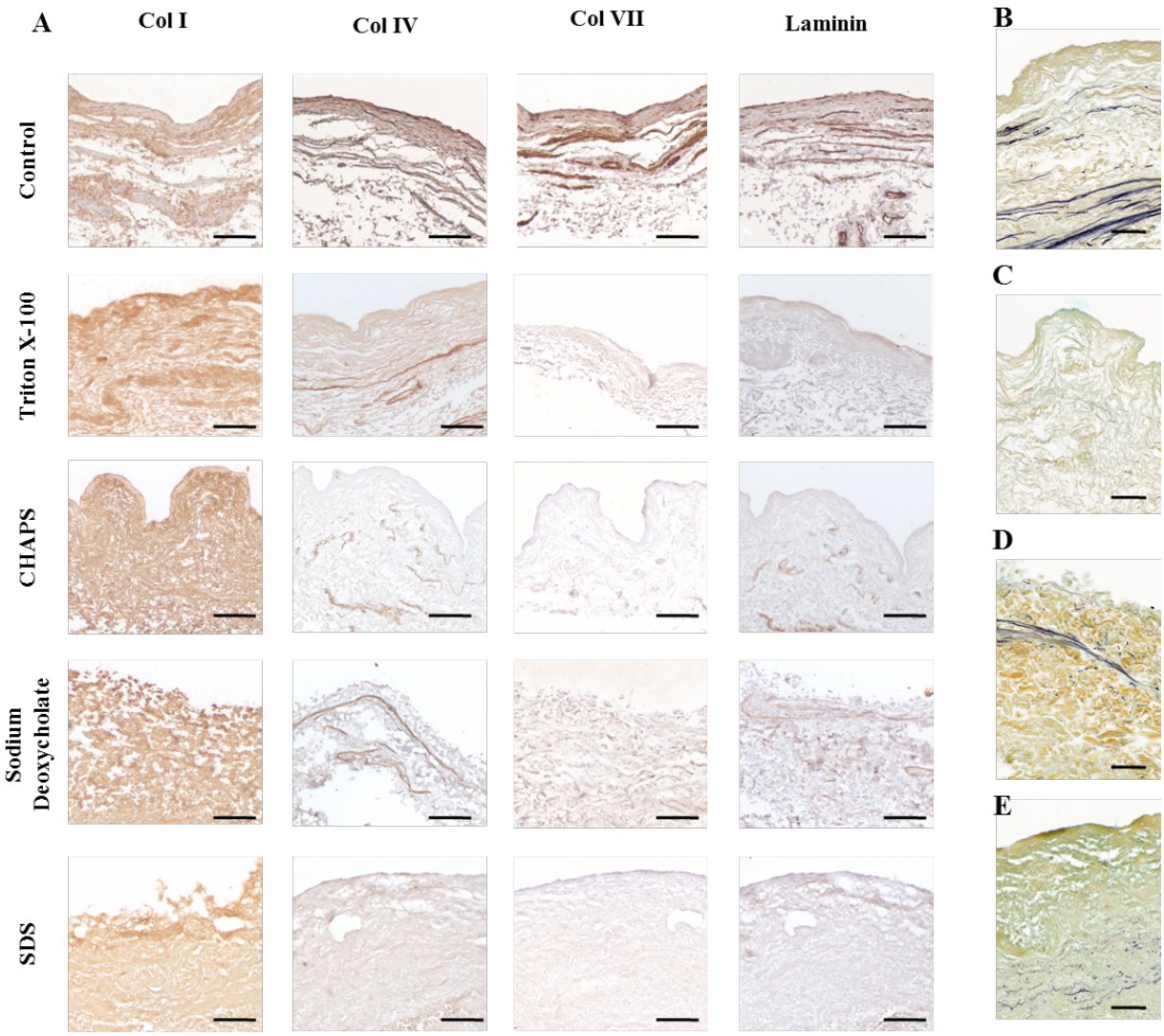

Figure 6. (A) Immunolabeling of collagen I, collagen IV, collagen VII and laminin for BMC scaffolds prepared with water, Triton X-100, CHAPS, sodium deoxycholate and SDS. (B) Movats Pentachrome stains for Triton X-100, (C) sodium deoxycholate, (D) CHAPS and (E) SDS, where yellow, blue and purple represent collagen, proteoglycans and GAG, and elastin, respectively. Scale bar represents 100 μm.

5.4.4 Movats Stain

Scaffolds treated with Triton X-100 and sodium deoxycholate retained elastin fibers, whereas CHAPS had no visible elastin fibers and SDS had only a small amount of thin fragmented fibers. GAGs were visible in both Triton X-100 and CHAPS while not visible for sodium deoxycholate and SDS confirming the observations from sulfated GAG quantification **(Figure 6B)**.

5.4.5 Analysis of the BMC Fiber Network

Quantitative assessment of the SEM of the BMC luminal surface showed that treatment without a detergent, with 3% Triton X-100, or with 4% sodium deoxycholate retained an intricate fiber network **(Figure 7 B, C& E)**. However, treatment with 8 mM CHAPS and 1% SDS resulted in an amorphous structure lacking distinct fibers **(Figure 7 D&F)**. The fiber diameter was not different with treatment of Triton X-100 or sodium deoxycholate compared to the no detergent control **(Figure 7I)**. While there was a slightly smaller pore size for Triton X-100 and sodium deoxycholate compared to the no detergent control**(Figure 7J)**, and a higher node density for Triton X-100 these changes were small compared to previously published variations**(Figure 7K)** [130, 260] . Thus, treatment with Triton X-100 and sodium deoxycholate were able to retain the original configuration of the fiber network. Multiphoton imaging confirmed a loss of a distinct fiber network for SDS compared to Triton X-100 beneath the surface of the sample **(Figure 7A-C)**. The lower collagen signal intensity for SDS indicates fiber denaturation **(Figure 8D)**. The higher signal intensity value for triton x-100 and sodium deoxycholate compared to the water

control may be due an increase in the density of ECM constituents due to loss of cellular material. These values provide a relative comparison of the effects of detergent treatments that are consistent in finding with visual observations of both SHG volumes and SEM images.

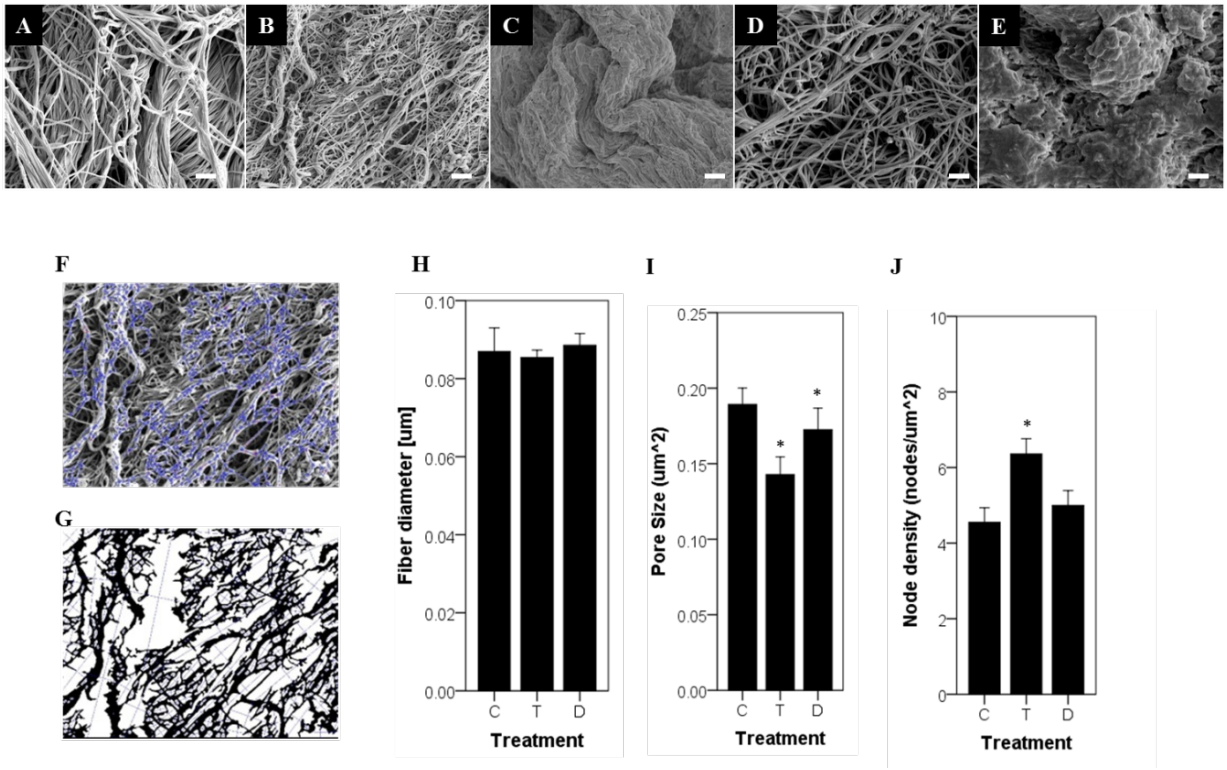

Figure 7. SEM of the BMC fiber network for scaffolds prepared with (A) water as a no-detergent control, (B) Triton X-100, (C) CHAPS, (D) sodium deoxycholate and (E) SDS. Scale bar represents 1 μm. (F, G) An automated algorithm was applied to quantify fiber network parameters of (H) fiber diameter, (I) pore size and (J) node density [24]. Graph shows mean ± standard error, and ⁄ indicates significance at $p < 0.05$ compared with the water control group. C, T and D denote the water control, Triton X-100 and sodium deoxycholate, respectively.

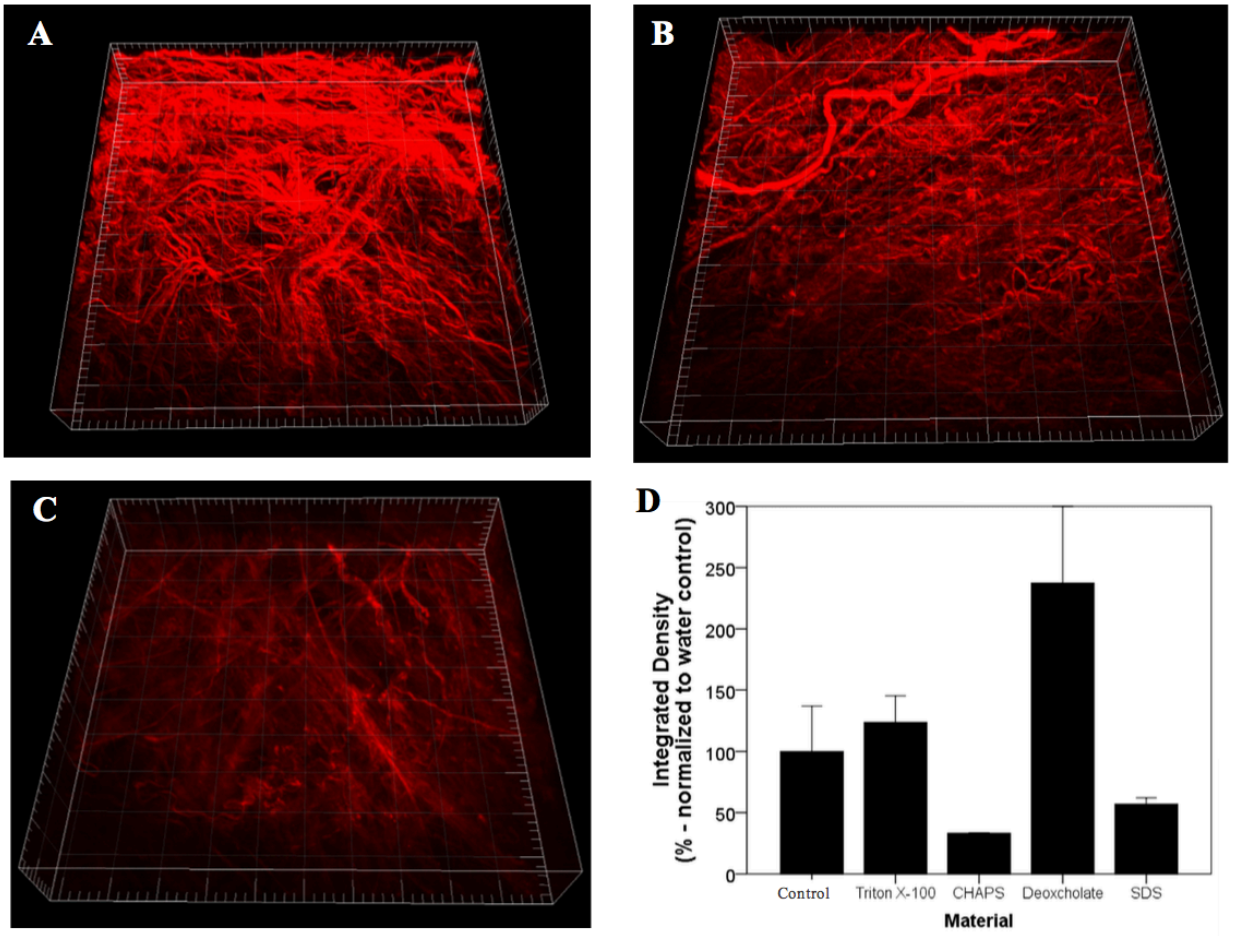

Figure 8. Three-dimensional rendering of collagen fiber network from SHG signal with two photon microscopy for BMC scaffolds prepared with (A) water, (B) Triton X-100 and (C) SDS. Major tick represents 50 μm, whereby the total length and depth is 500 μm and 100 μm, respectively. (D) An integrated density integrity was applied and normalized to the no-detergent control. Graph shows mean ± standard error, and ⁄ indicates significance at $p < 0.05$.5.3.6 Semi-Quantitative HMEC Scoring

5.4.6 Semi-quantitative HMEC Scoring

HMECs cultured on the BMC prepared with 3% Triton X-100 had a similar level of confluence, infiltration depth, and phenotype compared to cells cultured on scaffolds treated with type I water (control). These HMECs were characterized by a flat morphology **(Figure 9B)**. HMECs cultured on the BMC prepared with 8 mM CHAPS were less confluent, had a greater infiltration depth, and an atypical phenotype compared to HMECs cultured on the control **(Figure 9)**. HMECs cultured on scaffolds prepared with 4% sodium deoxycholate were less confluent, had a similar infiltration depth, and an atypical phenotype compared to cells cultured on a no detergent control **(Figure 9)**. HMECs cultured on scaffolds prepared with 1% SDS had a similar percentage of confluence, similar infiltration depth, but a less normal phenotype compared to cell cultured on a no detergent control **(Figure 9)**.

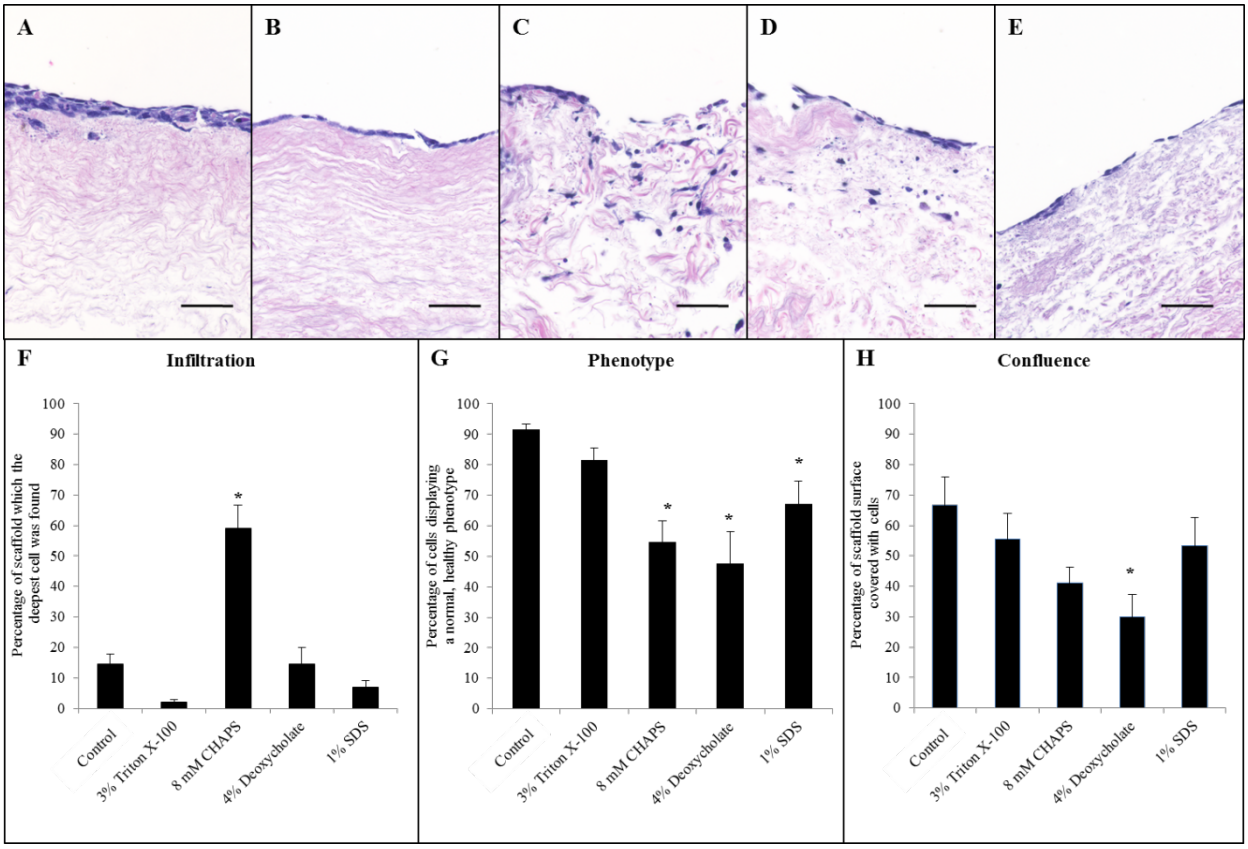

Figure 9. H&E stained sections of endothelial cells cultured on the BMC of porcine urinary bladders subjected to (A) water, (B) Triton X-100, (C) CHAPS, (D) sodium deoxycholate and (E) SDS for 24 h. Semi-quantitative analysis of (F) cellular infiltration, (G) phenotype and (H) level of confluence was performed by five blinded scores. Scale bar represents 50 μm. Graph shows mean ± standard error, and ⁄ indicates significance at $p < 0.05$.

5.4.7 Integrin β-1 Expression, Ki67, and TUNEL

HMECs cultured on the BMC prepared with 8 mM CHAPS and 1% SDS had a lower number of cells stain positive for integrin β-1 compared to HMECs cultured on the BMC not subjected to a detergent **(Figure 10)**. HMECs cultured on the BMC prepared with 3% Triton X-100 and 4%

sodium deoxycholate had a similar percentage of cells expressing integrin β-1 compared to cells cultured on the no detergent control tissue **(Figure 10)**. The percent of cells positive for Ki67 was below 3% for all groups and no significant differences were seen when comparing to the control **(Figure 11)**. Minimal TUNEL-positive cells were found on the BMC prepared with 3% Triton X-100 **(Figure 16)**.

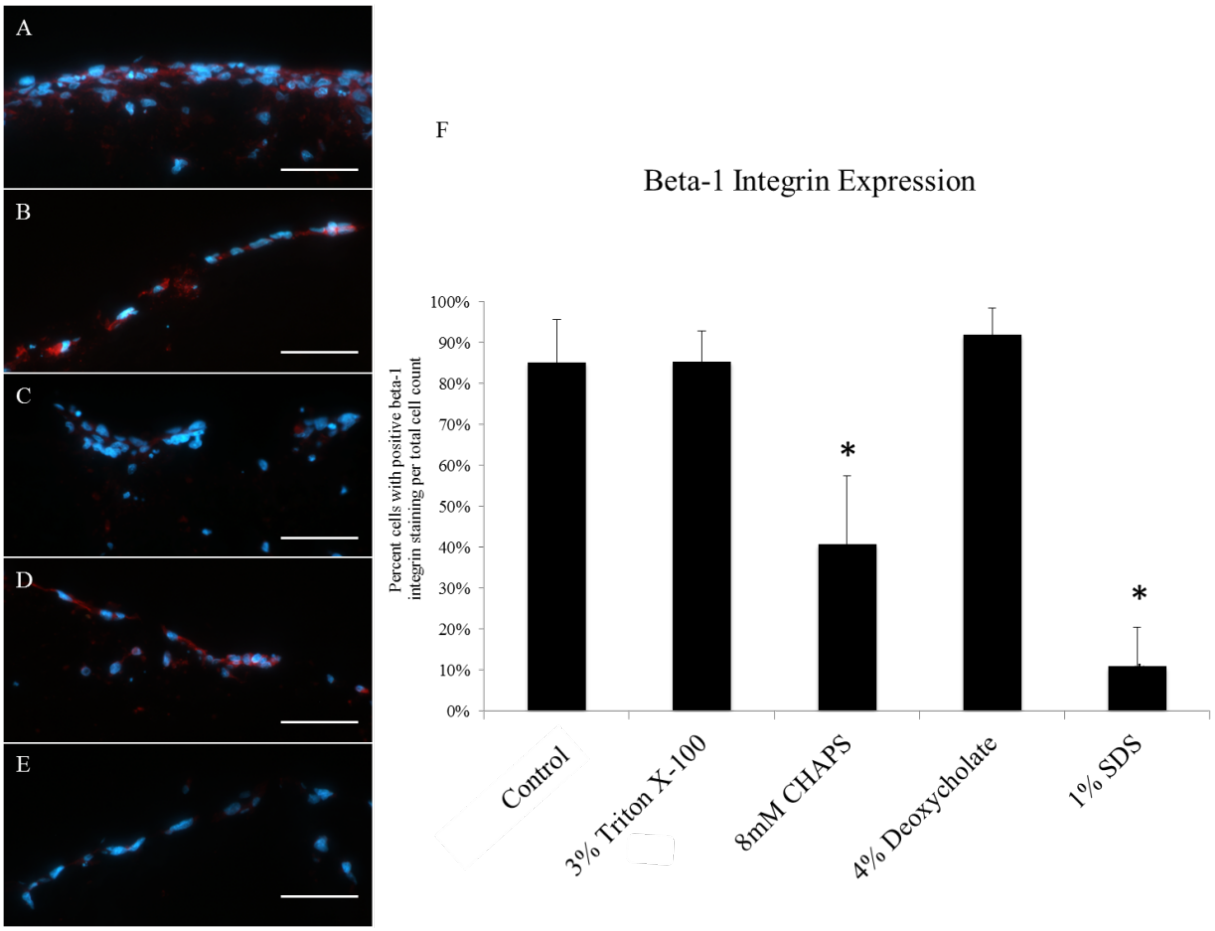

Figure 10. Immunofluorescent images of integrin b-1 (red) and DAPI (blue) of HMEC cultured on the BMC of porcine urinary bladders exposed to (A) water, (B) Triton X-100, (C) CHAPS, (D) sodium deoxycholate and (E) SDS for 24 h. (F) Percentage of cells positive for integrin b-1 was determined for each group. Scale bar represents 50 lm. Graph shows mean ± standard error, and ⁄ indicates significance at $p < 0.05$.

5.4.8 SEM of Seeded Endothelial Cells

SEM images of HMECs cultured on the BMC prepared with 3% Triton X-100 are similar to the no detergent control in terms of cell morphology and coverage of the BMC. SEM images of

seeded scaffolds prepared with 4% sodium deoxycholate showed areas of endothelial cell coverage as well as exposed ECM. 8 mM CHAPS and 1% SDS, however, showed greater area of exposed ECM and less endothelial cell coverage **(Figure 11)**.

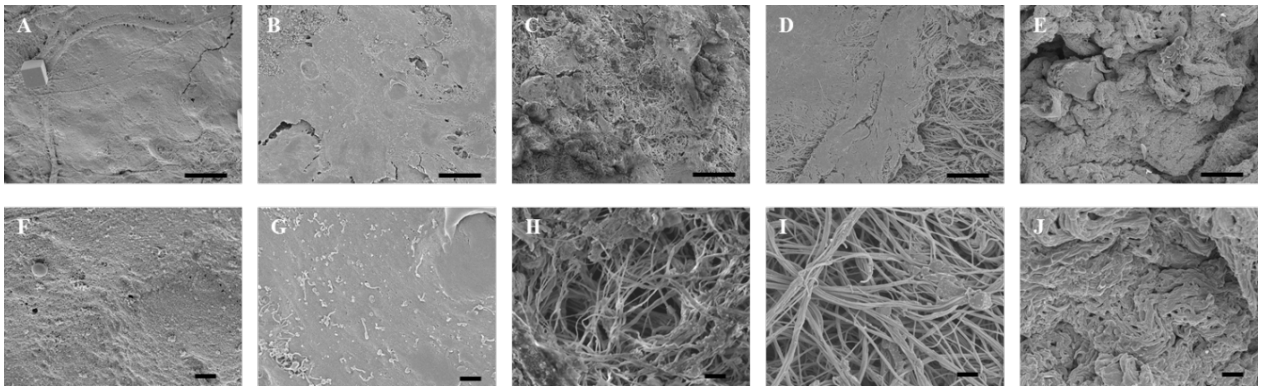

Figure 11. SEM images (2000x) of HMEC cultured for 7 days on BMC scaffolds prepared with (A) water, (B) Triton X-100, (C) CHAPS, (D) sodium deoxycholate and (E) SDS. Scale bar represents 10 lm. SEM images (10,000x) of HMEC cultured for 7 days on BMC scaffolds prepared with (F) water, (G) Triton X-100, (H) CHAPS, (I) sodium deoxycholate and (J) SDS. Scale bar represents 1 μm.

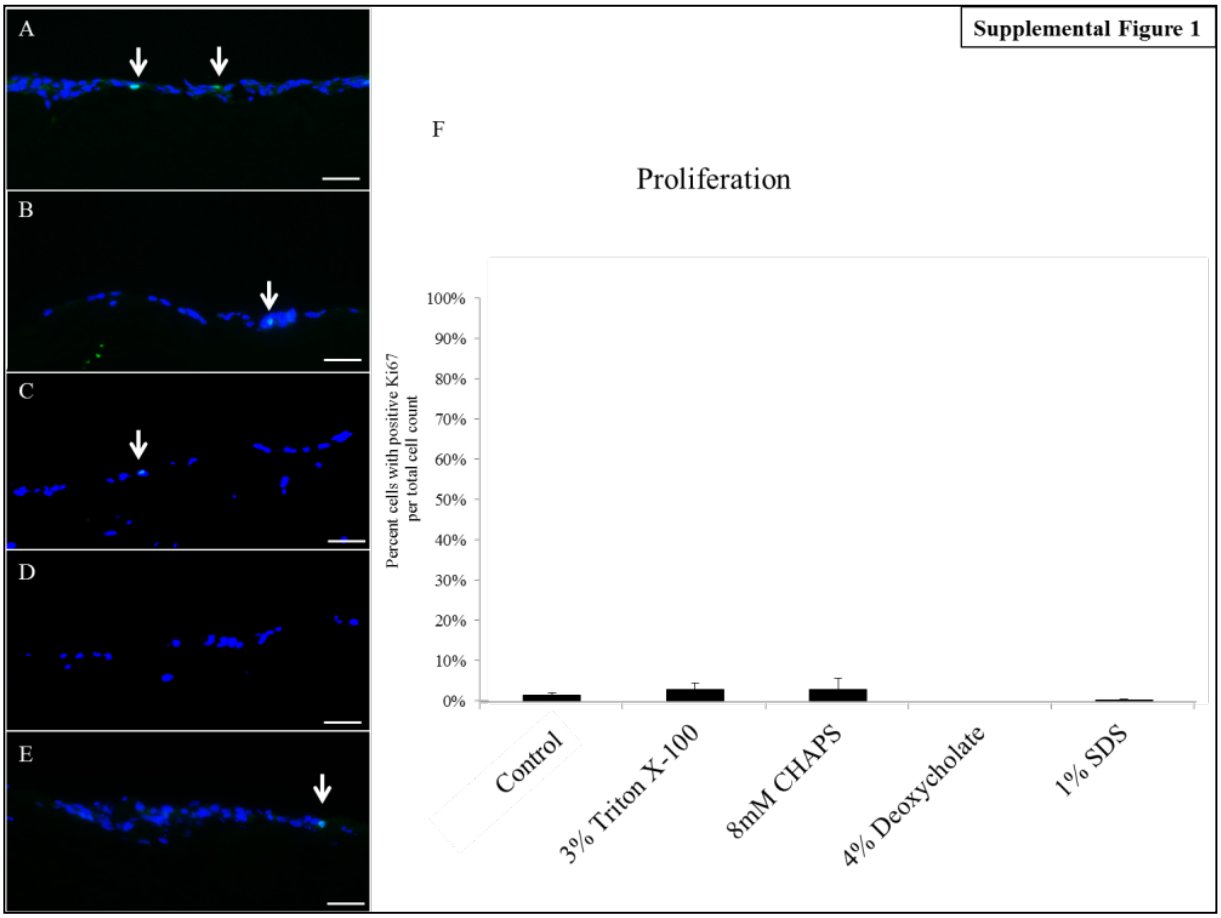

Figure 12. Immunofluorescent images of Ki-67 positive cells (green) and DAPI (blue) of HMEC cultured on the BMC of porcine urinary bladders exposed to (A) water, (B) Triton X-100, (C) CHAPS, (D) sodium deoxycholate and (E) SDS for 24 h. Percentage of cells positive for Ki-67 was determined for each group (F). Scale bar represents 50 mm. Graph shows mean ± standard error, and * indicates significance at $p<0.05$.

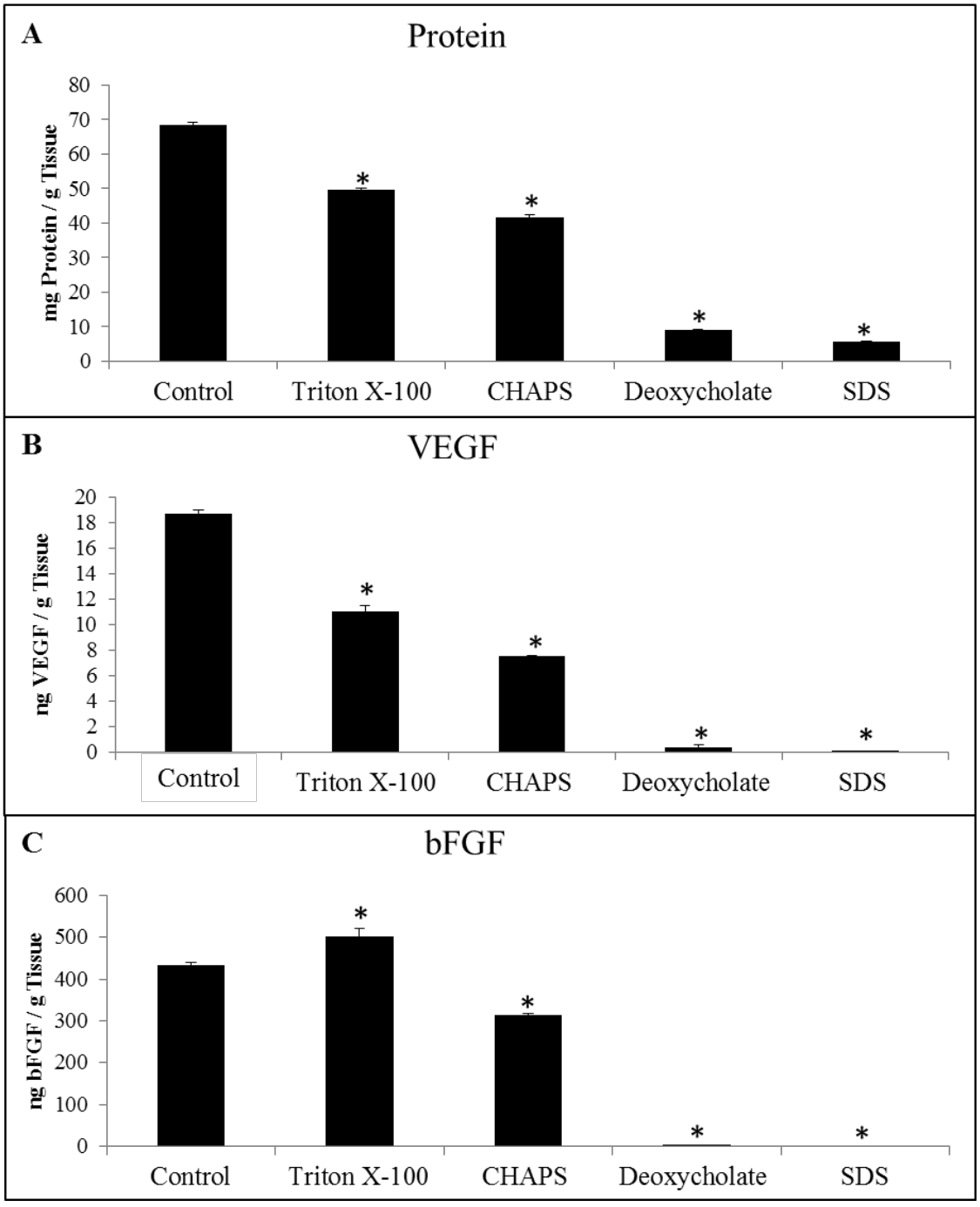

Figure 13. Biochemical assays to quantify (A) soluble protein, (B) VEGF and (C) bFGF normalized to dry weight tissue. Graph shows mean ± standard error.

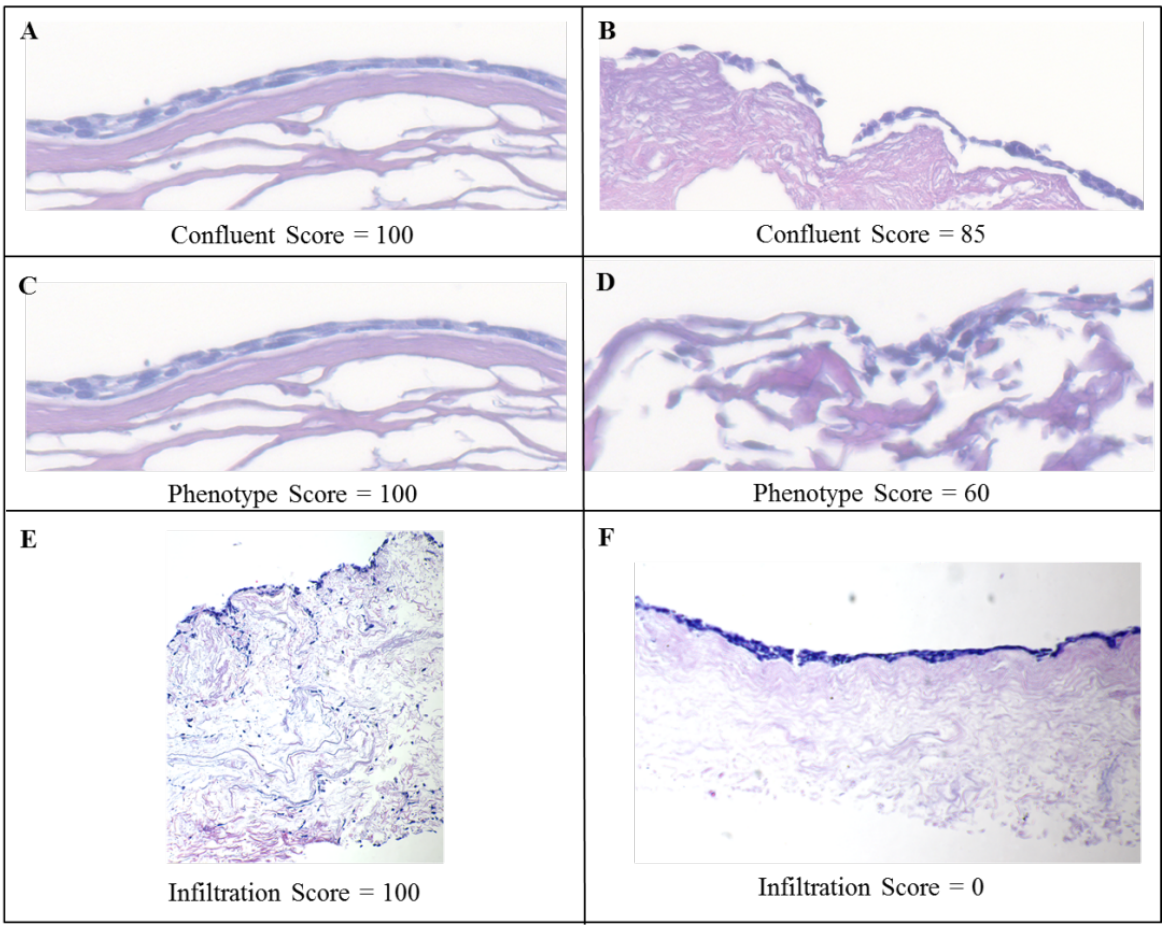

Figure 14. Graphical examples of the semi-quantitative scoring of the HMEC. H&E images were evaluated by five blinded investigators using a standardized system. Criteria included confluence, phenotype and infiltration. The confluence score is defined as the percentage of the BMC surface covered with cells. A score of 100 would indicate a fully coated surface with adjoining cells and no gaps (A). A score of 85 indicates 15% of the BMC surface is absent of cells, as in image (B). They phenotype score is defined as the percentage of healthy appearing cells. A healthy cell is flat and fully adhered to surrounding tissue and other cells (C). An unhealthy cell is round and does not adhere to the surrounding tissue or other cells. Approximately 40% of the cells in image D appear unhealthy. The infiltration score is defined as the percentage of the total depth in which cells have migrated within the tissue. For example, in

image (E), cells are found throughout the entire depth of the scaffold. Thus, image (E) would correspond to an infiltration score of 100. The opposite can be said about image (F), where no cells are infiltrating the scaffold. Therefore, image (F) corresponds to a score of 0.

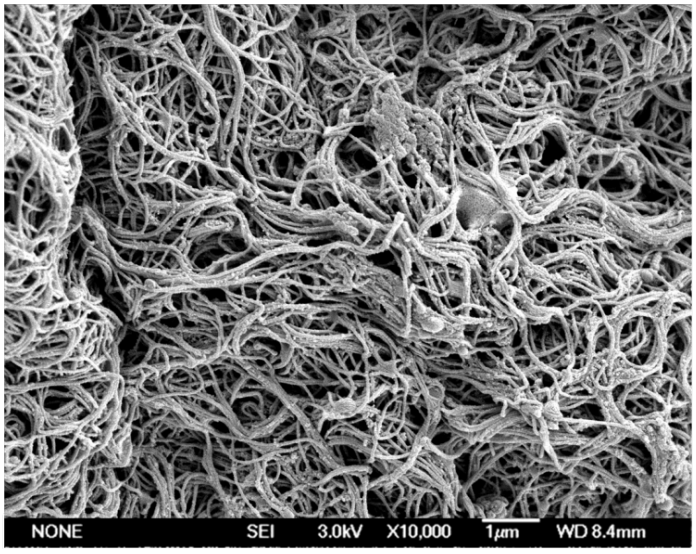

Figure 15. SEM image of a BMC fiber network where cells were physically removed and no chemical treatments were used.

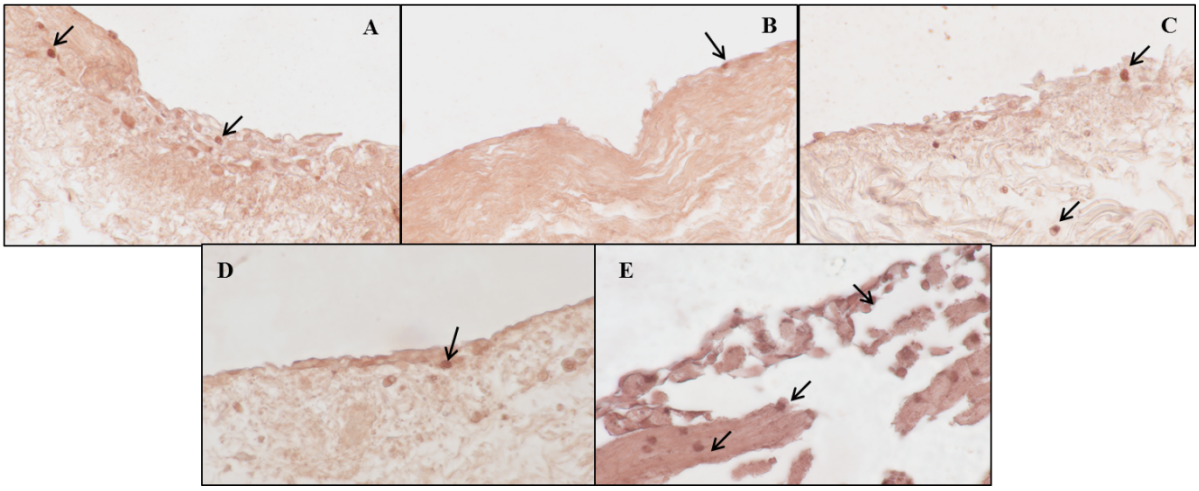

Figure 16. TUNEL staining of HMEC cultured on the BMC of porcine urinary bladders exposed to (A) water, (B) Triton X-100, (C) CHAPS, (D) sodium deoxycholate and (E) SDS for 24 h. Few TUNEL-positive cells were found on the BMC exposed to Triton X-100. Scale bar represents 50 µm.

5.5 DISCUSSION

Thorough decellularization of tissues and organs is essential for promoting a constructive remodeling host response when such decellularized structures are used as therapeutic bioscaffolds [55]. If a tissue is not thoroughly decellularized and residual cellular material is present, the in-vivo remodeling response is characterized by chronic inflammation, fibrotic encapsulation, and scar tissue formation [53, 55, 142]. The basement membrane is one of the first extracellular matrix structures made by the developing embryo with its major constituent laminin-111 synthesized at the eight cell stage[262]. This basement membrane is the first matrix structure with which embryonic stem cells interact and represents a key biosignal for separating endoderm from ectoderm; thus, it is logical that the BMC can represent an important structure in

a bioscaffold composed of ECM. Scaffolds containing a BMC are used in a variety of pre-clinical and clinical applications[153, 263-271]. Some of these scaffolds are seeded with cells before use[272-274]. Examples of ECM scaffolds with a BMC structure include several dermal ECM products such as Alloderm™ and Strattice®, urinary bladder matrix such as MatriStem™, and virtually all three dimensional whole organ scaffolds such as liver[131, 242, 257, 275-277], lung[243, 245, 255] and kidney[136, 244, 278-280]. Therefore, the results of the present study have relevance for a variety of biomaterial applications involving the use of ECM scaffold materials.

Four detergents commonly used for decellularization of tissues and organs were systematically evaluated and compared for their effect on the BMC and the ability of the resulting BMC to support human microvascular endothelial cells in vitro. The detergents investigated were 3% Triton X-100, 4% sodium deoxycholate, 8 mM CHAPS, and 1% SDS. The detergents and their respective concentrations were selected because of their frequent use as decellularization agents and their different chemical characteristics [1]. All detergents facilitate cell lysis and solubilize the released hydrophobic proteins through the formation of micelles. Triton X-100 is non-ionic containing an uncharged hydrophilic head group and disrupts lipid–lipid and lipid–protein interactions, while leaving protein–protein interactions intact. Non-ionic detergents are considered a non-denaturant and are widely used in the proteomics field for isolating membrane proteins in their biologically active form [281-283]. In contrast, sodium deoxycholate and SDS are anionic detergents containing a net negatively charged hydrophilic head group that can solubilize cytoplasmic and nuclear membranes, denature ECM proteins, and disrupt native tissue structure. SDS contains a straight hydrocarbon chain whereas sodium deoxycholate contains a more complicated rigid steroidal structure. CHAPS is zwitterionic,

contains a rigid steroid ring structure, and has properties of both non-ionic and anionic detergents while containing a net charge of zero. Therefore, it is not surprising that these detergents each have distinctly different effects on the BMC. Results of the present study show that these detergent specific effects change not only the ultrastructure and composition of the BMC, but also the behavior of seeded endothelial cells.

In its native state, the BMC defines the spatial relationships among various populations of cells, and influences cell behavior. For ECM scaffold materials that have a BMC on one surface but not the opposite surface (i.e., the material has a "sidedness"), it has been shown HMECs seeded on the non-BMC side invade below the surface of the material and populate the underlying connective tissues. In contrast, HMECs seeded on the BMC will form confluent layers on, but will not invade, the intact surface of the BMC[259]. Results of the present study are consistent with these previous findings. Of note however, the present study also shows that tissue exposed to SDS and CHAPS as part of the decellularization process is left with a BMC upon which the HMECs are less confluent, can migrate through the BMC into the subjacent tissue, and show an atypical phenotype compared to those seeded on an undamaged BMC. These findings, combined with the SEM results, altered collagen fiber organization, and loss of GAGs lead to the unavoidable conclusion that the ultrastructure and composition of the BMC are negatively affected when exposed to SDS and CHAPS. This conclusion, however, must be limited to the specific concentrations and exposure times investigated in the present study. These timeframes and concentrations were chosen because of their relatively common use. It is also unknown whether these findings will apply to tissues with a BMC other than the urinary bladder.

The compositional and structural complexity of the BMC is noteworthy [259]. The BMC contains laminin-111, collagen IV, heparan sulfate proteoglycan, entactin/nidogen, and several

growth factors arranged in a three dimensional ultrastructure which promotes cell adhesion, growth, migration, and invasion. This complexity provides a rational explanation for the potent biological activity of the BMC, and a plausible explanation, in fact expectation, for the finding that decellularization processes such as detergent exposure affect cell:matrix interactions. It is likely that cells interact with multiple components within the matrix. Components such as laminin-111, collagen IV, heparan sulfate proteoglycan, and entactin interact with adjacent cells via integrin receptors and in particular with integrins containing the β1 subunit. Exposure of the BMC to 8 mM CHAPS and 1% SDS decreased the number of cells staining positive for integrins containing the β1 subunit. These receptors regulate the cellular cytoskeleton and cell behavior. Furthermore, many of the major components, such as laminin-111, have multiple active sites for binding to cell surface receptors or other ECM components. Integrins are critical for cellular adhesion to the matrix and can induce either proliferative or differentiation responses. These factors emphasize the importance of understanding the effects of variables such as detergent exposure upon the subsequent biologic activity of materials composed of ECM derived by decellularization of source tissues, particularly when the resultant ECM has a BMC component.

Differences in scaffold surface fiber organization and evidence of collagen fiber denaturation were apparent from both SEM inspection and the results of automated image algorithms. SDS and CHAPS caused marked alterations of collagen fiber architecture while Triton X-100 and sodium deoxycholate were better tolerated and showed the surface of the BMC maintained an appearance that more closely resembled that of the no detergent control. These structural changes and the associated changes in the ligand landscape provide insight into the results of the cell seeding experiments. When HMECs were cultured on porcine urinary bladder basement membrane exposed to the chosen detergents, clear differences were seen in cell

morphology, confluence, infiltration depth, and integrin β-1 expression. Findings of the present study provide useful information for the rational design of decellularization protocols for various tissues and organs.

5.6 CONCLUSIONS

The choice of detergent used for the decellularization of a tissue or organ is an important factor in the preparation of an ECM scaffold for therapeutic applications. Each detergent, depending on its chemical characteristics, has unique and distinct effects on ECM composition and structure. Less disruptive detergents, such as Triton X-100 or other non-ionic detergents are preferred for maintaining the native BMC structure and composition compared to more harsh detergents, such as SDS, which can denature essential ligands and proteins within the BMC. The disruption or denaturing of the native BMC architecture can negatively impact the interaction of cells with the scaffold. The results of this study can aid in the formulation of tissue and organ decellularization protocols such that the native biological activity of the resulting extracellular matrix scaffold is maximally preserved.

6.0. SURFACE MOLECULAR FUNCTIONALITY OF BIOLOGIC SCAFFOLDS TREATED WITH VARIOUS DECELLULARIZATION AGENTS

6.1 ABSTRACT

Decellularization of tissues and organs is a successful platform technology for creating scaffolding materials for organ engineering and regenerative medicine applications. It has been suggested that the success of these materials upon implantation is due to the molecular signals provided by the remaining scaffold extracellular matrix (ECM) components presented to probing cells in vivo as they repopulate the surface. Detergents are frequently used to generate these biologic scaffolds composed of ECM due to their ability to solubilize cell membranes and dissociate DNA from proteins. However, the effect of detergent treatment on the surface molecular functionally of biologic scaffolds has yet to be investigated.

In the described study, decellularized matrices were created from market weight porcine bladders and subjected to decellularization agents commonly used for whole organ perfusion decellularization. The decellularized matrices were imaged using scanning electron microscopy of the surfaces to provide insight into the surface topography of the decellularized tissue following exposure to each decellularization agent. Time of flight secondary ion mass spectroscopy (ToF-SIMS) was utilized to characterize the surface molecular functionality of the basement membrane following detergent exposure. Principle component analysis of the positive and negative ion spectra highlighted high mass peaks associated with detergent fragments observed on the scaffolds exposed to SDS and deoxycholate. A phosphocholine peak, indicative of cell membrane, was observed in all samples, but to a greater extent with scaffolds not exposed

to a detergent. These results demonstrate the suitability of the ToF-SIMS technique to detect detergent fragments present in decellularized biological scaffolds. This study also demonstrates the potential of ToF-SIMS to be used as a criteria used for assessing extent of decellularization. Characterization of the effects of detergent exposure on BMC structure, composition and surface molecular functionality is critical for developing successful in vitro and in vivo recellularization strategies for engineering whole organ constructs.

6.2 INTRODUCTION

Decellularized tissue matrices are widely used for tissue engineering and regenerative medicine [67, 228, 284, 285]. It is suggested that their success is due to embedded biospecific signals found within their protein structures. These materials have been created from a variety of source tissues both allogeneic and xenogeneic [84]. The extracellular matrix (ECM) proteins, which comprise the bulk of these materials, are highly evolutionarily conserved [286-288]. The process of host remodeling of a biologically derived scaffold is dependent upon the immediate and subsequent events that occur at the surface of the material following in vivo implantation. For whole organ engineering, the ability of the scaffold to support engraftment and proliferation of seeded cells is also dependent upon maintaining a favorable surface of the material that is not damaged and prevents cellular attachment. The surface topography and ligand landscape of the scaffold material will determine the host molecules that bind and the type and behavior of cells that mediate the host response. The cellular components of tissue are primarily responsible for the antigenicity and adverse response when implanted in non-autologous hosts [84].

It is probable that the body may take embedded signaling cues from the biomolecular structures that comprise these decellularized extracellular matrices and uses these cues to direct the in vivo remodeling process. Acellular tissues have been explored in numerous applications including full heart constructs, cardiovascular grafts [44], heart valve [37, 289], nerves [290], skeletal muscle [291, 292], liver [59, 70, 293], bladder [50], and esophagus [240, 294, 295] among others.

There have been several published methods for decellularizing tissues and generating biologic scaffolds composed of ECM, each of which describes a unique and specific recipe of enzymes and detergents. Commonly used detergents include Triton X-100[131, 241], 3-[(3-cholamidopropyl)dimethylammonio]-1-propanesulfonate (CHAPS)[18], sodium deoxycholate[132], and sodium dodecyl sulfate (SDS)[23, 242-245]. Detergents are able to solubilize cell membranes and dissociate DNA from proteins, making such agents attractive for the decellularization process. Studies have shown that ionic detergents can be more effective for cellular removal than non-ionic and zwitterionic detergents[40]. However, subjecting tissue to harsh detergents, such as SDS, can disrupt the ECM structure[246], eliminate growth factors[258], and/or denature essential proteins[35].

Decellularized tissue scaffolds present a particularly challenging characterization problem due to their complex arrangement of interacting ECM components and the probable alterations of these structures during the decellularization process. Many different chemical and mechanical decellularization techniques have been employed and each method has the potential to alter the native three-dimensional ultrastructure of the ECM uniquely [84, 129]. However, largely, these ECM scaffolds induce a constructive remodeling response and favorable clinical outcome. To date, characterization methods for decellularized matrices have included

mechanical property testing along with imaging techniques such as scanning electron microscopy and immunohistochemistry [84, 129].

Time-of-flight secondary ion mass spectrometry (ToF-SIMS) represents a powerful surface-sensitive analytical method for the characterization of implantable decellularized materials. Using an energetic primary ion beam to eject surface species, the resulting secondary ions are collected and detected with a time-of-flight mass analyzer to yield an information-rich spectrum. This technique can detect all elements with masses ranging from hydrogen to molecules up to several thousands of Daltons without the need for specific markers or the addition of an analysis matrix. However, due to bombardment with highly energetic ions, the analyte is subject to fragmentation, which can complicate data interpretation.

Each ToF-SIMS spectrum thus represents a complete molecular fingerprint of the outermost 1-2 nm of the surface under analysis. For every spot analyzed, hundreds of individual spectral features can be identified. Multiple spots (spectra) are taken per sample and the spectra are overlaid so that comparisons of individual peak variance relationships of within-group and between-group changes can be assessed. To understand such complex data sets, multivariate analysis (MVA) techniques have been applied to statistically reduce the complexity to manageable patterns of captured variance [296-299].

For this study, principal component analysis (PCA) was employed as the multivariate technique. In PCA, a set of new variables called principal components (PCs) are calculated which represent new axes within the data space [300-302]. These new axes, or PCs, now bisect areas of variance within the original dataset. The first PC will capture the largest percentage of the variance in the dataset while each subsequent PC is orthogonal to its predecessor and captures sequentially less variance until there are no longer identifiable trends. Specifically, PCA

has been used previously to determine a set of protein-related peaks within ToF-SIMS data sets, which can be used to compare amino acid related structures [296]. Variations in the amino acid fragment intensities can be related to the identity, conformation and orientation of surface bound proteins [25].

ToF-SIMS characterization of decellularized ECM-based scaffolds is analytically challenging because of the scaffolds' surface chemical and structural complexity. This surface represents the first contact a given cell would encounter once seeded (in vitro) or repopulated (in vivo). With this in mind, characterizing surface chemistry precisely could provide vital insight into the mechanisms behind the in vivo success of decellularized matrices. ToF-SIMS has the power to assess the molecular chemistry and some aspects of the molecular organization associated with the outer layer of the scaffold. The challenge lies in the interpretation of the data. Previously in the characterization of biomaterials, this technique has been used to study adsorbed model protein films [303]. In a recent study, ECM proteins were analyzed after cell lift-off from poly(N-isopropyl acrylamide) (polyNIPAAM) [297, 298] and compared to an adsorbed protein film model. With the detailed molecular characterization of the surfaces investigated in the present study, researchers will have an enhanced understanding of the cellular interactions that occur upon implantation. This knowledge could help to improve functionality of future generations of these naturally-derived materials as well as guide the production of successful synthetic mimetics that incorporate molecular specificity [299].

6.3 MATERIALS AND METHODS

6.3.1 Scaffold Preparation and Decellularization

Porcine urinary bladders were obtained from animals (~120 kg) at a local abattoir (Thoma's Meat Market, Saxonburg, PA). Bladders were frozen (>16 h at −80 °C) and thawed completely before use. The BMC and underlying lamina propria were isolated and harvested from the bladders as previously described[50, 253, 259]. The tissue was then subjected to either, 0.1% Peracetic Acid (PAA), 3% Triton-X 100 (Sigma-Aldrich), 8 mM CHAPS (Sigma-Aldrich), 4% sodium deoxycholate (Sigma-Aldrich) , 1% SDS (Bio-Rad), 0.1% SDS (Bio-Rad) or Type I water (non-detergent control) for 24 hours with physical agitation (300 rpm on an orbital shaker). Scaffolds were next rinsed with 1X PBS for 15 min followed by water for 15 min and each repeated. Two 24 hour 1X PBS washes followed. Scaffolds were subsequently rinsed with 1X PBS followed by water for 15 min each and repeated.

6.3.2 Scanning Electron Microscopy

SEM was used to examine the surface topology of urinary bladders treated with each detergent. Scanning electron micrographs were also taken of the HMEC seeded scaffolds after 7 days of culture on each sample. Samples were fixed in 2.5% glutaraldehyde in 1X PBS, cut into blocks of approximately $8mm^3$, and washed thoroughly in 1X PBS for three times at 15 minutes each. Samples were then fixed in 1% OsO_4 in 1X PBS for 15 minutes each, dehydrated in graded series of alcohol (30%-100%) baths for 15 minutes each. Samples were then critically point

dried with hexamethyldisiloxane mounted on studs, sputter coated, and stored in a desiccator until imaged. SEM images were captured using a JEOL 6335F Field Emission SEM with backscatter detector.

6.3.3 Time of Flight Secondary Ion Mass Spectroscopy (ToF-SIMS)

ToF-SIMS spectra were acquired on an ION-TOF ToF.SIMS 5–100 spectrometer using a 25 keV Biþ ion source in the pulsed mode, at a pulse width of approximately 2 ns based on the hydrogen peak width, to enhance mass resolution of the spectra. Spectra were acquired for both positive and negative secondary ions over a mass range of m/z 1⁄4 0–700. The primary ion current was 0.8 pA. Secondary ions of a given polarity were extracted and detected using a reflectron time-of-flight mass analyzer. Spectra were acquired using an analysis area of 0.005–0.01 mm^2. Positive ion spectra and negative ion spectra were assessed in this study in order to identify characteristic peaks. Mass calibration errors were kept below 10 ppm. Mass resolution (m/Dm) for a typical spectrum was 3000–7000 at m/z 1⁄4 27.

6.3.4 Principal Components Analysis (PCA)

Multivariate analysis was conducted by selecting peak sets from the samples analyzed by ToF-SIMS. The selected peaks were then normalized to the total ion intensity of all peaks selected to account for fluctuations in secondary ion yield between different spectra. PCA was then employed to analyze the positive ToF-SIMS data using a Matlab (The MathWorks, Inc., Natick,

MA) based in-house program. All spectra were mean-centered before running PCA. PCA was used to determine the linear combination of peaks that captured the highest degree of variation in a dataset [32].

6.4 RESULTS

6.4.1 Analysis of the Basement Membrane Fiber Network via SEM

Qualitative assessment of the SEM of the BMC luminal surface showed that treatment with water alone, 3% Triton X-100, 4% deoxycholate or with 4% sodium deoxycholate retained an intricate fiber network (**Figure 17. A,C,D,E**). However, treatment with 1% PAA, 1% SDS, and 0.1% SDS resulted in an amorphous structure lacking distinct fibers (**Figure 17 B,F,G**). The fiber diameter did not appear significantly different with treatment of Triton X-100 or 8mM CHAPS compared with the no-detergent control (Fig. 4I). Samples treated with PAA, 1% SDS, and 0.1% SDS appear to have significant collagen denaturing, with the 0.1% SDS treated samples having less denaturing than the 1% SDS.

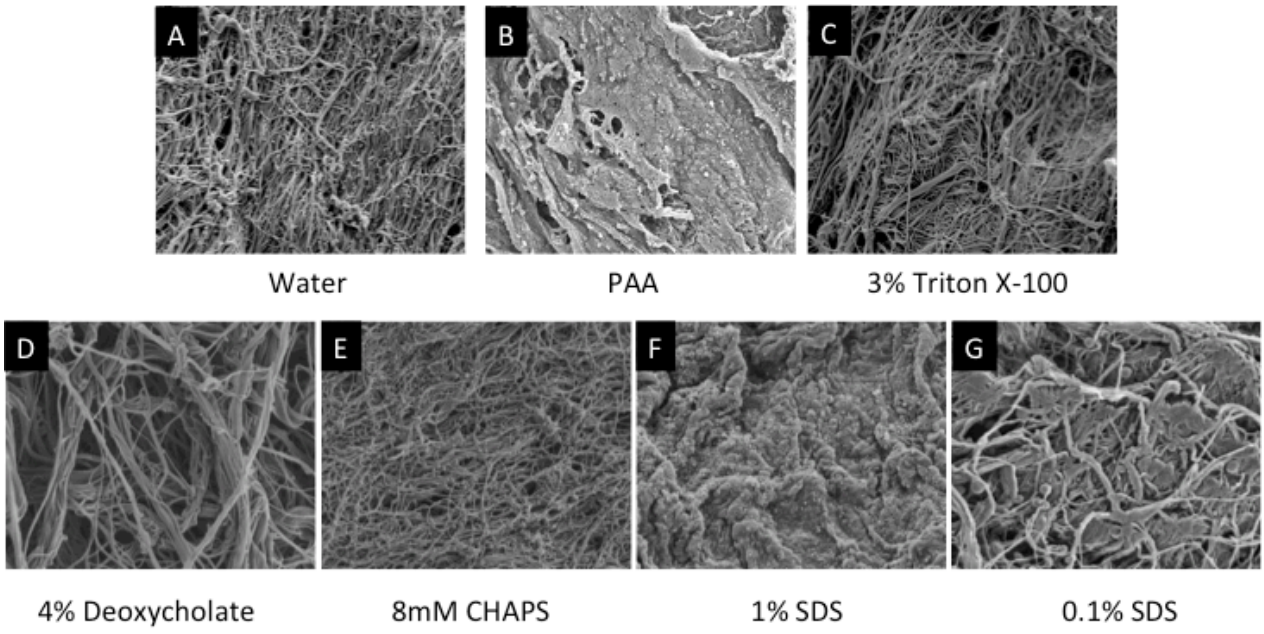

Figure 17. SEM of the BMC fiber network of porcine urinary bladders prepared with (A) water as a no-detergent control, (B) PAA, (C) Triton-X, (D) CHAPS, (E) sodium deoxycholate, (F) SDS (0.1%) and (G) SDS (1.0%).

6.4.2 Negative Ion Spectra

Representative negative ion spectra of each treatment group revealed clearly noticeable differences. High PO3 (m/z 79) signal in both native and PAA treated samples indicate the possible presence of residual DNA. Samples treated with SDS showed a high SO3- and SO4- peaks possibly associated with residual detergent. It is also clear that a series of distinctive higher mass peaks in SDS and dexocyholate treated indicative of residual detergent

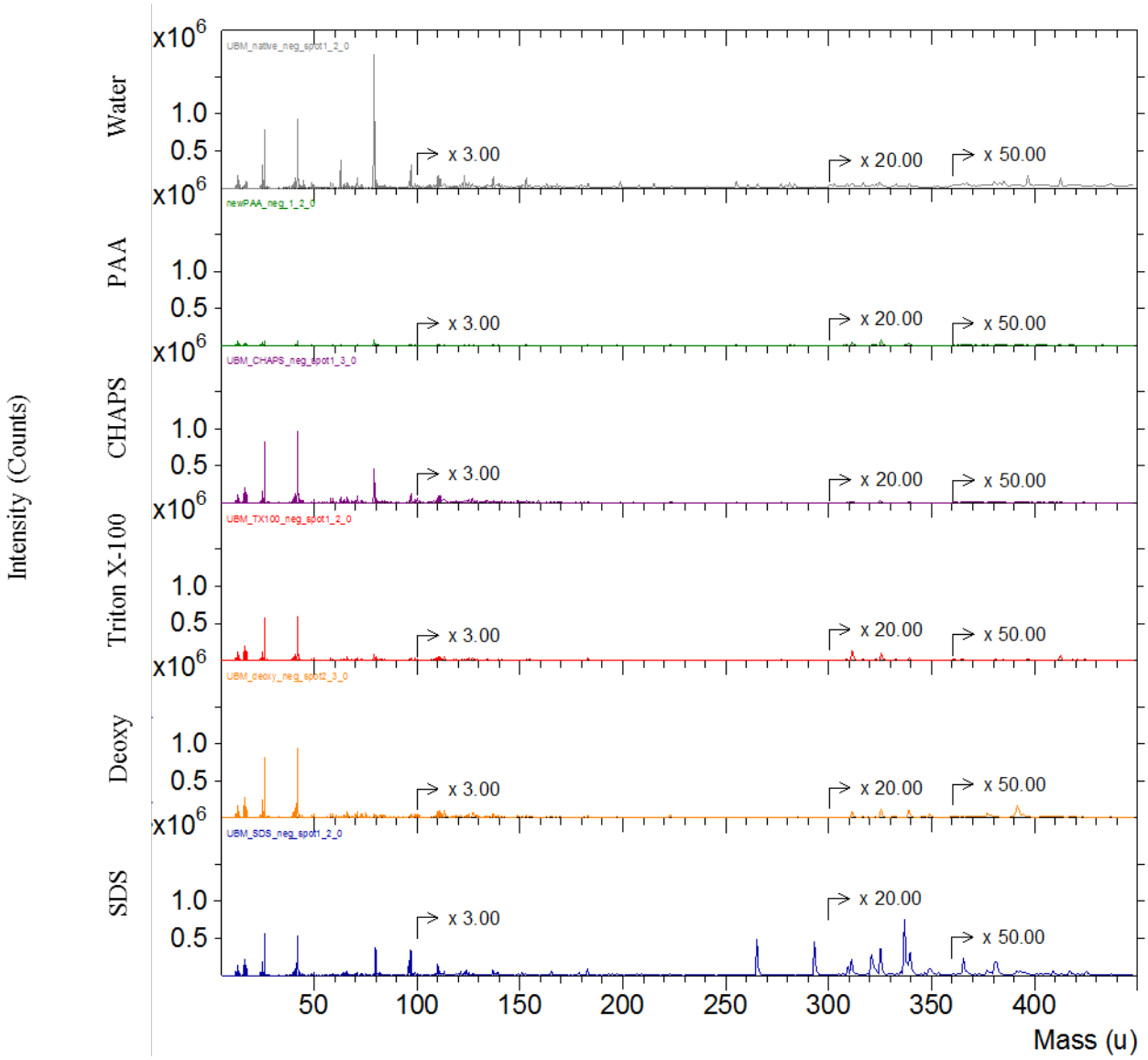

Figure 18. Representative negative ion spectra of porcine urinary bladders treated with Water, PAA, 3% Triton X-100, 8mM CHAPS, 4% sodium deoxycholate, and 1% SDS.

6.3.3 Principal Components Analysis of Negative Ion Spectra

After running a principal components analysis of the negative ion spectra there is evidence of trends separating the treatment groups. The water and PAA treated samples do not separate from each other in either principal components 1 or principal components 2. In principal components 1 the Triton X-100, Deoxycholate, and 0.1% SDS samples locate together, whereas the 1% SDS group is significantly higher than all groups. In principal components 2 the Triton X-100, CHAPS, and Deoxycholate samples locate together, whereas the 1% SDS and 0.1% SDS groups trend higher than all groups.

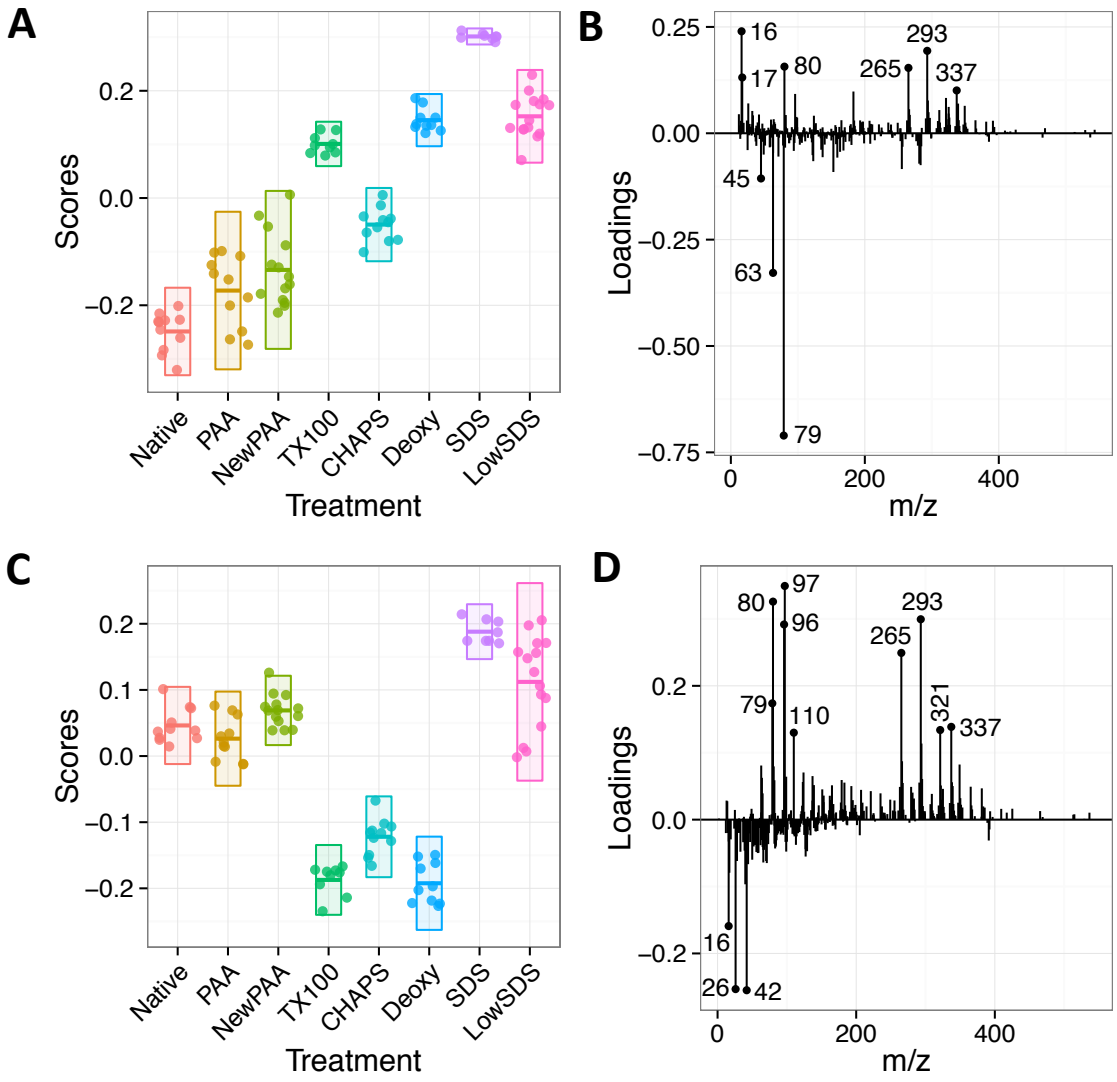

Figure 19. Principal component analysis (PCA) of negative ion spectra. Scores and loadings plots for principal components 1 (A, B) and 2 (C, D) are presented. In loadings plots (B, D) prominent highly loading peaks are marked and labeled.

Table 5: Summary of the polarity, mass, assignment, identity and association of highly loading peaks seen in PCA loadings plots shown in **Figure 19**.

Polarity	m/z	Assignment	Identity	Association	PC
Negative	63.0	PO3-	Phosphate	Residual nuclear material	1
Negative	79.0	PO4-	Phosphate		1
Negative	80.0	SO3-	Sulphate	SDS headgroup	2
Negative	97.0	SO4-			2
Negative	265.1	C12H25SO4-	Dodecylsulphate	SDS	2
Negative	293.1	C12H25O2Na4-	SDS micelle	SDS	2
Negative	391.3	C24H49O4	Deprotonated deoxycholate molecular ion	Deoxycholate	2

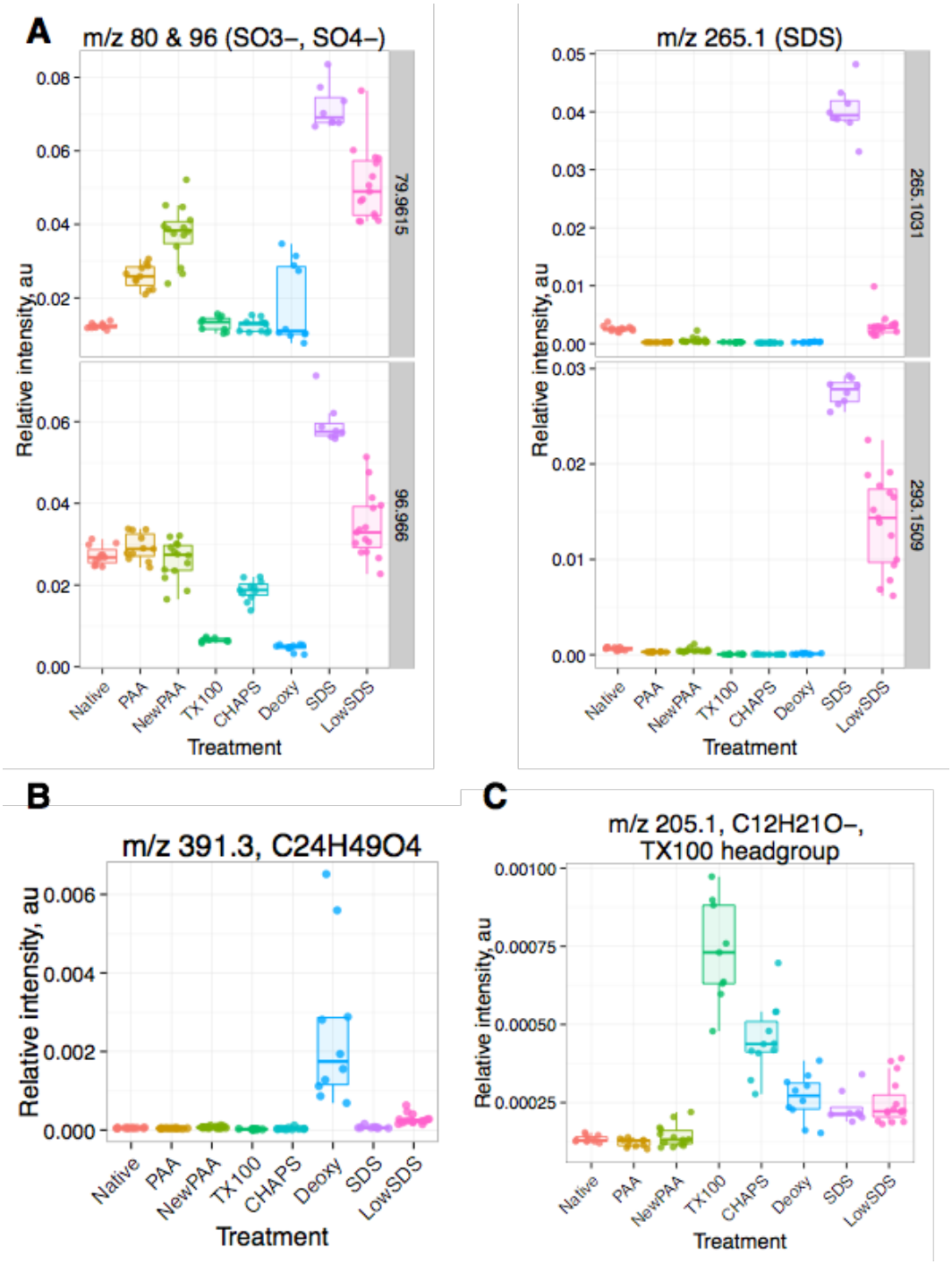

Figure 20. Peak intensities of residual SDS (A), Deoxycholate (B) and Triton X-100 (C)

6.3.4 Positive Ion Spectra

The positive ion spectrum reveals clearly noticeable differences between sample types. A high phosphocholine headgroup peak (m/z 184) indicating residual cell membrane were observed in native and PAA treated samples. The detergent treated groups did not show as high intensity of the phophocholine headgroup peak indicating they were potentially able to remove residual cell membrane. Many peaks indicative of PDMS contamination were seen in PAA treated samples. PDMS contamination was also seen during pilot study in PAA treated samples indicating possible contamination of PAA reagent. Lower levels in other treatment groups suggests contamination has not occurred during sample handling, transit, or analysis. Lastly, there are prominent lower mass peaks, characteristic of amino acid fragments.

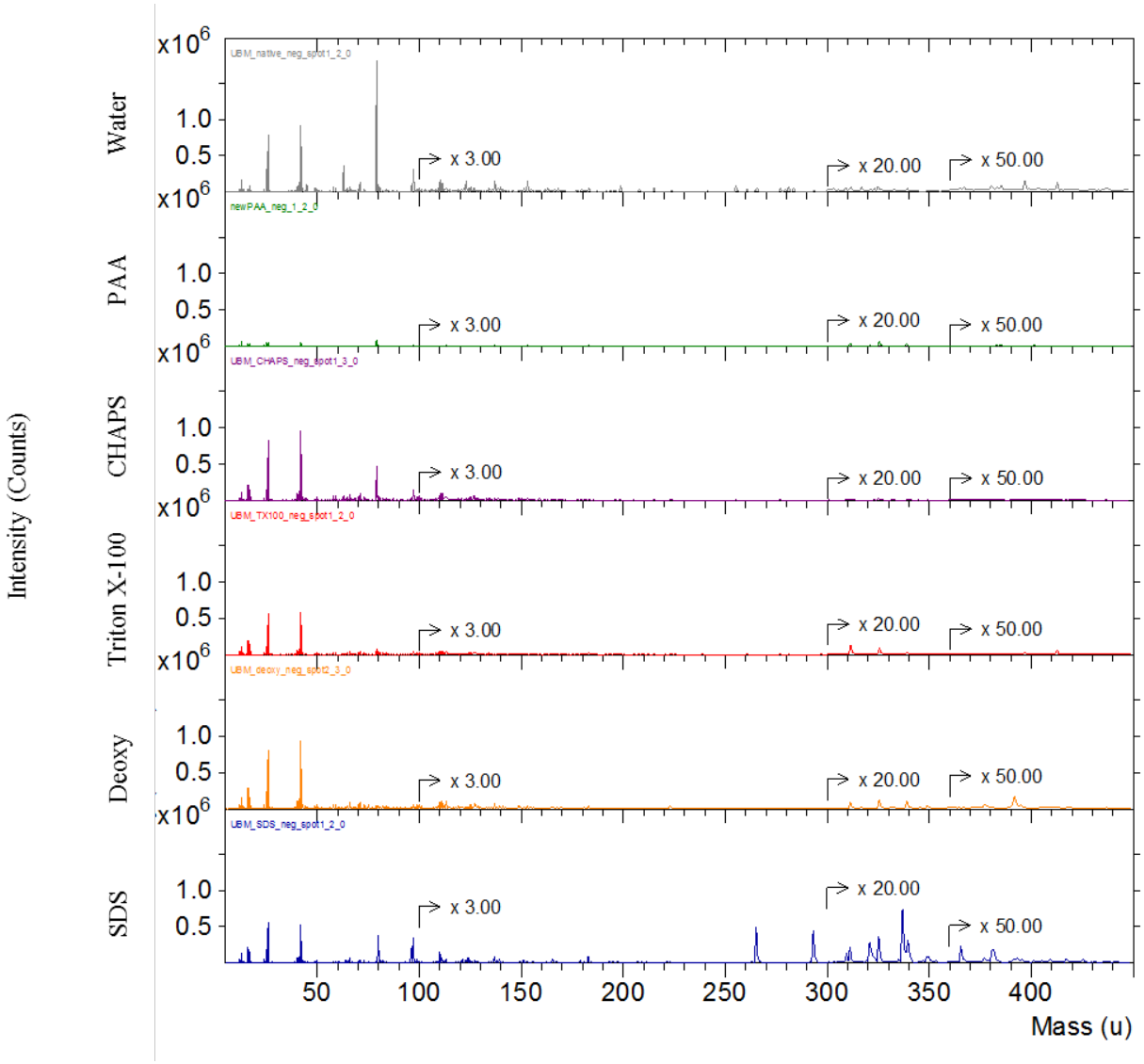

Figure 21. Representative positive ion spectra of porcine urinary bladders treated with Water, PAA, 3% Triton X-100, 8mM CHAPS, 4% sodium deoxycholate, and 1% SDS.

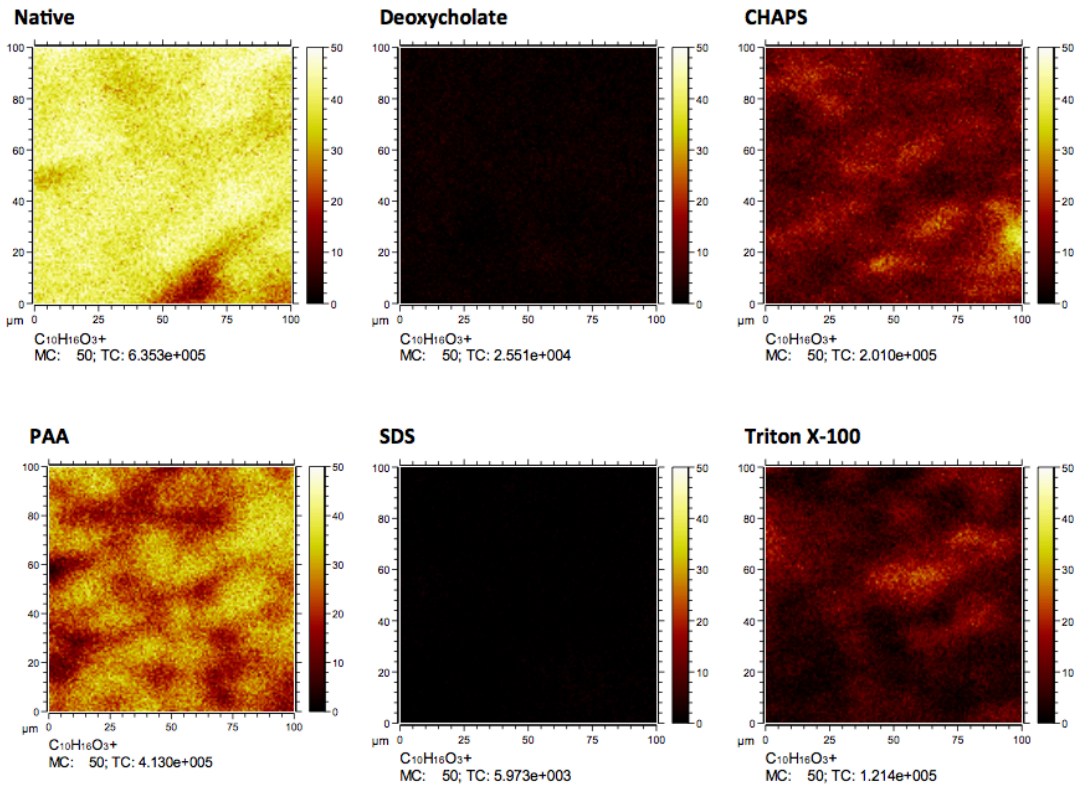

Figure 22. Spatial distribution of phosphocholine headgroup (m/z 183, positive ion spectra) indicative of cell membranes.

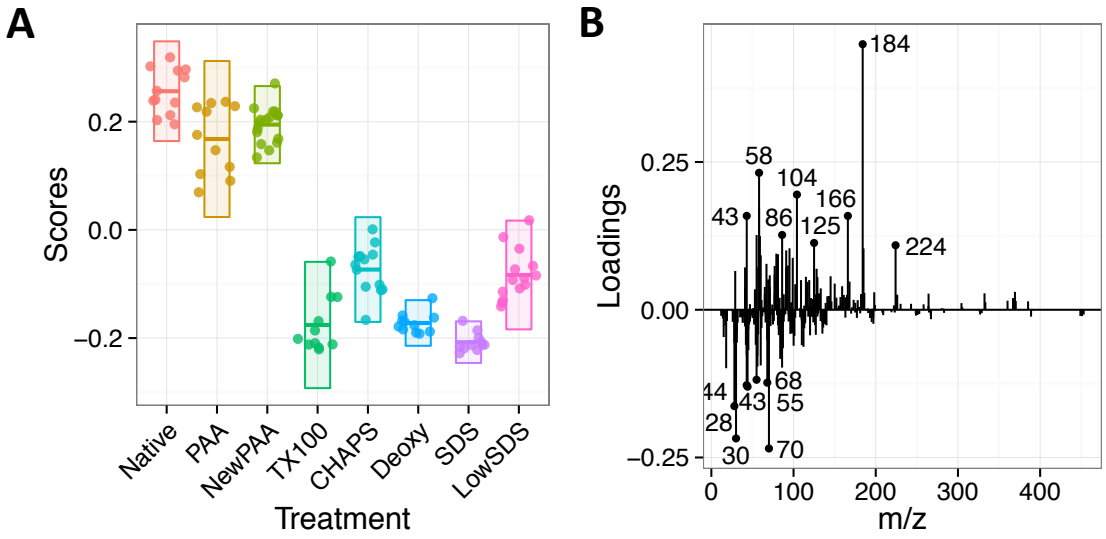

Figure 23. PCA of positive ion spectra with scores and loadings plots for principle component 1.

Table 6: Summary of the polarity, mass, assignment, identity and association of highly loading peaks seen in PCA loadings plots shown in **Figure 23**.

Polarity	m/z	Assignment	Identity	Association	PC
Positive	184.1	C5H15NPO4+	Phosphocholine	Residual cell membrane	1
Positive	224.1	C9H19NPO4+	Glycerophosphocholine		1
Positive	104.1	C5H14NO+	Choline		1

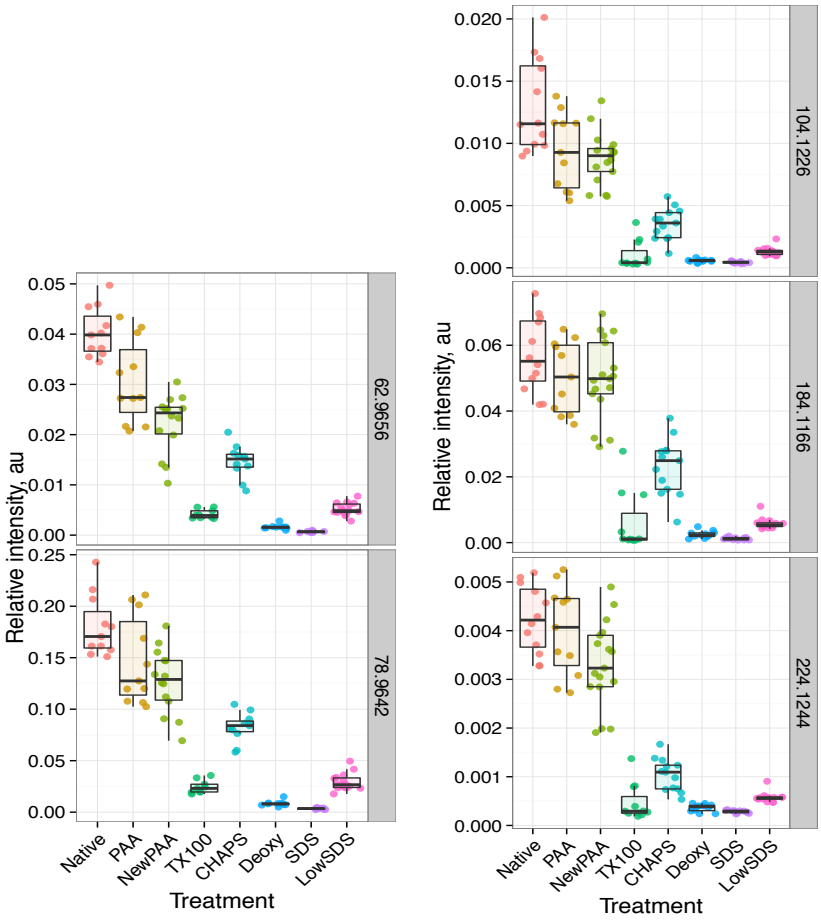

Figure 24. Peak intensities for cell membrane and nuclear associated compounds with PO2- (m/z 63.0), PO3- (m/z 79.0), C5H12NO+, choline (m/z 104.1), C5H15NPO4+, phosphocholine head group (m/z 184.1), C9H19NPO4+, phosphocholine (m/z 224.1).

6.5 DISCUSSION

Decellularized matrix scaffolds, such as porcine urinary bladder matrix (UBM) or decellularized liver scaffolds, may be prepared through a range of decellularization techniques, commonly using ionic, zwitterionic or nonionic detergents. Whilst removal of cellular material is regularly assessed, the impact of detergent selection on ECM structure and composition is less commonly investigated. Time-of-flight secondary ion mass spectrometry (ToF-SIMS) is a powerful surface analysis technique to probe biological structures with high mass resolution and surface specificity. In the described study we report the use of ToF-SIMS to distinguish the basement membrane complex of UBM prepared by treatment with water, 0.1% SDS 1% SDS, 4% Deoxycholate, 8 mM CHAPS or 3% Triton X-100 for 24 hours. All samples were rinsed thoroughly with water following treatment in an attempt to remove any residual detergent.

Results indicate clear evidence of significant retention of nuclear and membrane components with water and PAA treatment. This is not unexpected because these treatments do not adequately decellularize native tissue. Interestingly, there was a direction correlation between the PCA of the positive ion spectra and expected decellularization ability of each treatment. Stated differently, PCA of the positive ion spectra may be an adequate method of determining extent of decellularization. Imaging of phosphocholine headgroup peak at m/z 184 (positive) shows island like spatial distribution of residual cell membrance, particularly in PAA treated samples. It was also shown that PCA of the negative ion spectra is capable of separating sample types based on residual cellular components (Native and PAA treated) or detergent type (SDS vs. Deoxycholate). Furthermore, this study revealed the presence of residual detergent in

SDS treated and deoxycholate treated samples. However, the level of residual detergent content between deoxycholate samples varied. All dexocyholate samples were prepared from the sample porcine bladder, so source tissue variation does not explain the variation in residual deoxycholate

Principal components analysis (PCA) reveals spectral differences between treatment groups. In addition to insights into remaining cell debris and traces of residual detergent, we can further probe these data sets to investigate how detergent selection impacts proteinaceous ECM components. Using a reduced peak list of known characteristic amino acid fragments, PCA distinguishes native bladder tissue from decellularized UBM. Additionally, PCA highlights spectral differences between UBM treated with ionic and charge-neutral (zwitterionic and nonionic) detergents. Notably, the basement membrane surface of UBM prepared with ionic detergents SDS and Deoxycholate yield less intense characteristic peaks from hydrophobic amino acids than UBM treated with charge neutral detergents CHAPS and Triton X-100. Harsher ionic detergents may denature protein structure and break protein-protein interactions through binding of their hydrophobic tail to hydrophobic amino acid residues. Such damage is hypothesized to cause sub-optimal in vitro and in vivo responses.

6.6 CONCLUSIONS

The results of the present study demonstrate that each decellularization agent used to prepare a biologic scaffold creates in a unique surface. The resulting ECM scaffold is associated with distinct ultrastructural and compositional characteristics and that these surface characteristics are dependent on both the damage the decellularization agent has caused to the native extracellular matrix as well as the residual compoents left behind by the decellularization agent. It was also

demonstrated that ToF-SIMS is a highly sensitive method for the detection and differentiation of the molecular composition of the outermost surface of an ECM scaffold. Further, ToF-SIMS may represent a method for future identification of previously unknown surface species as well as for the prediction of cell–scaffold interactions and subsequent remodeling events. Finally, the richness of molecular detail in the ToF-SIMS spectra suggests that ToF-SIMS may be useful for quality control of commercialized ECM-based regenerative scaffold products and for standardization of these scaffolds.

7.0 RECONSTRUCTION OF A FUNCTIONAL VASCULAR NETWORK WITHIN A DECELLULARIZED RAT LIVER SCAFFOLD

7.1 ABSTRACT

More than 120,000 patients are on the organ transplant list in the United States alone, and 18 patients will die every day waiting for a donor organ. Recently, the concept of whole organ engineering has emerged as a potential solution for the donor organ shortfall. This concept involves the decellularization of an allogeneic or xenogeneic homologous organ followed by recellularization of the resultant three-dimensional stromal scaffold with site appropriate cells. Studies by our group and others have shown that decellularization of whole organs such as liver, lung, and heart with preservation of the underlying matrix scaffold is possible. However, current limitations of this approach for translation to pre-clinical animal models include the re-establishment of a functional non-thrombotic microvasculature capable of being connected to recipient's circulation upon implantation.

The objective of the present work was two-fold. The first was to systematically investigate key variables associated with reconstructing a functional hepatic vascular network. Four such variables including rate of media perfusion, endothelial cell seeding density, duration of culture, and the addition of an anti-thrombotic heparin coating were investigated for their effect upon two outcome measures: endothelial coverage of the scaffold vasculature and cell viability. The second objective was to develop a preferred method of delivering human endothelial cells through the venous and arterial networks within a 3-dimensional liver scaffold and achieve cell engraftment, high viability, and microvascular formation.

Results showed that of the four factors investigated for endothelial seeding, cell density and rate of media perfusion had the greatest effect on endothelialization of the vascular network. As seeding density and media perfusion rate were increased, endothelial coverage and viability also increased. A multi-day seeding approach also resulted in increased engraftment and re-endothelialization of the decellularized rat liver scaffold.

Within three days of culture, seeded endothelial cells attached to the scaffold, displayed a normotypic-flattened appearance, and a microvascular network was formed. The location of endothelial cells delivered through the portal vein and the hepatic vein were determined using a cell tracker fluorescent dye. Co-localization of these cells was found within major vessels and throughout the intralobular sinusoidal space. Methods were developed for re-endothelializing the arterial hepatic vasculature of a decellularized rat liver scaffold. Micro-vessels as small as 5-10 microns in diameter were found within the scaffold after 3 days of culture. For hepatocyte seeding, results showed higher viability, albumin and urea production with a transcapsular injection method compared to infusion via the vasculature. These findings are important for eventual clinical translation of whole organ engineering.

7.2 INTRODUCTION

The critical shortage of viable donor organs for patients with end-stage organ failure continues to worsen with no immediate solution in sight. More than 120,000 patients are on the organ transplant list in the United States alone, and 18 patients will die every day waiting for a donor organ[304]. Artificial organ devices such as dialysis machines, ventricular assist devices, and extracorporeal membrance exygenation (ECMO) machines provide temporary support, but are

inadequate long-term replacement of organ function. Whole organ engineering using naturally occurring three-dimensional bioscaffolds has emerged in recent years as a potential solution to the donor shortage[83, 305, 306]. This approach is based upon the concept that functional organ tissue can be engineered by cell seeding a three-dimensional scaffold composed of extracellular matrix homologous (ECM). This approach would include immediate or near immediate in-situ transplantation of the cell seeded scaffold, providing the requisite perfusion by the host circulation with appropriate microenvironmental cues, nutrients, and signaling factors necessary for organ development. The long-term goal of this work is to establish the decellularization, recellularization and transplantation criteria necessary to produce adequate functional organ tissue to sustain life with minimal or no morbidity. We have chosen the liver as the model organ because of its' remarkable natural ability to regenerate in vivo.

In 2008, perfusion decellularization was reported as a technique to generate acellular whole organ scaffolds from cadaveric organs[23]. Decellularizing agents were delivered via the native vasculature of the organ and thereby distributed across the entire mass of the organ. By applying physiologic perfusion pressures, decellularization solutions effectively permeate the organ via the capillary bed and cellular debris is removed via the venous system. This technique produces an acellular three-dimensional bioscaffold composed of naturally occurring extracellular matrix (ECM)[48, 83]. Theoretically, the resultant bioscaffold is ideal because the biochemical composition, micro and macro architecture, and extracellular cues are all derived from the native organ. This technique has also been used to decellularize whole livers[193-195].

The generation of a fully functional organ has yet to be accomplished, but several intermediate milestones have been reached in heart [196], liver [24, 193-195, 197-200], lung [25, 201-203], pancreas[204], and kidney [205, 206] regeneration. Current hurdles to successful pre-

clinical animal studies include the re-establishment of a non-thrombotic microvasculature and an effective method for delivering and maintaining viable and functional parenchymal cells to their native location[25, 307]. Organ specific parenchymal cell function has been reported following bioreactor-assisted in vitro cell seeding[24, 194, 195]. However, seeding efficacy of the vascular component of the three dimensional liver bioscaffolds has received little attention. Variables such as cell seeding density, perfusion pressures, oxygen concentration, and other factors require a systematic approach for optimization.

Techniques employed in recellularization of whole-organ scaffolds are typically adaptations of methods from a wide range of procedures including traditional cell culture, tissue-engineering, cell-transplantation therapies, and isolated-organ perfusion. The recellularization process can be considered in two major steps. The first is cell seeding, in which the goal is distribution of parenchymal and non-parenchymal cell types to their native three-dimensional location within the liver scaffold. The second is perfusion culture, which is typically utilized to prepare the cells for in vivo transplantation by providing them with physiological conditions in-vitro. Typically, cells are either injected directly into the organ with a needled syringe or introduced via vascular perfusion with the expectation that the cells will migrate to their native site, proliferate, and self-assemble. Cell seeding efficiency has varied greatly.

The objective of the present study was two-fold: 1) to systematically analyze key variables associated with reconstructing a functional vascular network within the 3-dimesnional liver bioscaffold, and 2) to develop methods for the reconstruction of the venous and arterial vascular networks within a 3-dimensional rat liver bioscaffold.

7.3 MATERIALS AND METHODS

7.3.1 Experimental Overview

Healthy at livers from Sprague-Dawley rats were harvested and decellularized using a minimally disruptive non-ionic detergent, Triton X-100. The resulting scaffold was analayzed for growth factor content, cellular remnants, and DNA content. Experiments were then conducted with the aim of re-endothelializing the rat liver scaffold. Four factors of endothelial cell seeding rate of media perfusion, seeding density, duration of culture, and the addition of an anti-thrombotic heparin coating were selected and investigated by means of two outcomes: endothelial coverage of the scaffold vasculature and cell viability. A multi-day seeding technique was also investigated. Following analysis of each seeding variable, a preferred method was develop for delivering human endothelial cells into the venous and arterial vascular networks of the deellularized rat liver scaffold. Endothleial cells delivered into the each network were labeled with a fluorescent cell tracker in order to correlate the avenue of delivery with the spatial location within the scaffold after culture.

7.3.2 Animals

Female Sprague-Dawley rats (250–300g; Charles River Laboratories) were used for hepatocyte isolation and preparation of the three dimensional liver scaffolds. The animals were cared for in accordance with the guidelines set by the Committee on Laboratory Resources, National Institutes of Health, and Institutional Animal Care and Use Committee of University of Pittsburgh.

7.3.3 Donor Rat Liver Harvest

Surgical plane anesthesia was induced and maintained using inhalation of 1.5%–3% of isofluorane. The abdominal cavity was opened by a ventral midline incision extending from the pubis to the xyphoid process and the animals were injected intravenously with heparin (200 units). The inferior vena cava (IVC) and the portal vein were clamped. The portal vein and IVC were then cannulated with an 18G cannula, and 5–10mL of phosphate-buffered saline (PBS) containing heparin was injected. The diaphragm was cut to transect the superior vena cava and IVC. The liver was removed and stored in a cell culture dish filled with PBS solution. The liver was then rinsed with 10–20mL of PBS solution containing heparin (200 units). The livers were frozen at - 80ºC completely immersed in PBS solution before perfusion was performed for organ decellularization.

7.3.4 Whole Rat Liver Decellularization

The harvested livers of Sprague-Dawley rats were frozen at -80ºC for at least 24 h before decellularization to aid in cell lysis. The liver was thawed at room temperature in 1 x PBS. Decellularization was conducted by a retrograde perfusion technique at 8 mL/min, in which solutions flowed through the cannula, into the IVC, and throughout the vasculature of the liver. Livers were placed in 500mL of 0.02% trypsin/0.05% EGTA solution at 37ºC, allowing the solution to flow through the liver for 2 h. Deionized water was perfused through the liver for 15 min followed by 15 min of 2 x PBS. The 3% Triton X-100/0.05% EGTA solution was perfused through the liver vasculature for 18–24 h with the solution being changed after 1, 4, and 16 h. A deionized water wash for 15 min followed by 2 x PBS wash for 15 min was repeated once, followed by a deionized water wash for 30 min and 2 x PBS wash for 30 min to aid in cellular lysis and wash any recirculating debris. The three-dimensional liver ECM was then perfused with 0.1% (v/v) peracetic acid/4% EtOH for 1 h. Acidic conditions were neutralized by PBS and deionized water washes twice for 15 min each.

7.3.5 Growth Factor Assays

Two hundred fifty milligrams of minced rat whole liver or decellularized rat liver was suspended in * 3.75 mL of urea heparin extraction buffer. The extraction buffer consisted of 2 M urea and 5 mg/mL heparin in 50 mM Tris with protease inhibitors (protease inhibitors: 1 mM phenylmethylsulfonyl fluoride, 5 mM benzamidine, and 10 mM N-ethylmaleimide) at pH 7.4. The extraction mixture was rocked at 4C for 20 to 24 h and then centrifuged at 12,000 g for 30

min. Supernatants were collected, and 6 mL of natively prepared ureaheparin extraction buffer was added to each pellet. Pellets with extraction buffer were again rocked at 4[degrees]C for 20 to 24h, centrifuged at 12,000 g for 30 min, and supernatants were collected. Supernatants from first and second extractions were dialyzed against Barnstead filtered water (total of three changes of dialysis water, 80 to 100 volumes per change) in Slide-A-Lyzer Dialysis Cassettes, 3500 MWCO (Pierce). The concentration of total protein in each dialyzed extract was determined by the BCA protein assay (Pierce #23227; Pierce) following the manufacturer's protocol, and extracts were frozen in aliquots until time of assay. Concentrations of basic fibroblast growth factor (bFGF), vascular endothelial growth factor (VEGF), and HGF in urea-heparin extracts of liver samples were determined with the Quantikine Human FGF basic Immunoassay (R&D Systems # DFB50; R&D Systems), the Quantikine Rat VEGF Immunoassay (R&D Systems # DFE00; R&D Systems), and the Rat HGF ELISA Kit (B-Bridge International # K2002-1; B-Bridge International), respectively. Manufacturer's instructions were followed for all three growth factor assays. Each growth factor assay was performed in duplicate three times. Results are reported as mean [+ or -] standard error. A one-way analysis of variance with Dunnett's comparison test was used for each growth factor analysis to test the null hypothesis that the growth factor content of the decellularized liver was no different than that of native liver. A p-value of < 0.05 was considered significant. It should be noted that growth factor assays measured the concentration of each growth factor protein and did not measure growth factor activity.

7.3.6 DNA Quantification

DNA content was quantified using methods described previously. (19) In brief, the decellularized liver was cut into small strips and digested using Proteinase K (Invitrogen) for 24-48 h at 50°C until no visible material remained. Phenolchloroform-isoamyl alcohol (25:24:1; Acros) was then added in equal amounts to the decellularized liver digest and centrifuged for 10 min at 10,000 g. The aqueous top layer containing the DNA was then removed and added to 200 μL of 3M sodium acetate solution to reduce RNA content. Ethanol was then added and the solution frozen at - 80°C for at least 12 h. Ethanol was then removed, and samples were allowed to fully dry, at which point 1 x TE buffer (Invitrogen) was added. The total amount of DNA was quantified using the Picogreen DNA assay (Invitrogen) using the manufacturer's instructions.

7.3.7 Vascular Corrosion Casting

Catheterization of the infrahepatic vena cava, portal vein and hepatic artery was performed followed by injection of 1-4 mL polymer mixture depending on the liver size using Batson's 17 anatomic corrosion kit (Polysciences, Inc.) as recommended by the manufacturer. Polymerization took 4 h at 4°C and was followed by maceration in 1 N KOH solution or proteinase K for 8-24 h.

7.3.8 Corline Heparin Conjugate

The heparin conjugate is schematically presented in Figure 25. The conjugate consists of heparin (Mw ~ 13,000 Da, Figure 25a) covalently bound to a polyamine carrier chain (PAV) with disulphide bonds using a heterobifunctional coupling agent, SPDP3 (Figure 25c), approximately in the proportions 70 mol heparin per mole carrier chain. The SPDP derivate forms a coupling unit between heparin and PAV (Figure 25d) and contains a disulfide bond, which provides a useful marker unit for the structural evaluation of the PES results.

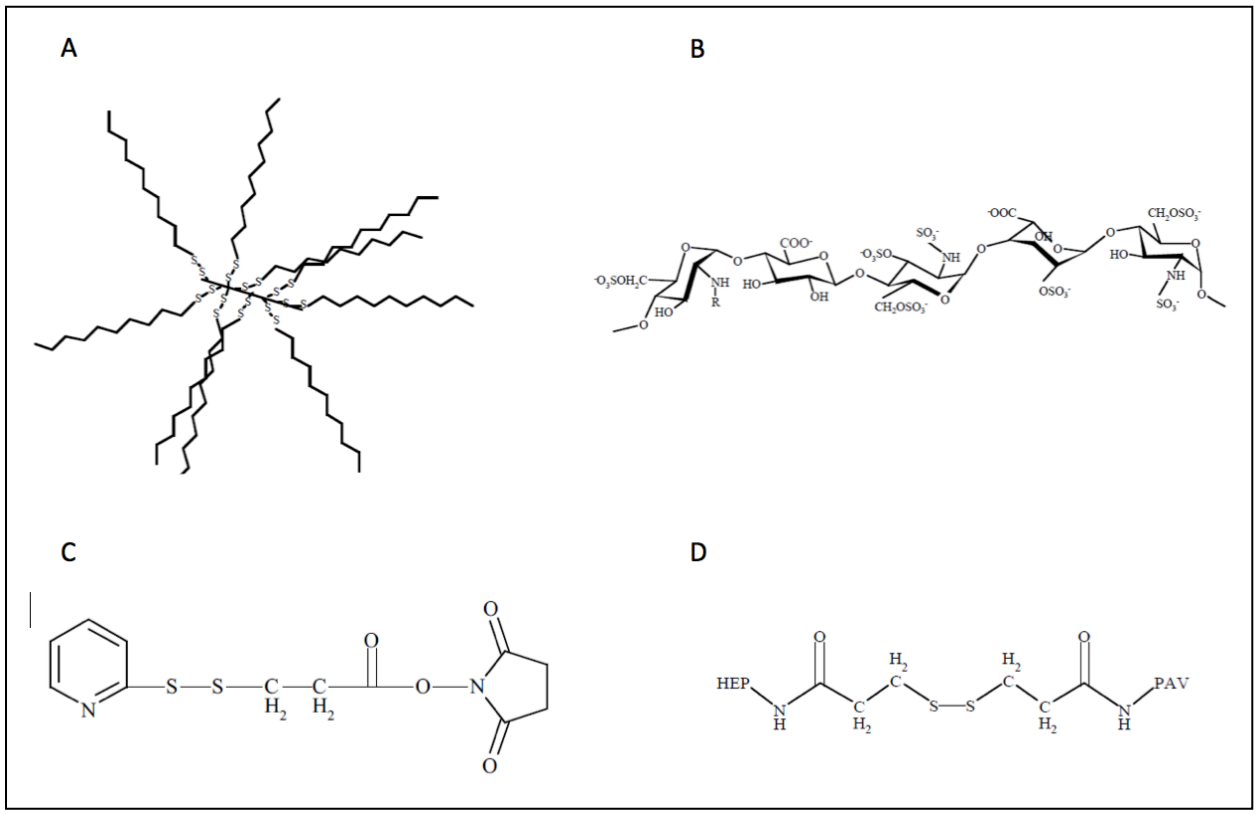

Figure 25. (A) Schematic drawing of the heparin conju gate. (B) The antithrombin binding heparin pentasaccharide unite. (C) The structure of the heterobifunctional coupling agent, SPDP. (D) The bond between the carrier chain PAV and the heparin chain. The –NH groups belong to PAV and heparin, respectively, but are shown for clarification.

7.3.9 Investigation of Key Endothelial Cell Seeding Variables

HMECs (a gift from Francisco Candal, Center for Disease Control and Prevention, Atlanta, GA) were cultivated in MCDB-131 medium containing 10% fetal bovine serum, 2 mM l-glutamine, 100 U ml−1 penicillin and 100 μg ml−1 streptomycin. MCDB-131 medium was from Invitrogen (Carlsbad, CA); all other reagents for cell growth were from Thermo Fisher Hyclone (Logan, UT). Cells were grown at 37 °C in 5% CO_2 and were harvested for seeding when they were

~100% confluent. Before seeding the decellularized rat scaffold the HMECs were suspended in 2ml of growth media. The remaining vascular structures of the decellularized liver were utilized for delivering the HMECs (**Figure 26).**

Half of the cell suspension (1ml) was delivered into the scaffold by infused through the portal vein. The remaining 1ml was then delivered through the hepatic vein. Four variables of endothelial cell seeding and culture process were investigated; seeding density ($10.0 – 30.0 \times 10^6$ HMECs per scaffold), media flow rate following seeding (0.0 – 4.0 ml/min), culture duration (0 – 7 days), and the addition of an anti-thrombotic heparin coating (before and after seeding). An overview of the various conditions can be seen in **Table 7** and **Figure 27**. Scaffolds were then placed in an incubator at 37°C in 5% CO_2. After culture, seeded scaffolds were fixed in 10% neutral buffered formalin for subsequent histologic analysis.

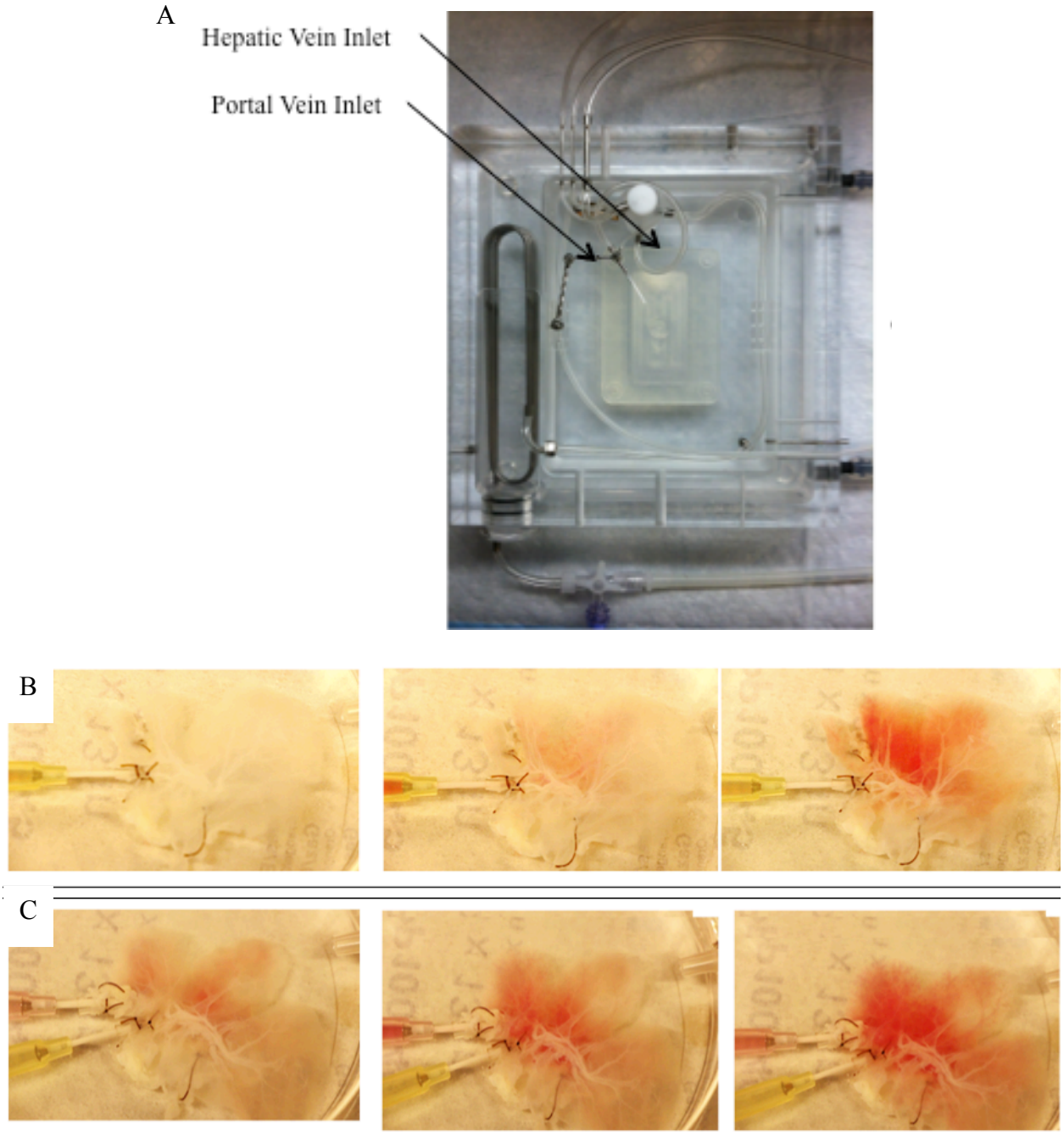

Figure 26. (A) Seeding chamber/bioreactor used for delivering human microvascular endothelial cells within the decellularized rat liver scaffolds. (B) Delivery of HMECs via the portal vein (C) Delivery of HMECs via the hepatic vain.

Table 7: Overview of human microvascular endothelial cell seeding conditions.

	Description of Culture Condition (N=2 for each condition)	Seeding Density (10^6 cells / scaffold)	Media Flow Rate (ml/min)	Culture Duration (days)	Heparin Coating
1	Starting Condition	20	2	3	No
2	Decreased Seeding Density	**10**	2	3	No
3	Increased Seeding Density	**30**	2	3	No
4	Decreased Media Flow Rate	20	**0**	3	No
5	Increased Media Flow Rate	20	**4**	3	No
6	Decreased Culture Duration	20	2	**0**	No
7	Increased Culture Duration	20	2	**7**	No
8	Heparin Coating Before Seeding	20	2	3	**Before Seeding**
9	Heparin Coating After Seeding	20	2	3	**After Seeding**

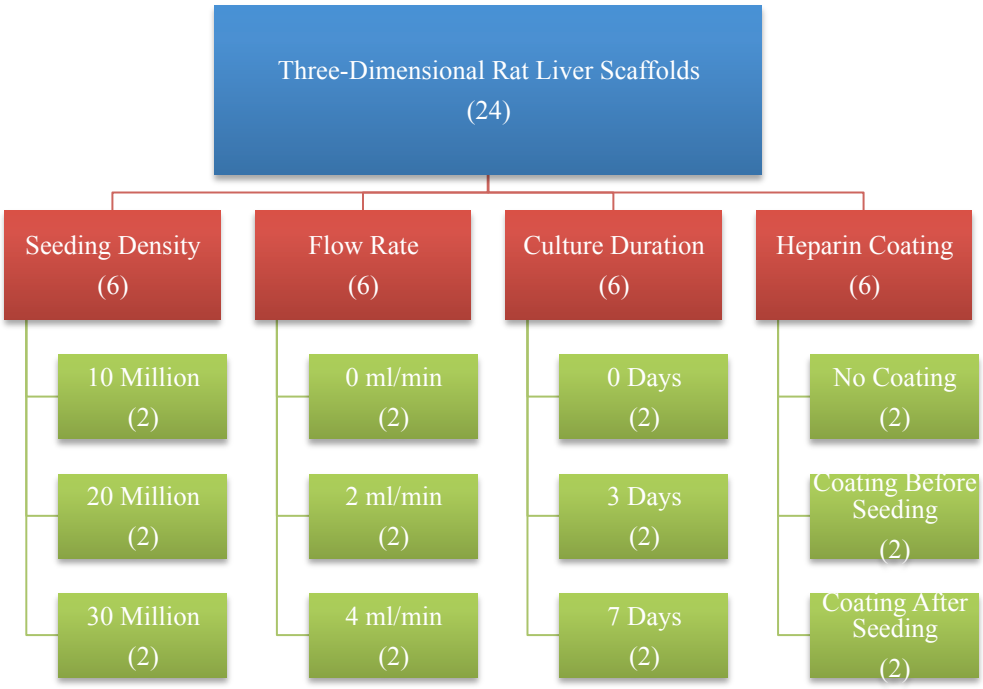

Figure 27. Schematic representation of the experiment design to systematically investigate key variables associated with endothelial cell seeding and culture within a three-dimensional rat liver scaffold.

7.3.10 Reconstruction of the Venous Network

HMECs (a gift from Francisco Candal, Center for Disease Control and Prevention, Atlanta, GA) were cultivated in MCDB-131 medium containing 10% fetal bovine serum, 2 mM l-glutamine, 100 U ml−1 penicillin and 100 μg ml−1 streptomycin. MCDB-131 medium was from Invitrogen (Carlsbad, CA); all other reagents for cell growth were from Thermo Fisher Hyclone (Logan, UT). Cells were grown at 37 °C in 5% CO_2 and were harvested for seeding when they were ∼100% confluent. Before seeding the decellularized rat scaffold the HMECs were suspended in 2ml of growth media. The portal vein and hepatic vein of the decellularized liver were utilized for delivering the HMECs (**Figure 26).**

A multi-day seeding approach was utilized for these experiments. For one decellularized rat liver, endothelial cell seeding was performed on 3 separate days (10 million per day) as opposed to the previous method of 30 million cells seeded at the same time. On day 1, 5 million cells were infused via the portal vein and 5 million cells were delivered via the hepatic vein. This seeding technique was repeated on days 2 and 3 for the same liver. Scaffolds were then placed in an incubator at 37°C in 5% CO_2 and cultured for an additional 24 hours following the 3rd seeding. After culture, seeded scaffolds were fixed in 10% neutral buffered formalin for subsequent histologic analysis.

7.3.11 Reconstruction of the Arterial Network

HMECs (a gift from Francisco Candal, Center for Disease Control and Prevention, Atlanta, GA) were cultivated in MCDB-131 medium containing 10% fetal bovine serum, 2 mM l-glutamine, 100 U ml−1 penicillin and 100 μg ml−1 streptomycin. MCDB-131 medium was from Invitrogen (Carlsbad, CA); all other reagents for cell growth were from Thermo Fisher Hyclone (Logan, UT). Cells were grown at 37 °C in 5% CO_2 and were harvested for seeding when they were ∼100% confluent. Before seeding the decellularized rat scaffold the HMECs were suspended in 2ml of growth media. The portal vein, hepatic vein, and hepatic artery of the decellularized liver were utilized for delivering the HMECs**.**

A multi-day seeding approach was utilized for these experiments in a similar fashion as section 7.3.6. However, 1 million HMECs were also seeded via the hepatic artery on days 1, 2, and 3. Scaffolds were then placed in an incubator at 37°C in 5% CO_2 and cultured for an additional 24 hours following the 3rd seeding. After culture, seeded scaffolds were fixed in 10% neutral buffered formalin for subsequent histologic analysis.

7.4 RESULTS

7.4 Rat liver perfusion decellularization

Figure 28 shows macroscopic and microscopic images of liver before decellularization and after various steps in the decellularization process. The decellularization protocol consisted first of a freezing-thawing technique for at least 24 h to induce cellular lysis. The liver was then retrograde perfused through the IVC using 0.02% trypsin/0.05% EGTA and 3% Triton X-100/0.05% EGTA with washing and disinfection cycles for a total of 28 h (Fig. 28a). Figure 28b shows the generation of a translucent acellular liver ECM, retaining the gross anatomical features of the liver.

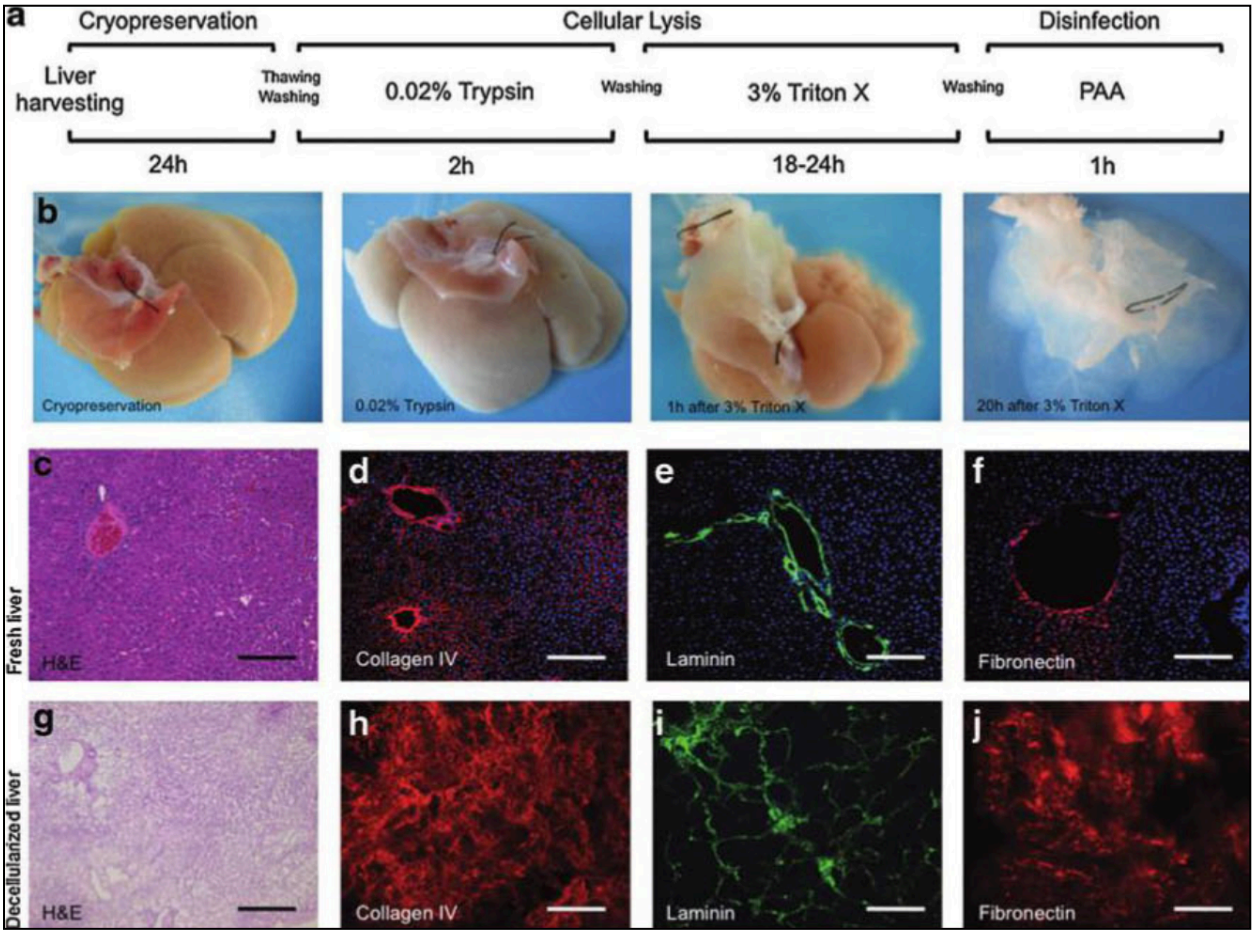

Figure 28. Schematic representation of the sequential whole-organ decellularization protocol (a) Representative macroscopic images of rat livers at various steps in the decellularization process (b). Histologic comparison of normal liver (c-f) and decellularized rat liver matrix (g-j): hematoxylin and eosin (c,g), collagen IV (red) (d,h), laminin (green) (e,i), and fibronective (red) (f, j). Sections were counterstained with DAPI (blue). Scale bars: 200 μm.

7.4.2 DNA Content

Evidence suggests that xenogeneic DNA remnants can be the cause of "inflammatory reactions" following the implantation of derived scaffolds. (19) Thus, DNA content was analyzed and gel

electrophoresis confirmed that the DNA content of the decellularized liver matrix was 25.8 -13 ng/ mg dry weight, which represents 0.47% of the DNA total content of a normal liver (547 [+ or -] 1176ng/mg dry weight) (Fig. 2i, note the logarithmic y-axis). Electrophoretic analysis confirmed that remaining DNA material consisted of fragments < 200 bp in length (Fig. 2j), confirming that degradation of cell contents was extensive. Histologic analysis with DAPI showed no visible nuclear material in the decellularized liver matrix (Fig. 2k).

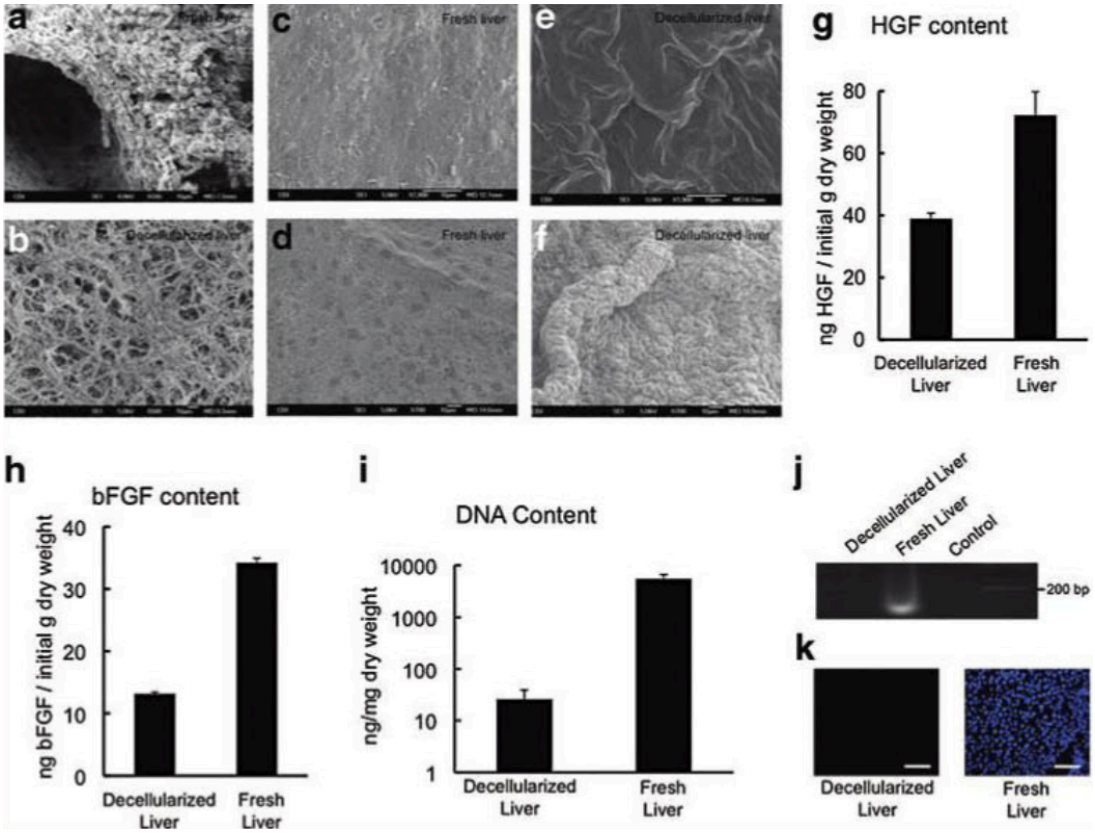

Figure 29. Scanning electron microscopy image showing the extracellular matrix within the parenchyma of normal liver (1), and decellularizved liver open spaces previously occupied by hepatic parenchymal cells (b). Representative SEM images of Glisson's capsul of fresh liver (C, D) after liver decellularization (e,f). Growth factor content of decellularized liver matrix and normal liver, hepatocyte growth factor (HGF) (G), and basic fibroblast growth factor (bFGF) (H) DNA content of the decellularized liver matrix and native liver as determined with a PicoGreen Assay (I,J) the presence of intact nuclear material was evaluated bys staining the decellularized liver and native liver using DAPI (K). Scale bars: 10um (A-F).

7.4.3 Morphology

Histologic analysis of the decellularized liver showed the absence of cellular components compared to native liver (Fig. 1c, g). Immunolabeling characterization of the liver ECM showed the preservation of collagen IV, laminin, and fibrin ogen, indicating a similar structural composition of the matrix to that of intact liver (Fig. 1d-f, h-j). Ultrastructural characterization of the decellularized liver matrix showed the absence of cells; the honey-comb spaces represent the footprint of hepatocyte removal (Fig. 2a, b). One important consideration in the organ decellularization process is the integrity of the collagenous capsule covering the external surface of the liver, that is, Glisson's capsule. A meticulous analysis of Glisson's capsule by both light microscopy and SEM in the present study showed complete integrity of the Glisson's capsule (Fig. 2e, f). Fresh liver from normal rats was used as control (Fig. 2c, d).

7.4.4 Growth Factor Content

The content of HGF in the decellularized liver matrix was 39 [+ or -] 1.7ng/g dry weight and the content of bFGF was 13 [+ or -] 1 ng/g dry weight. Native liver HGF content was 72 [+ or -] 7.5ng/g dry weight and bFGF was 34 [+ or -] 0.3ng/g dry weight. These results show that more than 50% of HGF and ~ 40% of bFGF were preserved in the decellularized liver matrix compared with the native liver (Fig. 2g, h).

7.4.5 Vascular Cast

Vascular casting of the hepatic portal and hepatic arterial vascular networks of the decellularized liver matrix were intact (Fig. 3a), an important feature for subsequent vascular endothelialization. In previous studies (4) it was demonstrated that only the portal and central venous system were preserved. Engineering of a complete liver graft would, however, require an intact and complete arterial system and, importantly, an intact bile drainage system. Thus, a corrosion cast of the decellularized liver matrix was created and showed the existence and preservation of the entire vascular system (portal vein, hepatic artery vasculature, central vein, and biliary tract) similar to normal liver (Fig. 3b, c).

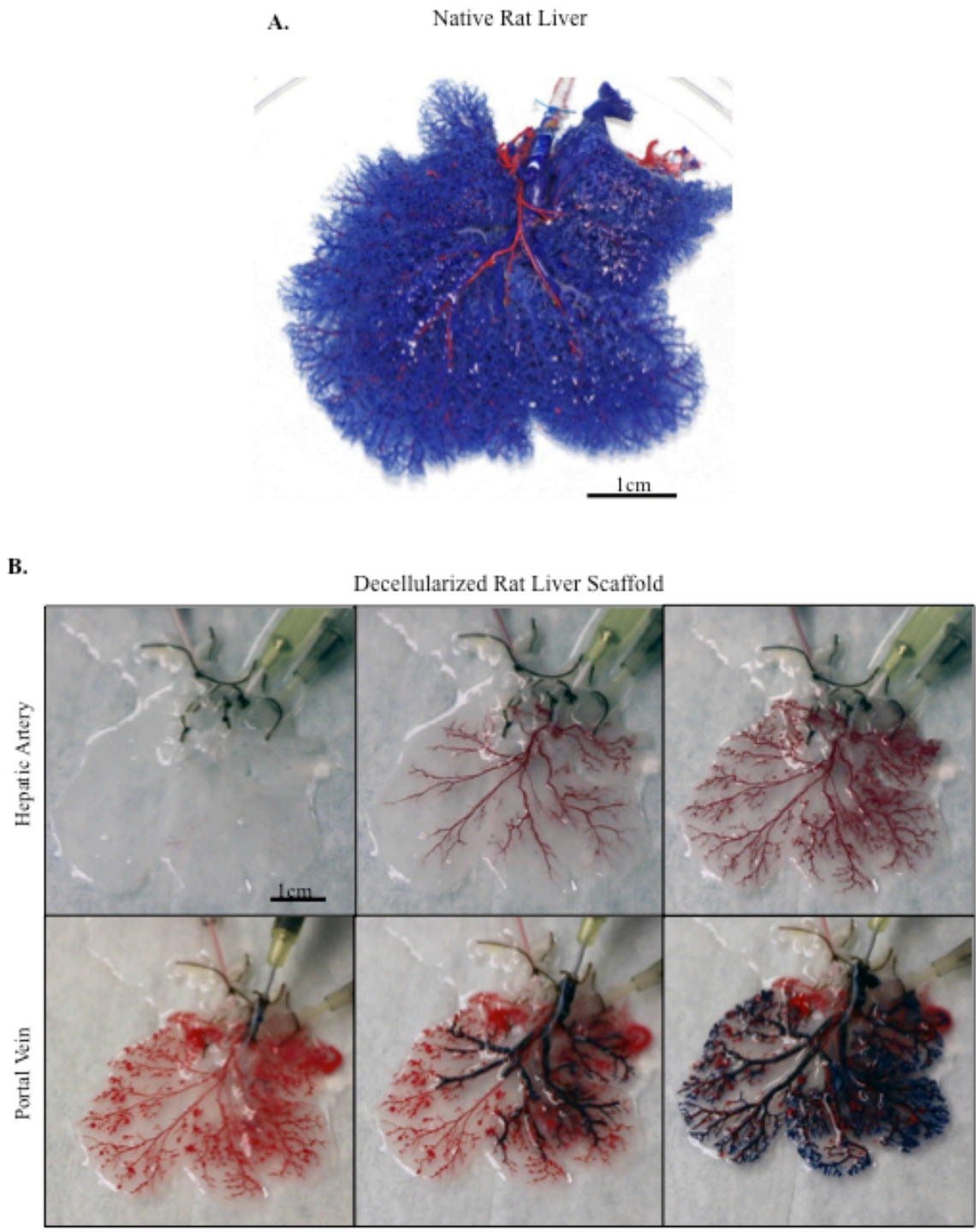

Figure 30. (A) Vascular cast of a native rat liver. (B) Vascular network of a decellularized rat liver scaffold. The venous network (blue) and the arterial network (red).

7.4.6 Investigation of Key Endothelial Cell Seeding Variables

Results showed that of the four factors investigated for endothelial seeding, cell density and rate of media perfusion had the greatest effect on the resulting vascular network. As seeding density and media perfusion rate were increased, endothelial coverage and viability also increased. Within three days of culture, seeded endothelial cells attached to the scaffold, displayed a flattened appearance, and a microvascular network was formed (Figure 31). Interestingly, cells seeded from the hepatic vein co-localized with cells seeded from the portal vein. Conclusions from this study are that endothelial coverage of major vessels within the decellularized liver scaffold is achievable after 3 days of culture. Increasing seeding density and media perfusion rate increases vessel coverage and cell viability

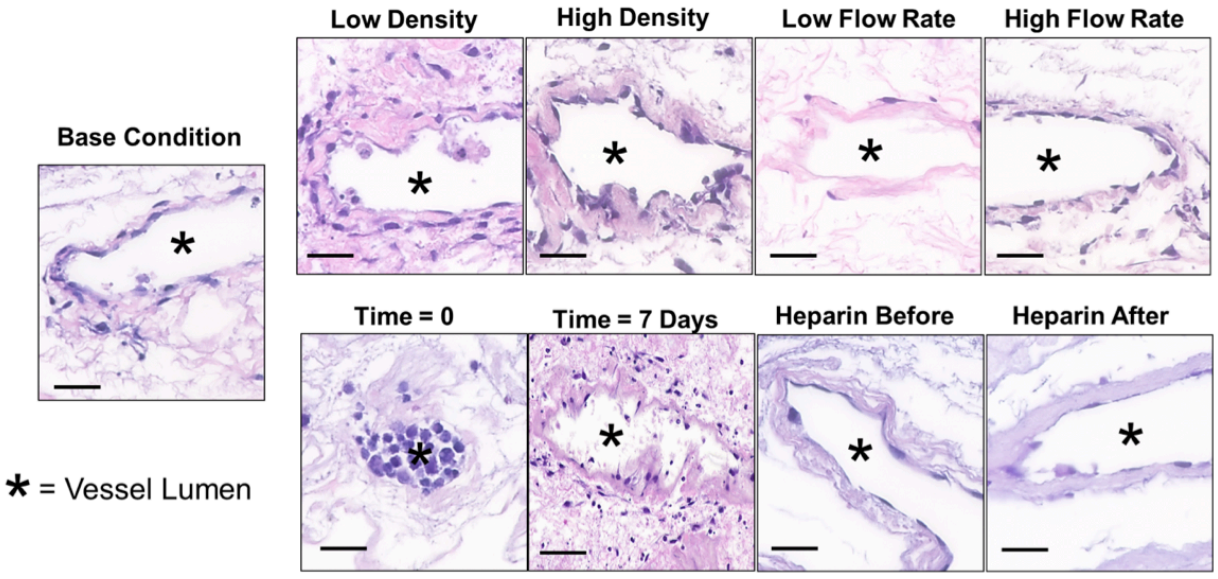

Figure 31. Representative H&E images from each seeding condition listed in Table 1. Scale bar = 50μm

7.4.7 Corline Heparin Coating and Its Effects on HMECs

Corline heparin product's interactions with Human Microvascular Endothelial Cells (HMECs) were determined. Specifically, we (1) determined the cytotoxicity, if any, of the Corline product on HMECs, (2) determined if the Corline product has an impact on endothelial cell attachment, and (3) determined if the Corline Heparin product can be applied on top of the HMECs after seeding.

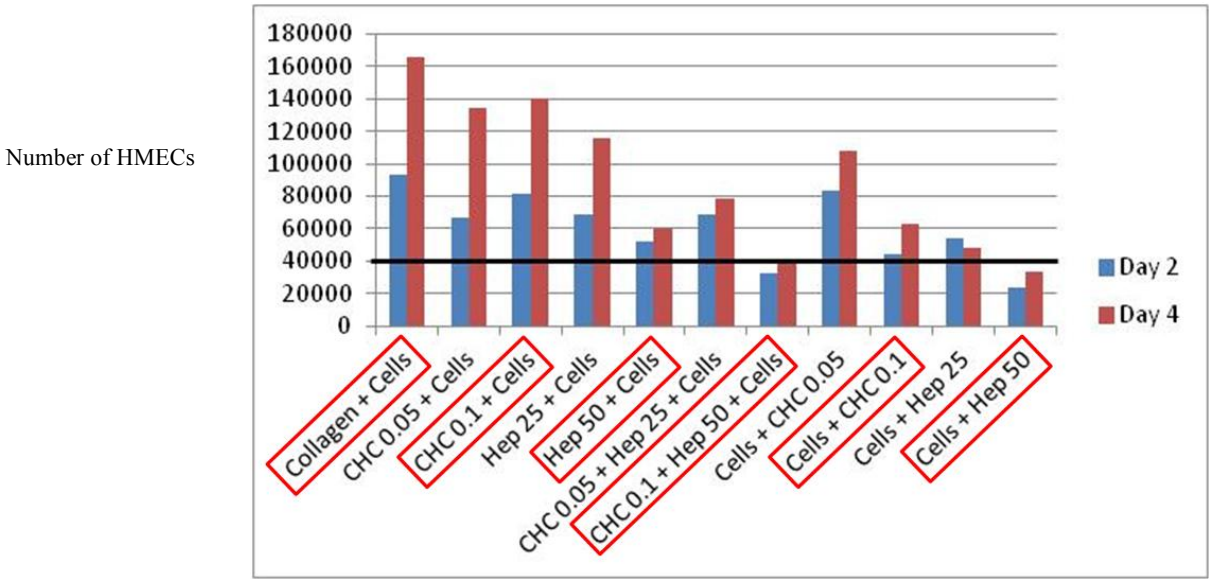

Figure 32: 40,000 HMECs were seeded onto collagen coated plates with the addition of CHC or free Heparin for a length of 2 and 4 days. Results show that free heparin inhibits the proliferation of HMECs, but CHC, at low concentrations, does not. Furthermore, higher cell proliferation was seen when CHC was added before seeding compared to adding CHC after seeding.

To test the effect of CHC upon endothelial cell attachment, native porcine hepatic vessels were isolated from healthy market weight pigs. These vessels were decellularized using our established published protocol for the decellularization of whole livers. Next, the decelled vessels were either coated with the Corline heparin conjugate or not coated. HMECs were cultured on the vessels for 4 and 7 days and fixed in 10% neutral buffered formalin.

At both 4 and 7 days there does not appear to be a difference in HMEC cell attachment, viability, or confluence when comparing the uncoated decellularized liver vessels with Corline coated decellularized liver vessels.

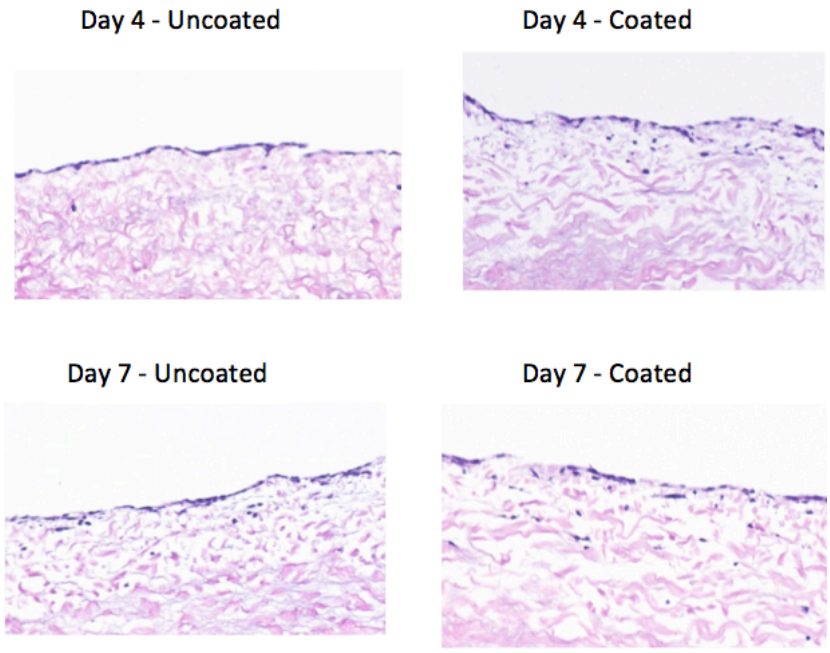

Figure 33: HMECs Cultured on uncoated decellularized liver vessels (left) and Corline coated decellularized liver vessels (right) for four (top) and seven (bottom) days. At both 4 and 7 days there does not seem to be a difference in HMEC cell attachment, viability, or confluence when comparing the uncoated decellularized liver vessels with Corline coated decellularized liver vessels.

To experimentally test the effect of CHC applied after HMEC seeding, native porcine hepatic vessels were isolated from healthy market weight pigs. These vessels were decellularized using our established published protocol for the decellularization of whole livers. Next, we coated the decellularized liver vessel with CHC, and HMECs were culture on it (count as day0). On day2 media containing CHC was added. Samples were collected on day 4 and 7.

The samples were fixed in 10% neutral buffered formalin and were stained with H&E to assess their attachment and viability. At both 4 and 7 days there was nodifference in HMEC viability or confluence between the samples with no CHC added on day 2 vs. samples with CHC added on day 2.

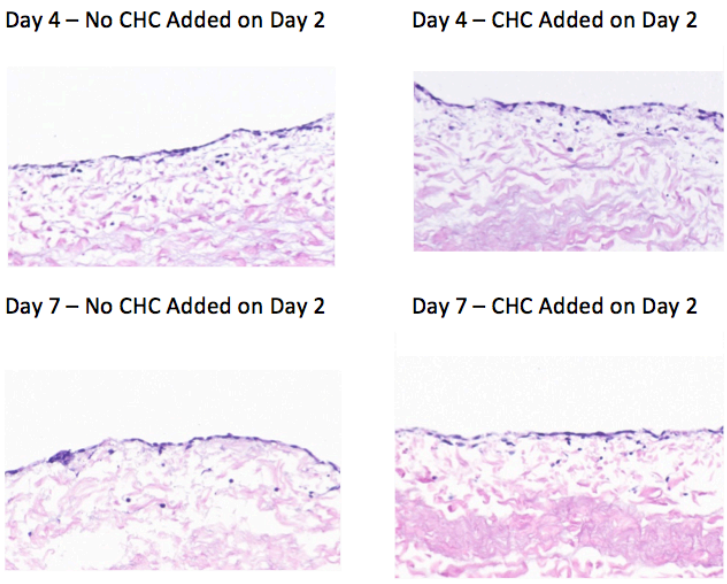

Figure 34. HMECs Cultured on CHC coated decellularized liver vessels with no CHC added on day 2 (left) and Corline coated decellularized liver vessels with CHC added on day two (right) for four (top) and seven (bottom) days. At both 4 and 7 days there does not appear to be a difference in HMEC viability or confluence between the samples with no CHC added on day 2 vs. samples with CHC added on day 2.

7.4.8 Reconstruction of the Venous Network

Following the first set of experiments conducted, in which we investigated key endothelial cell seeding variables, we then developed a new method for delivering endothelial cells within a decellularized rat liver. For one decellularized rat liver, endothelial cell seeding was performed on 3 separate days (10 million per day) as opposed to the previous method of 30 million cells seeded at the same time. Histologic assessment of the graft showed endothelial coverage of several major vessels within the decellularized rat liver as well as sinusoidal space. This microvascular formation within the sinusoidal space was not seen with previous seedings.

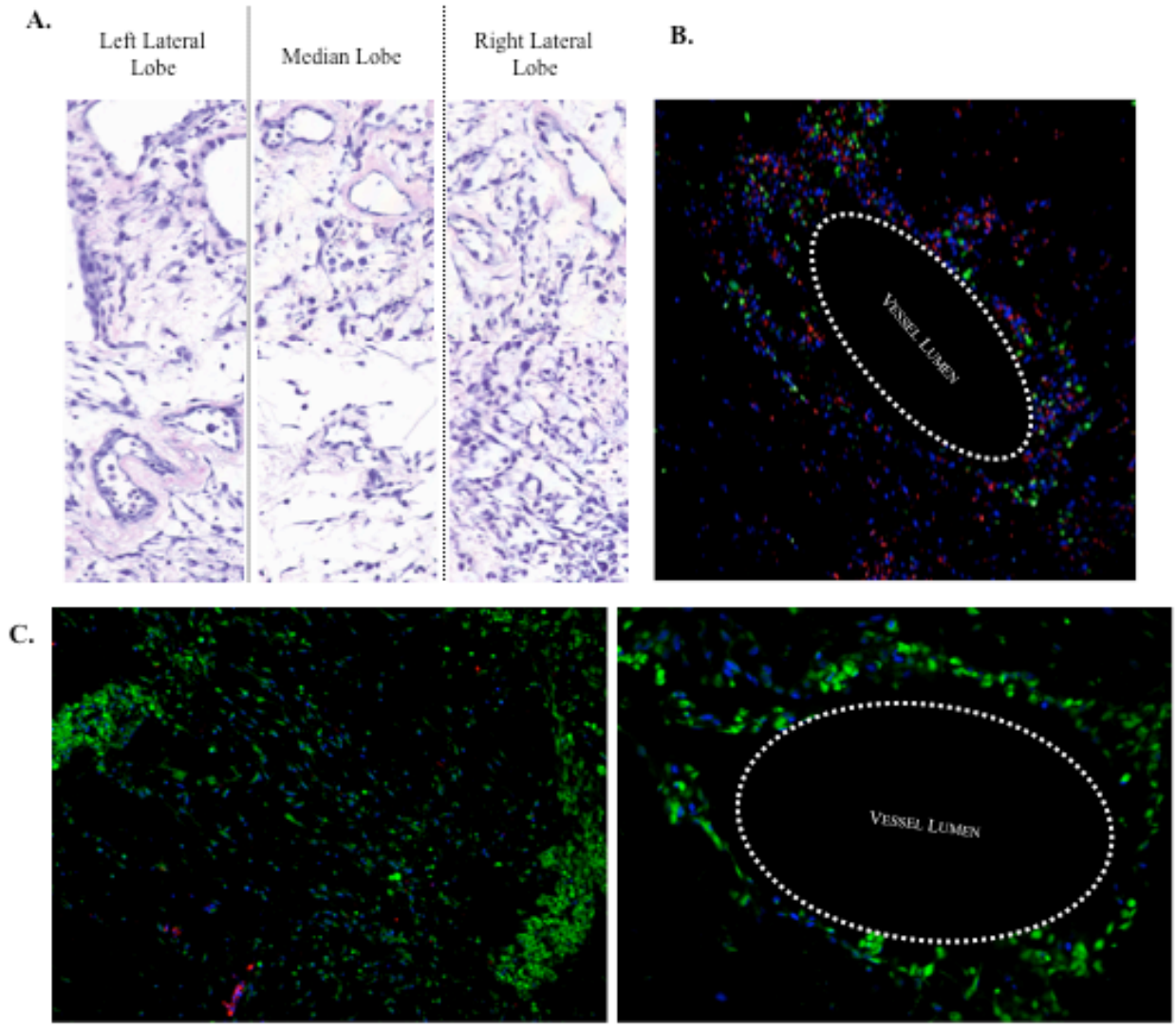

Figure 35. (A) Representative H&E images from our newly developed method of seeding microvascular endothelial cells within a decellularized rat liver. Endothelial cell coverage of major vessels as well as the sinusoidal space can be seen throughout the seeded scaffold. (B) HMECs delivered via the portal vein (red) co-localized with HMECs delivered via the hepatic vein (green)

7.4.9 Reconstruction of the Arterial Network

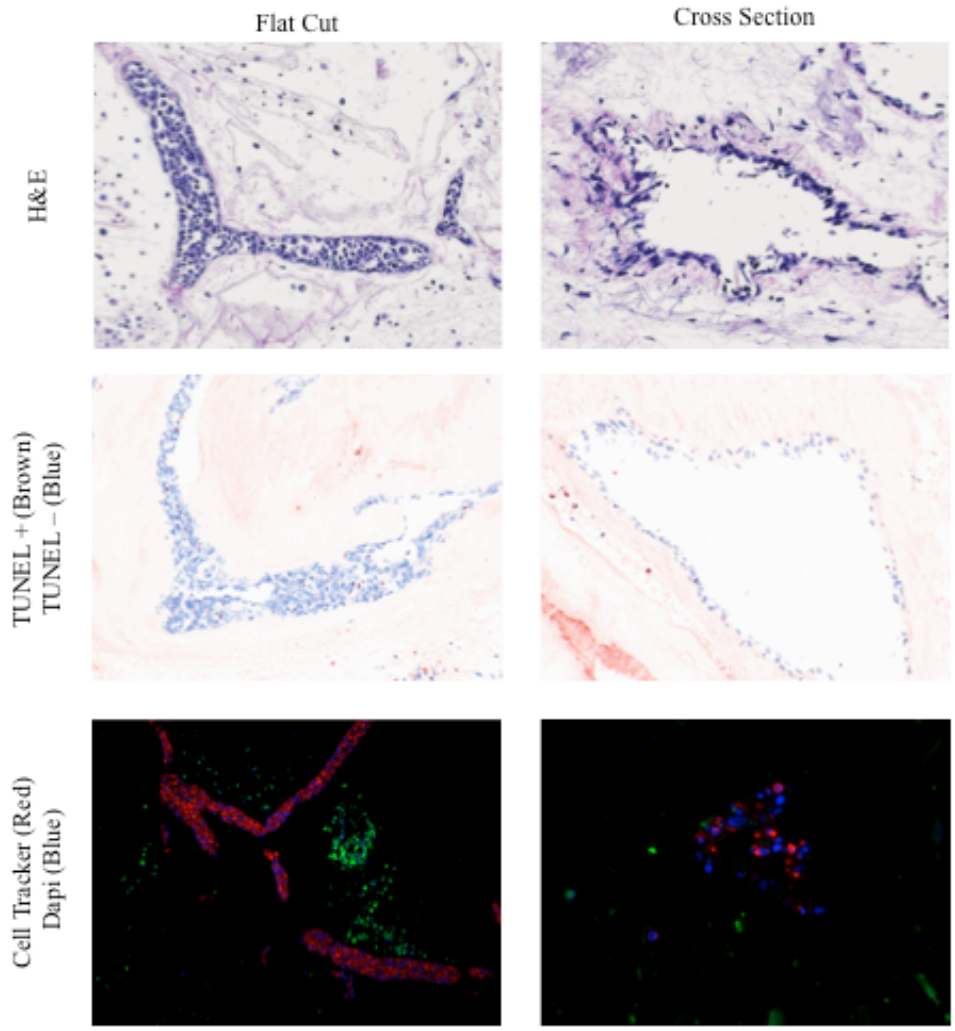

Figure 36. Isolation and cannulation of the hepatic artery allowed for endothelial cell delivery throughout the hepatic arterial network. After 3 days of culture an arterial network was formed and could be visualized via H&E. TUNEL stained showed a majority of cells are viable.

7.5 DISCUSSION

One of the major challenges for whole organ engineering is to produce large volume tissues capable of being connected to the recipient's blood supply for clinical applications. Pervious work in the field of bioengineer liver tissue has been met with many obstacles including cell sourcing, efficient cell seeding, vascularization of the engineered tissue, and provision of authentic cues for tissue development. The experiments conducted in this chapter were aimed at developing a technology that will provide meaningful progress toward engineering a fully functional hepatic vascular network within a decellularized liver scaffold. To do so, we presented here a method of decellularization that was used to fabricate a naturally derived whole-organ bioscaffold. We used the vascular channels as a conduit for reseeding human microvascular endothelial cells inside the bioscaffold. The three-dimensional liver bioscaffold provided spatial information for cell localization and engraftment, and supported cellular proliferation and phenotype maintenance. These developed methods offer a potential technique for fabrication of human liver tissue that can be readily transplanted into host animals or used for studies of liver cell biology, physiology, toxicology, and drug discovery with further development.

Previously, decellularization of tissue was performed by submersion of the tissue within a detergent solution under agitation to allow cell removal in bulk from the surface of the tissue moving inward. These approaches were successful for decellularization of smaller samples (up to 5 mm in thickness), whereas in thicker specimens the core of the tissue remained cellular. To circumvent this limitation, we took advantage of the native liver vascular network by perfusing the detergent through this network and distributing it throughout the entire liver. This gentle

procedure preserves the architecture of the liver matrix and vascular system. The choice of detergent for the production of whole organ bioscaffolds using perfusion may also impact the preservation of important biochemical cues. In chapters 5 and 6 we showed that harsh ionic detergents such as SDS facilitate rapid removal of cells from dense tissues and can yield a functional bioscaffold, but they may damage some ECM components. Therefore, we opted to use a mild nonionic detergent, Triton X-100. We found that this detergent could successfully decellularize the whole liver by the removal of a majority of cellular DNA. These studies highlight the utility of perfusion decellularization to generate whole organ bioscaffolds with significant potential for organ bioengineering.

Typically, neovascularization of bioengineered tissues was addressed by supplementing cells with angiogenic growth factors or fabricating scaffolds from synthetic material that allowed micro-patterning of vascular tree-like structures. When growth factors are used alone, they tend to create only a microvasculature consisting of small and fragile capillaries, and therefore this technique is only applicable for the engineering of smaller size tissues. An alternative fabrication method is using a micropatterning technique that can be scaled up to larger sizes by modular construction. However, currently this method cannot replicate the progressive complexity and ECM composition of the native liver vascular tree. The bioscaffolds generated from whole livers produced via our decellularization method retain the complexity of multiple size vessels that can deliver fluids from the larger vena cava or the portal vein and reach each individual liver lobule.

An additional advantage of this method is the retention of important ECM molecules required for site-specific engraftment and/or differentiation of different cell types that are present in the liver. Prior research showed that liver-specific stem cells can be isolated and differentiated to hepatic fate. We used human microvascular endothelial cells to recellularize the bioscaffolds.

The advantage of seeding human microvascular endothelial cells is that they are consistent in their proliferation rate, they are easy to maintain in culture, and they are associated with a low experimental cost. This allowed us to perform many recellularization experiments before moving to more clinically relevant iPSC derived human endothelial cells.

A major obstacle in producing large-volume tissues is the delivery of adequate numbers of cells to the entire thickness of the tissue. Commonly used methods for cell seeding into scaffolds employ static, dynamic, or perfusion bioreactor seeding, resulting in seeding of cells that can only penetrate several millimeters below the surface, with further engraftment dependent on active migration of the cells. Alternatively, previous methods to recellularize organ scaffolds have relied heavily on direct cell injection that damaged the scaffold microarchitecture and produced heterogeneous scaffold seeding. The perfusion method introduced here supports cell infusion through both the venous and arterial vascular networks and deposition throughout the thickness of the bioscaffold, achieving greater seeding efficiency without compromising the integrity of the bioscaffold. Furthermore, by accessing different vessels that feed into the liver, we were able to deliver cells selectively to different compartments of the liver tissue. Endothelial cells delivered through the vena cava selectively seeded larger and smaller blood vessels up to the pericentral area of the liver lobule, without reaching the periportal space of the lobule where the final branching vessels of portal vein are located. On the other hand, cells seeded through the portal vein, which delivers blood from the intestine and other organs to the liver, reached predominantly the periportal area of the liver lobule without extensive penetration to its pericentral space. These seeded endothelial cells cover the entire circumference of a vascular channel and maintained cell-cell junctions. Thus, simultaneous utilization of both vascular routes for cell seeding enables complete access to the entire length of the vascular network, which has

an essential importance for prevention of blood clotting and ultimately failure to transplant the bioengineered liver.

This study demonstrates that three-dimensional biologic scaffolds composed of liver extracellular matrix have the capability to become a completely re-endothelializes scaffold closely mimicking the native three-dimensional structure of liver tissue. The bioscaffold may also prove as a good tool to study normal tissue and organ development as well as liver pathology. Ultimately, this technology may bring us closer to the ultimate goal of providing bioengineered livers for transplantation.

8.0 SYSTEMATIC DEVELOPMENT OF METHODS FOR SEEDING HEPATOCYTES WITHIN A 3-DIMENSIONAL LIVER BIOSCAFFOLD

8.1 ABSTRACT

A major hurdle preventing whole organ engineering of the liver from translation to pre-clinical animal models includes the lack of an effective method for delivering hepatocytes to their native location. The objective of the work in this chapter was to develop a preferred method of delivering hepatocytes into a 3-dimensional liver scaffold achieving cell engraftment and functionality. Results showed higher viability, albumin and urea production with a trans-capsular injection method compared to infusion via the vasculature. These findings are important for eventual clinical translation of whole organ engineering.

8.2 INTRODUCTION

The critical shortage of viable donor organs for patients with end-stage organ failure continues to worsen with no immediate solution in sight. More than 120,000 patients are on the organ transplant list in the United States alone, and 18 patients die every day waiting for a donor organ[304]. Artificial organ devices such as dialysis machines, ventricular assist devices, and extracorporeal membrane oxygenation (ECMO) machines provide temporary support, but are inadequate and unsustainable long-term solutions. Whole organ engineering using naturally occurring three-dimensional bioscaffolds has emerged in recent years as a potential solution to the donor shortage [83, 305, 306]. This approach is based upon the concept that functional organ

tissue can be engineered by cell seeding a three-dimensional scaffold composed of homologous extracellular matrix (ECM). This approach would include immediate or near immediate in-situ transplantation of the cell seeded scaffold, providing the requisite perfusion by the host circulation with appropriate micro-environmental cues, nutrients, and signaling factors necessary for organ development, maintenance, and life-sustaining function.

In 2008, perfusion decellularization was described as a technique to generate acellular whole organ scaffolds from cadaveric organs [23]. Decellularizing agents were delivered via the native vasculature of the native heart and thereby distributed throughout the entire mass of the organ. This technique produced an acellular three-dimensional cardiac bioscaffold composed of naturally occurring extracellular matrix (ECM)[48, 83]. Theoretically, the resultant bioscaffold using this approach is ideal because the biochemical composition, micro and macro architecture, and extracellular cues would all be present. This technique has also been used to decellularize other whole organs such as heart [196], liver [24, 193-195, 197-200], lung [25, 201-203], pancreas[204], and kidney [205, 206].

\ The generation of a fully functional organ has yet to be accomplished, but several intermediate milestones have been reached. Current hurdles to successful long termpre-clinical animal studies include the re-establishment of a non-thrombotic microvasculature and an effective method for delivering and maintaining viable and functional parenchymal cells to their native location[25, 307]. Organ specific parenchymal cell function has been reported following bioreactor-assisted in vitro cell seeding[24, 194, 195].

The work described herein utilizes the liver as the test organ but the fundamental concepts may apply to all organs. Cell seeding techniques have not been systematically approached by isolating single key variables such as cell seeding density, perfusion pressure,

oxygen concentration, and other factors. Although such an effort can be exhaustive, a reasonable effort to identify a preferred technique is essential for success. Most reports to date have used perfusion techniques for both endothelial cell and parenchymal components.

Techniques employed in recellularization of whole-organ scaffolds are typically adaptations of methods from a wide range of procedures including traditional cell culture, tissue-engineering, cell-transplantation therapies, and isolated-organ perfusion. The recellularization process can be considered in two major steps. The first is cell seeding, in which the goal is distribution of parenchymal and non-parenchymal cell types to their native three-dimensional location within the liver scaffold. The second is perfusion culture, which is typically utilized to prepare the cells for *in vivo* transplantation by providing them with physiological conditions in-vitro. Typically, cells are either injected directly into the organ with a needled syringe or introduced via vascular perfusion with the expectation that the cells will migrate to their native site, proliferate, and self-assemble. Cell seeding efficiency has varied greatly.

The objective of the present study was to identify a perferred method of delivering parenchymal cells into the 3-dimensional liver bioscaffold and then to combine that method with the endothelial cell seeding methods developed in Chapter 7.

8.3 MATERIALS AND METHODS

Whole rat livers were decellularized using an established protocol to produce an acellular 3-dimensional liver bioscaffold. Two different methods of seeding hepatocytes into the 3-dimensional liver biscaffold were also evaluated: (1) direct parenchymal injection and (2) infusion via portal and hepatic veins. Metabolic activity of the engrafted hepatocytes was evaluated by quantification of albumin and urea production. Engrafted cell morphology and expression of hepatic specific genes were also used to evaluate the two seeding methods.

8.3.1 Animals

Female Sprague-Dawley rats (250–300g; Charles River Laboratories) were used for hepatocyte isolation and preparation of the three dimensional liver scaffolds. The animals were cared for in accordance with the guidelines set by the Committee on Laboratory Resources, National Institutes of Health, and Institutional Animal Care and Use Committee of University of Pittsburgh.

8.3.2 Preparation of 3-dimensional liver bioscaffold

The harvested livers of Sprague-Dawley rats were frozen at -80ºC for at least 24 h before decellularization to aid in cell lysis. The liver was thawed at room temperature in 1 x PBS. Decellularization was conducted by a retrograde perfusion technique at 8 mL/min, in which solutions flowed through the cannula, into the IVC, and throughout the vasculature of the liver.

Livers were placed in 500mL of 0.02% trypsin/0.05% EGTA solution at 37ºC, allowing the solution to flow through the liver for 2 h. Deionized water was perfused through the liver for 15 min followed by 15 min of 2 x PBS. The 3% Triton X-100/0.05% EGTA solution was perfused through the liver vasculature for 18–24 h with the solution being changed after 1, 4, and 16 h. A deionized water wash for 15 min followed by 2 x PBS wash for 15 min was repeated once, followed by a deionized water wash for 30 min and 2 x PBS wash for 30 min to aid in cell lysis and remove any recirculating debris. The three-dimensional liver bioscaffold was then perfused with 0.1% (v/v) peracetic acid/4% EtOH for 1 h. Acidic conditions were neutralized by PBS and deionized water washes twice for 15 min each.

8.3.3 Donor rat liver harvest

Surgical plane anesthesia was induced and maintained using inhalation of 1.5%–3% of isofluorane. The abdominal cavity was opened by a ventral midline incision extending from the pubis to the xyphoid process and the animals were injected intravenously with heparin (200 units). The inferior vena cava (IVC) and the portal vein were clamped. The portal vein and IVC were then cannulated with an 18G cannula, and 5–10mL of phosphate-buffered saline (PBS) containing heparin was injected. The diaphragm was cut to transect the superior vena cava and IVC. The liver was removed and stored in a cell culture dish filled with PBS solution. The liver was then rinsed with 10–20mL of PBS solution containing heparin (200 units). The livers were frozen at - 80ºC completely immersed in PBS solution before perfusion was performed for organ decellularization.

8.3.4 Primary rat hepatocyte isolation

Surgical plane anesthesia was induced and rats were maintained at this plane of anesthesia by inhalation of 1.5% – 3% isofluorane. Rat hepatocytes were harvested using a two-step collagenase digestion method. The isolation technique involved cannulation and perfusion through the hepatic portal vein with calcium and magnesium-free Hanks' salt solution followed by media containing collagenase at a flow rate of 12 mL/min as previously described. Viability was assessed by trypan blue exclusion and was routinely > 80%. The yield of the isolated hepatocytes was 5.0 – 7.0 x 10^8 viable cells per liver.

8.3.5 Hepatocyte seeding of three-dimensional liver scaffolds

Trans-capsular injection

A total of 1.5×10^6 cells (hepatocytes) suspended in 125 microliters of culture medium were delivered through twenty-five injections of 5 μL each into different hepatic lobes of the decellularized liver matrix with a 27G needle and a 1-cc tuberculin syringe. After 40 min of perfusion, the perfusate was collected, and the viability and the number of cells not retained in the liver were determined. To calculate the engraftment efficiency, the perfusate was collected and the number and viability of cells not retained in the liver (i.e., in the perfusate) was determined with a hemacytometer and trypan blue exclusion. The total number of cells retained in the decellularized liver represented the difference between the initial number of cells seeded

and the number of cells present in the perfusate after seeding. Reseeded scaffolds were perfused with hepatocyte culture media for 3 days flow through the portal and hepatic veins at a rate of 2 ml/min. Media was collected each day for albumin and urea quantification.

Infusion via the portal vein

A total of 1.5×10^6 cells (hepatocytes) suspended in 125 microliters of culture medium were delivered through a port located in the main chamber connected to the portal vein. The cells were infused via the portal vein at a rate of 2 ml/min until all cells entered the liver. After 40 min, the perfusate was collected, and the viability and the number of cells not retained in the liver were determined. Reseeded scaffolds were cultured in hepatocyte culture media for 3 days with continuous flow through the portal vein at a rate of 2 ml/min. Media was collected each day for albumin and urea quantification.

8.3.6 Investigating injection volume

Porcine liver ECM hydrogels, at a concentration of 8 mg/ml, were injected with varying injection bolus volumes of hepatocytes to determine the effect of injection volume on hepatocyte viability and functionality. Injection volumes of 5ul, 10ul and 20ul were investigated. The effect of varying injection volume on hepatocyte viability and function was assessed through ammonia metabolism, albumin production and transcription profiling of hepatocyte specific genes. Each porcine liver ECM hydrogel was injected with 500,000 primary rat hepatocytes and cultured

8.3.7 Functional assessment of seeded hepatocytes

Measurement of albumin secretion

Conditioned media was collected on days one, two, and three and stored at -80°C until analysis. Hepatocyte secretion of albumin was measured using a commercially available kit (Bethel Laboratories, Texas). At least three samples were collected from each culture condition and each sample was measured in triplicate.

Measurement of urea section

Primary rat hepatocyte metabolism of ammonia was measured. Media was aspirated and hepatocytes were incubated with 2.5 mM NH4Cl in hepatocyte maintenance media for two hours at 37°C. The conditioned media was collected and the concentration of NH3N was measured using a commercially available kit (Wako Pure Chemical Industries, Tokyo, Japan). At least three samples were collected from each culture condition and each sample was measured in triplicate.

Quantitative real-time PCR

Total RNA from cell lysates was isolated using Trizol reagent as instructed by the manufacturer. RNA concentration was determined by spectrophotometer at 260 nm. The purity of RNA was determined by spectrophotometry using the 280nm=260nm ratio, and the integrity checked by agarose gel electrophoresis stained with ethidium bromide.

RNA was stored at - 80ºC until further use. mRNA expression levels of albumin, BSEP, and NTCP were determined using TaqMan quantitative RT-PCR assays. From each group, 2 mg of total RNA was incubated with 5U RNA qualified (RQ) DNAse, 5 mL 10RQ buffer in a total volume of 10 mL at 378C for 30 min. The samples were then incubated with 1 mL RQ DNase Stop Solution at 65ºC for 10 min. The DNAse-treated RNA was then incubated with 1 mL of random hexamer primers (100 ng=L) at 70ºC for 5 min for cDNA synthesis. cDNA generation continued with incubation at 37ºC for 60 min with the following reagents: 1 mL deoxynucleotide triphosphate (dNTP) (10mM of each), 5 mL MMLV 5, and 1 mL MMLV RT for a total volume of 12 mL.

TaqMan one-step RT-PCR assays were performed with 4 ng of each RNA sample in a final reaction volume of 72 mL prepared from TaqMan one-step RT-PCR Master Mix Reagents Kit. Assays were performed using an Applied Biosystems' ABI Prism 7900HT sequence detection system. An initial RT step occurred for 30 min at 488 and was subsequently followed by heating to 95ºC for 10 min followed by 40 cycles of 95ºC for 15 s and 60ºC for 1 min.

8.3.8 Seeding of endothelial cells and hepatocytes within a decellularized rat liver

The addition of functional, viable hepatocytes to the re-endothelialized liver scaffold was also been achieved. Following re-endothelialization, primary rat hepatocytes were delivered via 5ul syringe injections into the parenchymal space of the decellularized scaffold. The hepatocytes were cultured for 3 days within the re-endothelialized scaffold. Histologic assessment confirms the hepatocytes are viable and they have integrated with the endothelial cells

8.4 RESULTS

8.4.1 Hepatocyte seeding portal vein infusion vs. trans-capsular injection

Representative H&E image of hepatocytes 3 days post seeding using the portal vein infusion technique and the trans-capsular syringe injection are shown in **Figure 37**. Seeding hepatocytes via the portal vein of the decellularized rat scaffold results is vascular occlusions and prevents media flow through the scaffold. Syringe injection of primary rat hepatocytes directly into the parenchymal space of the decellularized rat liver scaffold results in higher functionality compared to portal vein infusion **(Figure 37)**.

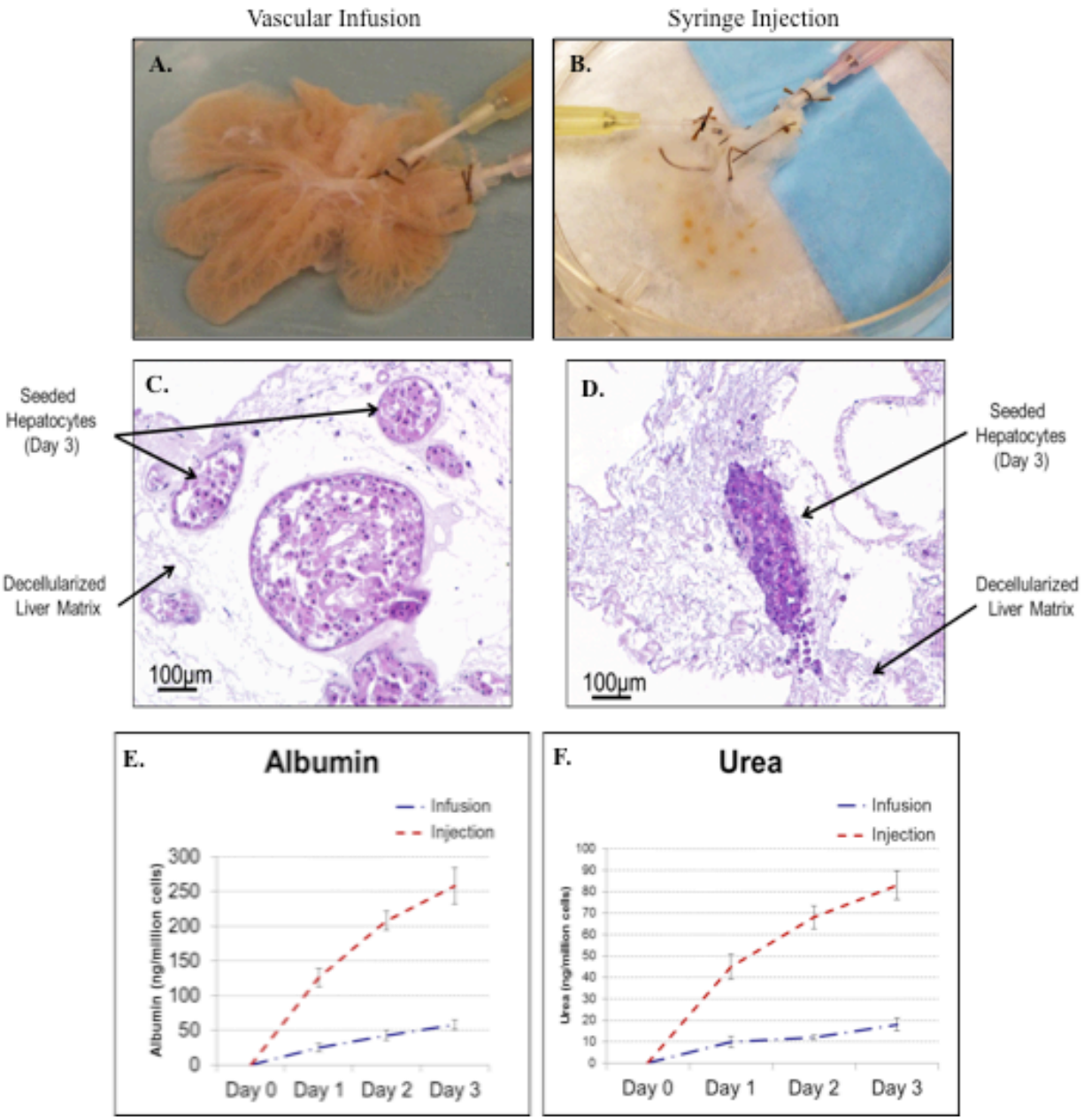

Figure 37. Representative H&E image of hepatocytes seeded via infusion (top left) and syringe injection (top right) three days post seeding. Engraftment efficiency, albumin production, and urea production from each technique (bottom row).

8.4.2 Optimization of injection size

Injection volume was also evaluated for its effect on hepatocyte function following seeding. The function of hepatocytes was assessed by analyzing the transcription profile of hepatocyte specific genes namely Albumin, CYP1A1, CYP1A2, CYP3A2, Connexin-32. Pig liver extracellular matrix (PLECM) gel was used for this experiment instead of whole decellularized rat livers. Results revealed that decreasing injection volume increased hepatocyte viability and functionality **(Figure 38)**. Studies that have been published on the effects of cell density on the hepatocyte viability, proliferation, and function indicate that for hepatocytes to survive in an in-vitro environment aggregation of hepatocytes is essential. Aggregation is postulated to promote viability and function. However, aggregation is double edge sword as large aggregation of cells would be toxic for the survival of tissue and minimal aggregation would hamper the viability of the cells.

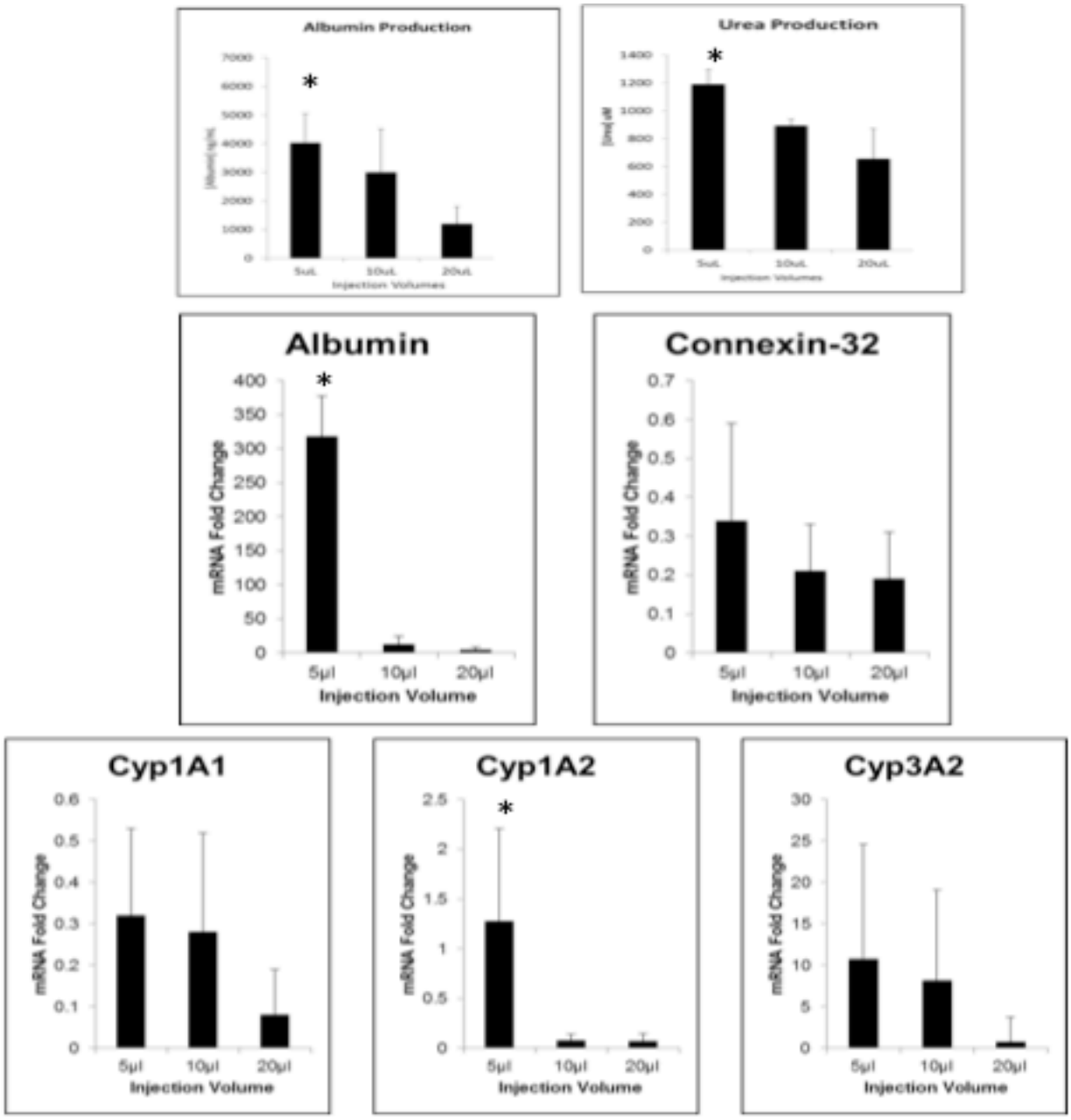

Figure 38. Albumin and Urea secretion from primary rat hepatocytes injected into porcine liver ECM gels using various injection volumes (top row). Effect of concentration and injection volume on function of hepatocytes seeded in PLECM gel. mRNA expression of Albumin, CYP1A1, CYP1A2, CYP3A2, Connexin-32(middle and bottom rows). mRNA expression normalized to Cyclophilin a gene. Error bars show mean ± standard deviation, and * indicates significance at $p<0.05$. Sample size is n=3.

8.4.3 Co-seeding of hepatocytes and endothelial cells

The addition of functional, viable hepatocytes to the re-endothelialized liver scaffold has also been achieved. Following re-endothelialization, primary rat hepatocytes were delivered via 5ul syringe injections into the parenchymal space of the decellularized scaffold. The hepatocytes were cultured for 3 days within the re-endothelialized scaffold. Histologic assessment confirms the hepatocytes are viable and they have integrated with the endothelial cells (**Figure 39**).

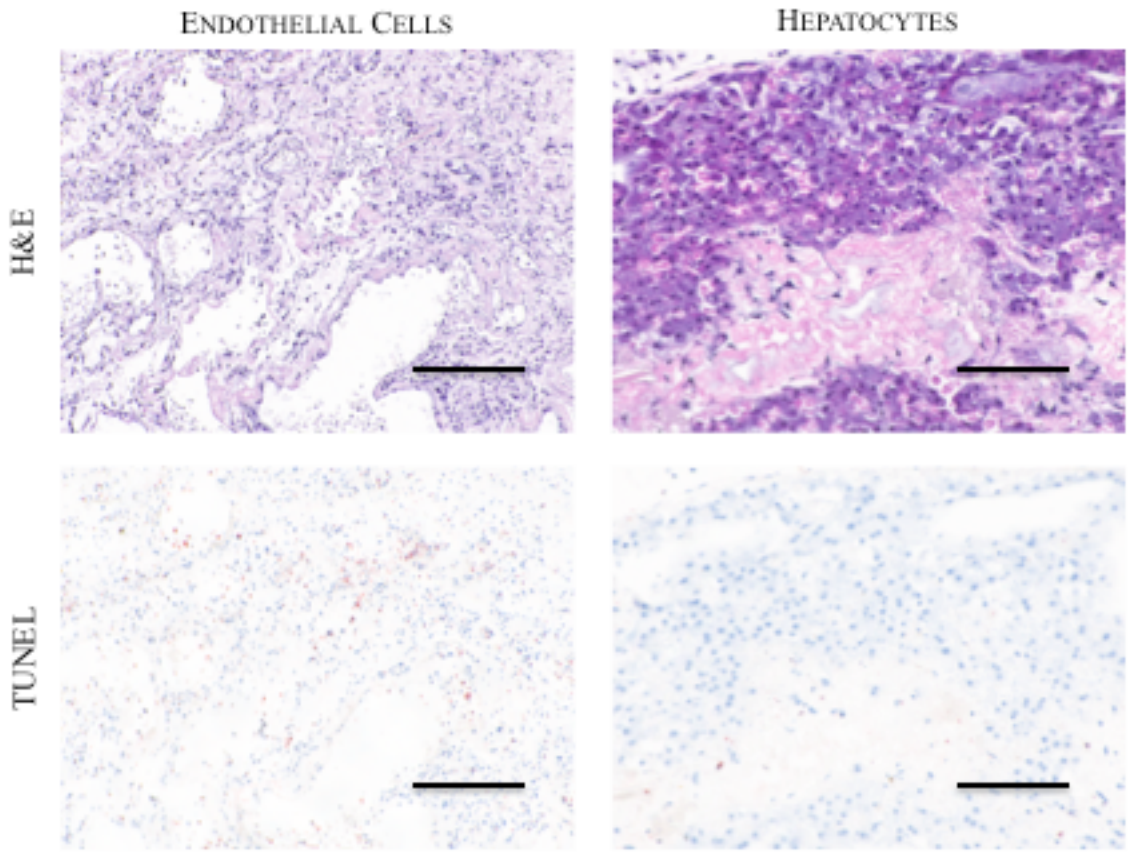

Figure 39. Viable endothelial cells and hepatocytes following culture within a decellularized rat scaffold. TUNEL is a common method for detecting DNA fragmentation that results from apoptotic signaling cascades. The TUNEL positive cells are brown and the TUNEL negative cells are glue. A majority of the hepatocytes and endothelial cells are negative, meaning they are not apoptotic. Scale bar = 50μm

8.5 DISCUSSION

The current study was motivated by the need to optimize hepatocyte seeding within a decellularized liver scaffold in order to enhance viability and functionality of the hepatocytes. The appropriate spatial distribution of hepatocytes following seeding into a 3-D liver scaffold is essential for regeneration of a native like hepatic tissue. The results of the study reveal that decreasing cell seeding density and injection volume increased hepatocyte viability and functionality. Studies that have been published on the effects of cell density on the hepatocyte viability, proliferation, and function indicate that for hepatocytes to survive in an in-vitro environment aggregation of hepatocytes is essential. Aggregation is postulated to promote viability and function. However, aggregation is double edge sword as large aggregation of cells would be toxic for the survival of tissue and minimal aggregation would hamper the viability of the cells. Falasca et al. showed that contact between hepatocyte cells was established following perfusion of hepatocyte into alginate beads, a weak adhesive matrix, within 6 hours of seeding. The cell-cell contacts were characterized by actin, and cytokeratin along adhesion junctions, as well as gap junctions characterized by connexins.

In the current study, the expression of Connexin-32 was found to be higher when 5ul of hepatocytes alone at a density of 8.36 x 106 /ml was injected into the PLECM gels compared to PLECM gels injected at 10ul or 20 ul and at a cell density of 12.5 x 106 /ml or 25 x 106 /ml. The higher fold expression of Connexin-32 transcripts at injection volume of 5ul and at a density of 8.36 x 106 /ml hepatocytes indicates that 5ul injection size and concentration of 8.3 x 10 6 are preferred for achieving cell-cell contact between adjacent hepatocyte cells without inducing clumping that would be toxic to tissue health. The expression of albumin was very high in

PLECM gels and in decellularized liver scaffolds seeded with hepatocytes alone. This is consistent with results from other studies wherein biodegradable polymers seeded with hepatocytes survived with high rate of albumin secretion (Vacanti et al., Dvir-ginzberg et al.). The high rate of albumin secretion is in fact observed in native rat livers too, which secrete 140–170 pg/cell/day(Takahashi et al.).

The current study highlights the significance of hepatocyte delivery and injection volume when reseeding a decellularized liver scaffold. This study demonstrates that three-dimensional biologic scaffolds composed of liver extracellular matrix have the capability to become a completely re-endothelializes scaffold closely mimicking the native three-dimensional structure of liver tissue. The bioscaffold may also prove as a good tool to study normal tissue and organ development as well as liver pathology. Ultimately, this technology may bring us closer to the ultimate goal of providing bioengineered livers for transplantation.

9.0 IMPROVING HEPATIC FUNCTION OF PRIMARY RAT HEPATOCYTES USING ENZYMATICALLY DIGEST LIVER ECM FROM VARIOUS SPECIES

9.1 ABSTRACT

Whole organ engineering and cell-based regenerative medicine approaches are being investigated as potential therapeutic options for end-stage liver failure. However, a major challenge of these strategies is the loss of hepatic specific function after hepatocytes are removed from their native microenvironment. The objective of the present study was to determine if solubilized liver extracellular matrix, when used as a media supplement, can better maintain hepatocyte phenotype compared to type I collagen alone or solubilized ECM harvested from a non-liver tissue source. Liver extracellular matrix (LECM) from four different species was isolated via liver tissue decellularization, solubilized, and then used as a media supplement for primary rat hepatocytes (PRH). The four species of LECM investigated were human, porcine, canine and rat. Cell morphology, albumin secretion, ammonia metabolism, and hepatic specific gene activity were used to assess maintenance of hepatocyte function. Biochemical and mechanical characterization of each LECM was also conducted. Results showed that PRH's treated with canine and porcine LECM maintained their phenotype to a greater extent compared to all other groups. PRH's treated with canine and porcine LECM showed increased bile production, increased albumin production, and the formation of multinucleated cells. The findings of the present study suggest that solubilized liver ECM can support in-vitro hepatocyte culture and should be considered for whole organ engineering and cell-based approaches for treating end-stage liver failure.

9.2 INTRODUCTION

In vitro culture of hepatocytes is associated with rapid dedifferentiation and decreased hepatocyte-specific functions such as albumin secretion and ammonia metabolism, and loss of hepatocyte polarity [308, 309]. The identification of a substrate or media supplement that can maintain a functional hepatocyte differentiation profile would represent a significant advancement toward development of a cell-based therapies, including tissue-engineered liver grafts for treatment of end-stage liver disease and 2-D hepatocyte culture systems.

Individual extracellular matrix (ECM) components or combinations of desired ECM components have been used as substrates for hepatocyte culture systems for several decades [310-314]. Although cell culture substrates composed of individual ECM proteins such as type-I collagen, laminin, and fibronectin have facilitated primary rat hepatocyte attachment, maintenance of selected liver-specific functions, and preservation of hepatocyte polarity and morphology for short periods of culture, these systems are insufficient to prevent dedifferentiation of hepatocytes [59, 315].

Conventional in vitro culture models for hepatocytes include the use of a sandwich configuration in which hepatocytes are either placed between two layers of type-I collagen or Matrigel (MG) or cultured on type-I collagen overlaid with MG [316-319]. Sandwich culture of primary hepatocytes maintains hepatocyte polarity and morphology better than hepatocytes cultured on a single layer of type-I collagen or MG [71, 320, 321]. Furthermore, hepatocyte-specific functions, such as albumin secretion, urea synthesis, and cytochrome P450 responsiveness and inducibility are enhanced when the sandwich culture model is used [308, 310, 322-325].

It is plausible that enzymatically digested ECM derived from the liver itself might be a useful media supplement for hepatocyte culture. Although rat liver matrix might theoretically be superior to that from other species for the maintenance of rat hepatocyte function, we compared liver ECM from various species using primary rat hepatocytes to determine species-specific advantages. The objective of the present study was to compare the ability of porcine, human, rat, and canine liver ECM, and heterologous ECM derived from porcine small intestinal mucosa and urinary bladder to support the primary rat hepatocyte (PRH) albumin secretion, ammonia metabolism and normal hepatocyte morphology. Biochemical and mechanical analysis of hydrogels created from these species of LECM was also conducted to more fully characterize species-specific differences.

9.3 MATERIALS AND METHODS

9.3.1 Overview of Experimental Design

Liver extracellular matrix was isolated from porcine, canine, human, and rat livers. Each liver tissue was subjected to the same decellularization protocol, which consisted of comminuting the liver into cubes of approximately 0.5 cm^2, exposing the tissue to trypsin/EGTA, inducing cell lysis with the detergent Triton X-100, rinsing with phosphate buffered saline and deionized water and disinfecting with peracetic acid. The resulting liver ECM from each species was lyophilized, powdered and pepsin solubilized. The composition of each was determined by quantifying DNA content, base pair length, sulfated glycosaminoglycan content and by performing a SDS-PAGE gel. Hydrogels from each group were formed and rheological properties were quantified. The

fiber network of the hydrogels was imaged using scanning electron microscopy. Finally, the ability of each liver ECM to support hepatocyte phenotype in-vitro was determined. Primary rat hepatocytes were isolated and cultured on rat tail collagen I. Solubilized liver ECM from each species was added to the culture media over a 7 day culture. Non-supplemented media, pepsin, and media supplemented with ECM from porcine small intestinal submucosa (SIS) or urinary bladder matrix (UBM) were used heterologous controls. Albumin production, ammonia metabolism, and hepatic specific cell morphology were assessed for each treatment group.

9.3.2 Tissue Decellularization

The methods used to isolate liver ECM have been previously described [52, 59, 195, 326]. Livers were harvested from market weight pigs (110–130 kg), adult dogs, and adult Sprague Dawley rats immediately after euthanasia. Non-diseased, human liver tissue was obtained with Institutional Review Board approval from one human donor liver of an unknown age. The tissues were rinsed with Type 1 water and frozen at -80ºC until used. Each liver tissue was cut into 0.5 cm^3 pieces with a scalpel and subjected to three separate 15-min washes in deionized water with mechanical agitation on an orbital shaker. The sections were then gently massaged to aid in cell lysis and soaked in 0.02% trypsin/0.05% EGTA at 37ºC for 2 h. The tissue was rinsed in type 1 water, and the massaging was repeated followed by mechanical agitation of the liver sections in 3% Triton X-100 for 18-24 h. The rinsing was repeated until all visible remnants of cellular material were removed. After processing, the liver ECM from each species was immersed in a solution of 0.1% peracetic acid followed by repeated rinses in type 1 water or

phosphate-buffered saline (PBS) at pH 7.4. The extent of decellularization was determined by quantification of remaining DNA (described below).

Harvest of small intestinal submucosa and urinary bladder matrix has been described previously in detail [142, 327-330]. In brief, to prepare SIS, small intestine was obtained from 6-month-old pigs and the majority of the mucosa and the entire serosa and muscularis externa layers were mechanically delaminated from the intestine. The remaining submucosa, muscularis mucosa, and stratum compactum layers were then washed with water and treated with 0.1% peracetic acid/4% ethanol for 1 hr.

Porcine urinary bladders were harvested from market weight pigs, and the urothelial, serosal, muscular and submucosal layers were removed by mechanical delamination. The remaining tissue consisted of intact basement membrane and tunica propria, which was rinsed with deionized water and then treated with 0.1% peracetic acid/4% ethanol on an orbital shaker for 2 h. The UBM was then rinsed twice with PBS for 15 min each followed by two 15 min rinses in deionized water

All decellularized tissues were embedded in paraffin, sectioned (5 μm), mounted onto microscope slides, and stained with hematoxylin and eosin (H&E) and DAPI.

9.3.3 Assessment of DNA and Glycosaminoglycan Content

DNA was extracted from all samples of liver ECM as previously described [240, 251, 331]. After lyophilization, LECM scaffolds were powdered using a Wiley Mill and filtered through a 60-mesh screen. One hundred milligrams of lyophilized, powdered liver ECM was digested with proteinase K digestion buffer (100 mM NaCl, 10 mM Tris HCl (pH = 8), 25 mM EDTA (pH =

8), 0.5% SDS, 0.1 mg/mL proteinase K) at 50ºC for 48 h. The digest was extracted twice using 25:24:1 (v/v/v) phenol/chloroform/isoamyl alcohol. DNA was precipitated from the aqueous phase at 20ºC with the addition of 2 volumes of ethanol and 0.1 volume of 3 M sodium acetate (pH = 5.2). The DNA was then centrifuged at 10,000 g for 10 min and resuspended in 1 mL of TE buffer (10 mM Tris (pH = 8), 1 mM EDTA).

The concentration of each extracted DNA sample was determined using Quant-iT PicoGreen dsDNA Assay Kit (Invitrogen) following the manufacturer's recommended protocol. A standard curve was constructed by preparing samples of known DNA concentrations from 0 to 1000 ng/mL and concentration of DNA was found by linear interpolation of the standard curve. Samples were read using SpectraMax M2 Plate Reader (Molecular Devices, Sunnyvale, CA). DNA samples were diluted to ensure their absorbance properties fell within the linear region of the standard curve.

Sulfated glycosaminoglycan (sGAGs) concentration in LECM samples was determined using the Blyscan Sulfated Glycosaminoglycan Assay Kit (Biocolor Ltd, Belfast, Northern Ireland). For extraction of sGAGs, lyophilized ECM scaffolds were powdered using a Wiley Mill and filtered through a 60-mesh screen. Samples were prepared by digestion of 50 mg/mL dry weight of each sample with 0.1 mg/mL proteinase K in buffer (10 mm Tris–HCl, pH 8, 100 mm NaCl, 25 mm EDTA) for 48 h at 50 °C. Digested samples were assayed following the manufacturer's protocol.

9.3.4 Enzymatic Digestion and Hydrogel Formation

The method used to prepare a hydrogel of harvested ECM has been previously described [251, 328]. The protocol was modified to produce a gel form of each liver ECM. First, a powdered form of the liver ECM was produced from cubic pieces of liver ECM. The hydrated, disinfected liver ECM was lyophilized overnight. Lyophilized tissue of liver ECM from each species was cut into small pieces, powdered using a Wiley Mill, and then filtered through a 60-mesh screen. One gram of lyophilized LECM powder and 100 mg of pepsin (2000–3000 U=mg) were mixed in 100 mL of 0.01 M HCl and stirred until all visible particles were soluble (between 24-72 h) at room temperature (25ºC). The final viscous solution of pepsin digested liver ECM had a pH of approximately 3.0–4.0. A hydrogel was formed from the solubilized liver ECM by neutralizing the pH to 7.4 and diluting the ECM pre-gel solution to 8 mg ECM/ mL, then incubating at 37 °C for approximately 40 minutes.

9.3.5 Scanning Electron Microscopy and Fiber Network Architecture Analysis

Scanning electron microscopy was used to examine the surface topography of human, porcine, rat, and canine LECM hydrogels. Five hundred micron thick hydrogels were prepared and then fixed in cold 2.5% glutaraldehyde (Electron Microscopy Sciences, Hatfield, PA) for 1 h followed by three 15 min washes in 1x PBS. Hydrogels were dehydrated in a graded series of alcohol (30, 50, 70, 90, 100% ethanol) for 15 min per wash, and then placed in 100% ethanol overnight. Hydrogels were washed 3 additional times in 100% ethanol for 15 min each and critical point dried using a Leica EM CPD030 Critical Point Dryer (Leica Microsystems, Buffalo Grove, IL,

USA) with carbon dioxide as the transitional medium. Hydrogels were then sputter-coated with a 4.5 nm thick gold/palladium alloy coating using a Sputter Coater 108 Auto (Cressington Scientific Instruments, UK) and imaged with a JEOL JSM6330f scanning electron microscope (JEOL, Peabody, MA, USA).

Fiber network descriptors were determined from SEM images of each liver ECM including: porosity, pore size, node density (number of fibers intersections per μm^2), connectivity (number of fibers connected at each node) and fiber diameter. Porosity was described as the percentage of each image composed of pores. Automated extraction of these fiber architectural features was achieved with a previously described algorithm [260]. Briefly, the SEM image was digitally processed by a cascade of steps including equalization with a 3x3 median filter, local thresholding through the Otsu method, thinning, smoothing, morphological operators, skeletonization, binary filtering for Delaunay network refinement, and ultimately the detection of fiber network architecture and its descriptors.

9.3.6 Liver ECM Hydrogel Rheological Testing

Rheological properties were determined for each of the various liver ECM hydrogels using a previously described method [251]. Briefly, the pH of the ECM digest was neutralized to 7.4 and the digest was then diluted to a concentration of 8 mg ECM/ ml. The pregel solution was then placed on a rheometer (AR 2000, TA Instruments) operating with a 40 mm parallel plate geometry, pre-cooled to 10 °C. Temperature was controlled within 0.1 °C using a Peltier plate. Mineral oil was spread along the edge to minimize evaporation of the sample. After loading, the steady sheer viscosity of each sample was measured by applying a stress of 1 Pa at a frequency

of 0.159 Hz. The temperature was then rapidly increased to 37 °C and a small oscillatory strain of 0.5% was imposed to track gelation kinetics. After complete gelation, a creep test of 1 Pa for 20s was performed to verify that there was no slip between the ECM hydrogel and the rheometer plates.

9.3.7 SDS-Page Gel Electrophoresis with Silver Stain

Protein composition of each LECM digest was compared qualitatively using SDS Page and gel electrophoresis. To compare proteins of a low molecular weight, 5 µg of each ECM digest was added to a 4-20% polyacrylamide gel and run at 120V for two hours. To compare proteins of a high molecular weight, 5 µg of each ECM digest was added to a 4-20% polyacrylamide gel and run at 120V for seven hours. The gels were stored in fixing buffer overnight and then stained with a Pierce™ Silver Stain for Mass Spectrometry Kit (Life Technologies) following the manufacturer's instructions.

9.3.8 Rat Hepatocyte Isolation and Culture

Primary rat hepatocytes (PRH) were isolated using a previously established method [195]. Surgical plane anesthesia was induced and mice were maintained at this plane of anesthesia by inhalation of 1.5%–3% isofluorane. Rat hepatocytes were harvested using a two-step collagenase digestion method. The isolation technique involved cannulation and perfusion through the hepatic vein with calcium and magnesium-free Hanks' salt solution followed by media containing 400µg/ml collagenase (Seromed, Collagenase Type CLS II) at a flow rate of 10

ml/min as previously described.[14] Viability was assessed by trypan blue exclusion and was routinely >90%. The yield of the isolated hepatocytes was $5.0–6.0\times10^7$ cells per liver. The cells were used immediately following isolation.

Cells were seeded on 6-well rat tail type I collagen coated plates and allowed to culture for one day in hepatocyte basal media. After one day, media was changed and supplemented with 50 μg/mL of human LECM, 50 μg/mL of porcine LECM, 50 μg/mL of canine LECM, or 50 μg/mL of rat LECM. Non-supplemented media, 10 μg/mL pepsin, and supplementation with 50 μg/mL UBM or 50 μg/mL of SIS were included as controls. Conditioned media from each well was collected on days 2, 5, and 7 and tested for albumin production. Images were taken on days 2, 5, and 7 to compare cell morphology. PRH metabolism of ammonia to urea was measured on day 7 of culture.

9.3.9 Measurement of albumin secretion

The conditioned media was collected from rat hepatocyte cultures on days 2, 5, and 7, and stored at -80ºC until analysis. Hepatocyte secretion of albumin was measured using a commercially available kit (Bethyl Laboratories, Montgomery, TX). At least three samples were collected from each culture condition and each sample was measured in duplicate.

9.3.10 Ammonia metabolism assay

Primary rat hepatocyte metabolism of ammonia was measured on day 7 of culture for each group. The media was aspirated and hepatocytes were incubated with 2.5 mM NH_4Cl in

hepatocyte basal media for two hours at 37ºC. The conditioned media was collected and the concentration of urea was measured using a commercially available kit (Bioassay Systems CA, USA). At least three samples were collected from each culture condition and each sample was measured in duplicate.

9.3.11 Statistical Analysis

The DNA quantification, sGAG content, fiber network analysis, rheological data, albumin production, and ammonia metabolism values are all presented as the mean ± the standard error of the mean. Statistical analysis was performed using a one-way ANOVA evaluating each treatment group (canine liver ECM, porcine liver ECM, etc.) within each assay using GraphPad software. A post-hoc Tukey test was conducted with a p-value <0.05 considered statistically significant.

9.4. RESULTS

9.4.1 Liver Tissue Decellularization and DNA Assessment

Hematoxylin and eosin (H&E) staining showed pink eosinophilic staining typical of collagen, whereas no basophilic staining typical of cellular nuclear material was observed. DAPI nuclear stain of the decellularized tissue was absent indicating loss of intact nuclear content **(Figure 40)**. Histologic examination of human liver ECM was not conducted due to the limited quantity of the material.

DNA quantification showed that human liver ECM contained 641 ng DNA/mg dry weight ECM, porcine liver ECM contained 98.0 ng DNA/mg dry weight ECM, canine liver ECM contained 563 ng DNA/mg dry weight ECM, and rat liver ECM contained 408 ng DNA/mg dry weight ECM. Only porcine liver ECM meets the previously established decellularization criteria of being below 200 ng DNA/mg dry weight ECM [83, 129]. However, all species show at least an 89% decrease in DNA content over native tissue and were considered adequately decellularized for the purposes of this study.

Quantification of sulfated glycosaminoglycan showed significant differences between species. Human LECM contained the most sGAG per g dry weight ECM while porcine LECM contained the least (10,907±124 μg sGAG/ g dry weight ECM and 583±183 μg sGAG/ g dry weight ECM respectively).

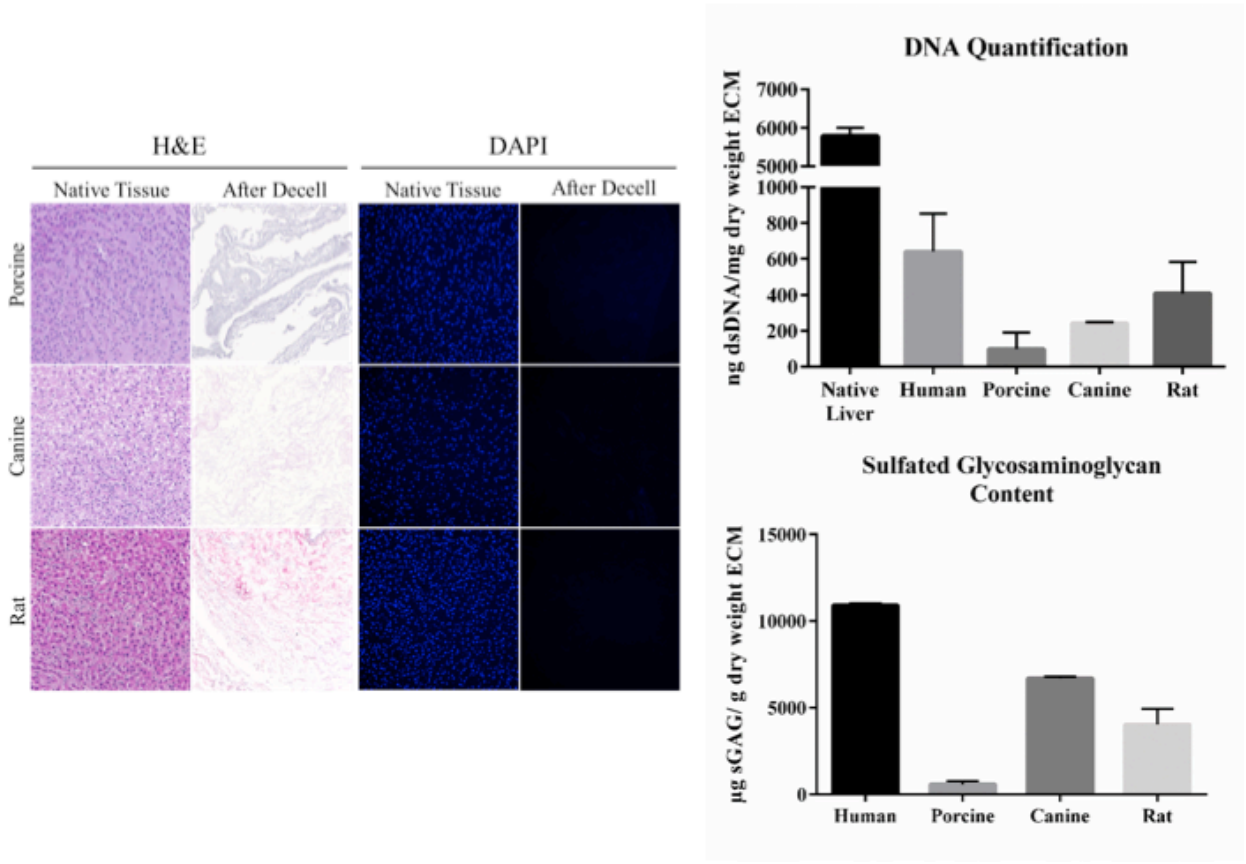

Figure 40. H&E and DAPI histologic staining of tissue following the decellularization process (a) for canine liver (top row), porcine (middle row), and rat (bottom row) (a). Double-stranded DNA quantification of the liver tissue from human, porcine, and rat species showed significant removal compared with native liver tissue (b). sGAG quantification indicates human LECM contained significantly more sGAGs per gram of dry weight when compared with the other groups (c).

9.4.2 Liver ECM Fiber Network Architecture

SEM images of liver ECM hydrogels derived from porcine, human, rat, and canine liver tissue showed that each species has a distinct collagen fiber architecture **(Figure 41)**. Quantitative analysis with the fiber architecture algorithm found that porcine liver ECM has a more dense fiber network as indicated by smaller pores compared to canine liver ECM.

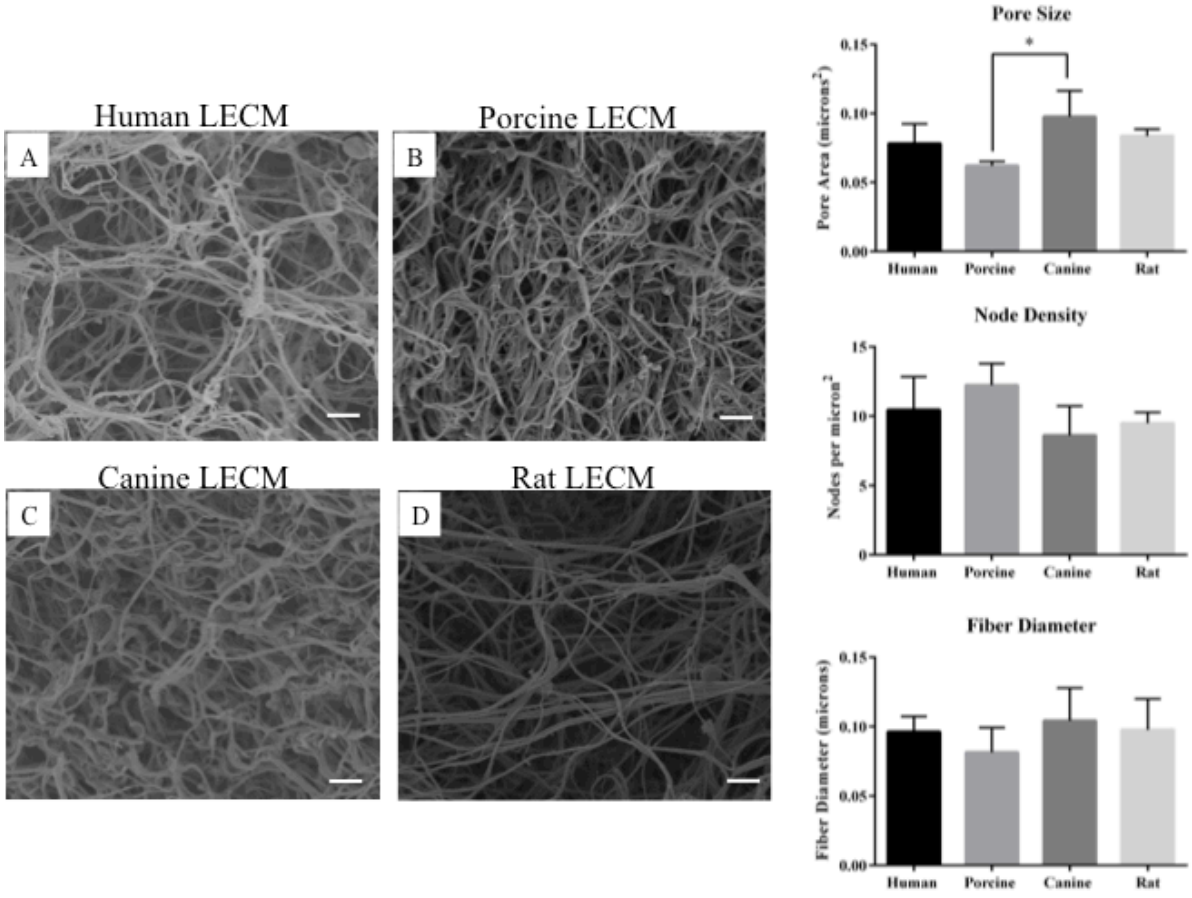

Figure 41. Scanning electron microscopy images of liver ECM hydrogels derived from human (a), porcine (b), canine (c), and rat (d). These images show a distinct species-specific collagen fiber architecture. Scale bar represents 1μm.

9.4.3 Liver ECM Hydrogel Rheological Testing

Results from the creep test showed porcine and canine LECM pre-gel to be more viscous than rat or human. The time sweep tests showed that porcine LECM has a higher storage modulus (G') than all other groups, indicating greater gel stiffness. Rat LECM gels more quickly than all other species, while the human, canine, and porcine LECM all reach fifty percent gelation in a similar time frame **(Figure 42)**.

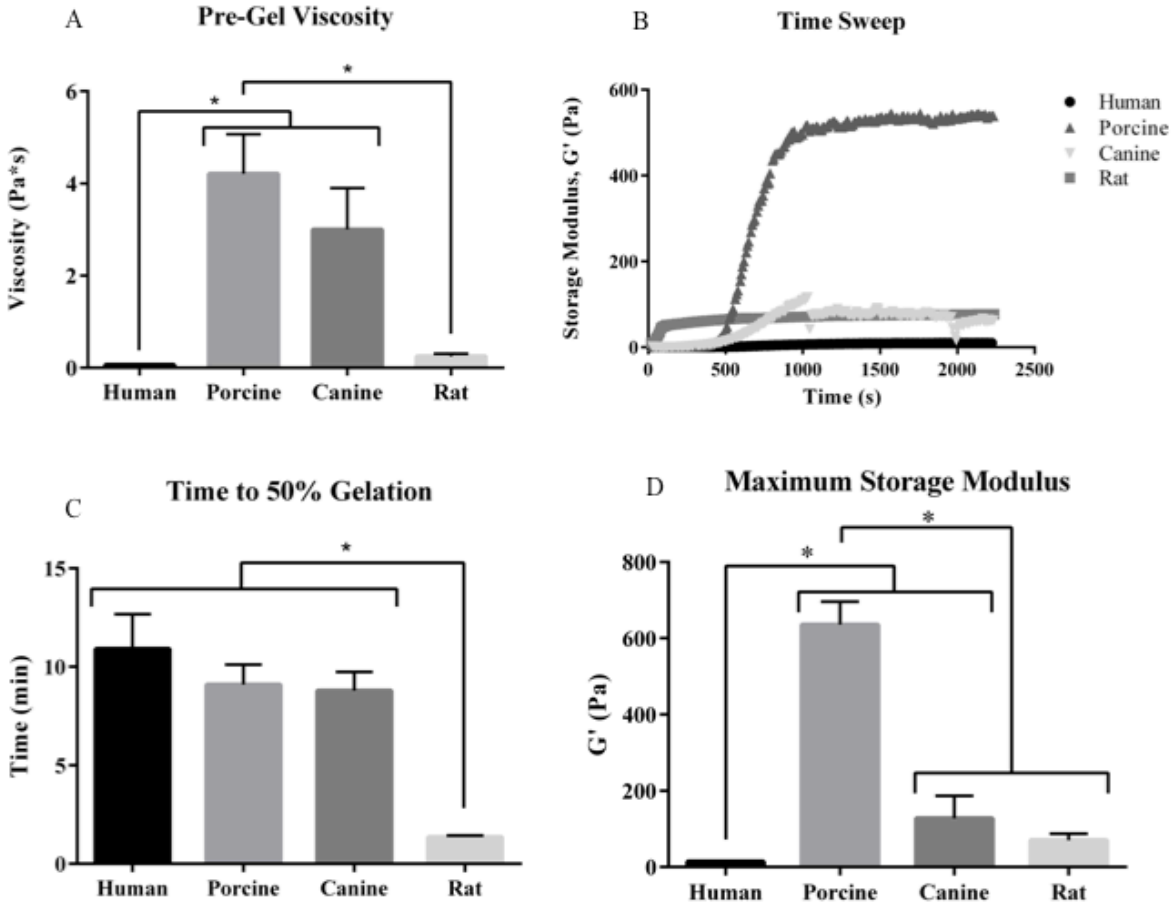

Figure 42. Rheological properties of human, porcine, canine, and rat liver ECM hydrogels at a concentration of 8mg/ml. Pre-gel viscosity (a), representative time sweep (b), time to 50% gelation (c), and maximum storage modulus (d).

9.4.4 SDS PAGE Gel Electrophoresis with Silver Stain

SDS PAGE analysis of the various liver ECMs showed that each species contained enriched quantities of high molecular weight components compared to SIS hydrogel while UBM hydrogel contained a greater quantity of high molecular weight fractions than all liver ECM hydrogels. The SIS hydrogel also contained fewer low molecular weight fractions compared to the liver ECM hydrogels and the UBM hydrogel **(Figure 43)**. Each liver ECM showed a distinctive banding pattern. For example, the canine liver ECM has a band ~200kD that does not appear in the human, porcine, or rat liver ECMs. There are also similarities across the various species of liver ECM. For example, all liver ECM hydrogels show a low molecular weight band ~12 kD and this band is shared with UBM hydrogel.

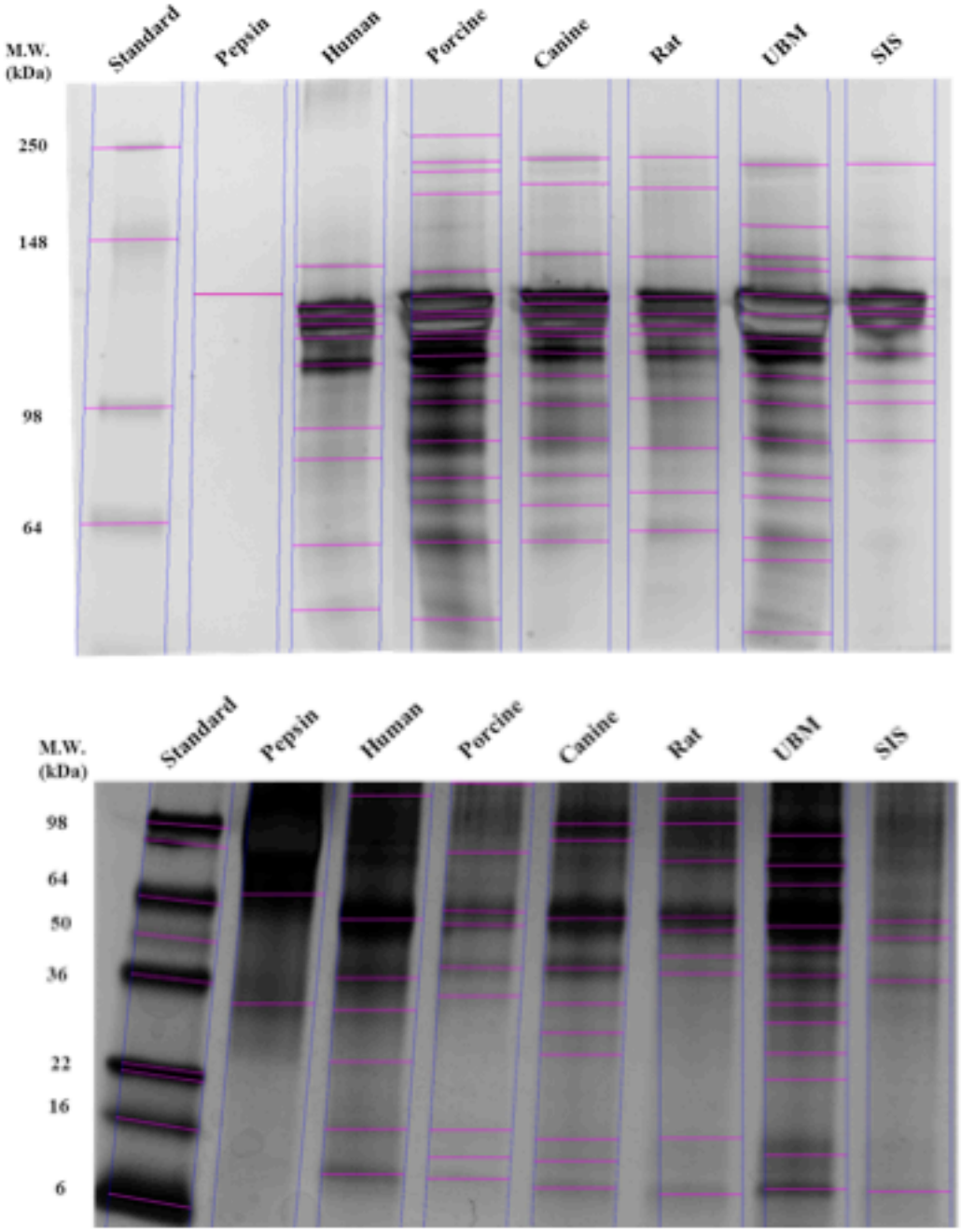

Figure 43. SDS PAGE gel followed by silver stain for human, porcine, canine, and rat liver ECMs. UBM and SIS were run as non-liver ECM controls. High molecular weight components (top) and low molecular weight components (bottom).

9.4.5 Primary Rat Hepatocyte Culture

PRH's treated with canine and porcine LECM maintained their phenotype to a greater extent than all other groups **(Figure 44)**. Images of PRH's treated with canine and porcine LECM show increased bile production and the formation of multinucleate cells, both markers of maintained hepatocyte phenotype.

Increased albumin production for hepatocytes treated with canine and porcine LECM on day 5 indicates these cells have increased function. Results showed a 472±70% increase in albumin production of hepatocytes treated with canine LECM and a 427±79% increase in albumin production of hepatocytes treated with porcine LECM over the collagen and pepsin controls from days 2-5 of culture. Ammonia metabolism was not different between groups.

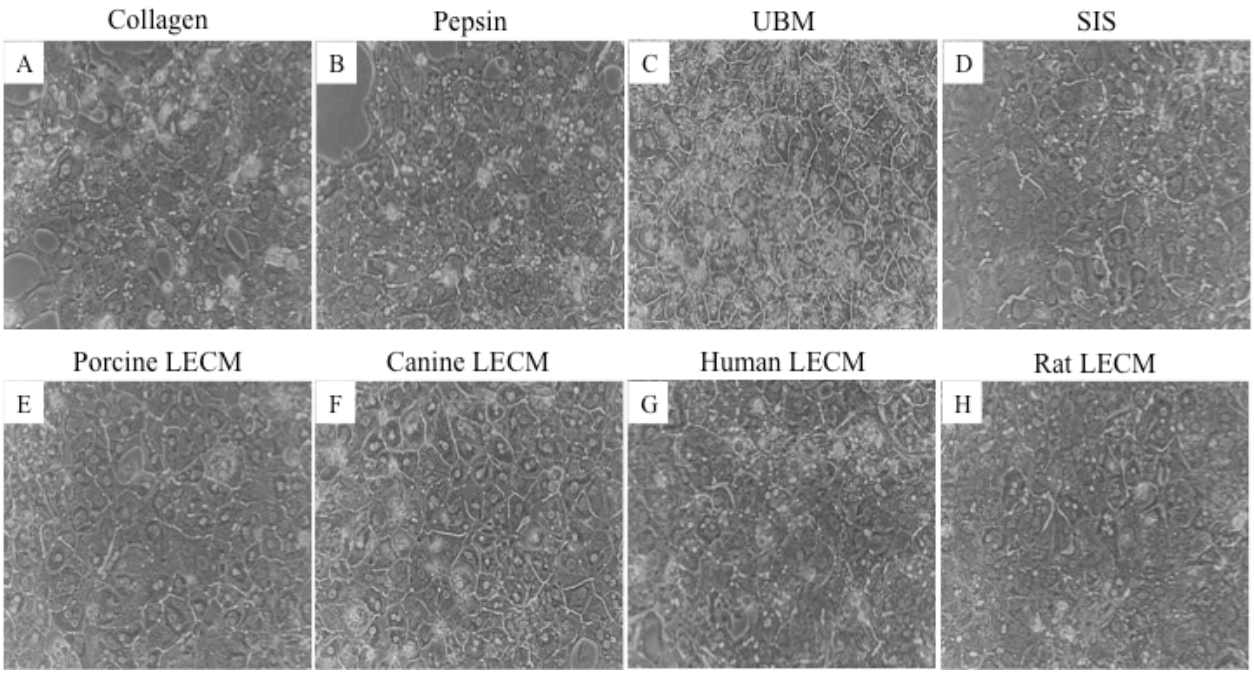

Figure 44. Representative morphologic images of primary rat hepatocytes cultured on rat tail collagen I alone (a), 1mg/ml pepsin (b), and 50ug/ml of UBM (c), SIS (d), porcine liver ECM (e), canine liver ECM (f), human liver ECM (g), and rat liver ECM (h) added to the media.

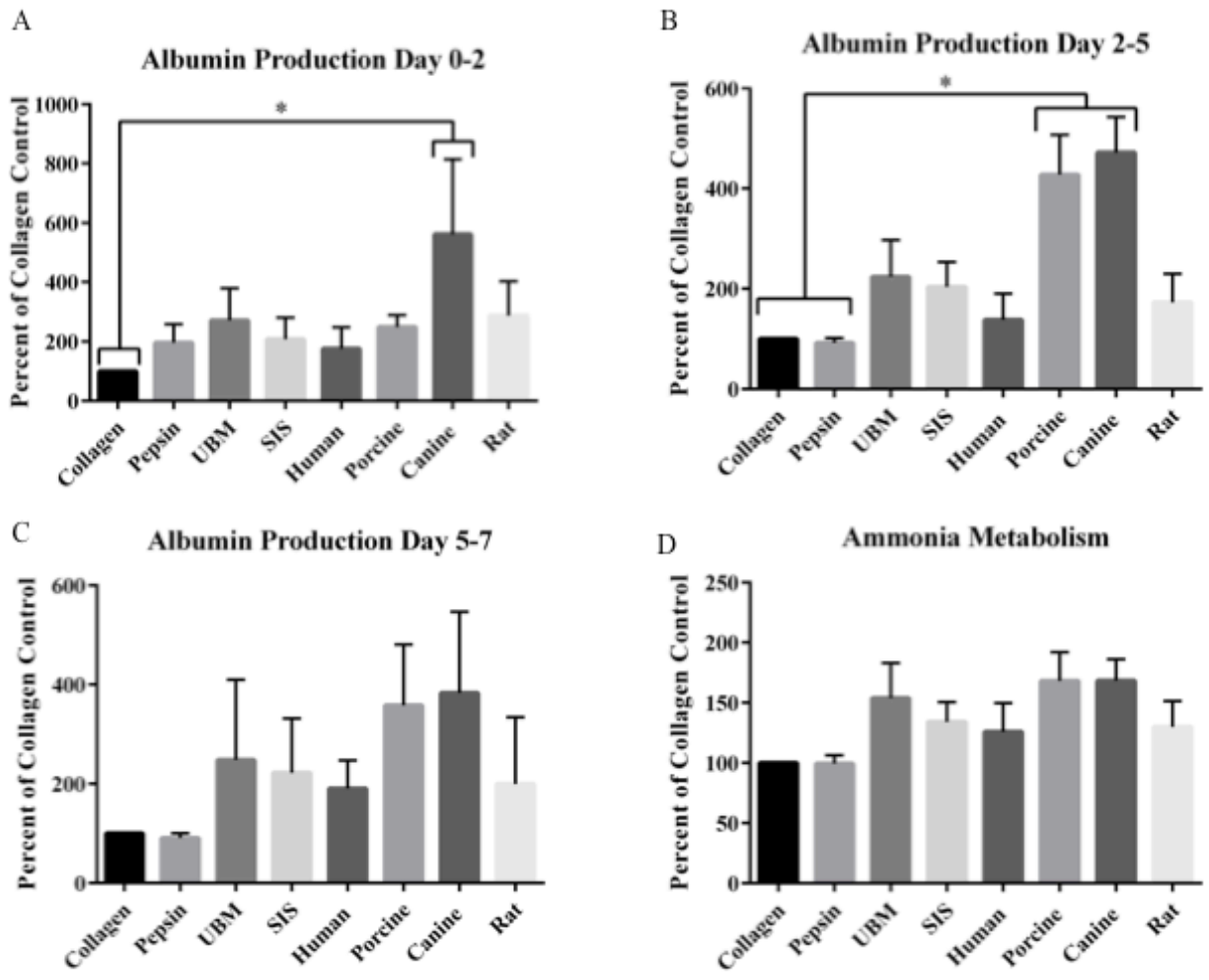

Figure 45. Functional rat hepatocyte data from day 7 of the in-vitro culture with the addition of pepsin, solubilized UBM, SIS, rat liver ECM, human liver ECM, canine liver ECM, and porcine liver ECM added to the media. Albumin secretion from day 0 to 2 (a), from day 2 to 5 (b), and from day 5 to 7 (c) and ammonia metabolism on day 7 of culture (d).

9.5 DISCUSSION

Media supplemented with pepsin solubilized ECM derived from porcine and canine liver was shown to support rat hepatocyte (PRH) function and better maintain hepatocyte phenotype compared to rat hepatocytes cultured with non-supplemented media. These findings are important because it has been well documented that during in-vitro culture hepatocytes quickly dedifferentiate and lose hepatic specific functions[316, 332, 333]. This study also showed that there are species differences in LECM and surprisingly, xenogeneic canine and porcine LECM supported primary rat hepatocytes better than rat LECM. Though it is not clear that similar results would be seen with human hepatocytes, the findings of the present study suggest that solubilized LECM could be a useful media supplement for hepatocytes and that the species source of the ECM should be an important consideration.

Cell based liver engineering strategies would benefit significantly from a culture supplement or substrate that maintains hepatocyte phenotype function during ex-vivo culture. It has been shown that biologic scaffolds composed of ECM provide a more physiologically relevant culture substrate compared to individual ECM proteins such as purified collagen[59, 315]. Liver tissue used in this study was processed in a manner designed to preserve ECM proteins derived from the liver in physiologically relevant amounts (e.g. Type-I, IV, VI, III, XI, XIX, heparin sulfate proteoglycan, ECM-bound growth factors, laminin, biglycan, tenascin, fibronectin).

Recent studies have suggested that tissue- and organ-specific ECM can promote site appropriate differentiation of progenitor cells and maintain site appropriate phenotype in in vitro culture systems, though this is not a requirement of all tissues [185, 334, 335]. Since the ECM of

each tissue and organ is produced by the resident parenchymal cells and logically represents the ideal scaffold or substrate for these cells, it is intuitive that a substrate composed of liver-derived ECM would be favorable for hepatocytes. Previous studies have shown that hepatic sinusoidal endothelial cells (SECs) maintained their differentiated phenotype the longest when cultured on ECM derived from the liver, as compared to SECs cultured on ECM derived from small intestine or urinary bladder [70]. Lin et. al. compared rat hepatocytes cultured on PLECM biologic scaffolds to well characterized hepatocyte culture models (type-1 collagen sandwich configuration or a single layer of type-1 collagen) [9]. Hepatocytes survived up to 45 days on a sheet form of PLECM and several liver-specific functions such as albumin synthesis, urea production, and P-450 IA1 activity were markedly enhanced compared to the growth and metabolism of cells cultured on a single layer of type-1 collagen. These results suggest that intact LECM biologic scaffolds provide tissue-specific signals. However, the use of a solubilized ECM media supplement has not previously been investigated for the purpose of hepatocyte culture.

The decellularization protocol used in this study was developed for porcine liver and designed to maintain as much of the native porcine LECM components while fully removing cellular content. Different decellularization methods can selectively affect the composition of ECM after processing [247], therefore we chose to decellularize all species of LECM according to the same protocol to eliminate this as a variable. However, the uniform method resulted in differences in both DNA and sulfated GAG composition.

The enhanced maintenance of primary rat hepatocytes function and phenotype for those cells cultured with porcine and canine liver ECM compared to cells cultured with human and rat liver ECM or rat tail collagen I may be due to differences in the composition and physical properties of the respective ECM. The results described herein indicate that liver ECM derived

from human, canine, porcine, and rat liver each have a distinct biochemical profile as well as differences in gel stiffness and fiber architecture. Just as tissue specific differences have been shown to modulate hepatic cell function[52, 70], the present study shows that species-specific differences can also modulate the function of hepatocytes. A comprehensive analysis of the biochemical composition and proteomic profile of each liver ECM would help identify these factors which of these differences contribute to maintenance of hepatocyte phenotype.

The present study shows that pepsin solubilized liver ECM, though far from perfect, provides a useful media supplement for hepatocyte culture. By helping to maintain hepatocyte phenotype and function, solubilized LECM has the potential to enhance drug discovery culture systems, whole organ engineering of the liver, and hepatocyte cell transplantation therapies.

10.0 DISCUSSION

The present dissertation was aimed at developing fundamental technology that will provide meaningful progress toward engineering organized functional hepatic tissue within a decellularized liver scaffold. One of the major challenges for whole organ engineering is to produce large volume tissues capable of being connected to the recipient's blood supply for clinical applications. Pervious work in the field of bioengineer liver tissue has been met with many obstacles including cell sourcing, efficient cell seeding, vascularization of the engineered tissue, and provision of authentic cues for tissue development. In order to overcome these challenges, we first conducted a set of experiments aimed at investigated the effect of commonly used decellularization agents on a biologic scaffold. Using that knowledge, we then developed a method of decellularization that was used to fabricate a naturally derived whole-liver bioscaffold. We used the vascular channels of this scaffold as a conduit for reseeding human microvascular endothelial cells throughout the bioscaffold. Next, we developed a method of delivering functional hepatocytes to their native parenchymal location within the liver bioscaffold. The three-dimensional liver bioscaffold provided spatial information for cell localization and engraftment, and supported cellular proliferation and phenotype maintenance. In the final study we developed a method of enhancing hepatic function of the seeded hepatocytes by using enzymatically digest liver ECM to the media as a supplement. These developed methods offer a potential technique for fabrication of human liver tissue that can be readily transplanted into host animals or used for studies of liver cell biology, physiology, toxicology, and drug discovery with further development.

Previously, decellularization of tissue was performed by submersion of the tissue within a detergent solution under agitation to allow cell removal in bulk from the surface of the tissue moving inward. These approaches were successful for decellularization of smaller samples (up to 5 mm in thickness), whereas in thicker specimens the core of the tissue remained cellular. To circumvent this limitation, we took advantage of the native liver vascular network by perfusing the detergent through this network and distributing it throughout the entire liver. This gentle procedure preserves the architecture of the liver matrix and vascular system. The choice of detergent for the production of whole organ bioscaffolds using perfusion may also impact the preservation of important biochemical cues. In chapters 5 and 6 we showed that harsh ionic detergents such as SDS facilitate rapid removal of cells from dense tissues and can yield a functional bioscaffold, but they may damage some ECM components. Therefore, we opted to use a mild nonionic detergent, Triton X-100. We found that this detergent could successfully decellularize the whole liver by the removal of a majority of cellular DNA. These studies highlight the utility of perfusion decellularization to generate whole organ bioscaffolds with significant potential for organ bioengineering.

Time-of-flight secondary ion mass spectrometry (ToF-SIMS) is a powerful surface analysis technique to probe biological structures with high mass resolution and surface specificity. In chapter 6 we report the use of ToF-SIMS to distinguish the basement membrane complex of scaffolds prepared by treatment with water, 0.1% SDS 1% SDS, 4% Deoxycholate, 8 mM CHAPS or 3% Triton X-100 for 24 hours. The results of the study demonstrate that each decellularization agent used to prepare a biologic scaffold creates in a unique surface. The resulting ECM scaffold is associated with distinct ultrastructural and compositional characteristics and that these surface characteristics are dependent on both the damage the

decellularization agent has caused to the native extracellular matrix as well as the residual components left behind by the decellularization agent. It was also shown by using principal component analysis of the negative ion spectra is capable of separating sample types based on residual cellular components (Native and PAA treated) or detergent type (SDS vs. Deoxycholate). Furthermore, this revealed the presence of residual detergent in SDS treated and deoxycholate treated samples. However, the level of residual detergent content between deoxycholate samples varied. All dexocyholate samples were prepared from the sample porcine bladder, so source tissue variation does not explain the variation in residual deoxycholate. It was also demonstrated that ToF-SIMS is a highly sensitive method for the detection and differentiation of the molecular composition of the outermost surface of an ECM scaffold. Further, ToF-SIMS may represent a method for future identification of previously unknown surface species as well as for the prediction of cell–scaffold interactions and subsequent remodeling events. Finally, the richness of molecular detail in the ToF-SIMS spectra suggests that ToF-SIMS may be useful for quality control of commercialized ECM-based regenerative scaffold products and for standardization of these scaffolds.

In Chapter 7 we addressed one of the major challenges in whole organ engineering, engineering a functional vascular network within a biologic scaffold. Typically, neovascularization of bioengineered tissues was addressed by supplementing cells with angiogenic growth factors or fabricating scaffolds from synthetic material that allowed micro-patterning of vascular tree-like structures. When growth factors are used alone, they tend to create only a microvasculature consisting of small and fragile capillaries, and therefore this technique is only applicable for the engineering of smaller size tissues. An alternative fabrication method is using a micropatterning technique that can be scaled up to larger sizes by modular

construction. However, currently this method cannot replicate the progressive complexity and ECM composition of the native liver vascular tree. The bioscaffolds generated from whole livers produced via our decellularization method retain the complexity of multiple size vessels that can deliver fluids from the larger vena cava or the portal vein and reach each individual liver lobule.

An additional advantage of this method is the retention of important ECM molecules required for site-specific engraftment and/or differentiation of different cell types that are present in the liver. Prior research showed that liver-specific stem cells can be isolated and differentiated to hepatic fate. We used human microvascular endothelial cells to recellularize the bioscaffolds. The advantage of seeding human microvascular endothelial cells is that they are consistent in their proliferation rate, they are easy to maintain in culture, and they are associated with a low experimental cost. This allowed us to perform many recellularization experiments before moving to more clinically relevant iPSC derived human endothelial cells.

A major obstacle in producing large-volume tissues is the delivery of adequate numbers of endothelial cells to the entire vascular network of the bioscaffold. The perfusion method developed in chapter 7 uses cell infusion through both the venous and arterial vascular networks and deposition throughout the thickness of the bioscaffold, achieving greater seeding efficiency without compromising the integrity of the bioscaffold. Furthermore, by accessing different vessels that feed into the liver, we were able to deliver cells selectively to different compartments of the liver tissue. Endothelial cells delivered through the vena cava selectively seeded larger and smaller blood vessels up to the pericentral area of the liver lobule, without reaching the periportal space of the lobule where the final branching vessels of portal vein are located. On the other hand, cells seeded through the portal vein, which delivers blood from the intestine and other organs to the liver, reached predominantly the periportal area of the liver lobule without

extensive penetration to its pericentral space. These seeded endothelial cells cover the entire circumference of a vascular channel and maintained cell-cell junctions. Thus, simultaneous utilization of both vascular routes for cell seeding enables complete access to the entire length of the vascular network, which has an essential importance for prevention of blood clotting and ultimately failure to transplant the bioengineered liver. This study demonstrates that three-dimensional biologic scaffolds composed of liver extracellular matrix have the capability to become a completely re-endothelializes scaffold closely mimicking the native three-dimensional structure of liver tissue. The bioscaffold may also prove as a good tool to study normal tissue and organ development as well as liver pathology. Ultimately, this technology may bring us closer to the ultimate goal of providing bioengineered livers for transplantation.

Next, in chapter 8 we aimed to optimize hepatocyte seeding concentration and volume within a decellularized liver scaffold in order to enhance viability and functionality of the hepatocytes. The appropriate spatial distribution of hepatocytes following seeding into a 3-D liver scaffold is essential for regeneration of a native like hepatic tissue. The results of the study reveal that decreasing cell seeding density and injection volume increased hepatocyte viability and functionality. Studies that have been published on the effects of cell density on the hepatocyte viability, proliferation, and function indicate that for hepatocytes to survive in an in-vitro environment aggregation of hepatocytes is essential. Aggregation is postulated to promote viability and function. However, aggregation is double edge sword as large aggregation of cells would be toxic for the survival of tissue and minimal aggregation would hamper the viability of

the cells. Falasca et al. showed that contact between hepatocyte cells was established following perfusion of hepatocyte into alginate beads, a weak adhesive matrix, within 6 hours of seeding. The cell-cell contacts were characterized by actin, and cytokeratin along adhesion junctions, as well as gap junctions characterized by connexins.

Lastly, in chapter 9 we showed that media supplemented with pepsin solubilized ECM derived from porcine and canine liver was shown to support rat hepatocyte (PRH) function and better maintain hepatocyte phenotype compared to rat hepatocytes cultured with non-supplemented media. These findings are important because it has been well documented that during in-vitro culture hepatocytes quickly dedifferentiate and lose hepatic specific functions [316, 332, 333]. This study also showed that there are species differences in LECM and surprisingly, xenogeneic canine and porcine LECM supported primary rat hepatocytes better than rat LECM. Though it is not clear that similar results would be seen with human hepatocytes, the findings of the present study suggest that solubilized LECM could be a useful media supplement for hepatocytes and that the species source of the ECM should be an important consideration.

Cell based liver engineering strategies would benefit significantly from a culture supplement or substrate that maintains hepatocyte phenotype function during ex-vivo culture. It has been shown that biologic scaffolds composed of ECM provide a more physiologically relevant culture substrate compared to individual ECM proteins such as purified collagen[59, 315]. Liver tissue used in this study was processed in a manner designed to preserve ECM proteins derived from the liver in physiologically relevant amounts (e.g. Type-I, IV, VI, III, XI, XIX, heparin sulfate proteoglycan, ECM-bound growth factors, laminin, biglycan, tenascin, fibronectin).

The enhanced maintenance of primary rat hepatocytes function and phenotype for those cells cultured with porcine and canine liver ECM compared to cells cultured with human and rat liver ECM or rat tail collagen I may be due to differences in the composition and physical properties of the respective ECM. The results described herein indicate that liver ECM derived from human, canine, porcine, and rat liver each have a distinct biochemical profile as well as differences in gel stiffness and fiber architecture. Just as tissue specific differences have been shown to modulate hepatic cell function [52, 70], the present study shows that species-specific differences can also modulate the function of hepatocytes. A comprehensive analysis of the biochemical composition and proteomic profile of each liver ECM would help identify these factors which of these differences contribute to maintenance of hepatocyte phenotype. This study shows that pepsin solubilized liver ECM, though far from perfect, provides a useful media supplement for hepatocyte culture. By helping to maintain hepatocyte phenotype and function, solubilized LECM has the potential to enhance drug discovery culture systems, whole organ engineering of the liver, and hepatocyte cell transplantation therapies.

REFERENCES

[1] Klosterhalfen B, Junge K, Klinge U. The lightweight and large porous mesh concept for hernia repair. Expert Rev Med Devices. 2005;2:103-17.

[2] Feola A, Barone W, Moalli P, Abramowitch S. Characterizing the ex vivo textile and structural properties of synthetic prolapse mesh products. Int Urogynecol J. 2013;24:559-64.

[3] Hernandez-Gascon B, Pena E, Melero H, Pascual G, Doblare M, Ginebra MP, et al. Mechanical behaviour of synthetic surgical meshes: finite element simulation of the herniated abdominal wall. Acta Biomater. 2011;7:3905-13.

[4] Chu CC, Welch L. Characterization of morphologic and mechanical properties of surgical mesh fabrics. J Biomed Mater Res. 1985;19:903-16.

[5] Cobb WS, Kercher KW, Heniford BT. The argument for lightweight polypropylene mesh in hernia repair. Surg Innov. 2005;12:63-9.

[6] Di Vita G, D'Agostino P, Patti R, Arcara M, Caruso G, Davi V, et al. Acute inflammatory response after inguinal and incisional hernia repair with implantation of polypropylene mesh of different size. Langenbecks Arch Surg. 2005;390:306-11.

[7] Leber GE, Garb JL, Alexander AI, Reed WP. Long-term complications associated with prosthetic repair of incisional hernias. Arch Surg. 1998;133:378-82.

[8] Garcia-Urena MA, Vega Ruiz V, Diaz Godoy A, Baez Perea JM, Marin Gomez LM, Carnero Hernandez FJ, et al. Differences in polypropylene shrinkage depending on mesh position in an experimental study. Am J Surg. 2007;193:538-42.

[9] Costello CR, Bachman SL, Ramshaw BJ, Grant SA. Materials characterization of explanted polypropylene hernia meshes. J Biomed Mater Res B Appl Biomater. 2007;83:44-9.

[10] Brandt CJ, Kammer D, Fiebeler A, Klinge U. Beneficial effects of hydrocortisone or spironolactone coating on foreign body response to mesh biomaterial in a mouse model. J Biomed Mater Res A. 2011;99:335-43.

[11] Ansaloni L, Catena F, Coccolini F, Gazzotti F, D'Alessandro L, Pinna AD. Inguinal hernia repair with porcine small intestine submucosa: 3-year follow-up results of a randomized controlled trial of Lichtenstein's repair with polypropylene mesh versus Surgisis Inguinal Hernia Matrix. Am J Surg. 2009;198:303-12.

[12] Medberry CJ, Tottey S, Jiang H, Johnson SA, Badylak SF. Resistance to infection of five different materials in a rat body wall model. J Surg Res. 2012;173:38-44.

[13] Holton LH, 3rd, Chung T, Silverman RP, Haerian H, Goldberg NH, Burrows WM, et al. Comparison of acellular dermal matrix and synthetic mesh for lateral chest wall reconstruction in a rabbit model. Plast Reconstr Surg. 2007;119:1238-46.

[14] Hiles M, Record Ritchie RD, Altizer AM. Are biologic grafts effective for hernia repair?: a systematic review of the literature. Surg Innov. 2009;16:26-37.

[15] Faulk DM, Londono R, Wolf MT, Ranallo CA, Carruthers CA, Wildemann JD, et al. ECM hydrogel coating mitigates the chronic inflammatory response to polypropylene mesh. Biomaterials. 2014;35:8585-95.

[16] Vorotnikova E, McIntosh D, Dewilde A, Zhang J, Reing JE, Zhang L, et al. Extracellular matrix-derived products modulate endothelial and progenitor cell migration and proliferation in vitro and stimulate regenerative healing in vivo. Matrix biology : journal of the International Society for Matrix Biology. 2010;29:690-700.

[17] Barkan D, Green JE, Chambers AF. Extracellular matrix: a gatekeeper in the transition from dormancy to metastatic growth. Eur J Cancer. 2010;46:1181-8.

[18] Nelson CM, Bissell MJ. Of extracellular matrix, scaffolds, and signaling: tissue architecture regulates development, homeostasis, and cancer. Annu Rev Cell Dev Biol. 2006;22:287-309.

[19] Taylor KR, Gallo RL. Glycosaminoglycans and their proteoglycans: host-associated molecular patterns for initiation and modulation of inflammation. FASEB J. 2006;20:9-22.

[20] Nagase H, Visse R, Murphy G. Structure and function of matrix metalloproteinases and TIMPs. Cardiovasc Res. 2006;69:562-73.

[21] Werner S, Grose R. Regulation of wound healing by growth factors and cytokines. Physiol Rev. 2003;83:835-70.

[22] Bornstein P, Sage EH. Matricellular proteins: extracellular modulators of cell function. Curr Opin Cell Biol. 2002;14:608-16.

[23] Ott HC, Matthiesen TS, Goh SK, Black LD, Kren SM, Netoff TI, et al. Perfusion-decellularized matrix: using nature's platform to engineer a bioartificial heart. Nat Med. 2008;14:213-21.

[24] Uygun BE, Soto-Gutierrez A, Yagi H, Izamis ML, Guzzardi MA, Shulman C, et al. Organ reengineering through development of a transplantable recellularized liver graft using decellularized liver matrix. Nat Med. 2010;16:814-20.

[25] Petersen TH, Calle EA, Zhao L, Lee EJ, Gui L, Raredon MB, et al. Tissue-engineered lungs for in vivo implantation. Science. 2010;329:538-41.

[26] Nakayama KH, Batchelder CA, Lee CI, Tarantal AF. Decellularized rhesus monkey kidney as a three-dimensional scaffold for renal tissue engineering. Tissue Eng Part A. 2010;16:2207-16.

[27] Allen RA, Seltz LM, Jiang H, Kasick RT, Sellaro TL, Badylak SF, et al. Adrenal extracellular matrix scaffolds support adrenocortical cell proliferation and function in vitro. Tissue Eng Part A. 2010;16:3363-74.

[28] Conklin BS, Richter ER, Kreutziger KL, Zhong DS, Chen C. Development and evaluation of a novel decellularized vascular xenograft. Med Eng Phys. 2002;24:173-83.

[29] Schmidt CE, Baier JM. Acellular vascular tissues: natural biomaterials for tissue repair and tissue engineering. Biomaterials. 2000;21:2215-31.

[30] Uchimura E, Sawa Y, Taketani S, Yamanaka Y, Hara M, Matsuda H, et al. Novel method of preparing acellular cardiovascular grafts by decellularization with poly(ethylene glycol). J Biomed Mater Res A. 2003;67:834-7.

[31] Woods T, Gratzer PF. Effectiveness of three extraction techniques in the development of a decellularized bone-anterior cruciate ligament-bone graft. Biomaterials. 2005;26:7339-49.

[32] Bader A, Schilling T, Teebken OE, Brandes G, Herden T, Steinhoff G, et al. Tissue engineering of heart valves--human endothelial cell seeding of detergent acellularized porcine valves. Eur J Cardiothorac Surg. 1998;14:279-84.

[33] Booth C, Korossis SA, Wilcox HE, Watterson KG, Kearney JN, Fisher J, et al. Tissue engineering of cardiac valve prostheses I: development and histological characterization of an acellular porcine scaffold. J Heart Valve Dis. 2002;11:457-62.

[34] Grauss RW, Hazekamp MG, Oppenhuizen F, van Munsteren CJ, Gittenberger-de Groot AC, DeRuiter MC. Histological evaluation of decellularised porcine aortic valves: matrix changes due to different decellularisation methods. Eur J Cardiothorac Surg. 2005;27:566-71.

[35] Kasimir MT, Rieder E, Seebacher G, Silberhumer G, Wolner E, Weigel G, et al. Comparison of different decellularization procedures of porcine heart valves. Int J Artif Organs. 2003;26:421-7.

[36] Korossis SA, Booth C, Wilcox HE, Watterson KG, Kearney JN, Fisher J, et al. Tissue engineering of cardiac valve prostheses II: biomechanical characterization of decellularized porcine aortic heart valves. J Heart Valve Dis. 2002;11:463-71.

[37] Rieder E, Kasimir MT, Silberhumer G, Seebacher G, Wolner E, Simon P, et al. Decellularization protocols of porcine heart valves differ importantly in efficiency of cell removal and susceptibility of the matrix to recellularization with human vascular cells. J Thorac Cardiovasc Surg. 2004;127:399-405.

[38] Schenke-Layland K, Vasilevski O, Opitz F, Konig K, Riemann I, Halbhuber KJ, et al. Impact of decellularization of xenogeneic tissue on extracellular matrix integrity for tissue engineering of heart valves. J Struct Biol. 2003;143:201-8.

[39] Chen RN, Ho HO, Tsai YT, Sheu MT. Process development of an acellular dermal matrix (ADM) for biomedical applications. Biomaterials. 2004;25:2679-86.

[40] Hudson TW, Liu SY, Schmidt CE. Engineering an improved acellular nerve graft via optimized chemical processing. Tissue Eng. 2004;10:1346-58.

[41] Kim BS, Yoo JJ, Atala A. Peripheral nerve regeneration using acellular nerve grafts. J Biomed Mater Res A. 2004;68:201-9.

[42] Borschel GH, Dennis RG, Kuzon WM, Jr. Contractile skeletal muscle tissue-engineered on an acellular scaffold. Plast Reconstr Surg. 2004;113:595-602; discussion 3-4.

[43] Tanaka T, Sun YL, Zhao C, Zobitz ME, An KN, Amadio PC. Effect of curing time and concentration for a chemical treatment that improves surface gliding for extrasynovial tendon grafts in vitro. J Biomed Mater Res A. 2006;79:451-5.

[44] Badylak SF, Lantz GC, Coffey A, Geddes LA. Small intestinal submucosa as a large diameter vascular graft in the dog. J Surg Res. 1989;47:74-80.

[45] Badylak SF, Tullius R, Kokini K, Shelbourne KD, Klootwyk T, Voytik SL, et al. The use of xenogeneic small intestinal submucosa as a biomaterial for Achilles tendon repair in a dog model. J Biomed Mater Res. 1995;29:977-85.

[46] Kropp BP, Eppley BL, Prevel CD, Rippy MK, Harruff RC, Badylak SF, et al. Experimental assessment of small intestinal submucosa as a bladder wall substitute. Urology. 1995;46:396-400.

[47] Singelyn JM, Sundaramurthy P, Johnson TD, Schup-Magoffin PJ, Hu DP, Faulk DM, et al. Catheter-deliverable hydrogel derived from decellularized ventricular extracellular matrix increases endogenous cardiomyocytes and preserves cardiac function post-myocardial infarction. J Am Coll Cardiol. 2012;59:751-63.

[48] Wainwright JM, Czajka CA, Patel UB, Freytes DO, Tobita K, Gilbert TW, et al. Preparation of cardiac extracellular matrix from an intact porcine heart. Tissue engineering Part C, Methods. 2010;16:525-32.

[49] Chen F, Yoo JJ, Atala A. Acellular collagen matrix as a possible "off the shelf" biomaterial for urethral repair. Urology. 1999;54:407-10.

[50] Freytes DO, Badylak SF, Webster TJ, Geddes LA, Rundell AE. Biaxial strength of multilaminated extracellular matrix scaffolds. Biomaterials. 2004;25:2353-61.

[51] Gilbert TW, Stolz DB, Biancaniello F, Simmons-Byrd A, Badylak SF. Production and characterization of ECM powder: implications for tissue engineering applications. Biomaterials. 2005;26:1431-5.

[52] Sellaro TL, Ranade A, Faulk DM, McCabe GP, Dorko K, Badylak SF, et al. Maintenance of human hepatocyte function in vitro by liver-derived extracellular matrix gels. Tissue Eng Part A. 2010;16:1075-82.

[53] Brown BN, Valentin JE, Stewart-Akers AM, McCabe GP, Badylak SF. Macrophage phenotype and remodeling outcomes in response to biologic scaffolds with and without a cellular component. Biomaterials. 2009;30:1482-91.

[54] Reing JE, Zhang L, Myers-Irvin J, Cordero KE, Freytes DO, Heber-Katz E, et al. Degradation products of extracellular matrix affect cell migration and proliferation. Tissue Eng Part A. 2009;15:605-14.

[55] Keane TJ, Londono R, Turner NJ, Badylak SF. Consequences of ineffective decellularization of biologic scaffolds on the host response. Biomaterials. 2012;33:1771-81.

[56] Tian XH, Xue WJ, Pang XL, Teng Y, Tian PX, Feng XS. Effect of small intestinal submucosa on islet recovery and function in vitro culture. Hepatobiliary Pancreat Dis Int. 2005;4:524-9.

[57] Tian XH, Xue WJ, Ding XM, Pang XL, Teng Y, Tian PX, et al. Small intestinal submucosa improves islet survival and function during in vitro culture. World J Gastroenterol. 2005;11:7378-83.

[58] Xiaohui T, Wujun X, Xiaoming D, Xinlu P, Yan T, Puxun T, et al. Small intestinal submucosa improves islet survival and function in vitro culture. Transplant Proc. 2006;38:1552-8.

[59] Lin P, Chan WC, Badylak SF, Bhatia SN. Assessing porcine liver-derived biomatrix for hepatic tissue engineering. Tissue Eng. 2004;10:1046-53.

[60] Hubbell JA. Materials as morphogenetic guides in tissue engineering. Curr Opin Biotechnol. 2003;14:551-8.

[61] Dow JA, Clark P, Connolly P, Curtis AS, Wilkinson CD. Novel methods for the guidance and monitoring of single cells and simple networks in culture. J Cell Sci Suppl. 1987;8:55-79.

[62] Clark P, Connolly P, Curtis AS, Dow JA, Wilkinson CD. Topographical control of cell behaviour: II. Multiple grooved substrata. Development. 1990;108:635-44.

[63] Clark P, Connolly P, Curtis AS, Dow JA, Wilkinson CD. Topographical control of cell behaviour. I. Simple step cues. Development. 1987;99:439-48.

[64] den Braber ET, de Ruijter JE, Smits HT, Ginsel LA, von Recum AF, Jansen JA. Quantitative analysis of cell proliferation and orientation on substrata with uniform parallel surface micro-grooves. Biomaterials. 1996;17:1093-9.

[65] Chehroudi B, Soorany E, Black N, Weston L, Brunette DM. Computer-assisted three-dimensional reconstruction of epithelial cells attached to percutaneous implants. J Biomed Mater Res. 1995;29:371-9.

[66] Zeltinger J, Sherwood JK, Graham DA, Mueller R, Griffith LG. Effect of pore size and void fraction on cellular adhesion, proliferation, and matrix deposition. Tissue Eng. 2001;7:557-72.

[67] Brown B, Lindberg K, Reing J, Stolz DB, Badylak SF. The basement membrane component of biologic scaffolds derived from extracellular matrix. Tissue Eng. 2006;12:519-26.

[68] Cepko CL. The roles of intrinsic and extrinsic cues and bHLH genes in the determination of retinal cell fates. Curr Opin Neurobiol. 1999;9:37-46.

[69] Jadhav AP, Mason HA, Cepko CL. Notch 1 inhibits photoreceptor production in the developing mammalian retina. Development. 2006;133:913-23.

[70] Sellaro TL, Ravindra AK, Stolz DB, Badylak SF. Maintenance of hepatic sinusoidal endothelial cell phenotype in vitro using organ-specific extracellular matrix scaffolds. Tissue Eng. 2007;13:2301-10.

[71] Zeisberg M, Kramer K, Sindhi N, Sarkar P, Upton M, Kalluri R. De-differentiation of primary human hepatocytes depends on the composition of specialized liver basement membrane. Mol Cell Biochem. 2006;283:181-9.

[72] Voytik-Harbin SL, Brightman AO, Kraine MR, Waisner B, Badylak SF. Identification of extractable growth factors from small intestinal submucosa. Journal of cellular biochemistry. 1997;67:478-91.

[73] Hodde JP, Badylak SF, Brightman AO, Voytik-Harbin SL. Glycosaminoglycan content of small intestinal submucosa: a bioscaffold for tissue replacement. Tissue Eng. 1996;2:209-17.

[74] Bissell MJ, Aggeler J. Dynamic reciprocity: how do extracellular matrix and hormones direct gene expression? Progress in clinical and biological research. 1987;249:251-62.

[75] Agrawal V, Tottey S, Johnson SA, Freund JM, Siu BF, Badylak SF. Recruitment of progenitor cells by an extracellular matrix cryptic peptide in a mouse model of digit amputation. Tissue engineering Part A. 2011;17:2435-43.

[76] Crapo PM, Medberry CJ, Reing JE, Tottey S, van der Merwe Y, Jones KE, et al. Biologic scaffolds composed of central nervous system extracellular matrix. Biomaterials. 2012;33:3539-47.

[77] DeQuach JA, Yuan SH, Goldstein LS, Christman KL. Decellularized porcine brain matrix for cell culture and tissue engineering scaffolds. Tissue Eng Part A. 2011;17:2583-92.

[78] Crapo PM, Tottey S, Slivka PF, Badylak SF. Effects of Biologic Scaffolds on Human Stem Cells and Implications for CNS Tissue Engineering. Tissue engineering Part A. 2013.

[79] Agrawal V, Kelly J, Tottey S, Daly KA, Johnson SA, Siu BF, et al. An isolated cryptic peptide influences osteogenesis and bone remodeling in an adult mammalian model of digit amputation. Tissue Eng Part A. 2011;17:3033-44.

[80] Valentin JE, Stewart-Akers AM, Gilbert TW, Badylak SF. Macrophage participation in the degradation and remodeling of extracellular matrix scaffolds. Tissue Eng Part A. 2009;15:1687-94.

[81] Brown BN, Ratner BD, Goodman SB, Amar S, Badylak SF. Macrophage polarization: an opportunity for improved outcomes in biomaterials and regenerative medicine. Biomaterials. 2012;33:3792-802.

[82] Brown BN, Londono R, Tottey S, Zhang L, Kukla KA, Wolf MT, et al. Macrophage phenotype as a predictor of constructive remodeling following the implantation of biologically derived surgical mesh materials. Acta Biomater. 2012;8:978-87.

[83] Crapo PM, Gilbert TW, Badylak SF. An overview of tissue and whole organ decellularization processes. Biomaterials. 2011;32:3233-43.

[84] Gilbert TW, Sellaro TL, Badylak SF. Decellularization of tissues and organs. Biomaterials. 2006;27:3675-83.

[85] Badylak SF. The extracellular matrix as a biologic scaffold material. Biomaterials. 2007;28:3587-93.

[86] Aouacheria A, Geourjon C, Aghajari N, Navratil V, Deleage G, Lethias C, et al. Insights into early extracellular matrix evolution: spongin short chain collagen-related proteins are homologous to basement membrane type IV collagens and form a novel family widely distributed in invertebrates. Molecular biology and evolution. 2006;23:2288-302.

[87] Kadler K. Matrix loading: assembly of extracellular matrix collagen fibrils during embryogenesis. Birth defects research Part C, Embryo today : reviews. 2004;72:1-11.

[88] Yoshimura Y. Integrins: expression, modulation, and signaling in fertilization, embryogenesis and implantation. The Keio journal of medicine. 1997;46:16-24.

[89] Kaneko Y, Murphy CR, Day ML. Extracellular matrix proteins secreted from both the endometrium and the embryo are required for attachment: a study using a co-culture model of rat blastocysts and Ishikawa cells. Journal of morphology. 2013;274:63-72.

[90] Sakurai M, Sato Y, Mukai K, Suematsu M, Fukui E, Yoshizawa M, et al. Distribution of tubulointerstitial nephritis antigen-like 1 and structural matrix proteins in mouse embryos during preimplantation development in vivo and in vitro. Zygote. 2012:1-7.

[91] Johnson KE. Extracellular matrix synthesis in blastula and gastrula stages of normal and hybrid frog embryos. I. Toluidine blue and lanthanum staining. Journal of cell science. 1977;25:313-22.

[92] Adams JC, Watt FM. Regulation of development and differentiation by the extracellular matrix. Development. 1993;117:1183-98.

[93] Gullberg D, Ekblom P. Extracellular matrix and its receptors during development. The International journal of developmental biology. 1995;39:845-54.

[94] Rozario T, DeSimone DW. The extracellular matrix in development and morphogenesis: a dynamic view. Developmental biology. 2010;341:126-40.

[95] Zagris N. Extracellular matrix in development of the early embryo. Micron. 2001;32:427-38.

[96] Perris R, Perissinotto D. Role of the extracellular matrix during neural crest cell migration. Mechanisms of development. 2000;95:3-21.

[97] Tsang KY, Cheung MC, Chan D, Cheah KS. The developmental roles of the extracellular matrix: beyond structure to regulation. Cell and tissue research. 2010;339:93-110.

[98] Daley WP, Peters SB, Larsen M. Extracellular matrix dynamics in development and regenerative medicine. Journal of cell science. 2008;121:255-64.

[99] Carnegie JA, Cabaca O. Extracellular matrix composition and resilience: two parameters that influence the in vitro migration and morphology of rat inner cell mass-derived cells. Biology of reproduction. 1993;48:287-99.

[100] Hay ED. Extracellular matrix alters epithelial differentiation. Current opinion in cell biology. 1993;5:1029-35.

[101] Lonai P. Epithelial mesenchymal interactions, the ECM and limb development. Journal of anatomy. 2003;202:43-50.

[102] Hardman P, Spooner BS. Extracellular matrix and growth factors in branching morphogenesis. Transactions of the Kansas Academy of Science Kansas Academy of Science. 1993;96:56-61.

[103] Berg LK, Chen SW, Wessel GM. An extracellular matrix molecule that is selectively expressed during development is important for gastrulation in the sea urchin embryo. Development. 1996;122:703-13.

[104] Harrisson F. Cellular origin of the basement membrane in embryonic chicken/quail chimeras. The International journal of developmental biology. 1993;37:337-47.

[105] Chiquet M. Tenascin: an extracellular matrix protein involved in morphogenesis of epithelial organs. Kidney international. 1992;41:629-31.

[106] Filla A, Hiripi L, Elekes K. Serotonergic and dopaminergic influence of the duration of embryogenesis and intracapsular locomotion of Lymnaea stagnalis L. Acta biologica Hungarica. 2004;55:315-21.

[107] Rifes P, Thorsteinsdottir S. Extracellular matrix assembly and 3D organization during paraxial mesoderm development in the chick embryo. Developmental biology. 2012;368:370-81.

[108] Czirok A, Rongish BJ, Little CD. Extracellular matrix dynamics during vertebrate axis formation. Developmental biology. 2004;268:111-22.

[109] Bellairs R, Veini M. An experimental analysis of somite segmentation in the chick embryo. Journal of embryology and experimental morphology. 1980;55:93-108.

[110] Kim HY, Nelson CM. Extracellular matrix and cytoskeletal dynamics during branching morphogenesis. Organogenesis. 2012;8:56-64.

[111] Wallner EI, Yang Q, Peterson DR, Wada J, Kanwar YS. Relevance of extracellular matrix, its receptors, and cell adhesion molecules in mammalian nephrogenesis. The American journal of physiology. 1998;275:F467-77.

[112] Kosher RA, Savage MP, Walker KH. A gradation of hyaluronate accumulation along the proximodistal axis of the embryonic chick limb bud. Journal of embryology and experimental morphology. 1981;63:85-98.

[113] Matsumoto K, Li Y, Jakuba C, Sugiyama Y, Sayo T, Okuno M, et al. Conditional inactivation of Has2 reveals a crucial role for hyaluronan in skeletal growth, patterning, chondrocyte maturation and joint formation in the developing limb. Development. 2009;136:2825-35.

[114] Chiquet M, Eppenberger HM, Turner DC. Muscle morphogenesis: Evidence for an organizing function of exogenous fibronectin. Developmental biology. 1981;88:220-35.

[115] Pavlov I, Lauri S, Taira T, Rauvala H. The role of ECM molecules in activity-dependent synaptic development and plasticity. Birth defects research Part C, Embryo today : reviews. 2004;72:12-24.

[116] Sheppard AM, Hamilton SK, Pearlman AL. Changes in the distribution of extracellular matrix components accompany early morphogenetic events of mammalian cortical development. The Journal of neuroscience : the official journal of the Society for Neuroscience. 1991;11:3928-42.

[117] Hanson KP, Jung JP, Tran QA, Hsu SP, Iida R, Ajeti V, et al. Spatial and temporal analysis of extracellular matrix proteins in the developing murine heart: a blueprint for regeneration. Tissue engineering Part A. 2013;19:1132-43.

[118] Behonick DJ, Werb Z. A bit of give and take: the relationship between the extracellular matrix and the developing chondrocyte. Mechanisms of development. 2003;120:1327-36.

[119] Peters C, O'Shea KS, Campbell AD, Wicha MS, Long MW. Fetal expression of hemonectin: an extracellular matrix hematopoietic cytoadhesion molecule. Blood. 1990;75:357-64.

[120] Bornstein P, Duksin D, Balian G, Davidson JM, Crouch E. Organization of extracellular proteins on the connective tissue cell surface: relevance to cell-matrix interactions in vitro and in vivo. Annals of the New York Academy of Sciences. 1978;312:93-105.

[121] Schultz GS, Davidson JM, Kirsner RS, Bornstein P, Herman IM. Dynamic reciprocity in the wound microenvironment. Wound repair and regeneration : official publication of the Wound Healing Society [and] the European Tissue Repair Society. 2011;19:134-48.

[122] Loganathan R, Potetz BR, Rongish BJ, Little CD. Spatial anisotropies and temporal fluctuations in extracellular matrix network texture during early embryogenesis. PloS one. 2012;7:e38266.

[123] Jafari G, Burghoorn J, Kawano T, Mathew M, Morck C, Axang C, et al. Genetics of extracellular matrix remodeling during organ growth using the Caenorhabditis elegans pharynx model. Genetics. 2010;186:969-82.

[124] Calve S, Odelberg SJ, Simon HG. A transitional extracellular matrix instructs cell behavior during muscle regeneration. Developmental biology. 2010;344:259-71.

[125] Calve S, Simon HG. Biochemical and mechanical environment cooperatively regulate skeletal muscle regeneration. FASEB journal : official publication of the Federation of American Societies for Experimental Biology. 2012;26:2538-45.

[126] Chen XD. Extracellular matrix provides an optimal niche for the maintenance and propagation of mesenchymal stem cells. Birth defects research Part C, Embryo today : reviews. 2010;90:45-54.

[127] Zeng D, Ou DB, Wei T, Ding L, Liu XT, Hu XL, et al. Collagen/beta(1) integrin interaction is required for embryoid body formation during cardiogenesis from murine induced pluripotent stem cells. BMC cell biology. 2013;14:5.

[128] Sandusky GE, Jr., Badylak SF, Morff RJ, Johnson WD, Lantz G. Histologic findings after in vivo placement of small intestine submucosal vascular grafts and saphenous vein grafts in the carotid artery in dogs. Am J Pathol. 1992;140:317-24.

[129] Badylak SF, Freytes DO, Gilbert TW. Extracellular matrix as a biological scaffold material: Structure and function. Acta Biomater. 2009;5:1-13.

[130] Wolf MT, Daly KA, Brennan-Pierce EP, Johnson SA, Carruthers CA, D'Amore A, et al. A hydrogel derived from decellularized dermal extracellular matrix. Biomaterials.33:7028-38.

[131] Soto-Gutierrez A, Zhang L, Medberry C, Fukumitsu K, Faulk D, Jiang H, et al. A whole-organ regenerative medicine approach for liver replacement. Tissue Eng Part C Methods.17:677-86.

[132] Wainwright JM, Czajka CA, Patel UB, Freytes DO, Tobita K, Gilbert TW, et al. Preparation of cardiac extracellular matrix from an intact porcine heart. Tissue Eng Part C Methods.16:525-32.

[133] Bloch O, Erdbrugger W, Volker W, Schenk A, Posner S, Konertz W, et al. Extracellular matrix in deoxycholic acid decellularized aortic heart valves. Med Sci Monit.18:BR487-92.

[134] Kneib C, von Glehn CQ, Costa FD, Costa MT, Susin MF. Evaluation of humoral immune response to donor HLA after implantation of cellularized versus decellularized human heart valve allografts. Tissue Antigens.80:165-74.

[135] Crapo PM, Gilbert TW, Badylak SF. An overview of tissue and whole organ decellularization processes. Biomaterials.32:3233-43.

[136] Badylak SF, Weiss DJ, Caplan A, Macchiarini P. Engineered whole organs and complex tissues. Lancet.379:943-52.

[137] Gilbert TW, Freund JM, Badylak SF. Quantification of DNA in biologic scaffold materials. J Surg Res. 2009;152:135-9.

[138] Badylak SF, Gilbert TW. Immune response to biologic scaffold materials. Semin Immunol. 2008;20:109-16.

[139] Keane TJ, Londono R, Turner NJ, Badylak SF. Consequences of ineffective decellularization of biologic scaffolds on the host response. Biomaterials.33:1771-81.

[140] Daly KA, Liu S, Agrawal V, Brown BN, Johnson SA, Medberry CJ, et al. Damage associated molecular patterns within xenogeneic biologic scaffolds and their effects on host remodeling. Biomaterials.33:91-101.

[141] Singelyn JM, Christman KL. Modulation of material properties of a decellularized myocardial matrix scaffold. Macromol Biosci.11:731-8.

[142] Freytes DO, Martin J, Velankar SS, Lee AS, Badylak SF. Preparation and rheological characterization of a gel form of the porcine urinary bladder matrix. Biomaterials. 2008;29:1630-7.

[143] Singelyn JM, Sundaramurthy P, Johnson TD, Schup-Magoffin PJ, Hu DP, Faulk DM, et al. Catheter-deliverable hydrogel derived from decellularized ventricular extracellular matrix increases endogenous cardiomyocytes and preserves cardiac function post-myocardial infarction. J Am Coll Cardiol.59:751-63.

[144] Medberry CJ, Crapo PM, Siu BF, Carruthers CA, Wolf MT, Nagarkar SP, et al. Hydrogels derived from central nervous system extracellular matrix. Biomaterials.34:1033-40.

[145] Sicari BM, Johnson SA, Siu BF, Crapo PM, Daly KA, Jiang H, et al. The effect of source animal age upon the in vivo remodeling characteristics of an extracellular matrix scaffold. Biomaterials.33:5524-33.

[146] Badylak SF. The extracellular matrix as a scaffold for tissue reconstruction. Semin Cell Dev Biol. 2002;13:377-83.

[147] Daly KA, Liu S, Agrawal V, Brown BN, Huber A, Johnson SA, et al. The host response to endotoxin-contaminated dermal matrix. Tissue Eng Part A.18:1293-303.

[148] Londono R, Jobe BA, Hoppo T, Badylak SF. Esophagus and regenerative medicine. World J Gastroenterol.18:6894-9.

[149] Sicari BM, Agrawal V, Siu BF, Medberry CJ, Dearth CL, Turner NJ, et al. A murine model of volumetric muscle loss and a regenerative medicine approach for tissue replacement. Tissue Eng Part A.18:1941-8.

[150] Turner NJ, Badylak JS, Weber DJ, Badylak SF. Biologic scaffold remodeling in a dog model of complex musculoskeletal injury. J Surg Res.176:490-502.

[151] Turner NJ, Badylak SF. Regeneration of skeletal muscle. Cell Tissue Res.347:759-74.

[152] Wainwright JM, Hashizume R, Fujimoto KL, Remlinger NT, Pesyna C, Wagner WR, et al. Right ventricular outflow tract repair with a cardiac biologic scaffold. Cells Tissues Organs.195:159-70.

[153] Badylak SF, Kochupura PV, Cohen IS, Doronin SV, Saltman AE, Gilbert TW, et al. The use of extracellular matrix as an inductive scaffold for the partial replacement of functional myocardium. Cell Transplant. 2006;15 Suppl 1:S29-40.

[154] Kochupura PV, Azeloglu EU, Kelly DJ, Doronin SV, Badylak SF, Krukenkamp IB, et al. Tissue-engineered myocardial patch derived from extracellular matrix provides regional mechanical function. Circulation. 2005;112:I144-9.

[155] Kastner T, Berkner P, DeSouza T, Wight D, Waran S. Rett syndrome and metabolic disorder. J Am Acad Child Adolesc Psychiatry. 1992;31:567-8.

[156] Rane AA, Christman KL. Biomaterials for the treatment of myocardial infarction: a 5-year update. J Am Coll Cardiol.58:2615-29.

[157] Agrawal V, Tottey S, Johnson SA, Freund JM, Siu BF, Badylak SF. Recruitment of progenitor cells by an extracellular matrix cryptic peptide in a mouse model of digit amputation. Tissue Eng Part A.17:2435-43.

[158] Agrawal V, Kelly J, Tottey S, Daly KA, Johnson SA, Siu BF, et al. An isolated cryptic peptide influences osteogenesis and bone remodeling in an adult mammalian model of digit amputation. Tissue Eng Part A.17:3033-44.

[159] Brown BN, Londono R, Tottey S, Zhang L, Kukla KA, Wolf MT, et al. Macrophage phenotype as a predictor of constructive remodeling following the implantation of biologically derived surgical mesh materials. Acta Biomater.8:978-87.

[160] Brown BN, Ratner BD, Goodman SB, Amar S, Badylak SF. Macrophage polarization: an opportunity for improved outcomes in biomaterials and regenerative medicine. Biomaterials.33:3792-802.

[161] O'Reilly MS, Boehm T, Shing Y, Fukai N, Vasios G, Lane WS, et al. Endostatin: an endogenous inhibitor of angiogenesis and tumor growth. Cell. 1997;88:277-85.

[162] Ramchandran R, Dhanabal M, Volk R, Waterman MJ, Segal M, Lu H, et al. Antiangiogenic activity of restin, NC10 domain of human collagen XV: comparison to endostatin. Biochem Biophys Res Commun. 1999;255:735-9.

[163] Colorado PC, Torre A, Kamphaus G, Maeshima Y, Hopfer H, Takahashi K, et al. Anti-angiogenic cues from vascular basement membrane collagen. Cancer Res. 2000;60:2520-6.

[164] Houghton AM, Grisolano JL, Baumann ML, Kobayashi DK, Hautamaki RD, Nehring LC, et al. Macrophage elastase (matrix metalloproteinase-12) suppresses growth of lung metastases. Cancer Res. 2006;66:6149-55.

[165] Vlodavsky I, Goldshmidt O, Zcharia E, Atzmon R, Rangini-Guatta Z, Elkin M, et al. Mammalian heparanase: involvement in cancer metastasis, angiogenesis and normal development. Semin Cancer Biol. 2002;12:121-9.

[166] Roy M, Marchetti D. Cell surface heparan sulfate released by heparanase promotes melanoma cell migration and angiogenesis. J Cell Biochem. 2009;106:200-9.

[167] Badylak SF, Coffey AC, Lantz GC, Tacker WA, Geddes LA. Comparison of the resistance to infection of intestinal submucosa arterial autografts versus polytetrafluoroethylene arterial prostheses in a dog model. J Vasc Surg. 1994;19:465-72.

[168] Sarikaya A, Record R, Wu CC, Tullius B, Badylak S, Ladisch M. Antimicrobial activity associated with extracellular matrices. Tissue Eng. 2002;8:63-71.

[169] Brennan EP, Reing J, Chew D, Myers-Irvin JM, Young EJ, Badylak SF. Antibacterial activity within degradation products of biological scaffolds composed of extracellular matrix. Tissue Eng. 2006;12:2949-55.

[170] Holtom PD, Shinar Z, Benna J, Patzakis MJ. Porcine small intestine submucosa does not show antimicrobial properties. Clin Orthop Relat Res. 2004:18-21.

[171] Li F, Li W, Johnson S, Ingram D, Yoder M, Badylak S. Low-molecular-weight peptides derived from extracellular matrix as chemoattractants for primary endothelial cells. Endothelium. 2004;11:199-206.

[172] Beattie AJ, Gilbert TW, Guyot JP, Yates AJ, Badylak SF. Chemoattraction of progenitor cells by remodeling extracellular matrix scaffolds. Tissue engineering Part A. 2009;15:1119-25.

[173] Badylak SF, Park K, Peppas N, McCabe G, Yoder M. Marrow-derived cells populate scaffolds composed of xenogeneic extracellular matrix. Exp Hematol. 2001;29:1310-8.

[174] Schenk S, Quaranta V. Tales from the crypt[ic] sites of the extracellular matrix. Trends Cell Biol. 2003;13:366-75.

[175] Ortega N, Werb Z. New functional roles for non-collagenous domains of basement membrane collagens. J Cell Sci. 2002;115:4201-14.

[176] Mott JD, Werb Z. Regulation of matrix biology by matrix metalloproteinases. Curr Opin Cell Biol. 2004;16:558-64.

[177] Ambesi A, Klein RM, Pumiglia KM, McKeown-Longo PJ. Anastellin, a fragment of the first type III repeat of fibronectin, inhibits extracellular signal-regulated kinase and causes G(1) arrest in human microvessel endothelial cells. Cancer Res. 2005;65:148-56.

[178] Ponce ML, Hibino S, Lebioda AM, Mochizuki M, Nomizu M, Kleinman HK. Identification of a potent peptide antagonist to an active laminin-1 sequence that blocks angiogenesis and tumor growth. Cancer Res. 2003;63:5060-4.

[179] Ponce ML, Kleinman HK. Identification of redundant angiogenic sites in laminin alpha1 and gamma1 chains. Exp Cell Res. 2003;285:189-95.

[180] Schenk S, Hintermann E, Bilban M, Koshikawa N, Hojilla C, Khokha R, et al. Binding to EGF receptor of a laminin-5 EGF-like fragment liberated during MMP-dependent mammary gland involution. J Cell Biol. 2003;161:197-209.

[181] Chen WY, Abatangelo G. Functions of hyaluronan in wound repair. Wound Repair Regen. 1999;7:79-89.

[182] Calve S, Odelberg SJ, Simon HG. A transitional extracellular matrix instructs cell behavior during muscle regeneration. Dev Biol.344:259-71.

[183] Adzick NS, Longaker MT. Scarless fetal healing. Therapeutic implications. Ann Surg. 1992;215:3-7.

[184] Bullard KM, Longaker MT, Lorenz HP. Fetal wound healing: current biology. World J Surg. 2003;27:54-61.

[185] Brennan EP, Tang XH, Stewart-Akers AM, Gudas LJ, Badylak SF. Chemoattractant activity of degradation products of fetal and adult skin extracellular matrix for keratinocyte progenitor cells. J Tissue Eng Regen Med. 2008;2:491-8.

[186] Brown BN, Freund JM, Han L, Rubin JP, Reing JE, Jeffries EM, et al. Comparison of three methods for the derivation of a biologic scaffold composed of adipose tissue extracellular matrix. Tissue Eng Part C Methods.17:411-21.

[187] Allen JW, Hassanein T, Bhatia SN. Advances in bioartificial liver devices. Hepatology. 2001;34:447-55.

[188] Strom SC, Fisher RA, Thompson MT, Sanyal AJ, Cole PE, Ham JM, et al. Hepatocyte transplantation as a bridge to orthotopic liver transplantation in terminal liver failure. Transplantation. 1997;63:559-69.

[189] Fuhrman C, Jougla E, Nicolau J, Eilstein D, Delmas MC. Deaths from chronic obstructive pulmonary disease in France, 1979-2002: a multiple cause analysis. Thorax. 2006;61:930-4.

[190] Bonavita AG, Quaresma K, Cotta-de-Almeida V, Pinto MA, Saraiva RM, Alves LA. Hepatocyte xenotransplantation for treating liver disease. Xenotransplantation. 2010;17:181-7.

[191] Fiegel HC, Kaufmann PM, Bruns H, Kluth D, Horch RE, Vacanti JP, et al. Hepatic tissue engineering: from transplantation to customized cell-based liver directed therapies from the laboratory. J Cell Mol Med. 2008;12:56-66.

[192] Diekmann S, Bader A, Schmitmeier S. Present and Future Developments in Hepatic Tissue Engineering for Liver Support Systems : State of the art and future developments of hepatic cell culture techniques for the use in liver support systems. Cytotechnology. 2006;50:163-79.

[193] Zhou P, Lessa N, Estrada DC, Severson EB, Lingala S, Zern MA, et al. Decellularized liver matrix as a carrier for the transplantation of human fetal and primary hepatocytes in mice. Liver transplantation : official publication of the American Association for the Study of Liver Diseases and the International Liver Transplantation Society. 2011;17:418-27.

[194] Barakat O, Abbasi S, Rodriguez G, Rios J, Wood RP, Ozaki C, et al. Use of decellularized porcine liver for engineering humanized liver organ. The Journal of surgical research. 2012;173:e11-25.

[195] Soto-Gutierrez A, Zhang L, Medberry C, Fukumitsu K, Faulk D, Jiang H, et al. A whole-organ regenerative medicine approach for liver replacement. Tissue Eng Part C Methods. 2011;17:677-86.

[196] Sampey BP, Stewart BJ, Petersen DR. Ethanol-induced modulation of hepatocellular extracellular signal-regulated kinase-1/2 activity via 4-hydroxynonenal. J Biol Chem. 2007;282:1925-37.

[197] Bao J, Shi Y, Sun H, Yin X, Yang R, Li L, et al. Construction of a portal implantable functional tissue-engineered liver using perfusion-decellularized matrix and hepatocytes in rats. Cell Transplant. 2011;20:753-66.

[198] Shupe T, Williams M, Brown A, Willenberg B, Petersen BE. Method for the decellularization of intact rat liver. Organogenesis. 2010;6:134-6.

[199] Mirmalek-Sani SH, Sullivan DC, Zimmerman C, Shupe TD, Petersen BE. Immunogenicity of decellularized porcine liver for bioengineered hepatic tissue. Am J Pathol. 2013;183:558-65.

[200] Lang R, Stern MM, Smith L, Liu Y, Bharadwaj S, Liu G, et al. Three-dimensional culture of hepatocytes on porcine liver tissue-derived extracellular matrix. Biomaterials. 2011;32:7042-52.

[201] Song JJ, Kim SS, Liu Z, Madsen JC, Mathisen DJ, Vacanti JP, et al. Enhanced in vivo function of bioartificial lungs in rats. Ann Thorac Surg. 2011;92:998-1005; discussion -6.

[202] Ott HC, Clippinger B, Conrad C, Schuetz C, Pomerantseva I, Ikonomou L, et al. Regeneration and orthotopic transplantation of a bioartificial lung. Nature medicine. 2010;16:927-33.

[203] Cortiella J, Niles J, Cantu A, Brettler A, Pham A, Vargas G, et al. Influence of acellular natural lung matrix on murine embryonic stem cell differentiation and tissue formation. Tissue Eng Part A. 2010;16:2565-80.

[204] Goh SK, Bertera S, Olsen P, Candiello JE, Halfter W, Uechi G, et al. Perfusion-decellularized pancreas as a natural 3D scaffold for pancreatic tissue and whole organ engineering. Biomaterials. 2013;34:6760-72.

[205] Sullivan DC, Mirmalek-Sani SH, Deegan DB, Baptista PM, Aboushwareb T, Atala A, et al. Decellularization methods of porcine kidneys for whole organ engineering using a high-throughput system. Biomaterials. 2012;33:7756-64.

[206] Song JJ, Guyette JP, Gilpin SE, Gonzalez G, Vacanti JP, Ott HC. Regeneration and experimental orthotopic transplantation of a bioengineered kidney. Nature medicine. 2013;19:646-51.

[207] Tzanakakis ES, Hess DJ, Sielaff TD, Hu WS. Extracorporeal tissue engineered liver-assist devices. Annu Rev Biomed Eng. 2000;2:607-32.

[208] Fausto N. Liver regeneration. J Hepatol. 2000;32:19-31.

[209] Reid LM, Fiorino AS, Sigal SH, Brill S, Holst PA. Extracellular matrix gradients in the space of Disse: relevance to liver biology. Hepatology. 1992;15:1198-203.

[210] Payen L, Courtois A, Campion JP, Guillouzo A, Fardel O. Characterization and inhibition by a wide range of xenobiotics of organic anion excretion by primary human hepatocytes. Biochem Pharmacol. 2000;60:1967-75.

[211] Rappaport AM, Borowy ZJ, Lougheed WM, Lotto WN. Subdivision of hexagonal liver lobules into a structural and functional unit; role in hepatic physiology and pathology. Anat Rec. 1954;119:11-33.

[212] Kudryavtseva MV, Sakuta GA, Stein GI, Kudryavtsev BN. The metabolic zonation of glycogen synthesis in rat liver after fasting and refeeding. Tissue Cell. 1992;24:31-5.

[213] Gebhardt R. Metabolic zonation of the liver: regulation and implications for liver function. Pharmacol Ther. 1992;53:275-354.

[214] Lindros KO. Zonation of cytochrome P450 expression, drug metabolism and toxicity in liver. Gen Pharmacol. 1997;28:191-6.

[215] Pathare DB, Jadhav AS, Shingare MS. Validated chiral liquid chromatographic method for the enantiomeric separation of Pramipexole dihydrochloride monohydrate. J Pharm Biomed Anal. 2006;41:1152-6.

[216] Jadhav JP, Govindwar SP. Biotransformation of malachite green by Saccharomyces cerevisiae MTCC 463. Yeast. 2006;23:315-23.

[217] Solaroglu I, Cahill J, Jadhav V, Zhang JH. A novel neuroprotectant granulocyte-colony stimulating factor. Stroke. 2006;37:1123-8.

[218] Suryawanshi NP, Bhutey AK, Nagdeote AN, Jadhav AA, Manoorkar GS. Study of lipid peroxide and lipid profile in diabetes mellitus. Indian J Clin Biochem. 2006;21:126-30.

[219] Turner NJ, Badylak SF. Biologic scaffolds for musculotendinous tissue repair. European cells & materials. 2013;25:130-43.

[220] Mantovani F, Trinchieri A, Castelnuovo C, Romano AL, Pisani E. Reconstructive urethroplasty using porcine acellular matrix. European urology. 2003;44:600-2.

[221] Crisan M, Yap S, Casteilla L, Chen CW, Corselli M, Park TS, et al. A perivascular origin for mesenchymal stem cells in multiple human organs. Cell stem cell. 2008;3:301-13.

[222] Londono R, Jobe BA, Hoppo T, Badylak SF. Esophagus and regenerative medicine. World journal of gastroenterology : WJG. 2012;18:6894-9.

[223] Valentin JE, Badylak JS, McCabe GP, Badylak SF. Extracellular matrix bioscaffolds for orthopaedic applications. A comparative histologic study. The Journal of bone and joint surgery American volume. 2006;88:2673-86.

[224] Smart NJ, Marshall M, Daniels IR. Biological meshes: a review of their use in abdominal wall hernia repairs. Surgeon. 2012;10:159-71.

[225] Agrawal V, Johnson SA, Reing J, Zhang L, Tottey S, Wang G, et al. Epimorphic regeneration approach to tissue replacement in adult mammals. Proc Natl Acad Sci U S A. 2010;107:3351-5.

[226] Mase VJ, Jr., Hsu JR, Wolf SE, Wenke JC, Baer DG, Owens J, et al. Clinical application of an acellular biologic scaffold for surgical repair of a large, traumatic quadriceps femoris muscle defect. Orthopedics. 2010;33:511.

[227] Nieponice A, McGrath K, Qureshi I, Beckman EJ, Luketich JD, Gilbert TW, et al. An extracellular matrix scaffold for esophageal stricture prevention after circumferential EMR. Gastrointest Endosc. 2009;69:289-96.

[228] Badylak SF, Vorp DA, Spievack AR, Simmons-Byrd A, Hanke J, Freytes DO, et al. Esophageal reconstruction with ECM and muscle tissue in a dog model. J Surg Res. 2005;128:87-97.

[229] Badylak SF, Hoppo T, Nieponice A, Gilbert TW, Davison JM, Jobe BA. Esophageal preservation in five male patients after endoscopic inner-layer circumferential resection in the setting of superficial cancer: a regenerative medicine approach with a biologic scaffold. Tissue Eng Part A. 2011;17:1643-50.

[230] Badylak S, Meurling S, Chen M, Spievack A, Simmons-Byrd A. Resorbable bioscaffold for esophageal repair in a dog model. J Pediatr Surg. 2000;35:1097-103.

[231] Boruch AV, Nieponice A, Qureshi IR, Gilbert TW, Badylak SF. Constructive remodeling of biologic scaffolds is dependent on early exposure to physiologic bladder filling in a canine partial cystectomy model. J Surg Res. 2010;161:217-25.

[232] Kropp BP, Badylak S, Thor KB. Regenerative bladder augmentation: a review of the initial preclinical studies with porcine small intestinal submucosa. Adv Exp Med Biol. 1995;385:229-35.

[233] Li F, Li W, Johnson S, Ingram D, Yoder M, Badylak SF. Low-molecular-weight peptides derived from extracellular matrix as chemoattractants for primary endothelial cells. Endothelium. 2004;11:199-206.

[234] Tottey S, Corselli M, Jeffries EM, Londono R, Peault B, Badylak SF. Extracellular matrix degradation products and low-oxygen conditions enhance the regenerative potential of perivascular stem cells. Tissue Eng Part A. 2011;17:37-44.

[235] Badylak SF, Valentin JE, Ravindra AK, McCabe GP, Stewart-Akers AM. Macrophage phenotype as a determinant of biologic scaffold remodeling. Tissue Eng Part A. 2008;14:1835-42.

[236] Gardner AB, Lee SK, Woods EC, Acharya AP. Biomaterials-Based Modulation of the Immune System. Biomed Res Int. 2013;2013:732182.

[237] Gilbert TW, Stewart-Akers AM, Simmons-Byrd A, Badylak SF. Degradation and remodeling of small intestinal submucosa in canine Achilles tendon repair. J Bone Joint Surg Am. 2007;89:621-30.

[238] Badylak SF. An Assay to Quantify Chemotactic Properties of Degradation Products from Extracellular Matrix. Methods in molecular biology. 2013.

[239] Weymann A, Loganathan S, Takahashi H, Schies C, Claus B, Hirschberg K, et al. Development and evaluation of a perfusion decellularization porcine heart model--generation of 3-dimensional myocardial neoscaffolds. Circulation journal : official journal of the Japanese Circulation Society. 2011;75:852-60.

[240] Keane TJ, Londono R, Carey RM, Carruthers CA, Reing JE, Dearth CL, et al. Preparation and characterization of a biologic scaffold from esophageal mucosa. Biomaterials. 2013;34:6729-37.

[241] Baptista PM, Siddiqui MM, Lozier G, Rodriguez SR, Atala A, Soker S. The use of whole organ decellularization for the generation of a vascularized liver organoid. Hepatology.53:604-17.

[242] Bao J, Shi Y, Sun H, Yin X, Yang R, Li L, et al. Construction of a portal implantable functional tissue-engineered liver using perfusion-decellularized matrix and hepatocytes in rats. Cell Transplant.20:753-66.

[243] Song JJ, Kim SS, Liu Z, Madsen JC, Mathisen DJ, Vacanti JP, et al. Enhanced in vivo function of bioartificial lungs in rats. Ann Thorac Surg.92:998-1005; discussion -6.

[244] Sullivan DC, Mirmalek-Sani SH, Deegan DB, Baptista PM, Aboushwareb T, Atala A, et al. Decellularization methods of porcine kidneys for whole organ engineering using a high-throughput system. Biomaterials.33:7756-64.

[245] Petersen TH, Calle EA, Zhao L, Lee EJ, Gui L, Raredon MB, et al. Tissue-engineered lungs for in vivo implantation. Science.329:538-41.

[246] Courtman DW, Pereira CA, Kashef V, McComb D, Lee JM, Wilson GJ. Development of a pericardial acellular matrix biomaterial: biochemical and mechanical effects of cell extraction. J Biomed Mater Res. 1994;28:655-66.

[247] Faulk DM, Carruthers CA, Warner HJ, Kramer CR, Reing JE, Zhang L, et al. The effect of detergents on the basement membrane complex of a biologic scaffold material. Acta Biomater. 2014;10:183-93.

[248] Kmiec Z. Cooperation of liver cells in health and disease. Advances in anatomy, embryology, and cell biology. 2001;161:III-XIII, 1-151.

[249] Bhatia SN, Balis UJ, Yarmush ML, Toner M. Microfabrication of hepatocyte/fibroblast co-cultures: role of homotypic cell interactions. Biotechnol Prog. 1998;14:378-87.

[250] Bhatia SN, Balis UJ, Yarmush ML, Toner M. Effect of cell-cell interactions in preservation of cellular phenotype: cocultivation of hepatocytes and nonparenchymal cells. FASEB J. 1999;13:1883-900.

[251] Wolf MT, Daly KA, Brennan-Pierce EP, Johnson SA, Carruthers CA, D'Amore A, et al. A hydrogel derived from decellularized dermal extracellular matrix. Biomaterials. 2012;33:7028-38.

[252] Petersen TH, Calle EA, Colehour MB, Niklason LE. Matrix composition and mechanics of decellularized lung scaffolds. Cells Tissues Organs. 2012;195:222-31.

[253] Freytes DO, Stoner RM, Badylak SF. Uniaxial and biaxial properties of terminally sterilized porcine urinary bladder matrix scaffolds. J Biomed Mater Res B Appl Biomater. 2008;84:408-14.

[254] Sellaro TL, Ranade A, Faulk DM, McCabe GP, Dorko K, Badylak SF, et al. Maintenance of human hepatocyte function in vitro by liver-derived extracellular matrix gels. Tissue Eng Part A.16:1075-82.

[255] Petersen TH, Calle EA, Colehour MB, Niklason LE. Matrix composition and mechanics of decellularized lung scaffolds. Cells Tissues Organs.195:222-31.

[256] Ott HC, Clippinger B, Conrad C, Schuetz C, Pomerantseva I, Ikonomou L, et al. Regeneration and orthotopic transplantation of a bioartificial lung. Nat Med.16:927-33.

[257] Uygun BE, Soto-Gutierrez A, Yagi H, Izamis ML, Guzzardi MA, Shulman C, et al. Organ reengineering through development of a transplantable recellularized liver graft using decellularized liver matrix. Nat Med.16:814-20.

[258] Reing JE, Brown BN, Daly KA, Freund JM, Gilbert TW, Hsiong SX, et al. The effects of processing methods upon mechanical and biologic properties of porcine dermal extracellular matrix scaffolds. Biomaterials.31:8626-33.

[259] Brown BN, Barnes CA, Kasick RT, Michel R, Gilbert TW, Beer-Stolz D, et al. Surface characterization of extracellular matrix scaffolds. Biomaterials.31:428-37.

[260] D'Amore A, Stella JA, Wagner WR, Sacks MS. Characterization of the complete fiber network topology of planar fibrous tissues and scaffolds. Biomaterials.31:5345-54.

[261] Theodossiou TA, Thrasivoulou C, Ekwobi C, Becker DL. Second harmonic generation confocal microscopy of collagen type I from rat tendon cryosections. Biophys J. 2006;91:4665-77.

[262] Wu TC, Wan YJ, Chung AE, Damjanov I. Immunohistochemical localization of entactin and laminin in mouse embryos and fetuses. Dev Biol. 1983;100:496-505.

[263] Parekh A, Mantle B, Banks J, Swarts JD, Badylak SF, Dohar JE, et al. Repair of the tympanic membrane with urinary bladder matrix. Laryngoscope. 2009;119:1206-13.

[264] Lecheminant J, Field C. Porcine urinary bladder matrix: a retrospective study and establishment of protocol. J Wound Care.21:476, 8-80, 82.

[265] Zhang L, Zhang F, Weng Z, Brown BN, Yan H, Ma X, et al. Effect of an Inductive Hydrogel composed of Urinary Bladder Matrix upon Functional Recovery Following Traumatic Brain Injury. Tissue Eng Part A.

[266] Liu L, Deng L, Wang Y, Ge L, Chen Y, Liang Z. Porcine urinary bladder matrix-polypropylene mesh: a novel scaffold material reduces immunorejection in rat pelvic surgery. Int Urogynecol J.23:1271-8.

[267] Robinson KA, Li J, Mathison M, Redkar A, Cui J, Chronos NA, et al. Extracellular matrix scaffold for cardiac repair. Circulation. 2005;112:I135-43.

[268] Nieponice A, Gilbert TW, Badylak SF. Reinforcement of esophageal anastomoses with an extracellular matrix scaffold in a canine model. Ann Thorac Surg. 2006;82:2050-8.

[269] Eberli D, Susaeta R, Yoo JJ, Atala A. Tunica repair with acellular bladder matrix maintains corporal tissue function. Int J Impot Res. 2007;19:602-9.

[270] Boruch AV, Nieponice A, Qureshi IR, Gilbert TW, Badylak SF. Constructive remodeling of biologic scaffolds is dependent on early exposure to physiologic bladder filling in a canine partial cystectomy model. J Surg Res.161:217-25.

[271] Kelly DJ, Rosen AB, Schuldt AJ, Kochupura PV, Doronin SV, Potapova IA, et al. Increased myocyte content and mechanical function within a tissue-engineered myocardial patch following implantation. Tissue Eng Part A. 2009;15:2189-201.

[272] Rosario DJ, Reilly GC, Ali Salah E, Glover M, Bullock AJ, Macneil S. Decellularization and sterilization of porcine urinary bladder matrix for tissue engineering in the lower urinary tract. Regen Med. 2008;3:145-56.

[273] Shah U, Bien H, Entcheva E. Microtopographical effects of natural scaffolding on cardiomyocyte function and arrhythmogenesis. Acta Biomater.6:3029-34.

[274] Eweida A, Saad M, Gabr E, Marei M, Khalil MR. Cultured keratinocytes on urinary bladder matrix scaffolds increase angiogenesis and help in rapid healing of wounds. Adv Skin Wound Care.24:268-73.

[275] Soto-Gutierrez A, Navarro-Alvarez N, Yagi H, Nahmias Y, Yarmush ML, Kobayashi N. Engineering of an hepatic organoid to develop liver assist devices. Cell Transplant.19:815-22.

[276] Baeck C, Streetz K. The recellularized liver matrix: a novel way of transplantation? Hepatology.52:1509-11.

[277] Shupe T, Williams M, Brown A, Willenberg B, Petersen BE. Method for the decellularization of intact rat liver. Organogenesis.6:134-6.

[278] Baptista PM, Orlando G, Mirmalek-Sani SH, Siddiqui M, Atala A, Soker S. Whole organ decellularization - a tool for bioscaffold fabrication and organ bioengineering. Conf Proc IEEE Eng Med Biol Soc. 2009;2009:6526-9.

[279] Arenas-Herrera JE, Ko IK, Atala A, Yoo JJ. Decellularization for whole organ bioengineering. Biomed Mater.8:014106.

[280] Song JJ, Guyette JP, Gilpin SE, Gonzalez G, Vacanti JP, Ott HC. Regeneration and experimental orthotopic transplantation of a bioengineered kidney. Nat Med.19:646-51.

[281] Arnold T, Linke D. The use of detergents to purify membrane proteins. Curr Protoc Protein Sci. 2008;4:1-4.

[282] Seddon AM, Curnow P, Booth PJ. Membrane proteins, lipids and detergents: not just a soap opera. Biochim Biophys Acta. 2004;3:1-2.

[283] Prive GG. Detergents for the stabilization and crystallization of membrane proteins. Methods. 2007;41:388-97.

[284] Bhrany AD, Beckstead BL, Lang TC, Farwell DG, Giachelli CM, Ratner BD. Development of an esophagus acellular matrix tissue scaffold. Tissue Eng. 2006;12:319-30.

[285] Seif-Naraghi SB, Singelyn JM, Salvatore MA, Osborn KG, Wang JJ, Sampat U, et al. Safety and efficacy of an injectable extracellular matrix hydrogel for treating myocardial infarction. Sci Transl Med. 2013;5:173ra25.

[286] Bernard MP, Chu ML, Myers JC, Ramirez F, Eikenberry EF, Prockop DJ. Nucleotide sequences of complementary deoxyribonucleic acids for the pro alpha 1 chain of human type I procollagen. Statistical evaluation of structures that are conserved during evolution. Biochemistry. 1983;22:5213-23.

[287] Exposito JY, D'Alessio M, Solursh M, Ramirez F. Sea urchin collagen evolutionarily homologous to vertebrate pro-alpha 2(I) collagen. J Biol Chem. 1992;267:15559-62.

[288] Faulk DM, Johnson SA, Zhang L, Badylak SF. Role of the extracellular matrix in whole organ engineering. J Cell Physiol. 2014;229:984-9.

[289] Zeltinger J, Landeen LK, Alexander HG, Kidd ID, Sibanda B. Development and characterization of tissue-engineered aortic valves. Tissue Eng. 2001;7:9-22.

[290] Apel PJ, Garrett JP, Sierpinski P, Ma J, Atala A, Smith TL, et al. Peripheral nerve regeneration using a keratin-based scaffold: long-term functional and histological outcomes in a mouse model. J Hand Surg Am. 2008;33:1541-7.

[291] Sicari BM, Rubin JP, Dearth CL, Wolf MT, Ambrosio F, Boninger M, et al. An acellular biologic scaffold promotes skeletal muscle formation in mice and humans with volumetric muscle loss. Sci Transl Med. 2014;6:234ra58.

[292] Sicari BM, Dearth CL, Badylak SF. Tissue engineering and regenerative medicine approaches to enhance the functional response to skeletal muscle injury. Anat Rec (Hoboken). 2014;297:51-64.

[293] Marongiu F, Gramignoli R, Dorko K, Miki T, Ranade AR, Paola Serra M, et al. Hepatic differentiation of amniotic epithelial cells. Hepatology. 2011;53:1719-29.

[294] Londono R, Badylak SF. Regenerative Medicine Strategies for Esophageal Repair. Tissue Eng Part B Rev. 2015.

[295] Nieponice A, Ciotola FF, Nachman F, Jobe BA, Hoppo T, Londono R, et al. Patch esophagoplasty: esophageal reconstruction using biologic scaffolds. Ann Thorac Surg. 2014;97:283-8.

[296] Lhoest JB, Wagner MS, Tidwell CD, Castner DG. Characterization of adsorbed protein films by time of flight secondary ion mass spectrometry. J Biomed Mater Res. 2001;57:432-40.

[297] Canavan HE, Graham DJ, Cheng X, Ratner BD, Castner DG. Comparison of native extracellular matrix with adsorbed protein films using secondary ion mass spectrometry. Langmuir. 2007;23:50-6.

[298] Canavan HE, Cheng X, Graham DJ, Ratner BD, Castner DG. Surface characterization of the extracellular matrix remaining after cell detachment from a thermoresponsive polymer. Langmuir. 2005;21:1949-55.

[299] Brown BN, Barnes CA, Kasick RT, Michel R, Gilbert TW, Beer-Stolz D, et al. Surface characterization of extracellular matrix scaffolds. Biomaterials. 2010;31:428-37.

[300] Sosnik A, Sodhi RN, Brodersen PM, Sefton MV. Surface study of collagen/poloxamine hydrogels by a 'deep freezing' ToF-SIMS approach. Biomaterials. 2006;27:2340-8.

[301] Holzweber M, Heinrich T, Kunz V, Richter S, Traulsen CH, Schalley CA, et al. Principal component analysis (PCA)-assisted time-of-flight secondary-ion mass spectrometry (ToF-SIMS): a versatile method for the investigation of self-assembled monolayers and multilayers as precursors for the bottom-up approach of nanoscaled devices. Anal Chem. 2014;86:5740-8.

[302] Muramoto S, Graham DJ, Wagner MS, Lee TG, Moon DW, Castner DG. ToF-SIMS Analysis of Adsorbed Proteins: Principal Component Analysis of the Primary Ion Species Effect on the Protein Fragmentation Patterns. J Phys Chem C Nanomater Interfaces. 2011;115:24247-55.

[303] Brunelle A, Laprevote O. Recent advances in biological tissue imaging with Time-of-flight Secondary Ion Mass Spectrometry: polyatomic ion sources, sample preparation, and applications. Curr Pharm Des. 2007;13:3335-43.

[304] Preface. OPTN/SRTR 2013 Annual Data Report. American journal of transplantation : official journal of the American Society of Transplantation and the American Society of Transplant Surgeons. 2015;15 Suppl 2:4-7.

[305] Faulk DM, Wildemann JD, Badylak SF. Decellularization and cell seeding of whole liver biologic scaffolds composed of extracellular matrix. Journal of clinical and experimental hepatology. 2015;5:69-80.

[306] Song JJ, Ott HC. Organ engineering based on decellularized matrix scaffolds. Trends in molecular medicine. 2011;17:424-32.

[307] Soto-Gutierrez A, Wertheim JA, Ott HC, Gilbert TW. Perspectives on whole-organ assembly: moving toward transplantation on demand. The Journal of clinical investigation. 2012;122:3817-23.

[308] Du Y, Han R, Wen F, Ng San San S, Xia L, Wohland T, et al. Synthetic sandwich culture of 3D hepatocyte monolayer. Biomaterials. 2008;29:290-301.

[309] Wang S, Nagrath D, Chen PC, Berthiaume F, Yarmush ML. Three-dimensional primary hepatocyte culture in synthetic self-assembling peptide hydrogel. Tissue Eng Part A. 2008;14:227-36.

[310] Xia L, Arooz T, Zhang S, Tuo X, Xiao G, Susanto TA, et al. Hepatocyte function within a stacked double sandwich culture plate cylindrical bioreactor for bioartificial liver system. Biomaterials. 2012;33:7925-32.

[311] Maher JJ. Primary hepatocyte culture: is it home away from home? Hepatology. 1988;8:1162-6.

[312] Gautam A, Ng OC, Boyer JL. Isolated rat hepatocyte couplets in short-term culture: structural characteristics and plasma membrane reorganization. Hepatology. 1987;7:216-23.

[313] Ferrini JB, Ourlin JC, Pichard L, Fabre G, Maurel P. Human hepatocyte culture. Methods Mol Biol. 1998;107:341-52.

[314] Bhandari RN, Riccalton LA, Lewis AL, Fry JR, Hammond AH, Tendler SJ, et al. Liver tissue engineering: a role for co-culture systems in modifying hepatocyte function and viability. Tissue Eng. 2001;7:345-57.

[315] Watt FM. Cell culture models of differentiation. FASEB J. 1991;5:287-94.

[316] Hamilton GA, Jolley SL, Gilbert D, Coon DJ, Barros S, LeCluyse EL. Regulation of cell morphology and cytochrome P450 expression in human hepatocytes by extracellular matrix and cell-cell interactions. Cell Tissue Res. 2001;306:85-99.

[317] Gross-Steinmeyer K, Stapleton PL, Tracy JH, Bammler TK, Lehman T, Strom SC, et al. Influence of Matrigel-overlay on constitutive and inducible expression of nine genes encoding drug-metabolizing enzymes in primary human hepatocytes. Xenobiotica. 2005;35:419-38.

[318] LeCluyse EL, Fix JA, Audus KL, Hochman JH. Regeneration and maintenance of bile canalicular networks in collagen-sandwiched hepatocytes. Toxicol In Vitro. 2000;14:117-32.

[319] Dunn JC, Tompkins RG, Yarmush ML. Long-term in vitro function of adult hepatocytes in a collagen sandwich configuration. Biotechnol Prog. 1991;7:237-45.

[320] LeCluyse EL, Audus KL, Hochman JH. Formation of extensive canalicular networks by rat hepatocytes cultured in collagen-sandwich configuration. Am J Physiol. 1994;266:C1764-74.

[321] Moghe PV, Berthiaume F, Ezzell RM, Toner M, Tompkins RG, Yarmush ML. Culture matrix configuration and composition in the maintenance of hepatocyte polarity and function. Biomaterials. 1996;17:373-85.

[322] Wang YJ, Liu HL, Guo HT, Wen HW, Liu J. Primary hepatocyte culture in collagen gel mixture and collagen sandwich. World J Gastroenterol. 2004;10:699-702.

[323] Kono Y, Yang S, Letarte M, Roberts EA. Establishment of a human hepatocyte line derived from primary culture in a collagen gel sandwich culture system. Exp Cell Res. 1995;221:478-85.

[324] Dunn JC, Yarmush ML, Koebe HG, Tompkins RG. Hepatocyte function and extracellular matrix geometry: long-term culture in a sandwich configuration. FASEB J. 1989;3:174-7.

[325] Choi HJ, Choi D. Successful mouse hepatocyte culture with sandwich collagen gel formation. J Korean Surg Soc. 2013;84:202-8.

[326] Gilbert TW, Agrawal V, Gilbert MR, Povirk KM, Badylak SF, Rosen CA. Liver-derived extracellular matrix as a biologic scaffold for acute vocal fold repair in a canine model. Laryngoscope. 2009;119:1856-63.

[327] Meng FW, Slivka PF, Dearth CL, Badylak SF. Solubilized extracellular matrix from brain and urinary bladder elicits distinct functional and phenotypic responses in macrophages. Biomaterials. 2015;46:131-40.

[328] Gilbert TW, Wognum S, Joyce EM, Freytes DO, Sacks MS, Badylak SF. Collagen fiber alignment and biaxial mechanical behavior of porcine urinary bladder derived extracellular matrix. Biomaterials. 2008;29:4775-82.

[329] Record RD, Hillegonds D, Simmons C, Tullius R, Rickey FA, Elmore D, et al. In vivo degradation of 14C-labeled small intestinal submucosa (SIS) when used for urinary bladder repair. Biomaterials. 2001;22:2653-9.

[330] Lindberg K, Badylak SF. Porcine small intestinal submucosa (SIS): a bioscaffold supporting in vitro primary human epidermal cell differentiation and synthesis of basement membrane proteins. Burns. 2001;27:254-66.

[331] Meng F, Modo M, Badylak SF. Biologic scaffold for CNS repair. Regen Med. 2014;9:367-83.

[332] Michalopoulos G, Sattler G, Sattler C, Pitot HC. Interaction of chemical carcinogens and drug-metabolizing enzymes in primary cultures of hepatic cells from the rat. Am J Pathol. 1976;85:755-72.

[333] Schuetz EG, Li D, Omiecinski CJ, Muller-Eberhard U, Kleinman HK, Elswick B, et al. Regulation of gene expression in adult rat hepatocytes cultured on a basement membrane matrix. J Cell Physiol. 1988;134:309-23.

[334] Shaffiey SA, Jia H, Keane T, Costello C, Wasserman D, Quidgley M, et al. Intestinal stem cell growth and differentiation on a tubular scaffold with evaluation in small and large animals. Regen Med. 2015.

[335] French KM, Boopathy AV, DeQuach JA, Chingozha L, Lu H, Christman KL, et al. A naturally derived cardiac extracellular matrix enhances cardiac progenitor cell behavior in vitro. Acta Biomater. 2012;8:4357-64.